ISSN 1997-1397 (Print)
ISSN 2313-6022 (Online)

Журнал Сибирского федерального университета

Математика и физика

Journal of Siberian Federal University

Mathematics & Physics

2026 19 (4)

ISSN 1997-1397
(Print)

ISSN 2313-6022
(Online)

2026 19 (4)

ЖУРНАЛ СИБИРСКОГО ФЕДЕРАЛЬНОГО УНИВЕРСИТЕТА
Математика и Физика

JOURNAL OF SIBERIAN FEDERAL UNIVERSITY
Mathematics & Physics

Издание индексируется Scopus (Elsevier), Emerging Sources Citation Index (WoS, Clarivate Analytics), Российским индексом научного цитирования (НЭБ), представлено в международных и российских информационных базах: Ulrich's periodicals directiory, ProQuest, EBSCO (США), Google Scholar, MathNet.ru, КиберЛенинке.

Включено в список Высшей аттестационной комиссии «Рецензируемые научные издания, входящие в международные реферативные базы данных и системы цитирования».

Все статьи представлены в открытом доступе http://journal.sfu-kras.ru/en/series/mathematics_physics.

Журнал Сибирского федерального университета.
Математика и физика.
Journal of Siberian Federal University. Mathematics & Physics.

Учредитель: Федеральное государственное автономное образовательное учреждение высшего образования "Сибирский федеральный университет"(СФУ)
Главный редактор: А.М. Кытманов. Редакторы: В.Е. Зализняк, А.В. Щуплев.
Компьютерная верстка: Г.В. Хрусталева.
№ 4 от 26.08.2026. Индекс: 42327. Тираж: 1000 экз. Свободная цена
Адрес редакции и издателя: 660041 г. Красноярск, пр. Свободный, 82, стр. 24, оф. 117.
Отпечатано в типографии Издательства БИК СФУ
660041 г. Красноярск, пр. Свободный, 82.
Свидетельство о регистрации СМИ ПИ № ФС 77-28724 от 29.06.2007 г., выданное Федеральной службой по надзору в сфере массовых коммуникаций, связи и охраны культурного наследия
http://journal.sfu-kras.ru
Подписано в печать 15.08.26. Формат 84×108/16. Усл.печ. л. 12,1.
Уч.-изд. л. 11,9. Бумага тип. Печать офсетная.
Тираж 1000 экз. Заказ 25231
Возрастная маркировка в соответствии с Федеральным законом № 436-ФЗ:16+

CONTENTS

СОДЕРЖАНИЕ

Editorial

In memory of Valter Alekseevich Ignatchenko

Editorial

This issue is dedicated to Valter Alekseevich Ignatchenko, doctor of physical and mathematical sciences, professor, Honored Scientist of the Russian Federation, a distinguished specialist in the physics of magnetic phenomena and a scientific lieder. A native of Odessa and a graduate of Odessa University, Ignatchenko arrived in Krasnoyarsk in 1957 and began working at the newly established Institute of Physics as part of the experimental laboratory. Heading a small experimental group, he was the first in our country to conduct research on spin-wave resonance in thin magnetic films. However, intrigued by the nature of this phenomenon, he became fascinated with the theory of magnetism, became a theoretician, and organized a theoretical group, which eventually grew into the theoretical department he heads, consisting of three laboratories. Many graduates of Siberian Federal University, having trained in the theoretical department, have become world-renowned scientists, pioneers of new fields in various fields of physics. The distinguishing features of his scientific style were always innovation and a broad range of scientific interests, a profound understanding of the phenomena being studied, physical intuition, a desire to refine the results of theoretical calculations to a point where they could be experimentally verified, and a critical approach to his own findings. His favorite sayings were: "Regardless of whether a physicist is engaged in theory or experiment, he knows and understands the nature of the phenomena being studied not only in the brain but also in the spinal cord" and "If you see an effect, look for a defect". Ignatchenko's fundamental work on the theory of the domain structure of bulk ferromagnets and magnetic films, a series of studies on spin dynamics and magnetoelastic resonance in thin films, pioneering work on phenomena in the field of the frequencies crossing of nuclear and electron magnetic resonances, his works on stochastic magnetic structure, its influence on dynamic properties, the law of approaching magnetization saturation, and the spectrum and attenuation of waves of various natures in superlattices with inhomogeneities have become recognized classics in the field of physics of magnetic phenomena. This issue contains contributions from students and successors of Valter Alekseevich's research, colleagues from various institutes who knew him and his work, and students of his students.

EDN: GDKZSV
УДК 538.9

The Nature of the Formation of the Pseudogap State in HTSC Cuprates

Valerii I. Kuz'min*
Kirensky Institute of Physics
Federal Research Center KSC SB RAS
Krasnoyarsk, Russian Federation
Sergey G. Ovchinnikov†
Kirensky Institute of Physics Federal Research Center KSC SB RAS
Krasnoyarsk, Russian Federation
Siberian Federal University
Krasnoyarsk, Russian Federation

Received 10.02.2026, received in revised form 11.03.2026, accepted 17.04.2026

Abstract. This paper discusses the current progress in studying the nature of the mysterious pseudogap state in high-temperature superconductors based on cuprates of the $La_{2-x}Sr_xCuO_4$-type and other similar quasi-two-dimensional compounds whose common structural elements are CuO_2 layers.

Keywords: high-temperature cuprate superconductors, Hubbard model, cluster perturbation theory, pseudogap.

Citation: V.I. Kuz'min, S.G. Ovchinnikov, The Nature of the Formation of the Pseudogap State in HTSC Cuprates, J. Sib. Fed. Univ. Math. Phys., 2026, 19(4), 429–436.
EDN: GDKZSV.

This article is intended for the special issue of the journal dedicated to the memory of Valter Alekseevich Ignatchenko. His name is associated with the development of theoretical physics in Krasnoyarsk. It was V. A. Ignatchenko who founded and for many years led the work of the Theoretical Department of the L.V. Kirensky Institute of Physics. Seminars held at the Theoretical Department presented a wide range of scientific fields, not only in the theory of magnetism, which formed the basis of his scientific interests, but also in many other areas of physics, mathematics, and biology. One of the authors of this article, S. G. Ovchinnikov, had the opportunity to work in the Theoretical Department at the beginning of his professional career. From the memoirs of S. G. Ovchinnikov: "For a third-year student, and that was the age at which I began attending the Theoretical Department seminars, V. A. Ignatchenko's concluding remarks were especially valuable, helping me understand the content of the paper. It was at these seminars that I learned about superconductors, which are a remarkable class of materials whose properties are formed by quantum physics. Not only I, but also many of my other young colleagues from the Theory Department, owe the breadth of our worldview to this scientific school founded by V. A. Ignatchenko". Therefore, he deservedly was highly respected among his colleagues, not only at the Institute of Physics in Krasnoyarsk but also among Soviet physicists in general. His active work with young students after he reached his 90th birthday is also admirable. His last paper was published in 2025 [1].

When V. A. Ignatchenko was in his prime, his colleague V. A. Borisyuk was working on problems of superconductivity in the Theoretical Department of the Institute of Physics. E. V. Kuz'min's group began working on the superconductivity of strongly correlated electrons (I. S. Sandalov, S. G. Ovchinnikov). These studies became especially relevant after the discovery

*kuz@iph.krasn.ru https://orcid.org/0000-0001-8744-2407
†sgo@iph.krasn.ru https://orcid.org/0000-0003-1209-545X

of high-temperature superconductivity. This article provides a brief overview of some aspects of our current understanding of the achievements and unresolved problems in the field of high-temperature superconductivity.

Introduction

One of the most important problems in modern physics is unraveling the nature of high-temperature superconductivity in layered cuprates. Although their critical temperature rarely exceeds 100 K and is inferior to current records in hydrides under pressures of approximately 300 GPa, where the critical temperature reaches room temperature, cuprates are already used in wires with negligible resistance and other quantum electronic devices. However, from a fundamental standpoint, superconductivity in hydrides is of a fairly standard nature, whereas in cuprates it has remained a mystery for almost 40 years. The reason is that they are a special class of materials with so-called strong electron correlations. In ordinary metals, the role of the Coulomb interaction was understood by L. D. Landau and described in his Fermi liquid theory. A theory of such superconductors was proposed by Bardeen, Cooper, and Schrieffer (BCS theory) [2]. In materials with strong electron correlations, the BCS theory does not work, since the Coulomb interaction destroys the Fermi liquid state. Nevertheless, some progress in understanding the properties and mechanisms of superconductivity in HTSC cuprates has been achieved to date [3]. In this paper, we describe the current state of the problem. It has now been reliably established that the electronic properties of the normal phase are determined by strong electronic correlations within two-dimensional copper-oxygen layers. The mechanism of formation of the superconducting phase is determined by the simultaneous action of two channels of Cooper pair formation with $d_{x^2-y^2}$-symmetry. The total parameter of superconducting pairing is formed by the antiferromagnetic interaction of the pair of nearest neighboring electrons and the interaction of these electrons with phonons [4]. This total mechanism allowed us not only to explain the high values of the critical temperature, but also to understand the unusual type of isotope effect, which is minimal precisely at the point of optimal doping concentration $p = 0.15$ [5]. Despite the significant progress in describing the superconducting phase in cuprates, the question of the formation of the electronic properties of the normal phase remains open. Without an answer to this question, the general phase diagram of cuprates on the hole concentration-temperature (p, T)-plane remains unclear. The particular uncertainty is associated with the so-called pseudogap states first discovered in experiments on nuclear magnetic resonance [6] and inelastic neutron scattering [7]. These states are most clearly manifested in the angle-resolved photoelectron (ARPES) spectra, in which it is possible to measure not only the energy distribution of emitted electrons, but also the their angle distribution [8]. This makes it possible to directly obtain information on the spectral density of photoelectrons at a fixed energy and a wave vector. The magnitude of the imaginary part of the electron Green's function $A(\mathbf{k}, \mathbf{E}) = \dfrac{-1}{\pi} G(\mathbf{k}, \mathbf{E})$ is determined by the number of emitted photoelectrons with an energy E and a given wave vector $\mathbf{k}$.

For ordinary metals described by Fermi-liquid theory, this method reveals the electron distribution over wave vectors, i.e. the Fermi surface, where each state with a wave vector on the Fermi surface corresponds to two states, one spin up and one spin down. The unusual nature of the ARPES results in cuprates lies in the fractional number of electrons on the Fermi surface for different wave vectors, varying from zero to two depending on the temperature and hole concentration. As a result, for some wave vectors, the states with a Lorentzian-like spectral line shape typical of Fermi systems, peaking at the Fermi level, are retained on the Fermi surface. For other states, a dip appears at the Fermi level, and the number of states is suppressed. In other words, in such a case an electron statistics atypical for usual Fermi systems exists, with the number of states depending on the momentum, temperature and hole concentration. The entire body of experiments on the detection of pseudogap states below the pseudogap temperature's

$T^*(p)$-line has led to the identification of an unknown region of the pseudogap state in the phase diagram of cuprates, with the critical $T^*(p)$-lines differing among different authors. Two main types of diagrams are known. For the first type, the $T^*(p)$-line rests on the superconducting phase boundary at a hole concentration $p_c \sim 0.15$ corresponding to the optimal doping point. For the second type, the $T^*(p)$ line rests on the $T = 0$ axis in the region of overdoped hole concentrations $p_{c_2} \sim 0.25$ at the boundary of the superconducting and normal metallic phases. Thus, the presence of a mysterious pseudogap state has been established below the $T^*(p)$-boundary in the phase diagram.

However, even above this limit, things are not so simple. In a normal metal at high temperatures in the non-superconducting state, a linear dependence of resistance on temperature is expected. Instead, over the most of the phase diagram, resistance measurements show a quadratic dependence, and only for highly overdoped compositions with a hole concentration $p > p_{c_2} \sim 0.25$ does the linear dependence typical of metals occur. Thus, pseudogap states represent terra incognita in the modern physics of high-temperature superconductivity. A detailed discussion of pseudogap states can be found in a recent review [9].

1. The pseudogap within cluster perturbation theory

The main focus of our research is on the electronic properties in the presence of strong electron correlations. The existence of such correlations is evident already when examining the properties of the undoped cuprate La_2CuO_4, which, when doped with holes by replacing the trivalent La^{3+} ion with Sr^{2+} in $La_{2-x}Sr_xCuO_4$, gives rise to a superconducting phase with a maximum T_c at $p = p_{c_1} \sim 0.15$ (the optimal doping point). We generalized the methods known for describing the region of strong electron correlations in the Hubbard model (when the energy of Coulomb interaction U is much greater than the kinetic energy of free electrons W) to describe their electronic properties in the so-called generalized tight-binding (GTB) method [10]. Within the framework of this approach, the insulating state in the undoped La_2CuO_4 is reproduced, and the electronic structure changes upon doping with holes. There are two Lifschitz electron transitions with a change in the Fermi surface topology at the points $p = p_{c_1}$ and $p = p_{c_2}$ [11]. Moreover, we were able to describe not only the superconducting phase with the correct $d_{x^2-y^2}$-type gap symmetry, taking into account the magnetic and phonon pairing mechanisms, with a maximum of the critical temperature T_c at the optimal doping concentration p_{c_1}, but also the isotopic shift of T_c upon substitution of O_{16} isotopes by O_{18}, with a minimum of T_c at the optimal doping point, in complete agreement with the isotopic substitution experiments [5]. However, our version of the theory [10] was unable to reproduce the shapes of the Fermi surfaces with the pseudogap states known from the ARPES experiments.

In constructing the version of the theory [10], we proceeded from the so-called Hubbard-1 approximation, although not in the standard Hubbard model, but taking into account the real oxygen and copper electron states in cuprates. In this approximation, strong intra-atomic Coulomb interactions of copper d-electrons are accurately taken into account. This turned out to be sufficient to describe the main features of the phase diagram of cuprates, namely: the insulating state of the undoped cuprate La_2CuO_4, the evolution of the electronic properties upon doping with two Lifschitz electronic transitions including the changes in the topology of the Fermi surfaces at p_{c_1} and p_{c_2}. To describe less trivial properties, such as the pseudogap state, an accurate consideration of only local correlations within Hubbard-1 turned out to be insufficient. For this purpose, we generalized our theory to take into account strong electron correlations within the framework of cluster perturbation theory (CPT). The essence of this method is to account for nonlocal electronic and magnetic correlations while accurately accounting for all local Coulomb interactions. The idea is to partition a square lattice into periodically repeating clusters. The smallest such cluster is a 2×2 square unit of four Cu^{2+} ions.

In the first stage of CPT, the exact diagonalization is performed within the unit cell and all eigenstates $|p\rangle$ with the number of holes 0, 1, 2, 3, 4 are found. Based on these eigenstates, the Hubbard cluster operators $X^{pq} = |p\rangle \langle q|$ are defined the same way as local operators in the standard Hubbard model. The difference is in the dimension of the eigenstate space and in the Hubbard operator matrices. For the standard definition of the local Hubbard operators, there are four single-site intra-atomic states $|p\rangle = |0\rangle, |\uparrow\rangle, |\downarrow\rangle, |\uparrow\downarrow\rangle$. For 2×2 clusters in the cluster, the number of eigenstates is 4^4. Therefore, the dimension of the Hilbert space increases sharply. Next, all intercluster interatomic electron hoppingss between nearest neighbors are taken into account using the cluster generalization of the Hubbard-1 approximation. Thus, a perturbation theory similar to the Hubbard-1 approximation is constructed, but with precise consideration of short-range order within the cluster [12]. For a 2×2 cluster, correlations for the first and second neighbors are accurately taken into account. This approach taught us to consider nonlocal correlations, but the correlation radius up to the second neighbors turned out to be too small for significant progress in the problem of the pseudogap formation. Real progress was achieved within the framework of CPT with 4×4 clusters, where interatomic correlations up to the ninth neighbors can be taken into account [13].

For such clusters, the Fermi surface at low doping (see Fig. 1(a) and (b)) is not closed and has the shape of arcs of finite length with the maximum spectral weight in the diagonal (nodal) direction of the Brillouin zone. In the off-diagonal (antinodal) direction, the spectral weight is close to zero — this is exactly what is observed in the ARPES spectra as a pseudogap. With an increase in the doping concentration to 0.1875 (Fig. 1(c)), the Fermi surface becomes continuous, but the spectral weight is still distributed non-uniformly along the Fermi contour. And only at a hole concentration of 0.25, where in the experiment the superconducting phase already ends and a normal Fermi liquid is observed, does the Fermi surface in Fig. 1(d) have a simple shape, in agreement with the ARPES data. The results of [13] made it possible to compare the changes in the Fermi surface and the spin correlation functions. Without doping, the correlation functions at zero temperature exhibited alternating signs, characteristic of the antiferromagnetic phase. With increasing doping at T=0 and at zero doping, the long-range antiferromagnetic order is

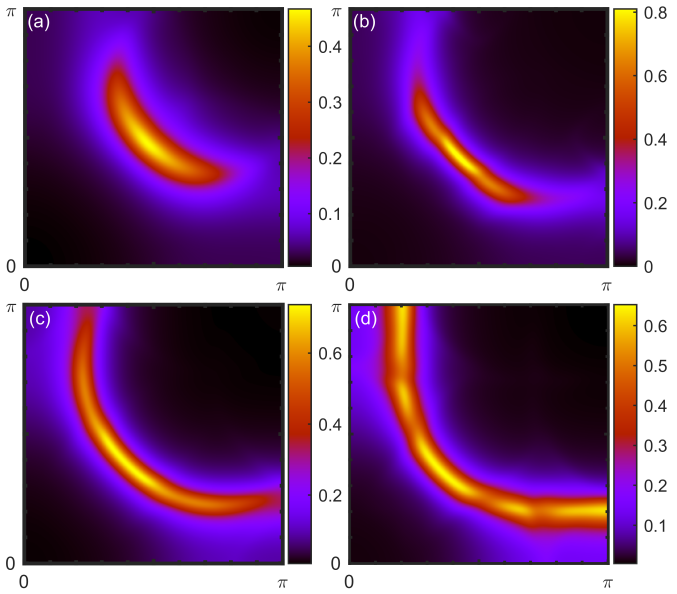

Fig. 1. The Fermi surface in the framework of CPT with 4×4 clusters at $T = 0$ for doping concentration (a) 0.0625, (b) 0.125, (c) 0.1875, (d) 0.25. Adapted from the paper [13]

disrupted with increasing temperature, manifested by a change in the sign of the correlation functions for the third and more distant neighbors. Figure 2 complements the above picture, showing the spectral intensity ratios (a) and the spectral line shapes in the antinodal direction at different doping concentrations (b). These figures demonstrate that Fermi-liquid properties appear only for heavily doped compounds with $p = 0.25$.

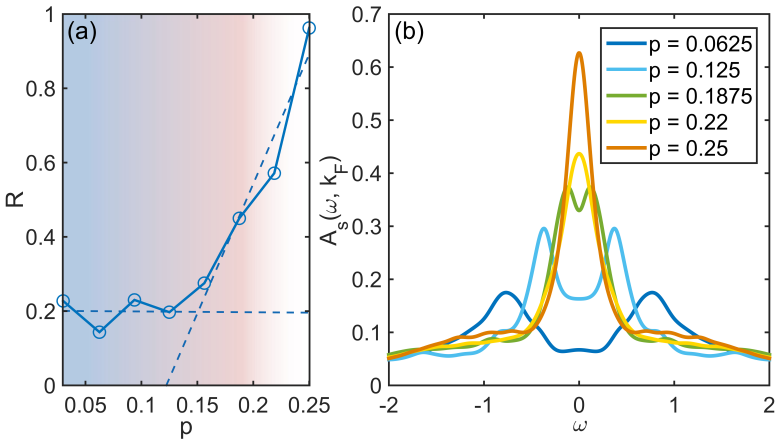

Fig. 2. (a) The dependence of the antinodal to nodal spectral weight ratio at the Fermi surface on doping p and (b) the changes in the antinodal spectral intensity from the Fermi-liquid-like at = 0.25 through the weak pseudogap at = 0.18 with a small drop around $\omega = 0$ to the strong pseudogap at = 0.125. Adapted from the paper [13]

CPT also allowed us to trace the evolution of electronic properties with increasing temperature (Figs. 3 and 4) from the pseudogap at low temperatures to a Fermi-liquid-like state at high temperatures. Note that the spectral weight ratio in Fig. 3 allows us to distinguish three regions: $R << 1$, $R \sim 1$, and the transition region from small ratios to $R \sim 1$. We called the $R << 1$ region "the strong pseudogap", the $R \sim 1$ region corresponds to the normal Fermi liquid, and the intermediate region corresponds the "weak pseudogap". Thus, if we trace the changes from

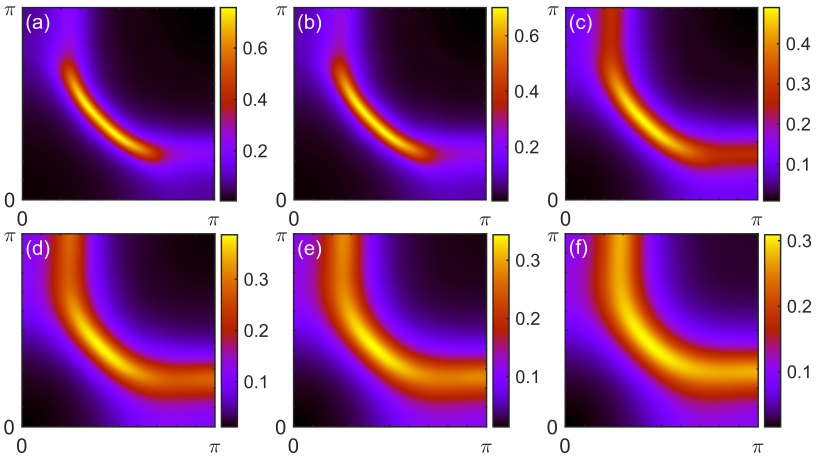

Fig. 3. The temperature evolution of the Fermi surface at $p = 0.167$ for different inverse temperatures $\beta = 1/kT$ in units of the hopping integral: (a) $\beta = 100$, (b) $\beta = 24$, (c) $\beta = 12$, (d) $\beta = 8$, (e) $\beta = 6$, (f) $\beta = 4$. Adapted from the paper [13]

high to low temperatures in the phase diagram for a fixed hole concentration, we first encounter the Fermi-liquid state, then a smooth transition to a weak pseudogap state, and at low temperatures we arrive at the strong pseudogap state. A similar evolution occurs with increasing hole concentration for a fixed temperature: at low doping there is the strong pseudogap, then in the intermediate doping range there is the weak pseudogap, and finally the Fermi-liquid state at high doping. Similar conclusions about three regions for hole doping were obtained in [14] within the framework of the dynamic mean-field cluster theory. At the same time, for electron-doped cuprates, the authors of [14] obtained only two regions.

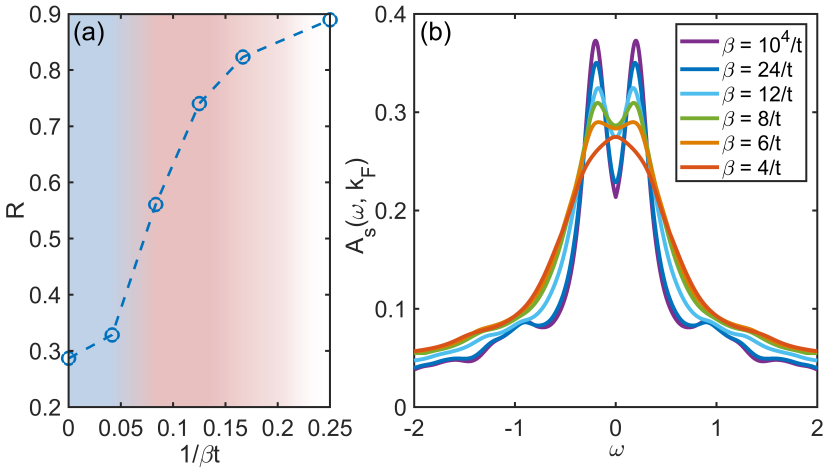

Fig. 4. (a) The dependence of the antinodal to nodal spectral weight ratio at the Fermi surface on doping and (b) the changes in the antinodal spectral intensity from the Fermi-liquid-like at = 0.25 through the weak pseudogap at = 0.18 with a small drop around $\omega = 0$ to the strong pseudogap at = 0.125. Adapted from the paper [13]

Conclusions

Here, we have shown that taking into account non-local spin correlations is important to obtain the doping and temperature evolution of the Fermi arcs and the pseudogap, and demonstrated it with an example of 4×4 CPT. Note that, due to the large size of the basis of eigenstates for a 4×4 cluster, the volume of numerical calculations is quite large. Note also that the conclusion regarding two possible pseudogap formation temperatures was not made in the experimental studies on the pseudogap using neutron magnetic resonance. However, the two characteristic Fermi arc temperatures were detected using ARPES [15]. In addition, in a recent inelastic neutron scattering study, the authors noted two different regions of the pseudogap state in their phase diagram [16].

This work was carried out within the framework of the state assignment of the Kirensky Institute of Physics of the Russian Academy of Sciences, project FWES-2024-0002.

References

[1] V.A.Ignatchenko, D.S.Tsikalov, D.S.Polukhin, The influence of local magnetic anisotropy on ferromagnetic resonance in a perpendicularly magnetized film, *ZhETF* **167**(2025), no. 2, 233–248 (in Russian). DOI: 10.31857/S0044451025020099

[2] J.Bardin, L.N.Cooper, J.R.Schrieffer, Theory of superconductivity, *Phys. Rev.*, **108**(1957), no. 5, 1175–1204.

[3] V.Z.Kresin, S.G.Ovchinnikov, S.A.Wolf, Superconducting State, *International Series of Monographs on Physics, Oxford University Press*, **170**(2021).

[4] E.I.Shneyder, S.G.Ovchinnikov, Phonon and magnetic pairing mechanisms in high-temperature superconductors in the strong correlation limit., *JETP Letters*, **83**(2006), no. 9, 394–398. DOI: 10.1134/S0021364006090062

[5] E.I.Shneyder, S.G.Ovchinnikov, Isotope effect in the model of strongly correlated electrons with the magnetic and phonon superconducting pairing mechanisms, *JETP*, **109**(2009), no. 6, 1017–1021. DOI: 10.1134/S1063776109120139

[6] W.W.Warren Jr, R.E.Walstedt, G.F.Brennert, R.J.Cava, R.Tycko, R.F.Bell, G.Dabbagh, Cu spin dynamics and superconducting precursor effects in planes above T_c in $YBa_2Cu_3O_{6.7}$., *Phys. Rev. Lett.*, **62**(1989), no. 10, 1193–1196.

[7] J.Rossat-Mignod, L.P.Regnault, C.Vettier, P.Bourges, P.Burlet, J.Bossy, J.Y.Henry, G.Lapertot, Neutron scattering study of the $YBa_2Cu_3O_{6+x}$ system., *Physica C*, **185**(1991), 86–92.

[8] Z-X.Shen, D.S.Dessau, Electronic structure and photoemission studies of late transition-metal oxides - Mott insulators and high-temperature superconductors., *Phys. Rep.*, **253**(1995), no. 1-3, 1–162. DOI: 10.1016/0370-1573(95)80001-A

[9] S.I.Vedeneev, Pseudogap problem in high-temperature superconductors., *Phys. Usp.*, **64**(2021), no. 9, 890–922. DOI: 10.3367/UFNr.2020.12.038896

[10] S.G.Ovchinnikov, I.S.Sandalov, The band structure of strong-correlated electrons in $La_{2?x}Sr_xCuO_4$ and $YBa_2Cu_3O_{7?y}$, *Physica C*, **161**(1989), no. 5-6, 607–617.

[11] S.G.Ovchinnikov, M.M.Korshunov, E.I.Shneyder, Lifshits quantum phase transitions and rearrangement of the Fermi surface upon a change in the hole concentration in high-temperature superconductors., *J. Exp. Theor. Phys.*, **109**(2009), no. 5, 775–785. DOI: 10.1134/S1063776109110077

[12] S.V.Nikolaev, S.G.Ovchinnikov, Cluster Perturbation Theory for the Hubbard Model: the Pinning of Chemical Potential, *J. Sib. Fed. Univ., Math. Phys.*, **4**(2011), no. 2, 162–167.

[13] V.I.Kuz'min, M.A.Visotin, S.V.Nikolaev, S.G.Ovchinnikov, Doping and temperature evolution of pseudogap and spin-spin correlations in the two-dimensional Hubbard model, *Phys. Rev. B*, **101**(2020), no. 11, 115141(12). DOI: 10.1103/PhysRevB.101.115141

[14] E.Gull, M.Ferrero, O.Parcollet, A.Georges, A.J.Millis, Momentum-space anisotropy and pseudogaps: A comparative cluster dynamical mean-field analysis of the doping-driven metal-insulator transition in the two-dimensional Hubbard model., *Phys. Rev. B*, **82**(2010), no. 15, 155101(14). DOI: 10.1103/PhysRevB.82.155101

[15] T.Kondo, A.D.Palczewski, Y.Hamaya, T.Takeuchi, J.S.Wen, Z.J.Xu, G.Gu, A.Kaminski, Formation of Gapless Fermi Arcs and Fingerprints of Order in the Pseudogap State of Cuprate Superconductors, *Phys. Rev. Lett.*, **111**(2013), no. 15, 157003(5). DOI: 10.1103/PhysRevLett.111.157003

[16] Z.W.Anderson et al., Gapped commensurate antiferromagnetic response in a strongly underdoped model cuprate superconductor., *npj Quantum Mater.*, **10**(2025), no. 93, 1–9.

Природа формирования псевдощелевого состояния в ВТСП купратах

Валерий И. Кузьмин
Институт физики им. Л. В. Киренского
Федеральный исследовательский центр КНЦ СО РАН
Красноярск, Российская Федерация
Сергей Г. Овчинников
Институт физики им. Л. В. Киренского
Федеральный исследовательский центр КНЦ СО РАН
Красноярск, Российская Федерация
Сибирский федеральный университет
Красноярск, Российская Федерация

Аннотация. В настоящей статье обсуждается современный прогресс в исследовании природы загадочного псевдощелевого состояния в высокотемпературных сверхпроводниках на основе купратов типа $La_{2-x}Sr_xCuO_4$ и других им подобных квазидвумерных соединений, общим структурным элементом которых являются слои CuO_2.

Ключевые слова: высокотемпературные купратные сверхпроводники, модель Хаббарда, кластерная теория возмущений.

EDN: JBSHKA
УДК 512.54

Correlation Properties of Magnetization and Effective Anisotropy of Nanostructured Low-dimensional Structures

Vitaly A. Orlov*
Siberian Federal University
Krasnoyarsk, Russian Federation
L. V. Kirensky Institute of Physics
Federal Research Center KSC SB RAS
Krasnoyarsk, Russian Federation
Anatoly A. Ivanov†
Siberian Federal University
Krasnoyarsk, Russian Federation

Received 10.02.2026, received in revised form 05.03.2026, accepted 07.04.2026

Abstract. The correlation length of the magnetization is theoretically calculated in the model of a two-dimensional unlimited sample, which is a conglomerate of crystallites with random parameters of local anisotropy. Estimates of the effective anisotropy constant of the stochastic domain are carried out, taking into account fluctuations in the directions of the light axes of anisotropy, constants and sizes of crystallites of the structure of arbitrary dimension.

Keywords: magnetic anisotropy, stochastic domain, correlation length.

Citation: V.A. Orlov, A.A. Ivanov, Correlation Properties of Magnetization and Effective Anisotropy of Nanostructured Low-dimensional Structures, J. Sib. Fed. Univ. Math. Phys., 2026, 19(4), 437–447. EDN: JBSHKA.

Introduction

Modern functional materials, promising for use in new generation devices for various purposes, have a complex structure that provides them with unusual physical properties. The most interesting and sought-after structures are heterogeneous in chemical composition, physical properties, etc.

At the same time, there are factors that are still difficult to control: defects in the crystal lattice, large (polyatomic) random structural inhomogeneities, etc.

In any case, there is a need to develop theoretical methods for studying the magnetic properties of structurally inhomogeneous objects. Structures with random defects are the most difficult to analytically describe. Such systems, due to their stochastic magnetic structure (SMS), they have unusual magnetic properties that can be both useful and harmful in the context of obtaining samples with predefined parameters.

Theoretical methods for describing the properties of randomly and regularly inhomogeneous magnets have a long history. Spectral methods of SMS research are actively developing, starting with the thorough pioneering work of the Krasnoyarsk School of Physics [1–3], the results of which

*vaorlov@sfu-kras.ru https://orcid.org/0000-0002-9025-0075
†aaivn@yandex.ru

are successfully used to interpret experimental data on static and dynamic magnetic properties (see, for example, [4–9]). Methods for describing the magnetic properties of regular structures with a controlled distribution of inhomogeneities over the volume of samples are also reflected in the developed theory [10, 11].

Somewhat later, methods for describing the properties of SMS using the correlation function of inhomogeneities of magnetic parameters and the correlation function of magnetization [12–16] arose and were developed. This approach has been successfully applied to interpret the observed mechanisms of orientation transitions in low dimensional structures [17–19], experimental and numerical investigation of the properties of stochastic magnetic domains [7, 20–23] and their effective parameters [24–27].

Despite the thoroughness and depth of developed theoretical approaches both in our country and abroad (see reviews of [28, 29]), well-known and emerging new problems of an applied nature remain, the solution of which can contribute to more meaningful actions in the development of systems with predefined magnetic properties.

As is known, in structures with random directions of the local axis of magnetic anisotropy, the homogeneous state of magnetization is not stable — ripples occur in the distribution of magnetization with a division into magnetic blocks. or stochastic magnetic domains (SMD). When such a sample is remagnetized, individual magnetic blocks are reoriented, almost independently of neighboring ones. Unlike the traditional domain structure, SMDs can have a significant variation in their parameters: dimensions, directions of the axes of the effective axes of anisotropy, effective constants of anisotropy, etc. This complicates the analytical description of effective macroscopic properties. At the same time, some properties of magnetic blocks are amenable to analytical calculations.

This paper is devoted to the question of the combined and separate influence of fluctuations in various structural and magnetic parameters of the system on the properties of the effective magnetic anisotropy of such an SMS element as a stochastic magnetic domain or magnetic block.

1. Effective anisotropy of the stochastic domain

To estimate the parameters of effective magnetic anisotropy, we consider a stochastic domain model in the form of a certain region of sample space, which is a conglomerate of densely arranged crystallites in the form of parallelepipeds (see Fig. 1). The division into crystallites occurs in secant planes with randomly distributed coordinates. The crystallites have randomly oriented directions of local axes of anisotropy (LAA) and values of anisotropy constants K. The LOA directions are set by vectors $\mathbf{l}$. Further the calculations are carried out under the assumption that the linear dimensions of the crystallites are small compared to the width of the domain wall of a homogeneous material δ_0.

The idea of calculating the effective constant of a magnetic block is based on comparing the expression for the resulting torque acting on magnetization from a conglomerate of crystallites with the expression for the moment in a parallelepiped of the same volume as the domain. Let us write expressions for the magnetic anisotropy energies.

The energy of the magnetic anisotropy of the block has the form:

$$E_a = -\sum_{i=1}^{N_x}\sum_{j=1}^{N_y}\sum_{k=1}^{N_z} K_{i,j,k} V_{i,j,k} \left(\mathbf{ml}\right)^2 = -\sum_{i=1}^{N_x}\sum_{j=1}^{N_y}\sum_{k=1}^{N_z} K_{i,j,k} \Delta x_i \Delta y_j \Delta z_k \left(\mathbf{ml}\right)^2 . \qquad (1)$$

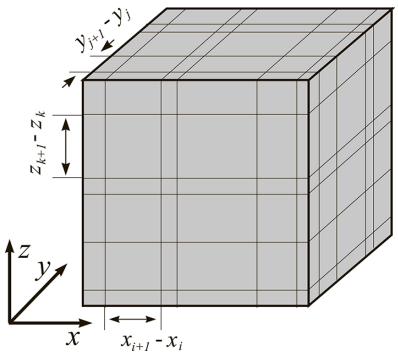

Fig. 1. The model of the sample section is a stochastic domain

Here $\mathbf{m}$ is a single magnetization vector, which we will consider unchanged throughout the magnetic block (due to the fulfillment of the condition $\Delta x, \Delta y, \Delta x \ll \delta_0$), the crystallites are numbered and have indexes i, j, k along the corresponding axes, $\Delta x_i = x_{i+1} - x_i$, $\Delta y_i = y_{i+1} - y_i$, $\Delta z_i = z_{i+1} - z_i$, $V_{i,j,k} = \Delta x_i \Delta y_j \Delta z_k$ and $K_{i,j,k}$ are the volume of the crystallite and its local anisotropy constant, respectively, with the indices i, j, k. The length of the magnetic block along In the general case, the coordinate axes are different and the number of rows is N_x, N_y, and N_z, respectively.

On the other hand, abstracting from the nanostructured of the block structure, and considering this area as a homogeneous area with some effective anisotropy constant K_{ef} and the direction of the effective axis $\mathbf{l}_{ef}$, we can write:

$$E_{a_{ef}} = -K_{ef} L_x L_y L_z \left(\mathbf{ml}_{ef}\right)^2, \tag{2}$$

where L_x, L_y, and L_z are the length of the block along the corresponding coordinate axes.

Then for the torques we get:

$$M_a = -\frac{\partial E_a}{\partial \vartheta} = \sum_{i=1}^{N_x} \sum_{j=1}^{N_y} \sum_{k=1}^{N_z} K_{i,j,k} \left(x_{i+1} - x_i\right) \left(y_{j+1} - y_j\right) \left(z_{k+1} - z_k\right) (\mathbf{ml}) \frac{\partial (\mathbf{ml})}{\partial \vartheta}, \tag{3}$$

$$M_{a_{ef}} = -\frac{\partial E_{a_{ef}}}{\partial \vartheta} = K_{ef} L_x L_y L_z \left(\mathbf{ml}_{ef}\right) \frac{\partial \left(\mathbf{ml}_{ef}\right)}{\partial \vartheta}, \tag{4}$$

where ϑ is the angle between the direction of the effective anisotropy axis and a single vector of magnetization.

After equating (3) and (4) for an effective constant, we get:

$$K_{ef} = \frac{\sum\limits_{i,j,k}^{N_x,N_y,N_z} K_{i,j,k} v_{i,j,k} \cos\left(2\alpha_{i,j,k}\right)}{\left| \sum\limits_{i,j,k}^{N_x,N_y,N_z} K_{i,j,k} v_{i,j,k} \cos\left(2\alpha_{i,j,k}\right) \right|} \left[\sum_{i,j,k}^{N_x,N_y,N_z} K_{i,j,k}^2 v_{i,j,k}^2 + \right.$$
$$\left. + \sum_{i,j,k}^{N_x,N_y,N_z} \sum_{n \neq i, m \neq j, l \neq k}^{N_x,N_y,N_z} K_{i,j,k} K_{n,m,l} v_{i,j,k} v_{n,m,l} \cos\left(2\left(\alpha_{i,j,k} - \alpha_{n,m,l}\right)\right) \right]^{\frac{1}{2}}. \tag{5}$$

Here α are the polar angles of the LOA direction, calculated from the direction of the effective anisotropy axis, in addition, the notation is introduced: $v_{i,j,k} = V_{i,j,k} / \left(L_x L_y L_z\right)$.

It is reasonable to assume the independence of the distribution of local constants, crystallite volumes, and LOA directions, and consequently the expression (5) can be rewritten in a more compact form:

$$K_{ef} = \frac{\langle K\rangle \langle\cos(2\alpha)\rangle}{|\langle K\rangle \langle\cos(2\alpha)\rangle|}\left[N\left\langle K^2\right\rangle \left\langle v^2\right\rangle + N\left(N-1\right)\langle K\rangle^2 \langle v_{i,j,k}v_{n,l,k}\rangle \phi\right]^{\frac{1}{2}}. \tag{6}$$

The notation used here is: $N = N_xN_yN_z$ — the number of crystallites in the magnetic block, $\langle K\rangle = \sum\limits_{i,j,k}^{N} K_{i,j,k}/N$ and $\left\langle K^2\right\rangle = \sum\limits_{i,j,k}^{N} K_{i,j,k}^2/N$ — RMS value of local anotropy constants, $\left\langle v^2\right\rangle = \sum\limits_{i,j,k}^{N} v_{i,j,k}^2/N$ — RMS dimensionless volume of crystallites,

$$\phi = \sum_{i,j,k}^{N}\sum_{n\neq i,m\neq j,l\neq k}^{N}\frac{\cos\left(2\left(\alpha_{i,j,k}-\alpha_{n,m,l}\right)\right)}{N(N-1)}. \tag{7}$$

The average of the product of the dimensionless volumes of crystallites requires separate consideration:

$$\langle v_{i,j,k}v_{n,l,k}\rangle = \frac{1}{L_xL_yL_z}\int\limits_V\int\limits_V V_{i,j,k}V_{n,m,l}\rho\left(V_{i,j,k}\right)\rho\left(V_{n,m,l}|V_{i,j,k}\right)dV_{i,j,k}dV_{n,m,l}. \tag{8}$$

Here $\rho\left(V_{i,j,k}\right)$ is the volume distribution density of the crystallite with the number $\{i,j,k\}$, $\rho\left(V_{n,m,l}|V_{i,j,k}\right)$ is the conditional distribution density of a crystallite with the number $\{n,m,l\}$, provided that the volume of the previous crystallite was equal to $V_{i,j,k}$.

After integration by all possible values of crystallite volumes from 0 to $V_d = L_xL_yL_z$ we get:

$$\langle v_{i,j,k}v_{n,l,k}\rangle = \frac{\langle v\rangle - \left\langle v^2\right\rangle}{N-1}. \tag{9}$$

Then, taking into account (9) for (6), we can write:

$$K_{ef} = \frac{\langle K\rangle \langle\cos(2\alpha)\rangle}{|\langle K\rangle \langle\cos(2\alpha)\rangle|}\left[N\left\langle v^2\right\rangle \left(\left\langle K^2\right\rangle - \langle K\rangle^2\phi\right) + N\langle K\rangle^2\langle v\rangle\phi\right]^{\frac{1}{2}}. \tag{10}$$

This expression defines a general method for calculating the effective constant of a magnetic block, but it is interesting to present (10) in a form that allows us to identify differences in K_{ef} for structures with inhomogeneities of different dimensions: multilayer, columnar, and 3D nanostructured (see Fig. 2).

To do this, let's return to the definition of linear sizes of crystallites (1) and introduce dimensionless dispersions of their linear sizes:

$$\sigma_x^2 = \frac{\left\langle\Delta x^2\right\rangle - \langle\Delta x\rangle^2}{\langle\Delta x\rangle^2}, \qquad \sigma_y^2 = \frac{\left\langle\Delta y^2\right\rangle - \langle\Delta y\rangle^2}{\langle\Delta y\rangle^2}, \qquad \sigma_z^2 = \frac{\left\langle\Delta z^2\right\rangle - \langle\Delta z\rangle^2}{\langle\Delta z\rangle^2}. \tag{11}$$

Taking into account (11), the expression (10) takes the form:

$$K_{ef} = \frac{\langle K\rangle \langle\cos(2\alpha)\rangle}{|\langle K\rangle \langle\cos(2\alpha)\rangle|}\left[\frac{1}{N}\left(\left\langle K^2\right\rangle - \langle K\rangle^2\phi\right)\left(\sigma_x^2+1\right)\left(\sigma_y^2+1\right)\left(\sigma_z^2+1\right) + \langle K\rangle^2\phi\right]^{\frac{1}{2}}. \tag{12}$$

It is important to note that the relationship between the number of crystallites in the magnetic block N and its volume V_d is determined differently for samples with different dimensions of

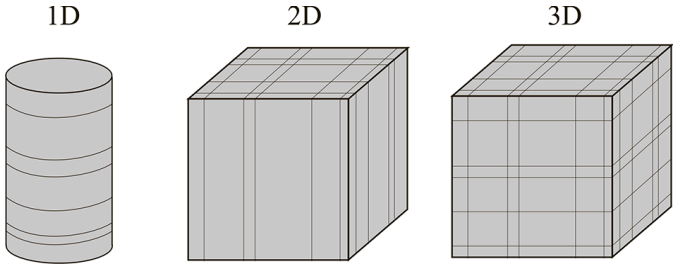

Fig. 2. Examples of models of polycrystalline structures with heterogeneities of different dimensions

inhomogeneities. For one-dimensional cases $V_d^{(1D)} \sim N\langle a\rangle$, two-dimensional — $V_d^{(2D)} \sim (N\langle a\rangle)^2$, three-dimensional — $V_d^{(3D)} \sim (N\langle a\rangle)^3$, where $\langle a\rangle$ is the characteristic linear size of crystallites in the direction of the axes along which the local anisotropy field fluctuates.

Let us further consider the limiting cases of the expression (12) for some practically interesting models. Note that in the limit of the total absence of fluctuations in all characteristics of the anisotropy field, i.e. for all $\sigma^2 = 0$, $\phi = 1/N$ (see (7)), $K = const$, we get $K_{ef} = K$, which should be the case.

For a simple model with one-dimensional inhomogeneities ($\sigma_y^2 = \sigma_z^2 = 0$), the same local constants K and crystallite sizes a ($\sigma_x^2 = 0$) and complete chaos in the LAA directions ($\phi = 0$) we get: $K_{ef} = K/\sqrt{N}$. This result is well-known [12, 19].

If the polar angles of LOA α are distributed within a narrow cone from $-\alpha_0$ to $+\alpha_0$, which can be provided, for example, during sample spraying, the expression for the effective constant takes the form:

$$K_{ef} \approx K\mu, \qquad \mu = \int\limits_{-\alpha_0}^{+\alpha_0} \cos(\alpha)\,\rho(\alpha)d\alpha. \tag{13}$$

Here μ is a texture parameter defined from (7), $\rho(\alpha)$ is the density of the polar angle distribution. The expression (13), as a limiting case, coincides with the previously obtained expression [30].

Interestingly, when the condition $\Delta x, \Delta y, \Delta x \ll \delta_0$ is met, models with complete chaos in the LOA directions ($\phi = 0$), fluctuations in crystallite sizes described by σ^2 dispersions will not change the functional dependence of the effective constant on other parameters. The correction is reduced only to the appearance of a multiplier of the order of one.

The opposite situation occurs with the regular distribution of directions. For example, when the polar angle of the axes alternates from crystallite to crystallite and takes only two values of $\pm\alpha_0$, the local constants do not fluctuate. In this case, for (7) we get: $\phi = (N\cos^2(2\alpha_0) - 1)/(N-1)$. Therefore, for an effective constant in this case, we will have:

$$K_{ef} = K\sqrt{\frac{\sin^2(2\alpha_0)\left(\sigma^2+1\right)^d + N\cos^2(2\alpha_0) - 1}{N-1}}, \tag{14}$$

where $d = 1, 2, 3$ is the dimension of magnetic inhomogeneities. In a special case $\alpha_0 = \pm\pi/4$, when, at first glance , torque compensation on the part of crystallites should occur, this does not happen due to differences in their linear dimensions [17]. Indeed, for this limiting case, we obtain:

$$K_{ef} = K\sqrt{\frac{\left(\sigma^2+1\right)^d - 1}{N-1}}. \tag{15}$$

For $\sigma^2 = 0$, we have $K_{ef} = 0$ — full compensation in the absence of volume fluctuations and the magnetization is in indifferent equilibrium.

2. Correlation length of magnetization and magnetic block

Next, let's ask about ways to estimate the size of the magnetic block (the number of crystallites N included in the block).

Methods for calculating the correlation length of magnetization, which is identified with the linear size of the stochastic domain, have been well developed for a long time (see, for example, the introduction and [31, 32]). However, the early approaches are somewhat abstract [33], i.e. they are not tied to the details of the magnetization distribution in nanostructured samples. Below, for example, consider the structure model with two-dimensional inhomogeneities (see Fig. 2) and apply a calculation method that echoes the method of calculating signal correlations in radiophysics [34].

It is easy to show that in the case of small crystallite sizes compared to the length of the domain wall of a homogeneous material, the anisotropy field can be represented by the sum δ-shaped outliers in the coordinates of the corresponding grains. In this case, the distribution of magnetization is actually determined by a discrete set of its guiding angles. However, due to the high concentration of crystallites with simultaneous smoothness of the magnetization reversals, the equilibrium equations are nothing more than a difference form of a differential equation for the equilibrium distribution of magnetization $\vartheta(x)$ of the form:

$$\frac{\partial^2 \vartheta}{\partial x^2} + \frac{\partial^2 \vartheta}{\partial y^2} = \frac{1}{\delta_0^2} \sin\left(2(\vartheta - \alpha)\right). \tag{16}$$

Here α is the polar angle of the direction of the local anisotropy axis.

Next, we obtain the solution of the equation (16) in general form, taking into account the specified boundary conditions. The solution of this equation can be represented as (Fourier series expansion):

$$\vartheta(x, y) = \sum_{k=1}^{\infty} \left(u_k(x) \sin\left(\frac{\pi k y}{L}\right) + g_k(x) \cos\left(\frac{\pi k y}{L}\right) \right). \tag{17}$$

Here, as before, L is the characteristic linear grain size in the directions along which the anisotropy fluctuates, k is an integer.

After substituting the trial solution (17) into the equation (16) for unknown functions depending on x, we obtain a system of equations:

$$\begin{cases} \dfrac{\partial^2 u_k}{\partial x^2} - \left(\dfrac{\pi k}{L}\right)^2 u_k = -\dfrac{1}{2\delta_0^2 L} \displaystyle\int_{-L}^{L} \sin(2\alpha) \sin\left(\frac{\pi k t}{L}\right) dt, \\ \dfrac{\partial^2 g_k}{\partial x^2} - \left(\dfrac{\pi k}{L}\right)^2 g_k = -\dfrac{1}{2\delta_0^2 L} \displaystyle\int_{-L}^{L} \sin(2\alpha) \cos\left(\frac{\pi k t}{L}\right) dt. \end{cases} \tag{18}$$

The fact that the function $\vartheta(x, y)$ varies slightly is used here, throughout the stochastic domain, and the selected axis is oriented in the direction of the average magnetization.

The joint solution of the equations (18) is represented as:

$$\vartheta(x,y) = -\frac{1}{2\pi\delta_0^2}\sum_{k=1}^{\infty}\int_0^x\int_{-L}^{L}\frac{1}{k}\sin(2\alpha)\cos\left(\frac{\pi k}{L}(t-y)\right)\exp\left(\pm\frac{\pi k}{L}(p-x)\right)dtdp. \tag{19}$$

Then, for the magnetization dispersion, we can write:

$$\begin{aligned}\left\langle\vartheta(x,y)^2\right\rangle = -\frac{1}{4\pi^2\delta_0^4}\sum_{k=1}^{\infty}\sum_{n=1}^{\infty}\int_0^x\int_0^x\int_{-L}^{L}\int_{-L}^{L}\frac{1}{kn}\cos\left(\frac{\pi k}{L}(t-y)\right)\cos\left(\frac{\pi k}{L}(t'-y)\right)\times\\ \times\ \exp\left(\pm\frac{\pi k}{L}(p-x)\right)\exp\left(\pm\frac{\pi k}{L}(p'-x)\right)\psi(p,p',t,t')dt\,dt'dp\,dp'.\end{aligned} \tag{20}$$

Here $\psi(p,p',t,t') = \delta\left(|p-p'|/a\right)\delta\left(|t-t'|/a\right)\left\langle\sin^2(2\alpha)\right\rangle$ is the correlation function of inhomogeneities, a is the characteristic linear size of the crystallite in the direction of the axes along which the anisotropy field fluctuates.

After sequential integration and summation (20), for the dependence of the variance on the coordinate r, we have:

$$D_\vartheta(r) = \frac{a^2r^2}{8\pi^2\delta_0^4}\sum_{k=1}^{\infty}\frac{1-e^{-2\pi k}}{k^3}\left\langle\sin^2(2\alpha)\right\rangle \approx 0.15\frac{a^2r^2}{\pi^2\delta_0^4}\left\langle\sin^2(2\alpha)\right\rangle = 0.15\frac{b^4}{\pi^2}N^2\left\langle\sin^2(2\alpha)\right\rangle, \tag{21}$$

where $b = a/\delta_0$, $N = r/a$.

It is reasonable to determine the characteristic correlation length of the magnetization and, consequently, the size of the stochastic domain from the equality: $D_\vartheta(r) = \left\langle\sin^2(2\alpha)\right\rangle$. From here, for r or N, we get:

$$N = \sqrt{\frac{\pi^2}{0.15}}b^{-2}, \qquad \delta_S \approx 7.9\delta_0 b^{-1}. \tag{22}$$

In conclusion of this section, we note that the specific type of correlation function of inhomogeneities does not affect the functional dependence of the size of the magnetic block. depends on the size of the crystallite. The only prerequisite is good localization ψ. That is, dependencies (22) would have a similar appearance not only for δ-shaped profile, but also for exponential, triangular, etc.

3. Conclusion

Combining formulas (22) and (12) makes it possible to fully determine the value of the effective constant of the uniaxial magnetic anisotropy of the sample section, identified with a stochastic magnetic domain or a magnetic block for two-dimensional structures.

Calculations of the size of magnetic blocks or the number of crystallites included in the stochastic domain for structures with one-dimensional and three-dimensional inhomogeneities can be carried out in the same way as it was done in the previous section:

$$\delta_S^{(1D)} \sim b^{-1/3}, \qquad \delta_S^{(3D)} \sim b^{-3}. \tag{23}$$

Expressions (23) paired with (12) It can also be used to estimate effective constants in 1D and 3D structures.

The calculated value (12) can also be used to estimate the width of the inter-domain wall:

$$\delta_W \approx \sqrt{\frac{A}{K_{ef}}}. \tag{24}$$

It is important to note here that the parameters δ_W and δ_S have different functional dependence on the magnetic and geometric parameters of the sample and can vary significantly. This circumstance can be especially vividly demonstrated by the example of a simple model with identical crystallite sizes, their local constants, but axes distributed in a relatively narrow cone of directions.

Indeed, regardless of the degree of texturing of μ, the size of the magnetic block is determined by the expression (22), and the wall size is determined by the expression (24), taking into account (13):

$$\delta_W \approx \sqrt{\frac{A}{K\mu}} = \frac{\delta_0}{\sqrt{\mu}}. \tag{25}$$

Qualitatively, this difference can be explained as follows. The size of the wall between stochastic domains is determined by the effective constant of these domains, the more pronounced it is, obviously, the more pronounced it is the direction in LAA orientations. This is exactly what is observed when there is a texture in the LAA directions.

In contrast, the size of the domain itself is determined by the correlation length of the magnetization, i.e. the distance at which the dispersion of the magnetization is equal to the dispersion of the local axes. This definition leads to an interesting property: in the simple model under consideration, the domain size is practically independent of the texture μ. Indeed, an increase in the angle of dispersion in the LAA directions (a decrease in μ leads to an increase in the dispersion in the LAA directions and at the same time, it leads to a commensurate increase in the dispersion in the guiding angles of magnetization. Thus, a change in μ leads to a kind of rescaling of the values of the polar angles with the characteristic lengths of the magnetization ripples unchanged.

As a result, this paper presents a theoretical calculation of the parameters of the stochastic magnetic structure of inhomogeneous ferromagnets: effective anisotropy parameters (without restrictions on the dimension of inhomogeneities) and the characteristic size of the magnetic block for the 2D model.

In conclusion, we note the range of unsolved research tasks. The range of static and dynamic magnetization properties of nanostructured ferromagnets is still wide. In particular, the dynamic properties of stochastic magnetic domains, taking into account magnetostatic energy, are awaiting their theoretical interpretation.

References

[1] V.A.Ignatchenko, Magnetic structure of thin magnetic films and FMR, *Sov. Phys. JETP*, **27**(1968), 162.

[2] I.S.Edelman, L.I.Chernyshova, Statistical characteristics of the fine magnetic structure of ferromagnetic films, *The Physics of Metals and Metallography,* **28**(1969), 51–57.

[3] V.A.Ignatchenko, R.S.Iskhakov, Stochastic magnetic structure and spin waves in amorphous ferromagnets, *Bulletin of the Academy of Sciences of the USSR: Physical Series*, **44**(1980), 59–62.

[4] F.G.Bass, V.A.Kagalovskii, V.V.Konotop, Inhomogeneous ferromagnetic resonance in magnets with fluctuating parameters, *Soviet Physics Solid State*, **32**(1990), 42–46.

[5] R.S.Iskhakov, S.V.Komogortsev, A.D.Balaev, L.A.Chekanova, Dimensionality of a system of exchange-coupled grains and magnetic properties of nanocrystalline and amorphous ferromagnets, *JEPT Lett.*, **72**(2000), 304–307. DOI: 10.1134/1.1328443

[6] R.S.Iskhakov, S.V.Komogortsev, Z.M.Moroz, E.E.Shalygina, Characteristics of the magnetic microstructure of amorphous and nanocrystalline ferromagnets with a random anisotropy: Theoretical estimates and experiment, *JEPT Lett.*, **72**(2000), 603–607.
DOI: 10.1134/1.1351199

[7] R.S.Iskhakov, V.A.Ignatchenko, S.V.Komogortsev, A.D.Balaev, Study of magnetic correlations in nanostructured ferromagnets by correlation magnetometry, *JEPT Lett.*, **78**(2003), 646–650. DOI:10.1134/1.1644310

[8] Y.I.Mankov, D.S.Tsikalov, Название: High-frequency susceptibility of a multilayered ferromagnetic system with two-dimensional inhomogeneities, *Physics of the Solid State,* **52**(2010), 544–553. DOI: 10.1134/S1063783410030157

[9] S.V.Komogortsev, R.S.Iskhakov, Magnetization curve and magnetic correlations in a nanochain of ferromagnetic grains with random anisotropy, *Physics of the Solid State,* **47**(2005), 495–501. DOI: 10.1134/S1063783410030157

[10] V.A.Ignatchenko, Yu.I.Mankov, A.V.Pozdnyakov, Spin-wave susceptibility of partially randomized ferromagnetic superlattices, *Journal of Experimental and Theoretical Physics*, **89**(1999), 712–720.

[11] V.A.Ignatchenko, Yu.I.Mankov, D.S.Tsikalov, High-frequency susceptibility of a superlattice with 2D inhomogeneities, *J. Exp. Theor. Phys.*, **107**(2008), 603–611.
DOI: 10.1134/S1063776108100075

[12] Y.Ymry, S.-K.Ma, Random field instability of the ordered state of continuous symmetry, *Phys. Rev. Letters*, **35**(1975), 1399–1401.

[13] E.M.Chudnovsky, Magnetic properties of amorphous ferromagnets. *J. Appl. Phys.*, **64**(1988), 5770–5775.

[14] A.A.Ivanov, G.O.Patrushev Stochastic Magnetic Anisotropy of an Ultradisperse Magnet, *The Physics of Metals and Metallography*, **84**(1997), 346–348.

[15] F.Porrati, W.Wulfhekel, J.Kirschner, An analytical model for ultrathin films with spatially varying magnetic anisotropies, *JMMM*, **270**(2004), 22–31.
DOI:10.1016/S0304-8853(03)00658-9

[16] A.A.Ivanov, V.A.Orlov, G.O.Patrushev, Correlation properties of the stochastic magnetic structure of ultradispersed ferromagnetic materials, *Physics of the Solid State,* **41**(1999), 1311–1314. DOI: 10.1134/1.1130989

[17] A.A.Ivanov, V.A.Orlov, G.O.Patrushev, On the formation of a given distribution of effective anisotropy axes in ferromagnets with regular inhomogeneities, *Physics of the Solid State,* **51**(2009), 756–760. DOI: 10.1134/S1063783409040192

[18] A.F.Kabychenkov, V.G.Shavrov, Inhomogeneous state of a uniaxial ferromagnet in the vicinity of an orientational phase transition (OPT) caused by a spatial inhomogeneity of the anisotropy, *Soviet Physics — Solid State*, **29**(1987), 111–112.

[19] A.A.Ivanov, V.A.Orlov, G.O.Patrushev, Properties of Effective Anisotropy of Magnetic Blocks in Ultradisperse Ferromagnets, *Physics of Metals and Metallography*, **103**(2007), 219–227. DOI: 10.1134/S0031918X07030015

[20] T.M.Vasilevskaya, D.I.Sementsov, Ferromagnetic Resonance in Metal Films with Angular Dispersion of Magnetic Anisotropy, *Physics of the Solid State,* **52**(2010), 1210–1216. DOI: 10.1134/S1063783410060156

[21] M.Gruyters, Exchange bias in two-dimensional layers of interacting nanoparticles with random magnetic anisotropy: A Monte Carlo study, *JMMM*, **320**(2008), 407–412. DOI: 10.1016/j.jmmm.2007.06.019

[22] B.A.Belyaev, A.V.Izotov, P.N.Solovev, Numerical Simulation of Magnetic Microstructure in Nanocrystalline Thin Films with the Random Anisotropy, *Journal of Siberian Federal University. Mathematics and Physic*, **10**(2017), 132–135. DOI: 10.17516/1997-1397-2017-10-1-132-135

[23] R.S.Iskhakov, S.V.Komogortsev, A.D.Balaev, et al., Fe nanowires in carbon nanotubes as an example of a one-dimensional system of exchange-coupled ferromagnetic nanoparticles, *JEPT Lett.*, **78**(2003), 236–240. DOI: 10.1134/1.1622038

[24] Z.V.Golubenko, L.P.Olkhovik, Y.A.Popkov, Z.I.Sizova, A.S.Kamzin, Magnetic anisotropy of a system of nanocrystalline $BaO\cdot 6Fe_2O_3$ particles, *Phys. Solid State*, **40**(1998), 1718–1720.

[25] D.S.Ilyushchenkov, V.I.Kozub, I.N.Yassievich, Domain Formation in Films of Magnetic Particles with a Random Distribution of Anisotropy Axes, *Physics of the Solid State*, **49**(2007), 1944–1948. DOI: 10.1134/S1063783407100216

[26] G.B.Han, R.W.Gao, S.S.Yan, H.Q.Liu, S.Fu, W.C.Feng, W.Li, X.M.Li, Effect of exchange-coupling interaction on the effective anisotropyin nanocrystalline Nd_2Fe_14B material, *JMMM*, **281**(2004), 6–10.

[27] N.A.Usov, A.Zhukov, J.Gonzalez, Single-domain particle with random anisotropy, *Journal of Non-Crystalline Solids*, **353**(2007), 79–798. DOI: 10.1016/j.jnoncrysol.2006.12.043

[28] V.A.Ignatchenko, Magnitnyye svoystva kristallicheskikh i amorfnykh sred, Sib. otd-niye: Nauka, 1989 (in Russian).

[29] R.S.Iskhakov, S.V.Komogortsev, Magnetic Microstructure of Amorphous, Nanocrystalline, and Nanophase Ferromagnets, *The Physics of Metals and Metallography*, **112**(2011), 666–681. DOI 10.1134/S0031918X11070064

[30] P.P.Dyachuk, E.V.Larikov, G.O.Patrushev, Influence of the misorientation of local anisotropy axes on the effective anisotropy constants of a uniaxial ferromagnet, *The Physics of Metals and Metallography,* **69**(1990), 25–31.

[31] A.A.Ivanov, G.O.Patrushev, Structure of Magnetization of a Stochastic Magnet, *Phys. Met. Metallogr,* **86**(1998), 331–336.

[32] E.M.Chudnovsky, D.A.Garanin, Topological Order Generated by a Random Field in a 2D Exchange Model, *Phys. Rev. Lett.*, **121**(2018), 017201.
DOI: 10.1103/PhysRevLett.121.017201

[33] A.A.Ivanov, V.A.Orlov, G.O.Patrushev, The Effect of the Profile of the Correlation Function of Structure Inhomogeneities on the Magnetic Structure in Ultradisperse Ferromagnetic Materials, *The Physics of Metals and Metallography,* **85**(1998), 639–641.

[34] S.M.Rytov, Y.A.Kravtsov, V.I.Tatarskii, Principles of Statistical Radiophysics 2. Correlation Theory of Random Processes, Springer Berlin, Heidelberg, 2011.

Корреляционные свойства намагниченности и эффективная анизотропия наноструктурированных низкомерных структур

В.А. Орлов
Сибирский федеральный университет
Красноярск, Российская Федерация
Институт физики им. Л. В. Киренского ФИЦ КНЦ СО РАН
Красноярск, Российская Федерация
А.А. Иванов
Сибирский федеральный университет
Красноярск, Российская Федерация

Аннотация. Теоретически рассчитана корреляционная длина намагниченности в модели двумерного неограниченного образца, представляющего собой конгломерат кристаллитов со случайными параметрами локальной анизотропии. Проведены оценки эффективной константы анизотропии стохастического домена с учетом флуктуаций в направлениях легких осей анизотропии, констант и размеров кристаллитов структуры произвольной размерности.

Ключевые слова: магнитная анизотропия, стохастический домен, корреляционная длина.

EDN: EDFJGG
УДК 537.6

The Law of Approach to Magnetic Saturation in Ferromagnets Nonuniform on the Nanometer Scale

Sergey V. Komogortsev*
Kirensky Institute of Physics
Federal Research Center KSC SB RAS
Krasnoyarsk, Russian Federation
Rauf S. Iskhakov†
Kirensky Institute of Physics
Federal Research Center KSC SB RAS
Krasnoyarsk, Russian Federation
Samarkand State University named after Sharof Rashidov
Samarkand, Uzbekistan

Received 10.02.2026, received in revised form 11.03.2026, accepted 17.04.2026

Abstract. The structural inhomogeneity of ferromagnetic materials on the nanometer scale plays a key role in the formation of excellent soft magnetic properties of nanocrystalline and amorphous alloys. The paper provides a brief overview of the main ideas behind the law of approach to magnetic saturation, which provides the basis for a method to study such inhomogeneities. Special attention is paid to the role of the works of the Krasnoyarsk school of magnetism researchers working in this direction: from the classic works of Kirensky and Ignatchenko to modern discoveries related to experimental studies of nanomaterials. The methodological options that open up to an experimentalist when studying the law of approach to saturation are discussed.

Keywords: ferromagnets, magnetic saturation, inhomogeneity, nanostructure, magnetic anisotropy.

Citation: S.V. Komogortsev, R.S. Iskhakov, The Law of Approach to Magnetic Saturation in Ferromagnets Nonuniform on the Nanometer Scale, J. Sib. Fed. Univ. Math. Phys., 2026, 19(4), 448–457. EDN: EDFJGG.

Introduction

The well-known dependence of the magnetization of a ferromagnetic material on an external magnetic field is characterized by hysteresis and is characterized by a nonlinear change in magnetization from zero to the maximum possible value – the saturation magnetization M_s. Most applied research is limited to studying the hysteresis loop. Since in fields significantly higher than the magnetic anisotropy field, the magnetization changes reversibly and rather fluently with increasing field. The magnetization in the maximum field is often taken as an estimate of M_s. To accurately determine the M_s, an experimentalist must take into account the so-called law of approach to magnetic saturation (LAMS). Furthermore, an experimentalist who does not neglect a careful study of this part of the magnetization curve near saturation obtains a remarkable source of useful, and sometimes unique, information about material inhomogeneities, local magnetic anisotropy, interactions, and magnetization correlations. In this work, we outline the history of ideas for studying the LAMS and delineate the range of opportunities for an experimentalist when using these ideas.

*komogor@iph.krasn.ru https://orcid.org/0000-0002-2686-3643
†rauf@iph.krasn.ru https://orcid.org/0000-0001-6077-2211

The law of approach to magnetic saturation is an equation (or formula) describing the part of the magnetization curve in strong magnetic fields, where the dependence of magnetization on field, associated with reversible rotation processes, has the character of an asymptotic approach to the maximum value – the saturation magnetization M_s. The first empirical form of this law is [1]:

$$M = M_s \left(1 - \sum \frac{a_i}{H^i}\right), \tag{1}$$

where the values i take the values $1/2, 1, 3/2, 2, \ldots$. The coefficients a_i are described by various theoretical models and can be determined experimentally when describing the magnetization curve by equation (1) [2]. When describing a part of an experimental magnetization curve near saturation using an equation of type (1), experimentalists sometimes add terms like χH and/or $bH^{1/2}$ describing the so-called paraprocess associated with the competition between the field and various kinds of excitations (mainly thermal) in the magnetic subsystem of a ferromagnet. In an experiment, the contributions from the paraprocess and reversible magnetization rotation processes can usually be separated, or the contribution from the paraprocess can be neglected.

The most well-known LAMS is the Akulov law for a ferromagnet with randomly oriented local easy magnetization axes [3]:

$$M = M_s \left(1 - \frac{1}{15}\left(\frac{H_a}{H}\right)^2\right), \tag{2}$$

where M_s is the saturation magnetization, H_a is the local magnetic anisotropy field, related to the magnetic anisotropy constant (K) as $H_a = 2K/M_s$. Starting from work [3], the LAMS became the basis for a method to determine magnetic anisotropy in crystallites of ferromagnetic polycrystals, and later for estimating elastic stresses in them [3, 4]. In deriving the Eq. (2), it was assumed that exchange correlations of magnetization are absent. This assumption is quite justified for an ensemble of misoriented non-interacting single-domain nanoparticles, or for a polycrystal with a crystallite size significantly exceeding the characteristic size $\sqrt{A/K}$, where A is the exchange interaction constant. For inhomogeneities with a size of the order of or smaller than $\sqrt{A/K}$, exchange correlations of magnetization play a significant role. As a result of the competition between the disordering effect of defects and the ordering influence of exchange interaction, magnetization demonstrates correlations on the scale $R_H = (2A/M_sH)^{1/2}$. A region of magnetic correlations of such extent turned out to be characteristic of nanocrystalline magnets. The magnetization inhomogeneity itself, first observed in thin films by Lorentz microscopy, was named "magnetization ripple" [5]. Consideration of these correlations led Brown to the conclusion about the possibility of observing terms in the LAMS of type (1) with values $i = 1/2, 1, 3/2$, for defects with different structures [6]. This idea was used in the works of Kronmuller, who linked various hyperbolic terms from equation (1) to specific structural defects (dislocation, vacancy, quasi-dislocation dipole, etc.) [7–12]. Kronmuller positioned his results as a theory of the LAMS for amorphous ferromagnets. Unfortunately, the identification of structural defects for amorphous materials is ambiguous. Ignatchenko and Iskhakov constructed a theory consistently linking the correlation or spectral properties of the inhomogeneities of the local anisotropy axis with magnetization inhomogeneities in a high field. They drew attention to the fact that when interpreting an experiment, matching a specific functional form of the LAMS with a specific structural defect cannot be considered reliable, since the same LAMS dependence could correspond to different structural defects [13, 14]. Using the theory of random functions, Ignatchenko and Iskhakov [2, 13, 14], and subsequently Chudnovsky, Saslow, and Serota [15, 16] showed that the functional form of the LAMS uniquely correlates only with the correlation function or the spectral density of the anisotropy inhomogeneity. It was established that for all LAMS arising in media with monotonically decreasing correlation functions of anisotropy inhomogeneity, the following behavior is common. A new, so-called exchange correlation field $H_R = 2A/M_sR_c^2$ appears

in the LAMS, above which the Akulov LAMS is valid, and below which a hyperbolic dependence of the form H^{-n} is realized, with an exponent depending on the dimensionality of the anisotropy inhomogeneity [17]. Thus, it was shown that observing the change in hyperbolic regimes in the LAMS could be used to determine the exchange field H_R. Initially, these theories were developed for the LAMS of amorphous alloys, so the first measurements of H_R, H_a, supplemented by independent measurements of A and M_s, were used to study the correlation radii of magnetic anisotropy and the local magnetic anisotropy field in a number of amorphous alloys [2]. For amorphous ferromagnets based on transition metals, it was experimentally established that the characteristic correlation size for the local easy magnetization axis is $10 \div 100$ nm [2,18,19]. Since, according to diffraction data, short-range order in amorphous metals is preserved over distances of about two or three interatomic distances, this led to new discussions about the structure of these alloys: from the special role of elastic stresses [7, 8, 19] to the specific crystallography of short-range order in amorphous media [2, 18, 19]. Subsequently, this theory of LAMS found application in the study of nanocrystalline alloys. Here, the correlation size of the local anisotropy axis in some cases acquires the more tangible meaning of the crystallite size [20–22], however, in nanocrystalline alloys it can also be associated with other scales, for example, the characteristic distance between twin boundaries [20]. In recent decades, a new understanding of the role of exchange magnetization correlations in the LAMS has provided an impetus for the development of both the method of approach to magnetic saturation and the study of nanoinhomogeneous materials in general. It became clear that the magnetic microstructure of nanostructured ferromagnets is represented by an ensemble of stochastic magnetic domains — regions with sizes equal to the magnetization correlation length. It was shown that experimental study of the LAMS allows one to determine the size of the stochastic domain and the effective anisotropy constant in this element, the size of the nanostructure element and its local anisotropy constant, as well as the dimensionality of the system of exchange-coupled ferromagnetic nanoparticles. The following presentation is devoted to a more detailed discussion of the current state of the LAMS method and the latest discoveries made with its help.

1. Theoretical basis

The various structural defects in a ferromagnet, affecting the local orientation of magnetization, leads to the fact that even in high magnetic fields, where there is no domain structure, the magnetization state is orientationally nonuniform (see Fig. 1). Magnetization in these fields

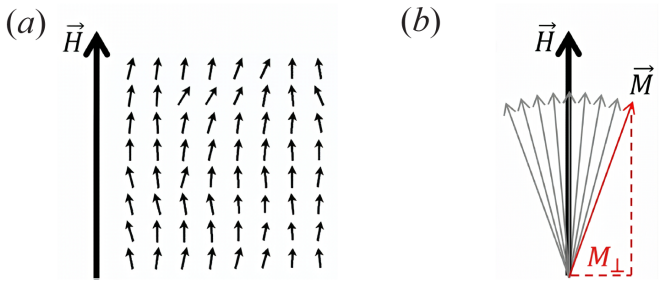

Fig. 1. The magnetization state of an inhomogeneous ferromagnet in a high field (a) and the corresponding magnetization hodograph (b)

occurs through inhomogeneous rotation: local magnetic moments rotate further towards the field direction, overcoming the stochastic influence of defects. For such a process, the LAMS is related to the normalized mathematical variance of the transverse components of the stochastic magnetic

structure d_m:

$$M = M_s \left(1 - d_m(H)\right), \tag{3}$$

$$d_m = \frac{\left\langle M_\perp^2 \right\rangle}{M_s^2}. \tag{4}$$

Nonuniform magnetization is characterized by correlations (Fig. 1(a)) associated with exchange interaction. A theory consistently linking the correlation or spectral properties of the inhomogeneities of the local anisotropy axis with magnetization inhomogeneities in a high field was developed by Ignatchenko and Iskhakov. This theory connects the LAMS with a specific type of correlation function of the local easy axis. For example, if an exponential is chosen as the modeling correlation function of the local easy axis, then for the dependence $d_m(H)$ one have:

$$d_m\left(H\right) = \frac{\left(aH_a\right)^2}{H^{1/2}\left(H_R^{1/2} + H^{1/2}\right)^3}, \tag{5}$$

here $H_a = 2K/M_s$ is the local anisotropy field, a is a symmetry coefficient equal to $1/\sqrt{15}$ for uniaxial anisotropy, $H_R = 2A/M_s R_c^2$ is the correlation field, R_c is the correlation radius of the local easy axis. It can be seen that near H_R, the field dependence of magnetization changes:

$$d_m(H) = (aH_a)^2 \begin{cases} H^{-2}, & H \gg H_R, \\ H^{-1/2}, & H \ll H_R. \end{cases} \tag{6}$$

In coordinates $\ln(d_m)$ vs $\ln(H)$, this corresponds to a characteristic bend in the experimental curve $d_m(H)$ near $H \sim H_R$ (see Fig. 2). Note that if instead of an exponential, any function from the class of monotonically decreasing functions is chosen as the model correlation function, the analytical expression for $d_m(H)$ will change. However, the asymptotes (6) and the value of the correlation field H_R will remain unchanged. The method for studying amorphous ferromagnets based on expressions (6), which allows estimating the correlation radius of the local easy axis, has been named correlation magnetometry.

2. Experimental results and new ideas

An important difference in analyzing experimental results using (1) and using (6) is that these approaches predict different behavior for $M(H)$ in the region of approach to magnetic saturation. In formula (1), the main contribution to the sum with increasing magnetic field will change in the sequence: $M(H) \propto H^{-2} \to\propto H^{-1} \to\propto H^{-1/2}$, thus, in an experiment, one should expect exactly this sequence of hyperbolic regimes with increasing field. According to formulas (5-6), the sequence of power-law regime changes is opposite. With increasing field, we have here: $M(H) \propto H^{-1/2} \to\propto H^{-2}$. This is due to the fundamental nonlinearity of expressions like (5) or (6) for the LAMS. As follows from the analysis of the literature, experimental groups investigating the LAMS are forced to choose one of these approaches, ignoring the other. That is, this difference is the reason for the lack of unity in experimental approaches. Expression (1) has an important flaw [11]. The magnetization work, proportional to the integral of $M(H)$ over magnetization, turns out to be infinite for all terms in expression (1) whose exponent is $\leqslant 1$. However, the magnetic anisotropy constants of a ferromagnet, determined precisely through the magnetization work of the material, are finite quantities. Describing the LAMS with nonlinear expressions like (5) eliminates this drawback – the magnetization work always turns out to be a finite quantity proportional to the average magnetic anisotropy constant. Experiment has shown that the sequence of power-law regime changes corresponds to expression (6), and not (1) [23].

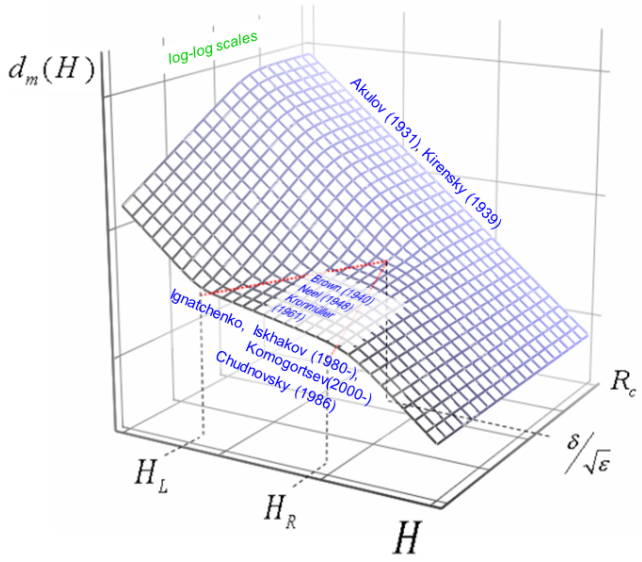

Fig. 2. The relationship between the magnetization variance near saturation, the external field, and the length of structural correlations (R_c) illustrates the main features of the LAMS method and the milestones in the development of LAMS ideas in ferromagnets inhomogeneous on the nanoscale

Further development of the LAMS method is associated with the concept of a stochastic magnetic domain – or a region of exchange magnetization correlations with a characteristic length $R_L \gg R_c$. This magnetic domain is observed in nanocrystalline alloys by various microscopic and diffraction techniques [24–26]. To date, based on the concepts of the stochastic magnetic domain, the following experimental data for nanostructured ferromagnets have been successfully explained: the dependence of the coercive force H_c, magnetic susceptibility χ, and the size of the stochastic magnetic domain on grain size: $H_c \propto R_c^6$, $\chi \propto R_c^{-6}$ [27], $R_L \propto R_c^{-3}$ [28]. As a result, the structure–property chain for nanostructured ferromagnets can be represented as: nanostructure–magnetic microstructure (stochastic magnetic domain) — magnetic properties. In recent decades, it has been shown that from the approach-to-saturation curves, one can determine the size of the micromagnetic structure element: the size of the stochastic domain and the value of the effective anisotropy in this element, the size of the nanostructure element and its local anisotropy, and the dimensionality of the exchange-coupled ferromagnetic nanoparticles. The correlation properties of the magnetic microstructure change qualitatively depending on the ratio R_c/R_c^*, where R_c^* is a unit of spatial scale composed of the fundamental constants (A, K) of the magnetic material. When $R_c > R_c^*$, the correlation properties of the magnetic structure are completely identical to the correlation properties of the atomic microstructure; when $R_c < R_c^*$, the magnetic microstructure is described by its own correlation characteristics, one of which is the size of the stochastic magnetic domain ($2R_L$), and the other is the field-dependent exchange correlation length R_H. The exchange correlation length satisfies the inequality $R_c \leqslant R_H \leqslant R_L$, under which the magnetization curve of a nanostructured ferromagnet can be represented through characteristic spatial scales as:

$$\frac{\Delta M}{M_s} = a^2 \frac{R_c^4}{\delta^4} \left(\frac{R_H}{R_c}\right)^{4-d} \equiv \frac{a^2}{\varepsilon^2} \left(\frac{R_H}{R_L}\right)^{4-d}, \tag{7}$$

where $\delta = \sqrt{A/K}$, and ε is a numerical coefficient in the range 0.4–0.7 [23]. In this version, the study of the magnetization curve $M(H)$ allows one to experimentally estimate two independent

characteristics: the value of the crossover field H_R (crossover field) and the value of the crossover ordinate of the functional dependencies $\Delta M(H)$ (from these values, R_c and R_L are calculated, respectively), and also to determine the packing dimensionality of nanoparticles in the material (or the topology of intergranular exchange bonds). The non-equi-axiality of particles can be accounted for by the anisotropy of the structural correlation radius: with a significant difference in these correlation radii, the crossover $\Delta M(H)$ occurs twice. Anisomery of the magnetic anisotropy inhomogeneity can lead to a dependence $d_m \propto H^{-1}$ for ribbons of rapidly quenched amorphous alloys [29].

Thus, for nanostructured ferromagnetic materials, a method has been developed for the experimental determination of the main characteristics of the micromagnetic structure from approach-to-saturation curves: correlation radii, the magnitude of the magnetic anisotropy of stochastic magnetic domains, and their spatial dimensionality [23, 30, 31]. It is shown that in a ferromagnetic system with random anisotropy and strong exchange interaction, the dependence of the magnetization correlation radius on the external field, besides the known crossover field H_R (above the field H_R, the magnetization is uniform within the crystallite), has a second crossover in the field $H_L < H_R$. In fields below H_L, a stochastic magnetic domain forms, whose size and anisotropy do not depend on the magnitude of the external field. In the range from H_L to H_R, the magnetization ripple regime is realized.

On reversible magnetization curves in the saturation region, in fields $H \leqslant H_L$, a section $\Delta M \propto H^{-2}$ has been experimentally discovered, associated with the limiting length of the magnetization ripple and with the formation of stochastic magnetic domains [30]. The power-law dependences of magnetization curves in the saturation region predicted by theory for nanostructured materials with different packing dimensionalities of exchange-coupled grains in the region where magnetization ripple exists ($H_L < H < H_R$) have been experimentally discovered. In bulk alloys ($d = 3$) — $M \propto H^{-1/2}$; in thin ferromagnetic films ($d = 2$) — $M \propto H^{-1}$; in ferromagnetic nanowires ($d = 1$) — $M \propto H^{-3/2}$ [32, 33]. In work [34], new analytical expressions for magnetization curves in the saturation region are proposed, which are fully consistent with the exact expressions of the theory in limiting cases but allow a more accurate description of the transition regime between power-law asymptotics. It is shown that in granular magnetic films FeCoB-SiO_2, near the "magnetic percolation threshold" [35], as well as in a nanoporous medium of aggregated CoPt nanoparticles [36], power-law dependences of the approach to magnetic saturation are observed, indicating a fractional packing dimensionality of exchange-coupled grains. The possibilities of studying the fractal dimensionality of exchange-coupled clusters of magnetic nanoparticles from their magnetization curves were demonstrated in [37] using micromagnetic modeling.

The dependences of the stochastic magnetic domain size and the random magnetic anisotropy energy, both of crystallites and stochastic magnetic domains, on heat treatment regimes were established for FeCuNbSiB alloys [38, 39], FeZrN [40, 41, 41–43], and the volume fraction of granules in nanogranular FeCoB-SiO_2 films [35]. Furthermore, it was experimentally demonstrated that the values of the coercive force and ferromagnetic resonance linewidth in FeCuNbSiB [44], FeCoB [45], and FeZrN [46] alloys increase with an increase in the effective anisotropy of the stochastic magnetic domain, and the dependences of the coercive force and ferromagnetic resonance linewidth on the crystallite size agree with the predictions of the random magnetic anisotropy model. The main milestones in the development of LAMS ideas in ferromagnets inhomogeneous on the nanoscale are given in Fig. 2, which shows the role played by researchers of the Krasnoyarsk school and, in particular, V. A. Ignatchenko.

Conclusion

The ideas associated with theoretical studies of the law of approach to magnetic saturation in ferromagnets have undergone a significant evolution: from empirical ideas for precise deter-

mination of the saturation magnetization value to a powerful method for the quantitative study of magnetization correlations in ferromagnets inhomogeneous on the nanometer scale. Recent achievements have stimulated significant experimental activity, related both to the search for new effects of structural and magnetic inhomogeneities on the magnetization curve and to the use of the new method for studying novel amorphous and nanostructured materials. The role of the Krasnoyarsk school of magnetism researchers in this direction is expressed by significant theoretical and experimental activity, which led both to the formation of new approaches for extracting information about inhomogeneities and to interesting discoveries in the study of new amorphous and nanocrystalline materials.

This work was carried out within the framework of a State Assignment (Federal Research Center KSC Siberian Branch Russian Academy of Sciences).

References

[1] P.Weiss, Les propriétés magnétiques de la pyrrhotine, *J. Phys. Théorique Appliquée*, **4**(1905), no. 1, 469.

[2] V.A.Ignatchenko, R.S.Iskhakov, Stochastic properties of inhomogeneities of amorphous magnetic materials, Magnetic properties of crystalline and amorphous media, Novosibirsk, Nauka, Sibyrskoe otdelenie, 1989, 128–147 (in Russian).

[3] N.S.Akulov, Uber den Verlauf der Magnetisierungskurve in starken Feldern, *Zeitschrift fur Phys. Phys.*, **69**(1931), no. 11–12, 822–831.

[4] N.S.Akulov, L.V.Kirensky, Magnetic method for study interal stress in ferromagnetic metall, *Zhurnal Tech Phys.*, **9**(1939), no. 13, 1145–1150 (in Russian).

[5] H.Hoffmann, Quantitative Calculation of the Magnetic Ripple of Uniaxial Thin Permalloy Films, *J. Appl. Phys.*, **35**(1964), no. 6, 1790.

[6] W.Brown, Theory of the Approach to Magnetic Saturation, *Phys. Rev.*, **58**(1940), no. 8, 736–743.

[7] H.Kronmüller, A.Seeger, Die einmündung in die ferromagnetische sättigung—II, *J. Phys. Chem. Solids.*, **18**(1961), no. 2–3, 93–115.

[8] M.Fähnle, H.Kronmüller, The influence of spatially random magnetostatic, magnetocrystalline, magnetostrictive and exchange fluctuations on the law of approach to ferromagnetic saturation of amorphous ferromagnets, *J. Magn. Magn. Mater.*, **8**(1978), no. 2, 149–156.

[9] A.Aharoni, Approach to Magnetic Saturation in the Vicinity of Impurity Atoms, *Phys. Rev. B.*, **2**(1970), no. 9, 3794–3805.

[10] A.Malozemoff, Laws of approach to magnetic saturation for interacting and isolated spherical and cylindrical defects in isotropic magnetostrictive media, *IEEE Trans. Magn.*, **19**(1983), no. 4, 1520–1523.

[11] L.Néel, La loi d'approche en a: H et une nouvelle théorie de la dureté magnétique, *J. Phys. le Radium.*, **9**(1948), no. 5, 184–192.

[12] E.Schlomann, Properties of Magnetic Materials with a Nonuniform Saturation Magnetization. I. General Theory and Calculation of the Static Magnetization, *J. Appl. Phys*, **38**(1967), no. 13, 5027.

[13] V.A.Ignatchenko, R.S.Iskhakov, Stochastic Magnetic Structure and Spin Waves in Amorphous Ferromagnetic Substance, *Izv. Akad. Nauk SSSR, Ser. Fiz.*, **44**(1980), 1434.

[14] V.A.Ignatchenko, R.S.Iskhakov, G.V.Popov, Law of approach to ferromagnetic saturation in amorphous ferromagnets, *Zh. Eksp. Teor. Fiz.*, **82**(1982), no. 5, 1518–1531.

[15] E.M.Chudnovsky, A theory of two-dimensional amorphous ferromagnet, *J. Magn. Magn. Mater.*, **40**(1983), no. 1–2, 21–26.

[16] E.M.Chudnovsky, W.M.Saslow, R.A.Serota, Ordering in ferromagnets with random anisotropy, *Phys. Rev. B.*, **33**(1986), no. 1, 251–261.

[17] V.A.Ignatchenko, R.S.Iskhakov, The Magnetization Curve of Ferromagnets with Anisotropic and Low-Dimensional Inhomogeneities, *Fiz. Met. Met.*, **73**(1992), 602–608.

[18] J.Tejada, Evidence of the extended orientational order in amorphous alloys obtained from magnetic measurements, *EPL*, **23**(1993), no. 7, 517–522.

[19] H.Kronmüller, Micromagnetism and microstructure of amorphous alloys (invited), *J. Appl. Phys.*, **52**(1981), no. 3, 1859–1864.

[20] A.Michels, et al., Range of Magnetic Correlations in Nanocrystalline Soft Magnets, *Phys. Rev. Lett.*, **91**(2003), no. 26, 267204. DOI: 10.1103/PhysRevLett.91.267204

[21] J.Weissmüller, et al., Analysis of the small-angle neutron scattering of nanocrystalline ferromagnets using a micromagnetics model, *Phys. Rev. B.*, **63**(2001), no. 21, 214414. DOI:10.1103/PhysRevB.63.214414

[22] A.Michels, J.Weissmüller, Magnetic-field-dependent small-angle neutron scattering on random anisotropy ferromagnets, *Reports Prog. Phys.*, **71**(2008), no. 6, 066501. DOI: 10.1088/0034-4885/71/6/066501

[23] R.S.Iskhakov, S.V.Komogortsev, Magnetic microstructure of amorphous, nanocrystalline, and nanophase ferromagnets, *Phys. Met. Metallogr.*, **112**(2011), no. 7, 666–681. DOI: 10.1134/S0031918X11070064

[24] S.Flohrer, et al., Interplay of uniform and random anisotropy in nanocrystalline soft magnetic alloys, *Acta Mater.*, **53**(2005), no. 10, 2937–2942. DOI: 10.1016/j.actamat.2005.03.008

[25] V.I.Petrov, G.V.Spivak, O.P.Pavlyuchenko, Electron microscopy of the magnetic structure of thin films, *Uspekhi Fiz. Nauk.*, **106**(1972), no. 2, 229.

[26] I.R.McFadyen, I.A.Beardsley, Micromagnetics of Co-based media: Experiment and model (invited), *J. Appl. Phys.*, **67**(1990), no. 9, 5540–5543.

[27] G.Herzer, Modern soft magnets: Amorphous and nanocrystalline materials, *Acta Mater.*, **61**(2013), no. 3, 718–734. DOI: 10.1016/j.actamat.2012.10.040

[28] J.Loffler, H.Braun, W.Wagner, Magnetic correlations in nanostructured ferromagnets, *Phys. Rev. Lett.*, **85**(2000), no. 9, 1990–1993. DOI: 10.1103/PhysRevLett.85.1990

[29] R.S.Iskhakov, et al., The manifestations of the two-dimensional magnetic correlations in the nanocrystalline ribbons Fe64Co21B15, *J. Magn. Magn. Mater.*, **374**(2015), 423–426. DOI:10.1016/j.jmmm.2014.08.078

[30] R.S.Iskhakov, et al., Study of magnetic correlations in nanostructured ferromagnets by correlation magnetometry, *J. Exp. Theor. Phys. Lett.*, **78**(2003), no. 10, 646–650. DOI: 10.1134/1.1644310

[31] R.S.Iskhakov, S.V.Komogortsev, Magnetic microstructure of nanostructured ferromagnets, *Bull. Russ. Acad. Sci. Phys.*, **71**(2007), no. 11, 1620–1622. DOI: 10.3103/S1062873807110470

[32] R.S.Iskhakov, et al., Dimensionality of a system of exchange-coupled grains and magnetic properties of nanocrystalline and amorphous ferromagnets, *J. Exp. Theor. Phys. Lett.*, **72**(2000), no. 6, 304–307. DOI: 10.1134/1.1328443

[33] R.S.Iskhakov, et al., Fe nanowires in carbon nanotubes as an example of a one-dimensional system of exchange-coupled ferromagnetic nanoparticles, *J. Exp. Theor. Phys. Lett.*, **78**(2003), no. 4, 236–240. DOI: 10.1134/1.1622038

[34] S.V.Komogortsev, R.S.Iskhakov, Law of approach to magnetic saturation in nanocrystalline and amorphous ferromagnets with improved transition behavior between power-law regimes, *J. Magn. Magn. Mater.*, **440**(2017), 213–216. DOI: 10.1016/j.jmmm.2016.12.145

[35] R.S.Iskhakov, et al., Fractal magnetic microstructure in the (Co41Fe39B20)x(SiO2)1-x nanocomposite films, *JETP Lett.*, **86**(2007), no. 7, 465–469. DOI: 10.1134/S0021364007190083

[36] S.V.Komogortsev, et al., The exchange interaction effects on magnetic properties of the nanostructured CoPt particles, *J. Magn. Magn. Mater.*, **401**(2016), 236–241. DOI: 10.1016/j.jmmm.2015.10.041

[37] S.V.Komogortsev, R.S.Iskhakov, V.A.Fel'k, Fractal Dimension Effect on the Magnetization Curves of Exchange-Coupled Clusters of Magnetic Nanoparticles, *J. Exp. Theor. Phys*, **128**(2019), no. 5, 754–760. DOI: 10.1134/S1063776119040095

[38] N.V.Ilin, et al., Magnetic correlations peculiarities in amorphous Fe-Cu-Nb-Si-B alloy ribbons, *J. Magn. Magn. Mater.*, **541**(2022), 168525. DOI 10.1016/j.jmmm.2021.168525

[39] S.V.Komogortsev, et al., Random Magnetic Anisotropy and Ferromagnetic Resonance in Nanocrystalline Alloy Fe73.5CuNb3Si13.5B9, *Solid State Phenom.*, **168–169**(2011), 365–368. DOI: 10.4028/www.scientific.net/SSP.168-169.365

[40] S.V.Komogortsev, et al., Magnetization correlations and random magnetic anisotropy in nanocrystalline films Fe78Zr10N12, *Solid State Phenom.*, **190**(2012), 486–489. DOI: 10.4028/www.scientific.net/SSP.190.486

[41] E.V.Harin, et al., Two-Mode Stochastic Magnetic Structure in Nanocrystalline Soft Magnetic Fe–Zr Films, *Phys. status solidi.*, **256**(2019), no. 10, 1900067. DOI: 10.1002/pssb.201900067

[42] E.N.Sheftel, E.V.Harin, Two modes of magnetic structure of nanocrystalline FeZrN films prepared by oblique-angle magnetron sputtering, *J. Magn. Magn. Mater.*, **479**(2019), 84–87. DOI: 10.1016/j.jmmm.2019.02.027

[43] E.N.Sheftel, et al., FeZrN Films: Magnetic and Mechanical Properties Relative to the Phase-Structural State, *Materials (Basel)*, **15**(2021), no. 1, 137. DOI: 10.3390/ma15010137

[44] S.V.Komogortsev, et al., Properties of ferromagnetic resonance in Fe73.5CuNb3Si13.5B9 nanocrystalline alloys, *Phys. Solid State.*, **52**(2010), no. 11, 2287–2290. DOI: 10.1134/S1063783410110132

[45] R.S.Iskhakov, et al., Ferromagnetic resonance and magnetic microstructure in nanocomposite films of Co x (SiO2)1 - x and (CoFeB) x (SiO2)1 - x, *Phys. Solid State.*, **52**(2010), no. 11, 2263–2266. DOI: 10.1134/S1063783410110089

[46] E.N.Sheftel', et al., Investigation of the magnetic properties and magnetic structure parameters of nanocrystalline Fe79Zr10N11 films, *Bull. Russ. Acad. Sci. Phys.*, **74**(2010), no. 10, 1449–1451. DOI: 10.3103/S1062873810100382

Закон приближения намагниченности к насыщению в ферромагнетиках неоднородных на нанометровом масштабе

Сергей В. Комогорцев
Институт физики им. Л. В. Киренского
Федеральный исследовательский центр КНЦ СО РАН
Красноярск, Российская Федерация
Рауф С. Исхаков
Институт физики им. Л. В. Киренского
Федеральный исследовательский центр КНЦ СО РАН
Красноярск, Российская Федерация
Самаркандский государственный университет имени Шарофа Рашидова
Самарканд, Узбекистан

Аннотация. Структурная неоднородность ферромагнитных материалов на нанометровом масштабе играет ключевую роль в формировании высоких магнитомягких свойств нанокристаллических и аморфных сплавов. В работе дается краткий обзор основных идей закона приближения намагниченности к насыщению, предоставляющего основу метода исследования таких неоднородностей. Уделено отдельное внимание роли работ красноярской школы магнитологов, работающих в этом направлении: от уже классических работ Киренского, Игнатченко до современных находок, связанных с экспериментальными исследованиями наноматериалов. Обсуждаются методические возможности, открывающиеся экспериментатору при исследовании закона приближения к насыщению.

Ключевые слова: ферромагнетики, магнитное насыщение, неоднородность, наноструктура, магнитная анизотропия.

EDN: KKHVFY
УДК 537.61.3

Structure and Properties of kπ-skyrmions in Ferromagnetic Films with Spatially Modulated Parameters

Robert Min. Vakhitov[*]
Galiya Fl. Ilyasova[†]
Rostislav V. Solonetsky[‡]
Mikhail Al. Filippov[§]
Institute of Physics and Technology
Ufa University of Science and Technology
Ufa, Russian Federation

Received 25.02.2026, received in revised form 26.03.2026, accepted 27.04.2026

Abstract. This paper examines the possibility of the existence of magnetic inhomogeneities such as kπ-skyrmions (k = 0, 1, 2, 3, ...) in a magnetically uniaxial film containing a columnar defect such as a "potential well." Two cases of such films are considered: an infinitely extended film and a finite (disk-like) film. It is shown that in both cases, skyrmions with a similar structure can exist at certain values of the material parameters. The features of their structure, properties, and methods for their production are studied. In particular, it was found that by varying the defect parameters, it is possible to transform kπ-skyrmions into (k+1)π-skyrmions, which will occur at the center of the disk.

Keywords: magnetically uniaxial film, disk, "potential well" type defect, skyrmions, non-topological soliton, core, demagnetizing fields.

Citation: R.Min. Vakhitov, G.Fl. Ilyasova, R.V. Solonetsky, M.Al. Filippov, Structure and Properties of kπ-skyrmions in Ferromagnetic Films with Spatially Modulated Parameters, J. Sib. Fed. Univ. Math. Phys., 2026, 19(4), 458–469. EDN: KKHVFY.

Introduction

Magnetic skyrmions, first discovered more than 15 years ago in magnetic films with a non-centrosymmetric lattice [1], continue to be the focus of attention for many leading research groups. This persistent interest is due to their topological protection, high mobility, and other unusual spin-electron properties, which can find application in spintronic devices and artificial neural networks [2–4]. The stability of skyrmions in these materials is ensured by the presence of the Dzyaloshinskii–Moriya interaction (DMI), which, however, for various reasons, has proven to be quite problematic [5–7]. As a result, alternative methods for stabilizing magnetic skyrmions in magnetically uniaxial films in the absence of DMI (non-chiral magnets) have been proposed [8, 9]. One such method was the artificial creation of modified films in which, by irradiating their surface with a localized beam of He^+ ions, a lattice of "potential wells" with a reduced uniaxial anisotropy constant is formed [9]. Magnetic skyrmions are stabilized in these wells. As calculations have shown [10], magnetic skyrmions in such modified films are stable formations over wide ranges of variation in the material parameters and characteristics of the defect.

As a rule, in most studies, a magnetic skyrmion is understood as a vortex-like inhomogeneity in which the magnetization vector $\mathbf{M}=\mathbf{M(r)}$ changes its direction by 180° when moving radially

[*]vakhitovrm@yahoo.com https://orcid.org/0000-0002-9828-4675
[†]galiya.siraeva2014@yandex.ru
[‡]rsolonetskiy@mail.ru
[§]mikhail.filippov.99@mail.ru https://orcid.org/0009-0007-9361-8705

from the center (r=0) to the periphery (r→∝) of the film (π-skyrmion). At the same time, already in work [11] it was theoretically predicted that in uniaxial ferromagnetic films with DMI, the existence of skyrmions with a more complex structure is also possible, the so-called kπ-skyrmions (k ∈ 1, 2, 3 . . .), in which the "twist" of the vector **M** occurs at an angle multiple of 180°. Subsequently, skyrmions of this type were discovered in work [12], where micromagnetic structures arising in Fe_3Sn_2 nanodisks were studied. As a result, stable states of 2π-, 3π- and 4π-skyrmions were detected in them at room temperature, and the following pattern in their appearance was observed: the larger the disk size, the more likely it is to detect a skyrmion in them with a greater value of the "twist" of the vector **M**. In particular, in zero field, the 2π-skyrmion is stabilized at a nanodisk size of D ∽ 730 nm, the 3π-skyrmion — at D ∽ 950 nm, and the 4π-skyrmion — at D ∽ 1150 nm. In addition, their behavior in a magnetic field perpendicular to the disk surface was studied, and it was found that as it increases, a transformation (collapse) of (k + 1)π-skyrmions into kπ-skyrmions occurs. Thus, the 3π-skyrmion "collapses" to a 2π-skyrmion when the external field increases to B ∽ 94 mT, and the 4π-skyrmion turns into a 3π-skyrmion at B ∽ 210 mT.

In [13–15], a theoretical analysis (micromagnetic modeling method using a software package) of the structure and properties of kπ-skyrmions, as well as their behavior in a magnetic field, was also carried out. These results generally correlate with the experimental data presented in [12]. However, despite the similarity of the results obtained in these theoretical studies, the studies in [13–15] were carried out for chiral magnets in which skyrmions are stabilized due to the presence of DMI in the film, while in [12], the stability of the skyrmion in a sample without DMI is achieved due to the demagnetizing fields of the disk. In this work, the possibility of nucleation of kπ-skyrmions in a magnetically uniaxial film with spatially modulated material parameters [10] in the absence of DMI is investigated.

1. Basic equations

Let us consider a uniaxial ferromagnetic disk (of thickness D and radius R) with a columnar defect located at its center [10]. Accordingly, we introduce a cylindrical coordinate system (r, α, z) with the center O located on the axis of symmetry of the defect (Oz) at the point of its intersection with the lower plane of the film (Fig. 1). It is also assumed that the easy axis of uniaxial anisotropy is collinear with the Oz axis.

The components of the unit magnetization vector $\mathbf{m}=\mathbf{M}/\mathrm{M}_s$, where M_s is the saturation magnetization, are determined through its polar and azimuthal angles (θ, ϕ) in the form: $\mathbf{m}=(\sin\theta\cos\phi, \sin\theta\sin\phi, \cos\theta)$. The expression for the energy density ε of the film under consideration takes into account the contributions of the exchange interaction (characterized by the parameter A), uniaxial anisotropy (K_u), and the demagnetizing field due to the finiteness of the sample. Accordingly, ε has the form

$$\varepsilon = \varepsilon_e + \varepsilon_u + \varepsilon_{ms}, \tag{1}$$

where

$$\varepsilon_e = \sum_{i,j} A\left(\frac{\partial m_i}{\partial x_j}\frac{\partial m_i}{\partial x_j}\right), \quad \varepsilon_u = K_u(m_x^2 + m_y^2), \quad \varepsilon_{ms} = -\frac{1}{2}M_s(\mathbf{m}\mathbf{H}_m), \tag{2}$$

Here m_i are the components of the vector **m** (the summation is carried out according to the indices i, j in the expression for ε_e, i, j=1,2,3), $\mathbf{H}_m$ is the demagnetizing field, which is found from the equations of magnetostatics

$$\mathrm{div}(\mathbf{H_m} + 4\pi\mathbf{M}) = 0, \quad \mathrm{rot}(\mathbf{H_m}) = 0, \tag{3}$$

taking into account the boundary conditions imposed on $\mathbf{H_m}$ [16].

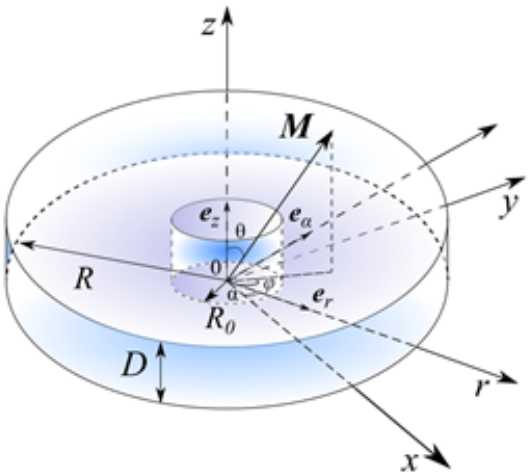

Fig. 1. Schematic representation of the film geometry. Here $(\mathbf{e}_r, \mathbf{e}_\alpha, \mathbf{e}_z)$ are unit vectors along the corresponding axes of the cylindrical coordinate system (r,α,z)

A cylindrical region of radius R_0 is considered as a defect, in which the parameters of the sample P = (A, K_u, M_s) change their values according to the relation

$$P = \begin{cases} P_1, r > R_0 \\ P_2, r \leqslant R_0 \end{cases} \tag{4}$$

where P_i = (A_i, K_{ui}, M_{si}) are the values of the material parameters outside (i=1) and inside (i=2) the defect. It is assumed that $K_{u2} < K_{u1}$ [17]. Such defects can be created artificially, as demonstrated in [9]. First, let us consider the case of an unlimited ferromagnetic film (R→∞) with a defect described by expression (4). The energy of such a sample can be represented as

$$E = 2\pi D \int_0^\infty (\varepsilon - \varepsilon_0) r \, dr, \tag{5}$$

where ε_0 is the energy of the homogeneous state.

The corresponding Euler–Lagrange equation [18], corresponding to the minimum of energy (5), will represent an integro-differential equation with non-constant coefficients, which can be solved only by numerical methods. The numerical integration of equation (3) was based on the method first demonstrated in [17]. Verification of this method was carried out in [19], in which the results of the study of the magnetization reversal processes of the films under consideration in a perpendicular magnetic field, obtained by this method, as well as by the method of micromagnetic modeling using the open-access software package OOMMF [20], completely coincided. In what follows, we will move on to the given quantities: r=R/△, r_0=R_0/△, d=D/△, where △ = $\sqrt{A/K_{u1}}$ is the characteristic width of the domain wall in a uniaxial crystal, Q=$K_{u1}/2\pi M_{s1}^2$ is the material quality factor.

2. Topological features of vortex-like inhomogeneities

An analysis of the corresponding Euler–Lagrange equations shows [18] that its solutions correspond to four types of vortex-like inhomogeneities, differing in the polarity of the core and the direction of the vector **m** at the film periphery (r→∞). Two of them (the first with $m_z(0)$ =

1 and $m_z(\infty) = -1$ and the second with $m_z(0) = -1$ and $m_z(\infty) = 1$) are degenerate states of the π-skyrmion, and the other two (the third with $m_z(0) = 1$, m_z $(\infty) = 1$ and with $m_z(0) = -1$ and $m_z(\infty) = -1$) are degenerate states of a non-topological soliton [17] or a 0-skyrmion [11]. In what follows, for definiteness, we will consider only one of the degenerate solutions, which corresponds to an inhomogeneity with $m_z(0) = -1$ (Fig. 2).

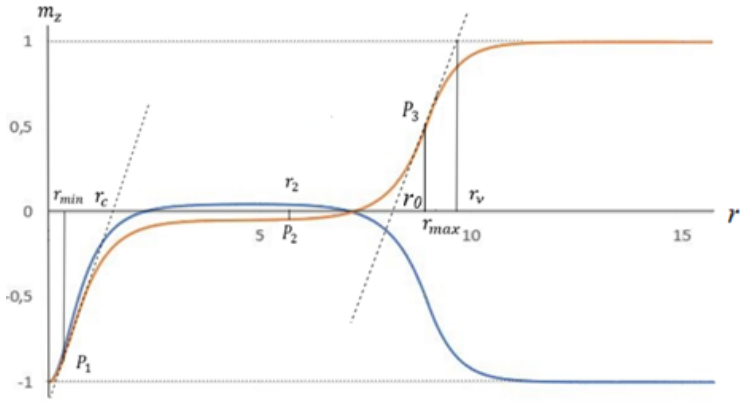

Fig. 2. Graphs of magnetization distribution ($m_z = m_z$ (r)) of different types: the red line corresponds to the π-skyrmion, and the blue line to the 0-skyrmion. Thin dashed lines represent asymptotes of the corresponding graphs, and dotted lines are tangents to the inflection points. The material parameters are as follows: $r_0 = 9$, Q = 5, K_{u2} = -2 K_{u1}, d=10

An analysis of the structure of 0- and π-skyrmions shows that, despite differences in their profiles, three regions of magnetic moment rotation can be conventionally distinguished: the core (central region), the intermediate region, and the boundary region. These regions differ in the nature of the change in the vector m: while in the core and boundary region it changes quite sharply (per unit length of the region), in the intermediate region it occurs less noticeably. This behavior of the vector m is explained by the competing influence of uniaxial anisotropy of exchange origin [18], uniaxial anisotropy, which also has a non-uniform character according to (4), and demagnetizing fields.

At the same time, the studied inhomogeneities differ in structure: the profile of the π-skyrmion has three inflection points, and that of the 0-skyrmion has two inflection points (Fig. 2). Here r_{min}, r_2, r_{max} are the points where the second derivative of the function $m_z = m_z$(r) vanishes, that is, $m_z''(r_i) = 0$ (i = 1, 2, 3). From them, one can determine the characteristic dimensions of the skyrmion and its core [17]. They also differ in the magnitude of the topological charge q: for the 0-skyrmion, q=0, and for the π-skyrmion, q=1. In addition, they differ in the magnitude of their energy: the energy of the 0-skyrmion is greater than that of the π-skyrmion and, therefore, the π-skyrmion represents an energetically more favorable state than the 0-skyrmion. This difference in their energies is explained by the difference in their profiles: if in the π-skyrmion there is a closure of the magnetic flux, then in the 0-skyrmion such a closure is practically absent.

The structure and properties of these inhomogeneities depend primarily on the characteristics of the defect: on its size r_0 and on the value of K_{u2}, which characterizes the depth of the potential well. As calculations show [17], there are always limiting values of r_{0c} and K_{u2c}, relative to which, at $r_0 < r_{0c}$ and $K_{u2} > K_{u2c}$, the π-skyrmion is not formed on the defect. Accordingly, with an increase in the defect size at $r_0 \geqslant r_{0c}$ (at: $A_2 = A_1$, $K_{u2} = -2K_{u1}$, $M_{s2} = M_{s1}$, Q=30, d=10, the value of r_{0c}=2.55), a solution arises corresponding to a π-skyrmion, the size of which (r_v) increases with increasing r_0 (Fig. 3).

However, for $r_0 \geqslant 7.45$, in addition to the π-skyrmion, another solution to equation (3) arises,

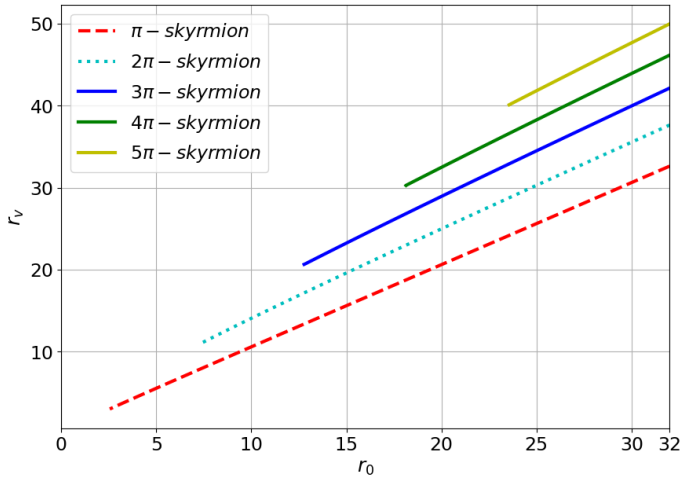

Fig. 3. Graphs of the dependence of the skyrmion size r_v on the defect size r_0, for the material parameters $A_2 = A_1$, $K_{u2} = -2K_{u1}$, $M_{s2} = M_{s1}$, Q=30, d=10. Here, the red line corresponds to the π-skyrmion, the light blue line to the 2π-skyrmion, the blue line to the 3π-skyrmion, the green line to the 4π-skyrmion, and the yellow line to the 5π-skyrmion

corresponding to the 2π-skyrmion. A further increase in r_0 leads to the fact that the sizes of the π- and 2π-skyrmions also increase, according to a linear law, and starting from $r_0 = r_{0c} = 12.8$, a solution corresponding to the 3π-skyrmion arises. Its size increases with increasing r_0 also according to a linear law. Further, with increasing r_0 at $r_0 = r_{0c} = 18.1$, a fourth solution appears, corresponding to the 4π-skyrmion, and at $r_0 = r_{0c} = 23.6$, a fifth solution appears, corresponding to the 5π-skyrmion, etc.

Similar patterns of kπ-skyrmion generation also occur with changes in the K_{u2} parameter. For example, a π-skyrmion emerges as a stable formation at $K_{u2} \leqslant -0.62$, a 2π-skyrmion already at $K_{u2} \leqslant -3.5$, a 3π-skyrmion at $K_{u2} \leqslant -7.55$, a 4π-skyrmion at $K_{u2} \leqslant -11.85$, and a 5π-skyrmion at $K_{u2} \leqslant -17.67$. It should be noted that the sizes of kπ-skyrmions increase with increasing $|K_{u2}|$, but to an extremely insignificant extent. If the magnetization distribution for all five types of skyrmions is combined in one figure, it can be seen (Fig. 4) that their initial profiles, including the core, intermediate, and almost the entire boundary region, coincide (here, only three skyrmions are shown in Fig. 4; with a larger number, such an overlap leads to confusion). This is explained by the fact that the formation of these regions is mainly due to uniaxial anisotropy of exchange origin [10], uniaxial anisotropy of the "easy plane" type (K_{u2}), and perpendicular uniaxial anisotropy (K_{u1}), which are short-range and make an equal contribution to their structure in the region r$<r_0 = 23.6$. At the same time, demagnetizing fields, which are long-range, also affect their profile, but to a lesser extent.

The most important characteristic of vortex-like inhomogeneities is their energy, which is zero-based, since in expression (2), the energy of the homogeneous state is subtracted from the total energy density. This means that if the energy E of a magnetic inhomogeneity is greater than zero (E>0), it is not realized, since in this case, the homogeneous state of the film has less energy than this inhomogeneity.

As can be seen from Fig. 5, kπ-skyrmions have negative energy, therefore, they can be stabilized in such films. Moreover, among them, the π-skyrmion has the lowest energy E, and the 5π-skyrmion has the highest. Accordingly, 2π-, 3π-, 4π-skyrmions occupy intermediate positions in energy. This means that in such films, π-skyrmions will predominantly nucleate, although the nucleation of other types of skyrmions is also possible. They are metastable structures, but can become stable inhomogeneities in the presence of other external factors: under the action of, for

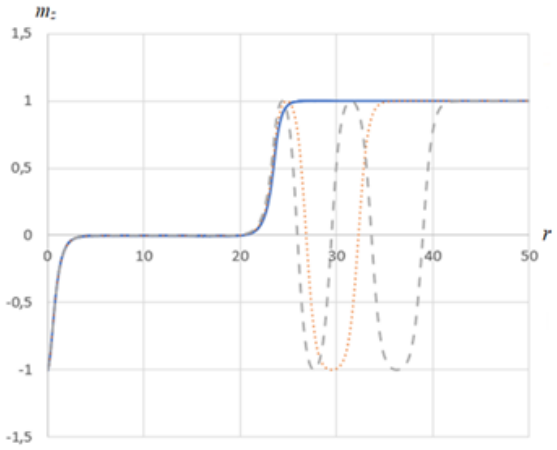

Fig. 4. Profiles of kπ-skyrmions determined by the dependence of m_z on the coordinate r at r_0=23.6, the values of the remaining material parameters are the same as in Fig. 3, here the solid line corresponds to the π-skyrmion, the dotted line to the 3π-skyrmion, the dashed line to the 5π-skyrmion

example, external magnetic fields [12, 21], local laser irradiation [22], the presence of antidotes [23], defects [24] in the film, etc.

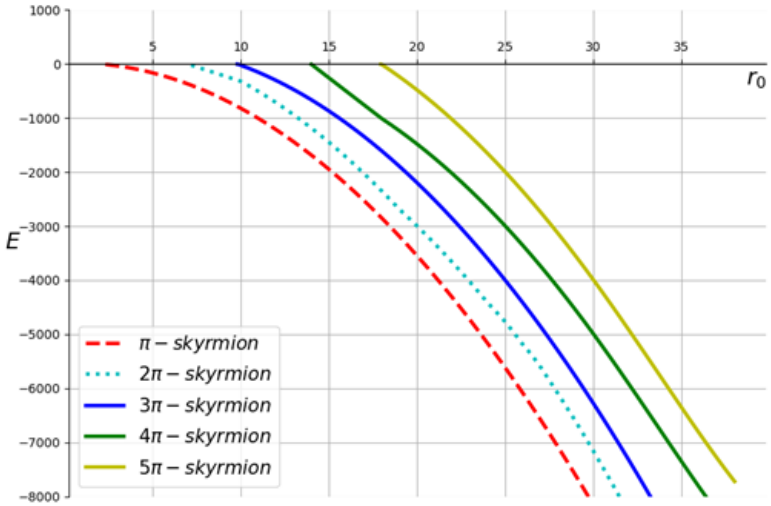

Fig. 5. Graphs of the dependence of the energy of kπ-skyrmions E on the size of the defect r_0, the values of the remaining material parameters, as well as the designations of the curves are the same as in Fig. 3

A similar picture holds for the dependence of the energies of kπ-skyrmions (k=1, 2, 3, 4, 5) on the parameter K_{u2}. It would seem that everything should be exactly the opposite, since the magnetostatic energy of a 2π-skyrmion, due to the greater number of magnetic flux closures (twists), should be lower than that of a π-skyrmion, and that of a 3π-skyrmion should be lower than that of a 2π-skyrmion, and so on. On the other hand, an increase in the number of rings (twists) in a kπ-skyrmion also leads to an increase in the exchange energy and the energy of uniaxial anisotropy, which fully compensates (and perhaps even to a greater extent) for the

negative contribution to ε from the energy of the demagnetizing fields. However, this will not happen, since a plate of infinite length is considered here. To better understand this problem, we examine it differently, using micromagnetic modeling based on the open-access OOMMF software package [20, 25]. For this purpose, we consider a finite-sized disk-shaped film (of thickness D and radius R), at the center of which is a columnar, through-type defect (of radius R_0). The defect, as before, is specified in the form (4). All sample parameters were taken to be close to experimental values corresponding to a Fe_2Sn_3 film [12]. They are presented in Tab. 1, where the ranges of their possible variations are also discussed.

Table 1. Material parameters of the sample used in modeling

Disk radius	(225-1025) nm
Film thickness	(120, 150) nm
Defect diameter	50 nm
Exchange stiffness outside the defect	$A_1 = 8.25 \times 10^{-12} J/m$
Exchange stiffness at a defect	$A_2 = 4.125 \times 10^{-12} J/m$
Saturation magnetization	$M_s = 622.7 \times 10^3 A/m$
Magnetic anisotropy constant outside the defect	$K_{u1} = 54.5 \times 10^3 J/m^3$
Magnetic anisotropy constant at a defect	$K_{u2} = 0 \quad J/m^3$

In the beginning, using numerical modeling, stable states of kπ-skyrmions were investigated in the considered disk in the absence of defects. In particular, by varying the disk dimensions, it was found that stabilization of the Bloch-type π-skyrmion will occur at a disk radius of R = 225 nm. It should be noted that this vortex-like formation differs in structure from a skyrmion in its central part there is a domain (homogeneous) region, which, as is known [26], is characteristic of bubble However, this inhomogeneity should not be completely identified with bubble, since the latter is stabilized only when an external magnetic field directed normal to the film surface acts on the sample. This hybrid formation was conditionally called a skyrmion bubble in [27].

A further increase in the disk radius leads to an increase in the central (domain) region, as well as (to a lesser extent) the peripheral part, which is a ring with $m_z = -1$. This process continues until a cylindrical domain boundary appears in the peripheral part at the edge of the disk with radius R = 250 nm, which will separate the peripheral region with $m_z = -1$ from the very thin ring region formed at the edge of the disk with $m_z = 1$. Thus, the transformation of π-skyrmion into 2π-skyrmion occurs. In a similar way, with a further increase in R, the transformation of 2π-skyrmion into 3π-skyrmion occurs. Tab. 2 presents the data on the critical disk sizes at

Table 2. Table of limiting values of R at which certain types of kπ-skyrmions are stabilized in the absence and presence of a defect; cases of film sizes that were not considered in [12] are marked with an asterisk (*)

Skyrmion type	Critical radius of the film for the occurrence of a kπ-skyrmion in the absence of a defect, nm	Critical film radius for the occurrence of kπ-skyrmion in the presence of a defect, nm
3π-skyrmion	500	400
4π-skyrmion	575	500
5π-skyrmion	675	575
6π-skyrmion	800	675
7π-skyrmion	900	800
8π-skyrmion	1025	925

which the corresponding transformations of kπ-skyrmions into (k+1) π-skyrmions (k = 1÷8)

occur. As can be seen from the obtained data, in the case of finite-sized films, the formation of kπ-skyrmions occurs due to the demagnetizing fields of the sample, which is impossible for films of unlimited size. In the latter case, even if new "twists" are formed, an infinite portion of the film always remains, which will inevitably negate any energy gain due to the formation of new "twists."

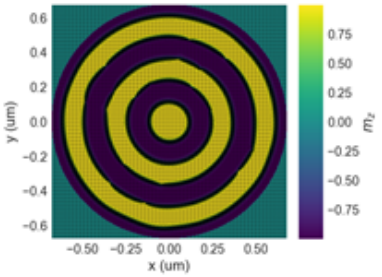

5π-skyrmion without a defect at R=675 nm

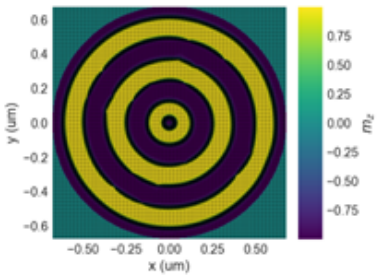

6π-skyrmion on a defect at R=675 nm

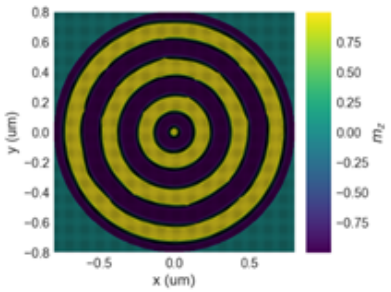

7π-skyrmion at R=800 nm

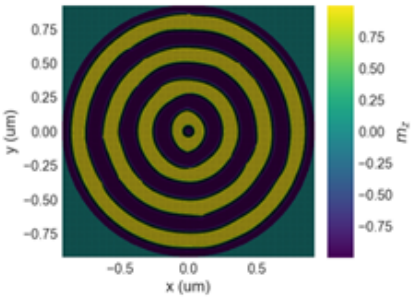

8π-skyrmion at R=925 nm

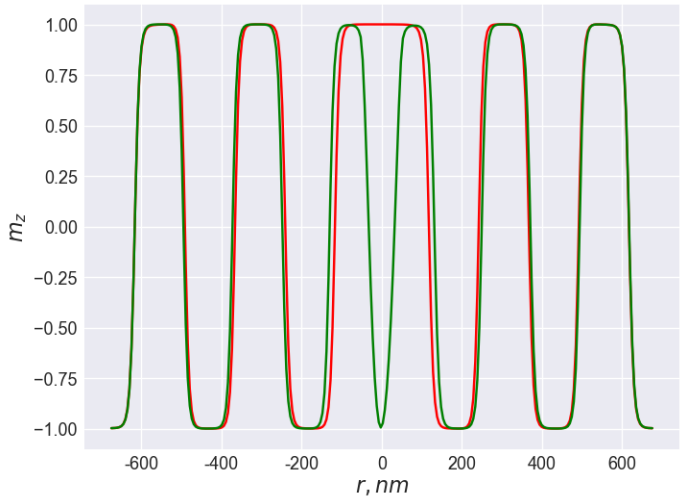

graph of the magnetization distribution of the 5π-skyrmion (red) and 6π-skyrmion (green)

Fig. 6. Images of kπ-skyrmions with different k, stabilized in the presence of a defect R_0=50 nm, $K_{u2} = 0 \quad J/m^3$ using Ubermag [25]

At the next stage of the research, the critical disk sizes at which kπ-skyrmions are formed

on it in the presence of a defect ($R_0 = 50, K_{u2} = 0, A_2 = 0,5A_1$) were again considered. The obtained results are presented in the right column of Tab. 2. Their analysis shows that the presence of a defect in the sample reduces the critical disk size at which a new type of skyrmion nucleates on it by approximately 10–15%. Moreover, the process of transformation of a kπ-skyrmion into a (k+1)π-skyrmion occurs in this case differently, namely, through the nucleation of a new structure in the center of the defect, which is a skyrmion-like inhomogeneity with dimensions close to R_0 (Fig. 6). In this case, the magnetic structure outside the defect remains unchanged. The study of the influence of the remaining parameters (M_{s2} and A_2) showed that the parameter M_{s2} has virtually no effect on these processes, while the value of A_2, on the contrary, has a significant effect. For example, if we reduce the value of A_2, which characterizes the exchange parameter at the defect, in a disk of radius R = 225 nm, in which a π-skyrmion is stabilized, then at $A_2 = 0.7A_1$ and below, a darkening appears in the central region in the form of a spot with a radius smaller than its domain part (Fig. 7). With a further decrease in A_2 down to $A_2 = 0.5\ A_1$, the color of the darkened area reaches the color of the peripheral area, which indicates the transformation of the π-skyrmion into a 2π-skyrmion. If we similarly perform these manipulations with the exchange parameter A_2 in a kπ-skyrmion (k>1), then we can transform it into a (k+1)π-skyrmion.

However, such transformations will occur in the center of the disk, rather than at its periphery. It should be noted that a similar effect was observed in [22], where the evolution of magnetization in a bismuth-containing ferrite garnet film induced by a laser pulse with an energy of $\Phi = 0.31$ J/s was investigated. A domain structure in the form of concentric rings was discovered at the site of local optical irradiation, which can be explained by heating of this region. The latter will lead to a local change (more precisely, a decrease) in the constants of uniaxial anisotropy and exchange, which can lead to the formation of a kπ-skyrmion.

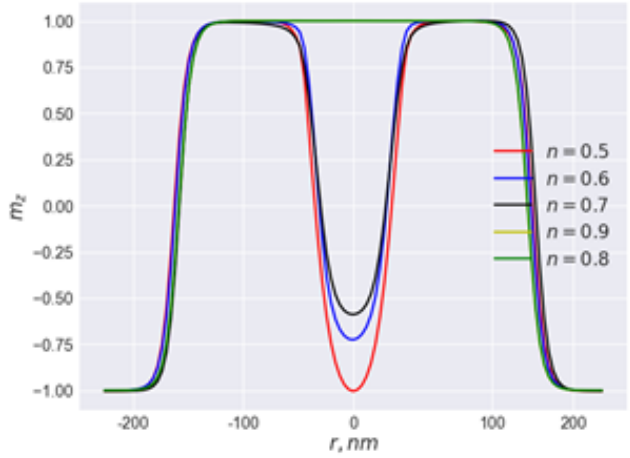

Fig. 7. Graphs of magnetization distribution in a disk with R=225 nm and $M_{s2} = M_{s1}$, $K_{u2} = 0$, $A_2 = nA_1$ for different coefficients n

Conclusion

According to the presented studies, vortex-like inhomogeneities such as kπ-skyrmions can form under certain conditions in a uniaxial ferromagnetic film containing a columnar defect such as a "potential well." Their structure, stability, and other properties depend significantly on the material parameters of the sample and the characteristics of the defect. When considering a film

with a finite thickness and unlimited thickness in the other two directions, it was found that the π-skyrmion is energetically most favorable, while the favorability of other skyrmion types decreases with increasing k. Furthermore, for each type of skyrmion, there are limiting values for the defect radius r_0, the "potential well" depth ($\triangle K_u = K_{u1} - K_{u2}$), and the quality factor Q, below which they do not form.

In the case where the film is limited and represents a ferromagnetic uniaxial nanodisk, then at a certain radius a skyrmion with a wide central part representing a cylindrical magnetic domain is formed on the disk. It is shown that with an increase in the disk radius, a transformation of different parts of the existing structure occurs, which ultimately leads to the transformation of the skyrmion into a 2π-skyrmion. Similarly (by increasing the radius R), it is possible to transform a 2π-skyrmion into a 3π-skyrmion, etc. In this case, such transformations occur at the edge of the disk and are caused by the magnetostatic fields of the sample. The presence of a defect leads to a decrease in the disk radii at which this occurs. In addition (with a decrease in ($\triangle K_u$), the defect affects the process of transformation of the kπ-skyrmion into a (k+1)π-skyrmion, which occurs already in the center of the defect. A similar effect occurs with a decrease in the exchange parameter, which helps explain the experimental results in [22].

The authors are grateful for the financial support of the State assignment of Russian Federation for the implementation of scientific research by laboratories (no. 075-03- 2024-123/1 15.02.2024).

References

[1] S.Mühlbauer, F.Jonietz, C.Pfleiderer, et al., Skyrmion lattice in a chiral magnet, *Science*, **323**(2009), 915–919.

[2] S.Luo, L.You, Skyrmion Devices for Memory and Logic Applications, *APL Mater.*, **9**(2021), 050901. DOI: 10.1063/5.0042917

[3] A.S.Samardak, A.G.Kolesnikov, A.V.Davydenko, et al., Topologically nontrivial spin textures in thin magnetic films, *Phys. Metals Metallogr.,* **123**(2022), 238–260. DOI: 10.1134/S0031918X22030097

[4] O.Lee, O.R.Msiska, M.A.Brems, et al., Perspective on unconventional computing using magnetic skyrmions, *APL Mater.*, **122**(2023), no. 26, 260501. DOI: 10.1063/5.0148469

[5] C.Moreau-Luchaire, C.Moutafis, N.Reyren, et al., Additive interfacial chiral interaction in multilayers for stabilization of small individual skyrmions at room temperature, *Nat. Nanotechnol.*, **11**(2016), no. 5, 444–448. DOI: 10.1038/nnano.2015.313

[6] P.Ho, A.K.Tan, S.Goolaup, et al., Geometrically Tailored Skyrmions at Zero Magnetic Field in Multilayered Nanostructures, *Phys. Rev. Applied*, **11**(2019), no. 2, 024064. DOI: 10.1103/PhysRevApplied.11.024064

[7] D.Navas, R.V Verba, A.Hierro-Rodriguez et.al., Route to form skyrmions in soft magnetic films, *APL Mater.*, **7**(2019), no. 8, 0811114. DOI:10.1063/1.5093371

[8] L.Sun, R.X.Cao, B.F.Miao, et al., Creating an artificial two-dimensional Skyrmion crystal by nanopatterning, *Phys. Rev. Lett.*, **110**(2013), no. 16, 167201. DOI: 10.1103/PhysRevLett.110.167201

[9] M.V.Sapozhnikov, S.N.Vdovichev, O.L.Ermolaeva, et al., Artificial dense lattice of magnetic bubbles, *Appl. Phys. Lett.*, **109**(2016), no. 4, 042406. DOI: 10.1063/1.4958300

[10] R.M.Vakhitov, A.A.Akhmetova, R.V.Solonetsky, Vortex-like formations on defects of magnetically uniaxial films, *Phys. Solid State*, **61**(2019), no. 3, 319–325. DOI: 10.1134/S1063783419030326

[11] A.Bogdanov, A.Hubert, The stability of vortex-like structures in uniaxial ferromagnets, *J. Magn. Magn. Mater.*, **195**(1999), no. 1, 182–192.

[12] J.Jiang, Y.Wu, L.Kong, et al., Magnetic kπ-skyrmions and their field-driven evolutions in a nanostructured centrosymmetric magnet, *Acta Materialia*, **215**(2021), 117084. DOI: 10.1016/j.actamat.2021.117084

[13] J.Hagemeister, A.Siemens, L.Rózsa, et al., Controlled creation and stability of kπ-skyrmions on a discrete lattice, *Phys.Rev. B*, **97**(2018), no. 17, 174436. DOI: 10.1103/PhysRevB.97.174436

[14] H.Vigo-Cotrina, D.L.Monteiro, J.P.V.Urruchua, et al., The emergence of kπ-skyrmions and their spin wave modes in a ferromagnetic disk, *J. Magn. Magn. Mater.*, **560**(2022), 169665.

[15] C.Song, Y.Ma, C.Jin, et al., Field-tuned spin excitation spectrum of kπ- skyrmion, *New J. Phys.*, **21**(2019), 083006. DOI: 10.1088/1367-2630/ab348e

[16] Y.O.Tu, Determination of magnetization of micromagnetic wall in bubble domains by direct minimization, *J. Appl. Phys.*, **42**(1971), no. 13, 5704–5709.

[17] R.M.Vakhitov, T.B.Shapaeva, R.V.Solonetsky, A.R.Yumaguzin, Structural features of micromagnetic formations on defects of ferrite-garnet films, *Phys. Metals Metallogr.*, **118**(2017), no. 6, 541–545. DOI: 10.1134/S0031918X17040111

[18] R.M.Vakhitov, R.V.Solonetsky, A.A.Akhmetova, Stable states of vortex-like magnetic formations in inhomogeneous magnetically uniaxial films and their behavior in a longitudinal magnetic field, *J. Appl. Phys.*, **128**(2020), no. 15, 153904. DOI: 10.1063/5.0035503

[19] R.M.Vakhitov, R.V.Solonetsky, A.A.Akhmetova, M.A.Filippov, Behavior of vortex-like inhomogeneities originating in magnetic films with modulated uniaxial anisotropy in a planar magnetic field, *Symmetry*, **14**(2022), no. 3, 612. DOI: 10.3390/sym14030612

[20] M.J.Donahue, D.G. Porter, OOMMF User's Guide, Version 2.0a3, *National Institute of Standard and Technolog: Gaithersburg, MD, USA* (2021). *Phys. Metals Metallogr*, **91**(2001), no. 4, 330–334.

[21] H.E.Khodenkov, H.H.Kudelkin, V.VRandoshkin, The breakdown of the 360° bloch domain wall in bubble magnetic films, *Phys.Status Solidi (A)*, **84**(1984), no. 2, 135–138.

[22] C.S.Davies, K.H.Prabhakara, M.D.Davydova, K.A.Zvezdin, T.V.Shapaeva et al., Anomalously damped heat-assisted route for precessional magnetization reversal in an iron garnet, *Phys. Rev. Lett.*, **122**(2019), no. 2, 027202. DOI: 10.1103/PhysRevLett.122.027202

[23] M.Xu, J.Zhang, D.Meng, et al., The influence of introducing holes on the generation of skyrmions in nanofilms, *Phys. Lett. A*, **433**(2022), 128034. DOI: 10.1016/j.physleta.2022.128034

[24] J.Muller, A.Rosch, Capturing of a magnetic skyrmion with a hole, *Phys. Rev. B*, **91**(2015), no. 5, 054410. DOI: 10.1103/PhysRevB.91.054410

[25] M.Beg, M.Lang, H.Fangohr, Ubermag: Toward More Effective Micromagnetic Workflows, *IEEE Transactions on Magnetics*, **58**(2022), no. 2, 1–5. DOI: 10.1109/TMAG.2021.3078896

[26] A.H.Eschenfelde, Magnetic bubble technology, Springer Science and Business Media, 2012.

[27] W.Jiang, P.Upadhyaya, W.Zhang, et al., Blowing magnetic skyrmion bubbles, *Science*, **349**(2015), no. 6245, 283–286. DOI: 10.1126/science.aaa1442

Структура и свойства kπ-скирмионов в ферромагнитных пленках с пространственно-модулированными параметрами

Роберт М. Вахитов
Галия Ф. Ильясова
Ростислав В. Солонецкий
Михаил А. Филиппов
Физико-технический институт
Уфимский университет науки и технологий
Уфа, Российская Федерация

Аннотация. В работе исследуется возможность существования магнитных неоднородностей типа kπ-скирмионов (k = 0, 1, 2, 3, . . .) в магнитоодноосной пленке, содержащей колумнарный дефект типа «потенциальная яма». Рассмотрены два случая таких пленок — бесконечно протяженная и конечная (типа диска). Показано, что в обоих случаях скирмионы с подобной структурой могут существовать при определенных значениях материальных параметров. Изучены особенности их структуры, свойства и способы их получения. В частности, было выявлено, что меняя параметры дефекта можно осуществить трансформацию kπ-скирмионов в (k+1)π-скирмионы, которая будет происходить в центре диска.

Ключевые слова: магнитоодноосная пленка, диск, дефект типа «потенциальная яма», скирмионы, нетопологический солитон, кор, размагничивающие поля.

EDN: LOIGMK
УДК 51 (09)

From the History of Quantum Chaos: Research from the Novosibirsk and Krasnoyarsk Schools of Nonlinear Dynamics

Ravil R. Mukhin*
Stary Oskol Technological Institute named after A. A. Ugarov (branch of NUST MISIS)
Stary Oskol, Russian Federation

Received 10.02.2026, received in revised form 30.03.2026, accepted 30.04.2026

Abstract. This paper examines the little-covered history of quantum chaos research in the literature at two centers of nonlinear dynamics in Russia: the Budker Institute of Nuclear Physics in Novosibirsk and the Kirensky Institute of Physics in Krasnoyarsk. The chosen timeframe — the early 1970s to the early 2000s — saw the appearance of the first works on quantum chaos, the development of concepts, and the formation of a conceptual framework. B. V. Chirikov and G. M. Zaslavsky played a key role in this regard. The work of these research centers largely determines the modern landscape of this field of knowledge.

Keywords: classical chaos, quantum chaos, semiclassical domain, quantum rotator, localization, energy spectrum statistics.

Citation: R.R. Mukhin, From the History of Quantum Chaos: Research from the Novosibirsk and Krasnoyarsk Schools of Nonlinear Dynamics, J. Sib. Fed. Univ. Math. Phys., 2026, 19(4), 470–482. EDN: LOIGMK.

1. Introduction. Early Research

In the 1960s, the main center for research on chaos in Hamiltonian physical systems was the G. I. Budker Institute of Nuclear Physics, Siberian Branch of the USSR Academy of Sciences (INP, Novosibirsk) [1, 2]. The founder of the Novosibirsk school of nonlinear dynamics was Boris Valerianovich Chirikov (1928–2008). Chirikov was a member of the first graduating class of the Physics and Engineering Department of Moscow State University (now the Moscow Institute of Physics and Technology). After graduating, he worked briefly at Laboratory No. 3 (now the Institute of Theoretical and Experimental Physics in Moscow). Then, at the invitation of A.M. Budker, head of the Laboratory of New Acceleration Methods, in 1954, Chirikov transferred to the Laboratory of Measuring Instruments (LIPAN, now the Russian Scientific Center "Kurchatov Institute"). In 1958, the Institute of Nuclear Physics began to form in the Novosibirsk Akademgorodok, with Budker as its first director. Chirikov became one of the new institute's first employees and moved to Novosibirsk the following year, where he began actively working at the INP and simultaneously taught classes at the newly opened Novosibirsk University. Here, a few words should be said about how the teams of the institutes of the newly opened Siberian Branch of the Academy of Sciences were formed. Their core consisted of employees of research institutes in Moscow, Leningrad, and other cities, as well as young graduates from various universities across the country. A few years later, a strong reinforcement was added from the so-called "zero" graduating class of the young Novosibirsk University. The first intake of which (24 students in the Physics Department, the same number in the Mathematics and Mechanics Department) consisted of students from universities across

*mukhiny@mail.ru

the country, recruited directly into their second year. Among those who came from the Institute of Atomic Energy to the INP, in addition to Budker and Chirikov, were S. T. Belyaev, V. M. Galitsky, R. Z. Sagdeev and others [1, 2]. Roald Zinurovich Sagdeev was born in 1932. After graduating from Moscow State University (1956), he intended to enroll in graduate school at the Institute for Physical Problems. However, his application to L. D. Landau's graduate program was rejected by the university's placement committee. Landau appealed to Kurchatov to intervene, but the only thing Kurchatov could do was hire Sagdeev at his institute [3]. Nevertheless, Sagdeev decided to hold his dissertation defense at the Institute for Physical Problems. V. I. Kogan, who was present at the defense, recalled that P. L. Kapitsa asked many questions at first, then others. L. D. Landau summed up the defense, noting that the candidate's ability to instantly find answers to any question was astonishing [4]. Such an admission from Landau, who himself was noted for his immediate response to questions, was quite unusual. In the late 1950s, Sagdeev taught one of the first courses on plasma physics at the Moscow Power Engineering Institute. Plasma physics was still a young field at the time, and the veil of secrecy had only just been lifted. After moving to Novosibirsk (1961), Sagdeev headed one of the INP laboratories. Just eight years after graduating, Sagdeev was elected a Corresponding Member of the USSR Academy of Sciences (1964). Sagdeev, at the height of his scientific career, was a very attractive figure to young physicists. Among Sagdeev's first graduate students were those from the "zero" class: A. A. Galeev, V. E. Zakharov, A. M. Fridman, and M. S. Moiseev; their names are now widely known. To them should be added G. M. Zaslavsky.

Georgy Moiseevich Zaslavsky (1935–2008) graduated from Odessa University in 1957. After the decision was made in 1957 to establish the Siberian Branch of the Russian Academy of Sciences with its center in Novosibirsk, G. M. Zaslavsky was among those sent there. He began working as an engineer at a research institute in Novosibirsk, then as a senior laboratory assistant at the Novosibirsk Electrotechnical Institute. In 1959, G. M. Zaslavsky began teaching at the then newly established Novosibirsk University, first as an assistant, and after defending a dissertation for a candidate of science degree in 1964, he became an associate professor. At the newly organized INP, the priority areas were research into accelerators based on new acceleration principles and plasma physics.

Akademgorodok, like other new scientific centers, attracted talented and active young people and experienced mature scientists whose potential was not fully utilized in Moscow and other established scientific centers. Scientists at Akademgorodok institutes were, to a certain extent, allowed to develop promising areas of research in the context of global fundamental science.

The creation of new accelerators and open-source magnetic plasma confinement systems required a thorough study of multidimensional nonlinear oscillations of a conservative system as a whole, i.e. over an unlimited time interval and under arbitrary initial conditions. Such problems provided a powerful stimulus for the progress of nonlinear physics, which began to develop rapidly. For tightly focused accelerators, the idea of which was then widely discussed, A. M. Budker believed that, due to the "forgetting" of the initial phase, oscillations would increase through diffusion, this will cause the particles to exit the acceleration regime and rapidly die. Computational experiments conducted at CERN confirmed Budker's prediction. It was shown that diffusion occurs even with very weak nonlinearity. However, the diffusion mechanism was completely unclear. Some new phenomena emerged here, requiring new approaches. These kinds of problems led Chirikov to study the phenomenon of chaos. Based on the overlap of nonlinear resonances, he first introduced a criterion for the appearance of chaotic oscillations in nonlinear Hamiltonian systems (the Chirikov criterion, 1959). Chirikov and Sagdeev determined Zaslavsky's interest in the problems of chaos, which became the subject of all his subsequent research. Zaslavsky's first works in this area were carried out with Chirikov and Sagdeev. Subsequently, two groups of chaos researchers emerged: B. V. Chirikov, V. V. Vecheslavov, F. M. Izrailev, D. L. Shepelyansky and G. M. Zaslavsky, G. P. Berman, P. I. Belobrov, A. R. Kolovsky, H.-R. Ya. Rachko, V. N. Synakh, N. N. Filonenko and others. The

research program of both groups can be formulated as follows: the study of the fundamental laws of chaos and the emergence of statistical behavior based on deterministic dynamics in classical and quantum systems [5].

It's difficult to overestimate the role of Valter Alekseevich Ignatchenko in the development of nonlinear dynamics research at the L. V. Kirensky Institute of Physics (IP SB USSR Academy of Sciences, Krasnoyarsk). He began working at the institute in 1957, practically from its founding. He headed the theoretical department, and it was on Valter Alekseevich's initiative that Zaslavsky, his friend and classmate from Odessa University, was invited to the institute in 1971 as a senior research fellow. Here, Zaslavsky was provided with all the necessary conditions for developing his research and forming a corresponding team of researchers. Based on this team, after Zaslavsky defended his doctoral dissertation, the Department of Nonlinear Process Theory was established in 1973, which he headed [2].

During this period, Zaslavsky began studying quantum chaos. The concept of mixing underlies Zaslavsky's approach to questions of chaos. More than two dozen of Zaslavsky's papers, completed in the 1960s and 1970s, were devoted to the study of nonlinear systems with mixing. They examined a variety of physical problems: the motion of charged particles in external fields, the instability of plasma particles, nonlinear waves, turbulence in dispersive media, and others. Here is what Zaslavsky himself says: "I started working on chaos problems in 1963 with Boris Chirikov, and we published a paper on Fermi acceleration. There was a time of the formation of new concepts, and we analyzed a real physical system. Soon after, turning to the problem of the existence and stability of magnetic surfaces, we discovered two important facts: 1) stochastic destruction of magnetic surfaces. These results are now broadly used in almost all cases of analysis in plasma confinement installations; 2) destruction of the separatrix and the formation of a stochastic (ergodic) layer, the width of which is estimated with a special, so-called separatrix map. These results are of principal significance since in Hamiltonian systems chaos starts from the formation of a stochastic layer . . . . The emotional part is that I had a few, but very strong supporters, such as R. Z. Sagdeev, M. A. Leontovich, B. B. Kadomtsev, and I. M. Lifshitz. There were many difficulties to find a positive attitude to the works on chaos. Partly it was due to my distant settlement in Krasnoyarsk. The main recognition of the results of chaos appeared after 1984. Another thing is that I had no access to good computers and many things were obtained analytically while all West used computers effectively. When I arrived in the US in 1990, I was surprised at how well known were my works" [6].

Communication with mathematicians was of great importance in the ongoing research. After B.V. Chirikov's visit to A.N. Kolmogorov, close contacts were established with his school: V. I. Arnold, Ya. G. Sinai, V. M. Alekseev, and others. Moreover, the interest was mutual. The influence of this communication is noticeable in many of Sinai and his disciples‘ works of the 1970s and 1980s [7, 8]. Since the late 1970s, international collaboration has been established, first with J. Ford, then with the addition of Italian physicists G. Casati, F. Vivaldi, and I. Guarneri. This opened up new possibilities for discussions, joint research, and publications, and the activity of Siberian physicists increased sharply. It should be noted here that Budker, while highly appreciating Chirikov as an experimentalist, did not welcome his transition to "pure" theory and did not accept his thesis on the special role of computers in modern physics. Unfortunately, true recognition of the significance of Chirikov's achievements came from abroad, when his work became available to foreign researchers [8]. To a certain extent, the same can be said of Zaslavsky.

In 1976, Chirikov's group shifted to the study of quantum chaos and, by the late 1970s, had almost entirely shifted its focus to this new field. At that time, very few physicists worldwide were working in the field of quantum chaos [5].

2. Quantum chaotic systems. Problem statement, semiclassical approximation

In the 1970s, the concept of dynamic chaos, which describes the stochastic behavior of classical mechanical systems with a small number of degrees of freedom, became firmly established. This concept fundamentally contradicted the deeply rooted belief in the scientific community that statistical descriptions are characteristic only of highly complex systems with a large number of degrees of freedom. Understanding the phenomenon of chaos has undergone a long historical development: from H. Poincaré's research on dynamic systems and the birth of ergodic theory to the creation of a consistent theory of dynamic chaos and experimental confirmation of this phenomenon (see, for example, [9]). The phenomenon of chaos was relatively independently discovered in two classes of systems — Hamiltonian and dissipative. The subject of our discussion is Hamiltonian systems, and we will limit ourselves to them in what follows. Necessary and sufficient conditions for dynamic chaos in Hamiltonian systems without any random parameter or external noise were established — local exponential instability of trajectories under arbitrarily weak perturbations of the initial conditions in systems with dimensions greater than one (the Alexseev–Brudno theorem) [10, 11]. Although the regions of chaos are very narrow, their presence is fundamentally important; chaos is inherent in the vast majority of dynamic systems.

The logic of the development of the subject inevitably led to the possibility of generalizing classical chaos to the quantum domain. What would happen if the system were described not by the equations of classical mechanics, but by the Schrödinger equation? At first glance, such a generalization seemed unjustified. In the classical case, the continuity of the phase space is of fundamental importance. No matter how small the distribution region of the initial conditions, it still contains an infinitely large amount of information, which manifests itself in the form of chaotic motion during strong instability. In the quantum domain, the phase space will be structured by Planck's constant h, and the concept of a trajectory loses its meaning. Therefore, in the quantum domain, one cannot speak of chaos in its classical sense. It should be noted that ideas about the possibility of quantum chaotic dynamics began to be discussed at the INP as early as the late 1960s. Chirikov repeatedly emphasized that the discreteness of the spectrum inherent in quantum systems can have a very significant impact on the dynamics of quantum chaos. Apparently, the first mention of the role of spectral discreteness is recorded in the transcript of Chirikov's doctoral dissertation defense, which took place in 1969 [12]. Let us note the years to which this applies. This was the time of the formation of the theory of dynamic chaos in classical systems, and the formation of its basic concepts. E. Lorenz's work, *Deterministic Nonperiodic Flow*, in which he derived his famous system of equations (the Lorenz attractor), received recognition only in the mid-1970s [9]. At first, everything was unclear. F. Izrailev recalled numerous discussions between B. V. Chirikov and J. Ford, who repeatedly visited the INP in the 1970s. As a result, a new approach was developed — quantum pseudo-chaos, although the term "quantum chaos" remained generally accepted. It can be added that for classical chaos, the nonlinearity of the system is of fundamental importance, whereas the Schrödinger equation is linear; the vectors of the Hilbert space, initially close to each other, remain close during evolution and do not diverge from each other. The fundamental distinction of quantum chaos is that it is based not on the instability of motion that arises in classical nonlinear systems, but on a completely different – linear – mechanism associated with a huge number of independent frequencies that determine the temporal evolution of a quantum system [8]. Radical physicists held the extreme position that quantum chaos does not exist at all. On the other hand, according to Bohr's correspondence principle, there is a region where, in the limit $h \to 0$, the classical and quantum descriptions are equivalent. Therefore, the semiclassical region requires more careful consideration. Moreover, the scope of research itself has expanded. Since the 1970s, interest has increased in the study of highly excited states in atomic and molecular physics, states with large

quantum numbers. In complex atoms, highly excited states are hydrogen-like, i.e., their wave functions coincide with those of the hydrogen atom, which significantly simplifies the analysis of such systems.

The time evolution of a quantum system in an external field $V(x)$ is determined by the Schrödinger equation:

$$ih\frac{\partial\psi}{\partial t} = -\frac{1}{2}h^2\Delta\psi + V(x)\psi. \tag{1}$$

In classical mechanics, the motion of particles in the same field $V(x)$ is determined by solving the system of Hamiltonian equations:

$$\frac{dx_i}{dt} = p_i,\ \frac{dp_i}{dt} = -\frac{\partial V(x)}{\partial x_i},\ i = 1, 2, \ldots, n. \tag{2}$$

If Planck's constant h is negligible compared to other parameters of the problem, system (2) is used. The relationship between (1) and (2) is established by substituting $\psi = \exp(iW/h)$. For W, we obtain the nonlinear Wenzel–Kramers–Brillouin equation (WKB method)

$$-ih\Delta W + \frac{\partial W}{\partial t} + |gradW|^2 + V(x) = 0. \tag{3}$$

For $h = 0$, this equation reduces to the Hamilton-Jacobi equation. However, the WKB method says nothing about the behavior of the solution to equation (1) [13].

Initially, the subject of quantum chaos was not entirely defined and included a wide range of seemingly unrelated topics: quantum nonlinear resonance, the interaction of quantum nonlinear resonances, the properties of wave functions of quantum chaotic systems, the evolution of nonstationary states, the statistics of the energy spectrum, nonautonomous quantum chaotic systems, etc. [14–16]. The few manifestations of complex behavior in quantum systems seemed more the exception than the rule. By the end of the last century, ideas about the subject of quantum chaos had taken shape. The concept of "quantum chaos" encompasses a range of problems related to the quantum-mechanical description of systems that exhibit chaotic behavior in the classical limit. Here, the differences between physical and mathematical approaches become clear. A mathematician will first try to clearly define the object of study, clearly formulate the conditions imposed, and only then proceed directly to solving the problem. In physics, the subject of research can acquire more or less clear contours during the course of the study itself. This is what happened with quantum chaos.

In quantum chaos research, it was entirely natural to first turn to the transition region between quantum mechanical and classical descriptions — the semiclassical region. This immediately presented significant challenges, as the very foundations of our understanding of the world were affected. The question of the validity of the correspondence principle and the Copenhagen interpretation arose. The first step was taken by Albert Einstein long before the phenomenon of dynamic chaos became known. On May 11, 1917, at a meeting of the German Physical Society, Einstein gave a report on the relationship between classical and quantum mechanics [17, 18]. Strictly speaking, this was the period of the old quantum theory; quantum mechanics emerged only in the following decade. Within the framework of the old quantum theory, the Bohr-Sommerfeld quantization rules were derived:

$$\frac{1}{2\pi}\oint p(q_i)dq_i = \hbar n_i\ (i = 1, 2, \ldots, N), \tag{4}$$

where N is the number of integrals of motion. These rules are applicable only in the case of complete separation of variables. Only then can one choose (p_i, q_i) such that the expressions $\oint p(q_i)dq_i$ are integrals of motion. However, this quantization procedure turned out to be ambiguous. Even if variables are separated in different coordinate systems, nonequivalent

results can be obtained [19]. Einstein notes in his work [17] that the condition of separation of variables significantly limits the applicability of the quantization conditions (4). Using a simple example of two-dimensional particle motion under the action of a central attractive potential, he generalized the quantization conditions (4)

$$I_k = \frac{1}{2\pi} \oint_{C_k} \sum_{i=1}^{N} p_i dq_i = \hbar n_k \ (k = 1, 2, \ldots, N), \tag{5}$$

where I_k are independent integrals of motion, C_k are irreducible contours, i.e., contours that cannot be contracted to a point and cannot be continuously transformed into each other. In modern language, the case of integrable systems is considered here. Linear integrals of the 1-form $\sum_i^N p_i dq_i$ taken over the entire set of topologically equivalent irreducible contours C_k, are invariant [18]. The trajectories of integrable systems wind onto N-dimensional tori, and the motion is regular.

The very end of Einstein's work [17] is of particular interest. Considering Poincaré's study of the three-body problem as an example, Einstein notes the possibility of a case where the number of integrals of motion is less than the number of degrees of freedom. Let us ponder this statement. In essence, this is where the problem was formulated that, four decades later, led to the creation of KAM theory. Recall that KAM theory addresses the following questions: the conservation of invariant tori; their stability under small perturbations; and the nature of motion when the integrals of motion are destroyed. I believe that Einstein's work can rightfully be considered the starting point for research into quantum chaos. It should be noted, however, that several decades passed between the formulation of the task and its implementation.

Einstein's remarkable work was far ahead of its time, and at the time it did not attract the attention it deserved. Interest was focused on solving more pressing problems, primarily the creation of a quantum mechanics free from the shortcomings of the old quantum theory. The concept of trajectory was banished from quantum mechanics. The correspondence principle, Ehrenfest's theorem, and the WKB approximation were considered sufficient for considering the semiclassical region.

Yet Einstein, like a number of other leading physicists (M. Planck, G. A. Lorentz, W. Heisenberg, E. Schrödinger), who were particularly keenly aware of the unity of physics, was not entirely satisfied with the approaches proposed in the intermediate region of the transition from the quantum-mechanical to the classical description. However, the problems posed in the report [17] only began to attract attention in the late 1950s.

A refinement of Einstein's quantization condition (5) in the general case of nonintegrable systems was carried out in 1958 by J. Keler [20]. In integrable systems, trajectories wind around submanifolds of the phase space with the topology of an N-dimensional tori. In the nonintegrable case, the situation is more complex. The motion occurs on a Lagrangian manifold–an isotropic submanifold of maximal dimension of a symplectic manifold. Lagrangian manifolds occupy an important place in the study of semiclassical asymptotics. Keler refined Einstein's quantization formula by introducing the following amendment:

$$I_k = \frac{1}{2\pi} \oint_{C_k} \sum_{i=1}^{N} p_i dq_i = \hbar(n_k + \frac{m_k}{4}), \tag{6}$$

where m_k are integers called Maslov indices. V. P. Maslov is the author of fundamental results on asymptotic methods for solving a wide range of problems in physics and mechanics. The Schrödinger equation is linear, while the WKB method yields a nonlinear equation. Mathematically, this leads to the theory of linear operators. Maslov's main results were obtained in the 1960s [13, 21, 22]. However, a second question remains, going back to Einstein: what changes will occur when invariant tori are destroyed, when in the classical limit the motion is chaotic?

A very important step was made by M. Gutzwiller, who investigated this question in a series of papers in the 1960s and 1970s (see, for example, [23] and the bibliography therein). Using the technique of Feynman path integrals, Gutzwiller obtained the formula that bears his name. The Gutzwiller trace formula allows one to establish a connection between the spectrum of a system and closed orbits in phase space. The Maslov index is equal to the number of turning points in the orbit, which provides an additional phase shift. Gutzwiller's formula can be considered a generalization of the semiclassical approximation to the case of chaotic systems.

3. Computational experiment. The multiple time scales. Kicked rotator. Dynamic polarization

The primary research method used by Siberian physicists was computational experimentation, which has now become an effective method of scientific research. Unlike traditional numerical methods, computational experiments involve experimenting with an initial mathematical model. A key feature is that the final result is unknown in advance. By varying parameters, initial conditions, and including or ignoring certain terms in the equations, researchers attempt to elucidate the characteristic features of the model as a whole, its behavioral characteristics, and so on. This use of computers was quite unusual in theoretical physics at the time. Furthermore, it is imperative that the model being studied be related to physical reality, and that the observed effects be confirmed by laboratory experiments and investigated using standard theoretical methods. Computational experiments complement these two research methods. According to Chirikov, "The human mind is weak, and it needs guidance to understand the complex behavior of a system. Numerical modeling, or, better yet, numerical experiments, provide such a clue. However, computer capabilities are limited, and therefore the scientist must select a good model that is, on the one hand, simple enough for modeling, and on the other, remains sufficiently general, given the typical patterns of the processes being studied" [5]. Here it is worth recalling the atmosphere in which, in the 1960s, chaos research was viewed with considerable skepticism in the scientific community, not only in our country but also abroad. Our physics journals refused to publish papers based on computational experiments. Only later, in the 1970s, did the validity of such research come to be recognized.

The combination of quantum and classical descriptions in the transition region must be achieved not only conceptually but also instrumentally. But first, let us dwell on the choice of mathematical models used. Here, Chirikov's astonishing intuition was expressed. The model had to be as simple as possible for analysis and, at the same time, nontrivial and as meaningful as possible. The most striking example of this approach is a simple system of two discrete equations, known as the standard Chirikov map. Its importance in the study of classical chaos cannot be overestimated. The standard map provides insight into the fundamental properties of dynamic chaos and, on the other hand, serves as a touchstone for testing various mathematical models used to study real physical systems. The very first paper on quantum chaos, jointly with foreign physicists [24], proved to be one of the foundational works in the new field and one of the most cited. Here, Chirikov, together with Ford, proposed a mathematical model called the "kicked rotator," which has occupied the same place in quantum chaos research as the standard map does in classical chaos research. Essentially, the kicked rotator is a quantum analog of the standard map and is obtained by quantizing it. It is also relatively simple and yet describes a vast number of quantum effects [5, 8].

How can discreteness be reconciled with the correspondence principle? The idea of multiple time scales emerged. In the work of G. Berman and G. Zaslavsky [25] the time scale t_E was introduced, later called the Ehrenfest time. This scale characterizes the spreading time of the wave packet and limits the time interval during which the wave packet can be associated with

a classical particle. Therefore, at times $t > t_E$ the influence of quantum effects becomes significant. According to the Ehrenfest theorem, the average values of the quantities characterizing the motion of a particle in the quantum domain are related by equations analogous to the equations of classical mechanics. On the t_E time scale, the system's behavior is close to classical, and quantum corrections are small. For unstable systems with complex behavior, the Ehrenfest time is logarithmically small, $t_E \sim (|lnq|)/h$, where q is the characteristic quantum parameter and h is the Kolmogorov–Sinai entropy.

There is another time scale of quantum dynamics with a characteristic time t_D, on which quantum diffusion processes occur, and $t_D \gg t_E$. To study the dynamics on the t_D scale, a quantum rotator model was used with the Hamiltonian

$$H = \frac{n^2}{2} + k \cdot \cos\theta \cdot \delta_T(t), \tag{7}$$

where (n, θ) are the action-angle variables, k and T are the magnitude and period of the perturbation, and $\delta_T(t)$ is a delta function with period T. The dynamics of the corresponding classical system are described using the map

$$\overline{n} = n + k \cdot \sin\theta, \ \overline{\theta} = \theta + \overline{n} \cdot T. \tag{8}$$

The only parameter in this map is $K = k \cdot T$ [24]. This simple model has proven to be very informative and applicable to many physical situations. Depending on the parameter K, there are two very different motion regimes: for $K < 1$, the motion is confined; for $K > 1$, the motion can be described as diffusion. In both cases, regular and chaotic motion coexist, and for $K \gg 1$, the motion becomes ergodic and exponentially unstable. At times $t \ll t_D$, quantum diffusion will be similar in all details to classical diffusion. The local instability of quantum motion disappears at $t > t_E$, and at times $t \gg t_D$, quantum diffusion ceases.

In the work of B. V. Chirikov, F. M. Izrailev, and D. L. Shepelyansky [26], it was established that on the diffusion time scale t_D, the behavior of quantum systems exhibits a number of peculiarities, the most interesting of which is the quantum limitation of diffusion. It was shown that in the case of a discrete spectrum with an average quasi-energy level density ρ_0, classical diffusion occurs on the time scale $t \sim t_D \sim \rho_0$. For ρ_0 the estimate $\rho_0 \sim \Delta n \sim t_D$ was obtained, where Δn is the number of effectively excited states during the evolution of one arbitrary unperturbed state, and $t_D \sim D_{cl}$. Hence,

$$l \sim \Delta n \sim D_{cl}. \tag{9}$$

Here D_{cl} is the classical diffusion rate, l is the localization length, i.e. effective number of unperturbed states involved in stationary oscillations after diffusion has ceased. In other words, the localization length l determines the size of the localization region of the eigenfunctions in the unperturbed basis. Note a remarkable feature of relations (9): they establish a connection between the essentially quantum characteristics of the system dynamics — the diffusion time scale t_D and the localization length l — and the classical diffusion rate D_{cl}. The analogy between the considered dynamic localization and the Anderson localization in a random potential, well known from solid state theory, was established in the work of S. Fishman et al. [27] and was substantially developed by D. L. Shepelyansky [28]. Although it is sometimes claimed that dynamic localization is a special case of Anderson localization, this similarity is more of an external nature. The mechanism of these two phenomena is completely different. In the considered model of dynamic localization, there are no random parameters. In this regard, the rotator-with-kicks model represents the first and entirely nontrivial example of dynamic localization in a deterministic system free of any randomness. It should be noted that in the kicked rotator model considered above, for $K \geqslant 1$ and $k > 1$, localization is associated with the suppression of classical diffusion due to quantum interference effects. When $K \leqslant 1\,(k > 1)$, quantum tunneling into a classically inaccessible region becomes decisive for localization.

These questions should not be considered the domain of only a narrow circle of theorists, with little connection to reality. All of this is currently supported by a solid experimental base. Experiments with hydrogen atoms in a strong radio-frequency field are crucial in the study of quantum chaos. The unusually strong microwave ionization of hydrogen atoms from Rydberg states was first observed by J. Baysfield and P. Koch of Yale University [29]. A good model for such a system is the kicked rotator. The phenomenon of dynamic localization was further studied experimentally in [30, 31]. In the work of M.G. Raizen and his co-workers, dynamic localization of atoms in magneto-optical traps was first observed [32]. They even managed to observe the transition from classical diffusion to quantum localization with ultracold atoms in a laser field [33]. The experimental study of dynamic localization is not limited to what has been said; today it is a reliably established phenomenon.

4. Energy spectrum structure

The applicability range of the semiclassical approximation covers problems involving highly excited states of atoms, and the quantization rules are directly related to the structure of the spectrum. In systems with chaotic behavior, integrals of motion are destroyed. According to KAM theory, invariant tori are preserved under sufficiently small perturbations, and the measure of destroyed tori is small. Under large perturbations, invariant tori are mostly destroyed, and the destruction is chaotic in nature, but islands of stability with regular motion are preserved. Many problems concerning the emergence of chaos can be reduced to billiard-type systems [34, 35]. One such problem is the problem of mixing in the motion of sliding electrons.

Here, the work of G. M. Zaslavsky and N. N. Filonenko [36] should be mentioned. This work was one of the first on quantum chaos in the Soviet Union, if not the very first in this area. The problem arose in connection with the analysis of the motion of metal electrons in an external magnetic field directed along the metal surface ("sliding" electrons). Electrons located near the surface drift, the nature of which depends on the properties of the surface. Mathematically, there is an isomorphism of the electron trajectories in this problem with the trajectories of the Sinai billiard, and the question of quantization can be reduced to the quantization of the billiard problem. Initially, the article [36] was rejected by the editors of JETP. At that time (the article was received by the editors on January 15, 1973), the issues raised in it did not seem relevant, and not many physicists were studying the problems of chaos. The time when nonlinear dynamics became a generally recognized field had not yet come. Only after the intervention of Ilya Lifshitz, who convinced Evgeny Lifshitz, who was a member of the editorial board of the journal, of the high level of this work and the fundamental importance of the problems raised in it, it was accepted for publication [6].

In the question of spectra, another approach is possible, which arose during the consideration of certain problems in the theory of the atomic nucleus. We are talking about the structure of the energy levels of nuclei. To explain the structure of low-lying levels of complex nuclei, it was possible to find theoretical approaches based on the shell model, using collective or individual quantum numbers. But this approach loses its validity when considering highly excited states of a series of energy levels from N to $(N+n)$, $1 \ll n \leqslant (N+n)$, if, say, $N \sim 10^6, n \sim 10^2$. Here, it is no longer possible to ignore the fluctuations of the distances between the levels, distorting the structure of the spectrum; the sequence of levels will be irregular. A statistical analysis becomes more adequate. E. Wigner [37] and L. Landau and Ya. Smorodinsky [38] pointed out that "repulsion" can take place between levels of the same symmetry, which should lead to the disappearance of arbitrarily close levels from the spectrum. The main works on the statistical theory of the spectrum are contained in a collection edited by C. Porter [39].

The effect of "repulsion" of levels turned out to be quite unusual. Energy is considered as a random variable, and for levels of the same symmetry, the probability $P(E|\Delta E)$ of detecting

two adjacent levels with energies E and $E + \Delta E$ should tend to zero as $\Delta E \to 0$; nearby levels turn out to be strongly correlated [39, p. 217]. The spectra of atoms and molecules also have a complex structure, and theoretical constructions for explaining nuclear spectra have a much wider range of applicability.

In [36], the problem of finding the probability $P(E, \Delta E)$ was solved using semiclassical asymptotics for the case of "gliding" electrons. It was assumed that the system is isomorphic to a Sinai billiard; all integrals of motion, with the exception of the energy integral, are destroyed. Zaslavsky later showed that the results obtained are of a much more general nature [40]. It turned out that in systems with stochastically destroyed integrals of motion it is possible to find the increment of local instability and, with its help, determine the time t_0, during which a small perturbation of the initial condition will lead to the statistical independence of trajectories. When trajectories are stochastic, the correlation between levels weakens and, in the limit $t_0 \to 0$, the correlation disappears, which is manifested in the structure of the irregular spectrum. All this began to attract close attention as early as the 1970s, including in experimental studies, such as the study of the spectra of highly excited molecules and molecules in a predissociation state, the study of electron motion in an anisotropic field, etc. All these studies heightened interest in a number of fundamental issues: the quantization of stochastically unstable systems, the wave functions in such systems, the correspondence principle, etc. [41]. Some of these questions were resolved in subsequent studies in Novosibirsk and Krasnoyarsk.

The statistical theory of spectra was based on the hypothesis of the equivalence of the distribution of energy levels E_k and eigenvalues λ_k of an ensemble of eigenvalues of random matrices with a certain symmetry. This approach was developed by E. Wigner [37], C. E. Porter [39], and F. Dyson [42]. The main result of these studies was the derivation of the probability distribution of distances ΔE between adjacent spectral levels with energies close to E:

$$P(E, \Delta E) = A(\Delta E)^{\alpha} exp(-B(\Delta E)^2), \tag{10}$$

where A and B are normalizing constants, and α is a critical exponent that takes values of 1, 2, or 4 depending on the type of symmetry of the system.

Computational experiments on a simple quantum model with two degrees of freedom by O. Bohigas et al. (1984) [43] showed remarkable agreement with the conclusions of random matrix theory. These studies were continued in the works of F. Izrailev [44] and B. Chirikov, F. Izrailev D. Shepelyansky [45]. In the model considered in them, the exponent $\alpha = 1$. Separate consideration was carried out for even and odd eigenstates. An important parameter $\Lambda = \frac{l}{N_1}$ was introduced, where l is the localization length, N_1 is the dimension of the set of eigenfunctions of the Hilbert space, i.e., the maximum number of unperturbed states associated with the eigenfunctions. It was shown that for $\Lambda \gg 1$ there is good agreement with the conclusions of random matrix theory. For $\Lambda < 1$, a deviation from distribution (10) already occurs. In the limit $\Lambda \to 0$, distribution (10) goes over to the Poisson distribution for completely integrable systems, although the classical analogue of a quantum system exhibits chaotic behavior. In the general case, for $\Lambda < 1$, there is an "intermediate statistic" with the distribution $P(E, \Delta E)$, which is somewhere between the Wigner–Dyson and Poisson distributions. It has been hypothesized that the $P(E, \Delta E, \Lambda)$ distribution is universal.

* * * *

The Novosibirsk and Krasnoyarsk schools of nonlinear dynamics have made enormous contributions to this field of knowledge, with many of their results considered classic. These achievements are invaluable; they largely define the modern face of this field of physics. Research continues to develop and is being continued in many countries around the world.

Darren Gill provided me with great assistance in preparing the manuscript, for which I express my sincere gratitude.

References

[1] R.R.Mukhin, From the history of Hamiltonian chaos: studies of stochasticity of nonlinear systems in the works of the Novosibirsk school, *Izvestiya VUZ. Applied Nonlinear Dynamics*, **16**(2008), 67 (in Russian). DOI: 10.18500/0869-6632-2008-16-5-67-82

[2] G.P.Berman, et al., Georgy Moiseevich Zaslavsky, *Izvestiya VUZ. Applied Nonlinear Dynamics*, **17**(2009), 137 (in Russian).

[3] R.Z.Sagdeev, How much porridge was eaten, Academician M.A. Leontovich, Moscow, 2003, 287 (in Russian).

[4] V.I.Kogan, Oral communication dated 12/17/2003.

[5] D.L.Shepelyansky, Boris Chirikov, Sputnik of Chaos. In: Memories of Boris Valerianovich Chirikov, Novosibirsk, 2014 (in Russian).

[6] G.M.Zaslavsky, Written message 02/12/2003.

[7] Ya.G.Sinai, Some mathematical problems in the theory of quantum chaos, *Physica A*, **163**(1990), 197.

[8] F.M.Izrailev, Boris Valerianovich Chirikov. In: Memories of Boris Valerianovich Chirikov, Novosibirsk, 2014 (in Russian).

[9] R.R.Mukhin, Essays on the history of dynamic chaos, Moscow, 2012 (in Russian).

[10] V.M.Alexeev, M.V.Jacobson, Symbolic dynamics and hyperbolic dynamic systems, *Phys. Rep.*, **75**(1981), 287.

[11] A.A.Brudno, The complexity of the trajectories of a dynamical system, *Russian Mathematical Surveys*, **33**(1978), Issue 1, 197 (in Russian).

[12] O.V.Zhirov, Near the Origins of Dynamic Chaos. In: Memories of Boris Valerianovich Chirikov, Novosibirsk, 2014 (in Russian).

[13] V.P.Maslov, The quasi-classical asymptotic solutions of some problems in mathematical physics, *J. Comp. Mathematics and Math. Physics*, **1**(1962), no. 1, 113.

[14] P.V.Elyutin, The quantum chaos problem, *Sov. Phys. Usp.*, **31**(1988), 597 (in Russian). DOI: 10.1070/PU1988v031n07ABEH003572

[15] G.P.Berman, A.R.Kolovskii, Quantum chaos in interactions of multilevel quantum systems with a coherent radiation field, *Sov. Phys. Usp.*, **35**(1992), no. 4, 303.
DOI: 10.1070/PU1992v035n04ABEH002228

[16] H-J.Stöckmann, Quantum Chaos: An Introduction, Cambridge, 2000.

[17] A.Einstein, Zum Quantensatz von Sommerfeld und Epstein, *Verh. Dtsch. Phys. Ges.*, **19**(1917), 82.

[18] F.Steiner, Quantum chaos, Schlaglichter der Forschung. Zum 75 Jahrestag der Universität Hamburg 1994, Berlin, 1994.

[19] M.Born, The Mechanics of the Atom, London, 1927.

[20] J.B.Keller, Corrected Bohr-Sommerfeld Quantum Conditions for Nonseparable Systems, *Annals of Physics*, **4**(1958), 180.

[21] V.P.Maslov, Théorie des Perturbations et Méthodes Asymptotiques, Paris, 1972.

[22] V.P.Maslov, M.V.Fedoriuk, Semi-Classical Approximation in Quantum Mechanics, Boston, 1981.

[23] M.C.Gutzwiller, Chaos in Classical and Quantum Mechanics, New York, 1990.

[24] G.Casati, B.V.Chirikov, J.Ford, F.M.Izrailev, Stochastic behavior of a quantum pendulum under a periodic perturbation, *Lecture Notes in Physics*, **93**(1979), 334.

[25] G.P.Berman, G.M.Zaslavsky, Condition of stochasticity in quantum nonlinear systems, *Physica A*, **91**(1978), 450.

[26] B.V.Chirikov, F.M.Izrailev, D.L.Shepelyansky, Dynamical stochastisity in classical and quantum mechanics, *Sov. Scien. Rev.*, **2**(1981), 209.

[27] S.Fishman, D.R.Grempel, R.E.Prange, Chaos, Quantum Recurrences, and Anderson Localization, *Phys. Rev. Lett.*, **49**(1982), 509. DOI: 10.1103/PhysRevLett.49.509

[28] D.L.Shepelyansky, Localization of diffusive excitation in multi-level systems, *Physica D.*, **28**(1987), 103.

[29] J.Baysfield, P.Koch, Multiphoton ionization of highly excited hydrogen atoms, *Phys. Rev. Lett.*, **33**(1974), 258.

[30] J.E.Bayfield, G.Casati, I.Guarneri, D.W.Sokol, Localization of classically chaotic diffusion for hydrogen atoms in microwave fields, *Phys. Rev. Lett.*, **63**(1989), 364.
DOI: 10.1103/PhysRevLett.63.364

[31] E.J.Galvez, B.E.Sauer, et al., Microwave Ionization of H Atoms: Breakdown of Classical Dynamics for High Frequencies, *Phys. Rev. Lett.*, **61**(1988), 2011.
DOI: 10.1103/PhysRevLett.61.2011

[32] M.G.Raizen, et al., Observation of Dynamical Localization in Atomic Momentum Transfer, *Phys. Rev. Lett.*, **73**(1994), 2974. DOI: 10.1103/PhysRevLett.73.2974

[33] F.L.Moore, J.C.Robinson, et al., Atom optics realization of the quantum delta - kicked rotor, *Phys. Rev. Lett.*, **75**(1995), 4598. DOI: 10.1103/PhysRevLett.75.4598

[34] Ya.G.Sinai, On the Justification of the Ergodic Hypothesis for a Dynamic System of Statistical Mechanics, *Doklady AN SSSR*, **153**(1963), no. 6, 1261 (in Russian).

[35] Ya.G.Sinai, Dynamical systems with elastic reflections. Ergodic properties of dispersing billiards, *Russian Mathematical Surveys*, **25**(1970), no. 2, 137 (in Russian).

[36] G.M.Zaslavsky, N.N.Filonenko, Statistical properties of the energy spectrum of "sliding" electrons with mixing classical trajectories, *JETP*, **65**(1973), no. 2, 643 (in Russian).

[37] E.P.Wigner, On a Class of Analytic Functions from the Quantum Theory of Collisions, *Ann. Math.*,**53**(1951), 36; Characteristic Vectors of Bordered Matrices with Infinite Dimensions, *Ann. Math.*, **62**(1955), 548; Characteristic Vectors of Bordered Matrices with Infinite Dimensions, *Ann. Math.*, **65**(1957), 203; On the Distribution of the Roots of Certain Symmetric Matrices, *Ann. Math.*, **67**(1958), 325.

[38] L.D.Landau, Ja.A.Smorodinsky, Lectures on the theory of the atomic nucleus, Moscow-Leningrad, 1955 (in Russian).

[39] C.E.Porter, Fluctuations of Quantal Spectra, Statistical Theories of Spectra: Fluctuations, Charles E. Porter (Ed.), 1965, 3.

[40] G.M.Zaslavsky, Statistics of Energy Levels in the Destruction of Integrals of Motion, *Sov. Phys. JETP*, **73**(1977), 2089 (Russian).

[41] G.M.Zaslavskii, Statistics of energy spectra, *Sov. Phys. Usp.*, **22**(1979), 788 (in Russian).

[42] F.J.Dyson, Statistical Theory of the Energy Levels of Complex Systems. *I, II, III J. Math. Phys.*, **3**(1962), 140, 157, 166.

[43] O.Bohigas, M.J.Giannoni, C.Schmit, Characterization of Chaotic Quantum Spectra and Universality of Level Fluctuation Laws, *Phys. Rev. Lett.*, **80**(1984) 157.

[44] F.M.Izrailev, Distribution of quasienergy level spacings for classically chaotic quantum systems, *Phys. Rev. Lett.*, **56**(1986) 541.

[45] B.V.Chirikov, F.M.Izrailev, D.L.Shepelyansky, Quantum chaos: Localization vs. ergodicity, *Physica D*, **33**(1988), 77.

Из истории квантового хаоса: исследования школ нелинейной динамики Новосибирска и Красноярска

Равиль Р. Мухин
Старооскольский технологический институт им. А. А. Угарова (филиал НИТУ «МИСиС»)
Старый Оскол, Российская Федерация

Аннотация. Работа посвящена мало освещенным в литературе исследованиям квантового хаоса в двух центрах нелинейной динамики в России — Институте ядерной физики им. Г. И. Будкера в Новосибирске и Институте физики им. Л. В. Киренского в Красноярске. выбранных временных рамках — начало 1970-х гг.— начало 2000-х гг. — появились первые работы по квантовому хаосу, сложились представления о предмете, сформировался понятийный аппарат. Здесь ключевая роль принадлежит Б. В. Чирикову и Г. М. Заславскому. Работы названных исследовательских центров в значительной степени определяют современный облик рассмотренной области знания.

Ключевые слова: классический хаос, квантовый хаос, квазиклассическая область, квантовый ротатор, локализация, статистика энергетического спектра.

EDN: LKMQKI
УДК 538.941(075)

Hubbard Boson Condensation Taking into Account the Kinematic Interaction from Distant Coordination Spheres

Valerii V. Val'kov*
Kirensky Institute of Physics
Federal Research Center KSC SB RAS
Krasnoyarsk, Russian Federation

Received 25.02.2026, received in revised form 25.03.2026, accepted 27.04.2026

Abstract. For the case of a strong one-site boson repulsion the temperature of the Bose-condensation have been calculated when boson hopping take into account for three co-ordinating spheres. In the solution the task an indefinite metric method was applied to provide an exact bose-analog of the Hamiltonian, written in the atomic representation. Through an unitary transformation the transition to a Hamiltonian with the break down global U(1) symmetry in the phase with condensate was realized. As this takes place the spectrum of excitations for small values of the quasimomentum has characteristics corresponding to the superfluid phase.

Keywords: Bose-condensation, superfluid, U(1) symmetry, indefinite metric method, unitary transformation.

Citation: V.V. Val'kov, Hubbard Boson Condensation Taking into Account the Kinematic Interaction from Distant Coordination Spheres, J. Sib. Fed. Univ. Math. Phys., 2026, 19(4), 483–490. EDN: LKMQKI.

This work is dedicated to the memory of Valter Alekseevich Ignatchenko. The Theoretical Department of the Institute of Physics, founded and directed by him for many years, continually pursued research into the formulation of new methods for the theoretical analysis of complex physical systems. V. A. Ignatchenko actively supported these areas of scientific inquiry. The presented research results belong to this class of works and define a new approach to the problem of condensation of strongly correlated bosons in optical lattices, using the atomic representation and bosonization of quantum Hamiltonians with the introduction of an indefinite metric.

The study of ultracold atoms in optical lattices led to the establishment of highly effective approaches to simulating quantum phenomena at the microscopic level. The research ultimately resulted in the experimental observation of Bose-Einstein condensation and the formation of matter-wave packets. This enabled the use of technical capabilities to realize Feshbach resonances, opening the way to control interatomic interactions. This demonstrated the experimental possibility of moving from the regime of weak interactions to the regime of strong interactions.

If the theory of weakly interacting Bose gases was developed sufficiently well [1], then the situation when the energy of interactions is comparable to or exceeds the kinetic energy of bosons was previously considered unattainable. The main problem is related to the need for a correct description of strong interactions. In the limit of low boson concentrations interactions are taken into account based on the ladder approximation [2–4].

The second difficulty of the theory of non-ideal Bose systems is related to the presence of a condensate in the low-temperature region. The basis for a consistent account of the condensate

*vvv@iph.krasn.ru https://orcid.org/0000-0002-3853-3633

in a weakly non-ideal Bose gas is the replacement of Bose operators with zero quasi-momentum by the $\sqrt{N_0}$, where N_0 is the number of bosons in the condensate, as proposed by Bogolubov. After such a replacement, the diagonalization of the quadratic form of the Hamiltonian leads to the energy spectrum of quasiparticles corresponding to the superfluid phase.

If the interaction of bosons at a single site is not weak, a correction to the theory is required. One possible scenario for the theory of such strongly interacting bose-systems is based on the use of the atomic representation. The ideology of such a description mirrors the concept used in the theory of strongly correlated electronic systems, where strong single-site interactions are included in the zero Hamiltonian and taken into account exactly [5,6]. In this case, the dynamical variables are represented by Hubbard operators (HO).

The complexity of commutation relations for HO reflects the presence of kinematic interaction between quasiparticles generated by new dynamic variables. To develop the theory of Bose-Einstein condensation in an ensemble of strongly interacting bosons, one can use an approach associated with the application of an indefinite metric [7] for constructing an exact Bose analog of the quantum Hamiltonian written in the atomic representation [8,9]. In this case, the kinematic interaction of Hubbard bosons is explicitly expressed through the seed scattering amplitude. In the work, this approach allowed studying the spectrum of elementary excitations and the concentration of the Bose condensate, taking into account the hops of bosons between nearest sites.

Since the process of Bose condensation is largely determined by the low-energy density of states, and this density is modified when considering long-range hopping, the question of the influence of hopping between non-nearest sites on the concentration of the Bose condensate and the properties of the energy spectrum becomes relevant. This work is devoted to this question.

1. Hamiltonian of ultracold atoms in an optical lattice

It is known the Hamiltonian of the ultracold atoms in the optical lattice may be written as followers [10]:

$$H = \sum_{fg}[(\varepsilon - \mu)\delta_{fg} - t_{fg}]c_f^\dagger c_g + \frac{1}{2}\sum_f U c_f^\dagger c_f^\dagger c_f c_f, \tag{1}$$

where c_g^+ and c_f are bosonic operators with the conventional commutation relations. The summation is over all sites of the optic lattice are numbered as f and g. Parameter ε is the one-site energy of the boson, μ is the chemical potential of the system, δ_{fg} is Kronecker symbol, t_{fg} is the hopping energy between sites g and f, U is the pair interaction energy between bosons at the same site.

Let us perform a Fourier transform for the operators

$$c_f = \frac{1}{\sqrt{N}}\sum_k \exp(ikf)c_k, \tag{2}$$

where N is the number of sites in the lattice, k is the quasimomentum. Its values are determined by the requirement to satisfy periodic boundary conditions.

In the quasimomentum representation the Hamiltonian (1) may be written as following

$$H = \sum_k(\varepsilon_k - \mu)c_k^\dagger c_k + \frac{U}{2N}\sum_{1-4} c_1^\dagger c_2^\dagger c_3 c_4 \Delta(1+2-3-4), \tag{3}$$

where $\varepsilon_k{=}\varepsilon - t_k$, $t_k = \sum_h t(h)\exp(ikh)$, h-lattice vectors.

Taking into account hoppings within three coordinative spheres t_k for a 3D cubic lattice is defined by the expression

$$t_k = 6t_1 \cdot \gamma_1(k) + 12t_2 \cdot \gamma_2(k) + 8t_3 \cdot \gamma_3(k). \tag{4}$$

Here are introduced the lattice functions corresponding to the first three invariants for a cubic lattice

$$\gamma_1(k) = \frac{1}{3}[\cos k_x + \cos k_y + \cos k_z],$$
$$\gamma_2(k) = \frac{1}{3}[\cos k_x \cdot \cos k_y + \cos k_y \cdot \cos k_z + \cos k_z \cdot \cos k_x],$$
$$\gamma_3(k) = \cos k_x \cdot \cos k_y \cdot \cos k_z.$$

The parameters t_1, t_2 and t_3 describe the intensities of boson hopping between sites of the first, second and third coordination spheres, respectively.

The second term in (3) describes the interaction of boson in the quasimomentum representation.

2. Symmetry breaking and Bogolyubov excitation spectrum

Bogolyubov was the first to point out the need for an explicit consideration of the condensate in boson system at low temperatures. For this purpose, terms containing operators with zero quasi-momentum were singled out in the Hamiltonian (3). After that, a substitution was made:

$$c_0 \longrightarrow \sqrt{N_0}, \quad c_0^+ \longrightarrow \sqrt{N_0}, \tag{5}$$

where N_0 is the number of bosons in condensate.

It was later proposed to use the shift transformation [11]

$$c_0 \longrightarrow \sqrt{N_0} + c_0, \quad c_0^+ \longrightarrow \sqrt{N_0} + c_0^+, \tag{6}$$

allowed the development of the theory of non-ideal Bose gas based on new approaches. In this context c_0 and c_0^+ came to be called fluctuation operators.

Note that the shift transformation (6) for operators corresponds to a unitary transformation of the Hamiltonian

$$H \longrightarrow H' = U(\alpha)HU^+(\alpha), \tag{7}$$

in which unitary operator is defined by the expression

$$U(\alpha) = \exp(\alpha^* c_0 - \alpha c_0^+). \tag{8}$$

In this case the transformation law for operators takes the form that fully corresponds to a shift transformation

$$c_0 \longrightarrow U(\alpha)c_0U^+(\alpha) = \alpha + c_0, \qquad c_0^+ \longrightarrow U(\alpha)c_0^+U^+(\alpha) = \alpha^* + c_0^+. \tag{9}$$

In the particular case when $\alpha = \sqrt{N_0}$ we obtain the previously used shift transformation in the theory of interacting bosons at low temperatures.

Establishing a connection between the shift transformation (6) and the unitary transformation of the Hamiltonian (7) allows the structure of the condensate wave function to be determined. Since a unitary transformation of the Hamiltonian (7) is accompanied by a change in

the basis vectors of the Hilbert space, after the transformation the new vacuum vector for zero quasimomentum is the coherent state defined by the equation

$$| \tilde{0} \rangle = U^{+}(\alpha)| 0 \rangle, \tag{10}$$

in which vector $| 0 \rangle$ denotes the state with number of bosons equal to zero.

The coherence property of state $| \tilde{0} \rangle$ follows from a chain of equalities

$$c_0| \tilde{0} \rangle = c_0 U^{+}(\alpha)| 0 \rangle = U^{+}(\alpha)U(\alpha)c_0 U^{+}(\alpha)| 0 \rangle = \alpha| \tilde{0} \rangle. \tag{11}$$

It is important to note that transformation (7) induces a violation of the global U1 symmetry. As a result the Hamiltonian H' loses invariance with respect to the group of homogeneous gauge transformations

$$c_k \longrightarrow c_k \exp(i\theta), \qquad c_k^{+} \longrightarrow c_k^{+} \exp(-i\theta), \tag{12}$$

whereas the original Hamiltonian H possessed this property. This is easy to verify if U is written up to terms quadratic in the operators

$$\begin{aligned} H' = \frac{UN_0^2}{2N} + \sqrt{N_0}(\varepsilon_0 - \mu + Un_0)(c_0 + c_0^{+}) + \\ + \frac{1}{2}Un_0[c_0^2 + (c_0^{+})^2] + (2Un_0 + \varepsilon_0 - \mu)c_0^{+}c_0 + \\ + \sum_{k\neq 0}\{(\varepsilon_k - \mu + 2Un_0)c_k^{+}c_k + \frac{1}{2}Un_0(a_k^{+}a_{-k}^{+} + a_{-k}a_k)\}. \end{aligned} \tag{13}$$

From the condition of the linear operator contributions summing to zero, we obtain that $\mu = \varepsilon_0 + Un_0$. At the same time, the spectrum of excitation is determined by the expression

$$\omega(k) = \sqrt{(t_0 - t_k)(2Un_0 + t_0 - t_k)}. \tag{14}$$

This expression follows that the breaking of the global calibration symmetry of the Hamiltonian leads to a transformation of the elementary excitation spectrum. At small values of the quasi-momentum, the spectrum acquires a linear character. This circumstance is of significant importance for the formation of the superfluid phase.

It should be emphasized that the expression for (14) is valid only when $U \ll |t_{fm}|$. If U is comparable to $|t_{fm}|$, or exceeds it, a different approach is required. This is addressed in the following paragraph.

3. Ensemble of boson with strong correlations

If the repulsion energy of bosons on a single site significantly exceeds their kinetic energy, the operator including all single-site interactions should be chosen as the zero Hamiltonian. By finding the eigenfunctions of such an operator, one can move to a representation in which single-site correlations are taken into account exactly. For fermions systems, this approach is described in detail in the book [6]. In our case, the eigenstates of the boson number operator are chosen as the basis states:

$$c^{+}c\ |n\rangle \quad = \quad n\ |n\rangle, \quad n = 0, 1, 2, \ldots . \tag{15}$$

Taking into account the rules of operators' influence on states

$$c|n\rangle = \sqrt{n}|n-1\rangle, \quad c^{+}|n\rangle = \sqrt{n+1}|n+1\rangle, \tag{16}$$

we will obtain the representation of Bose operators through the operators of the atomic representation

$$c = \sum_{n=1} \gamma(n) X^{n-1,n}, \qquad c^+ = \sum_{n=1} \gamma(n) X^{n,n-1}, \quad \gamma(n) = \sqrt{n}. \tag{17}$$

Here, the operators of atomic representation (Hubbard operators) are defined by equations

$$X^{n-1,n} = |n-1\rangle\langle n|, \quad X^{n,n-1} = |n\rangle\langle n-1|. \tag{18}$$

Hubbard operators satisfy the commutation relations,

$$[X_f^{n,m}, X_g^{p,q}]_- = \delta_{fg}(\delta_{mp} X_f^{n,q} - \delta_{nq} X_f^{p,m}), \tag{19}$$

corresponding to Lie algebra. The physical manifestation of these relationships is the emergence of kinematic interaction. Dyson was the first to draw attention to this.

In the case $U \longrightarrow \infty$ the Hamiltonian in the atomic representation has the form

$$H = \sum_f (\varepsilon - \mu) X_f^{1,1} \; + \; \sum_{fg} t_{fg} X_f^{1,0} X_g^{0,1}. \tag{20}$$

The operator $X_f^{1,0}$, acting on a state at the site f, in wich there is no boson, transforms this site into a state with a single boson. Due to the complex commutation properties of Hubbard operators, the excitation generated by the operator $X_f^{1,0}$ is called a Hubbard boson, similar to how Fermi excitations in an ensemble of strongly correlated electrons are called Hubbard fermions.

To study the influence of kinematic interaction on the condensation of Hubbard bosons, we will use a method based on the construction of an exact Bose analogue of the quantum Hamiltonian.

Its application, coupled with the introduction of an indefinite metric to cut off contributions from non-physical states, allows one to obtain an exact Bose representation for Hubbard operators

$$X_f^{10} = \hat{F}_f a_f^+, \quad X_f^{01} = \hat{F}_f (a_f - a_f^+ a_f a_f), \quad X_f^{11} = \hat{F}_f a_f^+ a_f. \tag{21}$$

In this equation $\hat{F}_f$ - metric operator [8]

$$\hat{F}_f = 1 + \sum_{n=2} A_n (a_f^+)^n a_f^n, \quad A_2 = -1/2, \quad A_3 = 1/3, \quad A_4 = -1/8, \ldots . \tag{22}$$

Using this representation, we can write a Bose analog of the Hamiltonian. Retaining only terms of the fourth order in operators in the Hamiltonian, we obtain

$$H_B = \sum_k (\varepsilon_k - \mu) a_k^\dagger a_k - \frac{1}{N} \sum_{1-4} (\varepsilon - \mu - t_1 - t_4) a_1^\dagger a_2^\dagger a_3 a_4 \Delta(1+2-3-4), \tag{23}$$

where a_k^+ and a_q are bosons operators with the conventional commutation relations.

Using Bogolyubov's method, we write down the quadratic form of the Hamiltonian, which reflects the kinematic interaction of the Hubbard bosons

$$H_{(2)} = \sum_{k \neq 0} \left[A_k a_k^+ a_k + \frac{1}{2} B_k (a_k^+ a_{-k}^+ + a_{-k} a_k) \right], \tag{24}$$

where

$$A_k = (1-4n_0)(\varepsilon_k - \mu - t_0) + t_0, \qquad B_k = -2n_0(\varepsilon_k - \mu - t_0). \tag{25}$$

The equation determining the value of the chemical potential is found from the condition that the first-degree terms of the Hamiltonian in terms of the operators vanish. With the accuracy considered, this equation can be written as

$$(1-2n_0)(\varepsilon - \mu - t_0) + 2n_0 t_0 = 0. \tag{26}$$

Diagonalization of Hamiltonian (24) leads to an expression for the spectrum [12]

$$\omega_k = \sqrt{(1-2n_0)(t_0 - t_k)[4n_0 t_0 + (1-6n_0)(t_0 - t_k)]}. \tag{27}$$

The equation that determines the relationship between the temperature of the system, the total concentration of bosons n and the concentration of the condensate n_0 is written as

$$n = n_0 + \frac{1}{2N}\sum_k \frac{A_k - \omega_k}{\omega_k} + \frac{1}{N}\sum_k \frac{A_k}{\omega_k} f_B(\omega_k/T), \tag{28}$$

where $f_B(x) = 1/(\exp(x) - 1)$ — Bose-Einstein function.

The use of this expression allows us to analyze the influence of the kinematic interaction of Hubbard bosons on the temperature of Bose condensation, as well as on the effect of condensate depletion, i.e., on the decrease of n_0 in comparison with n at zero temperature. Fig. 1 shows the

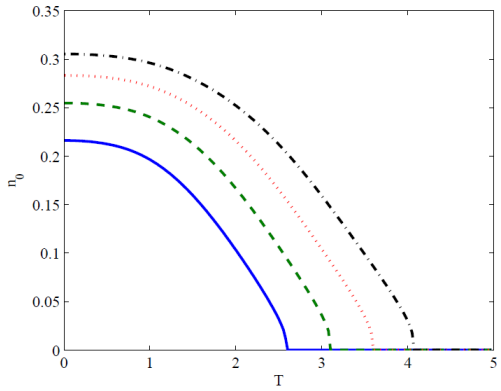

Fig. 1. Temperature behavior of the condensate concentration n_0 for four values of the total boson concentration n. Kinematic interaction is realized within one coordination sphere. The solid blue line corresponds to the case $n = 0.3$; the green dashed line — $n = 0.4$; the red dotted line — $n = 0.5$; the black dashed-dotted line — $n = 0.6$. The temperature is measured in units of the parameter t_1

temperature dependencies of the condensate concentration $n_0(T)$ for four values of the boson concentration in the system n. The kinematic interaction of Hubbard bosons is taken into account only within the first coordination sphere. Accordingly, the long-range hopping parameters are zero ($t_2 = 0$, $t_3 = 0$). It follows from the figure that the depletion of the condensate at $T = 0$ ($n_0(T = 0)/n$) reaches approximately 50 percent.

When hopping between non-nearest sites ($t_2 \neq 0$, $t_3 \neq 0$) is enabled, the kinematic interaction of Hubbard bosons is generated within three coordination spheres. Increasing the effective radius

of interaction between Hubbard bosons can significantly alter the condensation temperature in such a system.

Fig. 2 shows an example of such a change. The calculations were performed for ($t_2 = -0.145$, $t_3 = -0.1$). Comparing the curves presented in Figs. 1 and 2 reveals that enabling long-range interactions resulted in an eightfold decrease in the Bose condensation temperature.

A second effect associated with long-range interactions is a decrease in the condensate concentration n_0 at $T = 0$.

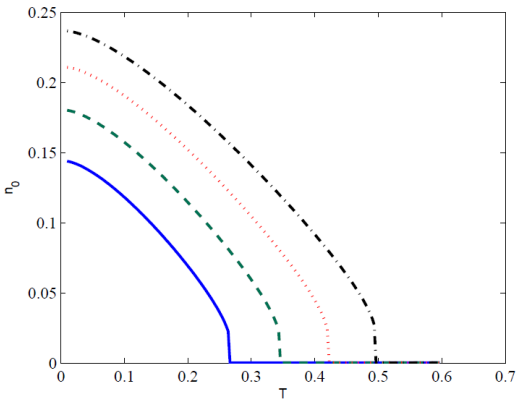

Fig. 2. Temperature behavior of the condensate concentration n_0 for four values of the total boson concentration n in the case when kinematic interaction is realized within three coordination spheres: $t_2 = -0.145$, $t_3 = -0.1$. The solid blue line corresponds to the case $n = 0.3$; the green dashed line — $n = 0.4$; the red dotted line — $n = 0.5$; the black dashed-dotted line — $n = 0.6$. All energy quantities are measured in units of t_1

This means that long-range boson hops in the strong correlation regime can have a significant impact on the thermodynamic characteristics of the boson ensemble.

Conclusion

The conducted studies have shown that the use of an atomic representation followed by a bosonization procedure based on the introduction of an indefinite metric is effective in constructing a theory of condensation of an ensemble of strongly interacting bosons.

With this approach, the system under consideration is represented by an ensemble of Hubbard bosons for which kinematic interaction is realized.

The paper demonstrates that the kinematic interaction of Hubbard bosons for significantly reduces the condensate concentration at T=0 (the depletion effect). Importantly, this interaction from distant coordination spheres for 3D lattice can reduce the boson condensation temperature by an order of magnitude.

The work was carried out within the framework of the state assignment of Kirensky Institute of Physics of the Siberian Branch of the Russian Academy of Sciences.

References

[1] N.N.Bogolyubov, On the Theory of Superfluidity, *J. of Physics USSR*, **11**(1947), 23.

[2] S.T.Beliaev, Application of the Methods of Quantum Field Theory to a System of Bosons, *JETP*, **7**(1958), 289.

[3] S.T.Beliaev, Energy-Spectrum of a Non-ideal Bose Gas, *JET*, **7**(1958), 299.

[4] N.M.Hugenholtz, D.Pines, Ground-State Energy and Excitation Spectrum of a System of Interacting Bosons, *Phys. Rev.*, **116**(1959), 489.

[5] J.Hubbard, Electron correlations in narrow energy bands - IV. The atomic representation, *Proc. Roy. Soc.*, **A285**(1965), 542.

[6] S.G.Ovchinnikov, V.V.Val'kov, Hubbard Operators in the Theory of Strongly Correlated Electrons, London: Imperial College Press, 2004.

[7] F.J Dyson, General Theory of Spin-Wave Interactions, *Phys.*, **102**(1965), 1217.

[8] V.V.Val'kov, T.A.Val'kova, Anomalies in the quantum excitation spectrum of a magnetic material with a strong quasiparticle interaction, *JETP Lett.*, **52**(1990), 589

[9] V.V.Val'kov, T.A.Val'kova, Application of an indefinite metric to go over to a Bose description of SU(3) Hamiltonians: The excitation spectrum of spin nematics, *JETP*, **72**(1991), 1053.

[10] D.Jaksch, C.Bruder, J.I.Cirac, C.W.Gardiner, P.Zoller, Cold Bosonic Atoms in Optical Lattices, *Phys. Rev. Lett.*, **81**(1998), 3108. DOI: 10.1103/PhysRevLett.81.3108

[11] D. van Oosten, P. van der Straten, H.T.C.Stoof, Cold Bosonic Atoms in Optical Lattices, *Phys. Rev.*, **A63**(2001), 053601.

[12] V.V.Val'kov, Excitation Spectrum in an Ensemble of Hubbard Bosons, *JETP Letters*, **116**(2022), 896. DOI:10.1134/S0021364022602664

Конденсация бозонов Хаббарда при учете кинематического взаимодействия из дальних координационных сфер

Валерий В. Вальков
Институт физики им. Л. В. Киренского
Федеральный исследовательский центр КНЦ СО РАН
Красноярск, Российская Федерация

Аннотация. Для режима сильного одноузельного отталкивания бозонов при учете перескоков между узлами в пределах трех координационных сфер вычислена температура бозе-конденсации. При решении задачи на основе введения индефинитной метрики использован алгоритм получения точного бозе-аналога оператора, записанного в атомном представлении. Посредством унитарного преобразования реализован переход к гамильтониану с нарушенной в фазе с конденсатом глобальной симметрией U(1). При этом спектр элементарных возбуждений для малых значений квазиимпульса приобретает характеристики, соответствующие сверхтекучей фазе.

Ключевые слова: бозе-конденсация, сверхтекучесть, U(1) симметрия, метод индефинитной метрики, унитарное преобразование.

EDN: SGDRGS
УДК 537.611

Tuning the Magnetic Structure and Phase Diagram of the Orthorhombic Antiferromagnets $Pb_2Fe_{2-x}Mn_xGe_2O_9$ via Mn Substitution

Anatoly I. Pankrats*
Kirensky Institute of Physics
Federal Research Center KSC SB RAS
Krasnoyarsk, Russian Federation

Received 10.11.2025, received in revised form 01.03.2026, accepted 07.04.2026

Abstract. This work presents a review of the magnetic properties and magnetic phase diagrams of three isostructural orthorhombic antiferromagnets from the $Pb_2Fe_{2-x}Mn_xGe_2O_9$ family, with $x = 0$, 0.16, and 0.43. In pure $Pb_2Fe_2Ge_2O_9$, the magnetic properties are determined solely by the magnetic S-ions Fe^{3+}. The magnetic structure of this crystal is characterized by an antiferromagnetic vector oriented along the orthorhombic c-axis and a weak ferromagnetic moment along the a-axis. The partial substitution of Fe^{3+} ions with highly anisotropic Mn^{3+} ions leads to a reorientation of the antiferromagnetic vector toward the orthorhombic b-axis in the crystal with the highest substitution level $x = 0.43$, accompanied by the disappearance of weak ferromagnetism. At an intermediate substitution level $x = 0.16$, the competition between the anisotropic contributions of the Fe^{3+} and Mn^{3+} ion subsystems results in a spontaneous spin-reorientation transition at $T_c = 22$ K. The temperature and field dependences of the magnetization for all three crystals were analyzed on the basis of a thermodynamic potential derived from symmetry considerations. Based on this analysis, magnetic field–temperature phase diagrams were constructed for each crystal for various orientations of the magnetic field relative to the orthorhombic axes.

Keywords: antiferromagnetism, weak ferromagnetism, spin-reorientation transition, magnetic phase diagram, Mn substitution.

Citation: A.I. Pankrats, Tuning the Magnetic Structure and Phase Diagram of the Orthorhombic Antiferromagnets $Pb_2Fe_{2-x}Mn_xGe_2O_9$ via Mn Substitution, J. Sib. Fed. Univ. Math. Phys., 2026, 19(4), 491–505. EDN: SGDRGS.

Introduction

Since its very foundation, the L. V. Kirensky Institute of Physics has been recognized as a leading center for research in the physics of magnetic phenomena, not only in our country but also worldwide. Among the first researchers invited by L. V. Kirensky to join the Institute was Valter Alekseevich Ignatchenko. V. A. Ignatchenko was one of the most highly qualified and versatile specialists in the field of magnetism, and he consistently maintained a keen interest in the search for novel magnetic materials with unusual properties.

The present work falls precisely within this research direction — namely the search for magnetic materials exhibiting magnetodielectric properties. One possible reason for the emergence of a coupling between the magnetic and electrical properties of a material is considered to be the presence of ions with unusual stereochemical features in the compound [1, 2]. Such ions include, for example, Bi^{3+} and Pb^{2+}, in which the $6s^2$ valence electrons form so-called "lone pairs." These lone pairs can, in turn, give rise to local dipole moments.

Single crystals of the orthorhombic weak ferromagnet $Pb_2Fe_2Ge_2O_9$ — a compound containing the stereochemically active Pb^{2+} ion — were first synthesized and reported in Ref. [3]. This

*pank@iph.krasn.ru https://orcid.org/0000-0002-8314-192X

material is a promising candidate for investigating magnetodielectric phenomena. Given that multiferroic properties are known to be extremely sensitive to the underlying magnetic structure, having the means to control this structure is a crucial advantage.

Doping with different ions is an effective strategy for modifying the magnetic structure of a crystal. For instance, in rare-earth ferroborates with the huntite structure, mixed doping of the rare-earth subsystem, along with its diamagnetic dilution, is routinely employed to control both the magnetic order and magnetoelectric properties [4–6]. In our previous study [7], we demonstrated that partial substitution of Fe^{3+} for Mn^{3+} ions transforms the initial ferromagnetic structure of $PbMnBO_4$ [8] into a ferrimagnetic-like one.

$Pb_2Fe_2Ge_2O_9$ belongs to the isostructural family $Pb_2M_2X_2O_9$ (M = Fe, Mn; X = Ge, Si). This structural relationship naturally suggested the possibility of synthesizing a series of $Pb_2Fe_{2-x}Mn_xGe_2O_9$ solid solutions. Such a series was of particular interest to us, as it involves the progressive substitution of the S-state Fe^{3+} ion — characterized by relatively weak magnetic anisotropy — with the highly anisotropic, Jahn-Teller active Mn^{3+} ion. In general, varying the substitution level in such families provides an effective means of tuning the magnetic structure and phase diagram.

A key requirement for conducting detailed investigations of magnetic properties — particularly magnetic phase diagrams — is the availability of high-quality single-crystal samples. Indeed, only measurements on single crystals can provide the detailed insight necessary to fully map out the phase diagram of a material.

This paper provides a comprehensive overview of the magnetic properties and phase diagrams of pure $Pb_2Fe_2Ge_2O_9$ single crystals [9] and their Mn^{3+}-doped counterparts, $Pb_2Fe_{2-x}Mn_xGe_2O_9$ with $x = 0.16$ [10] and $x = 0.43$ [11]. We analyze the temperature- and field-dependent magnetization measured for different orientations of the applied magnetic field relative to the crystallographic axes. By comparing these data and modeling them with a thermodynamic potential consistent with the crystal symmetry, we conclude that the highest Mn^{3+} concentration ($x = 0.43$) drives an abrupt reorientation of the antiferromagnetic vector: from the orthorhombic c-axis in the pristine crystal to the b-axis in the doped one. At the intermediate doping level ($x = 0.16$), the magnetic structure becomes inclined. For each composition, we map out the magnetic phase diagrams for various field orientations with respect to the crystal axes.

1. Experimental

The $Pb_2Fe_2Ge_2O_9$ single crystals were grown using a pseudo-flux technique modification of the spontaneous crystallization method described in [3, 9]. The partially substituted single crystals $Pb_2Fe_{2-x}Mn_xGe_2O_9$ were synthesized using minor modifications of this technology [10, 11]. Details on the characterization of the synthesized single crystals can be found in previous publications [3, 9–11]. X-ray diffraction analysis confirmed the orthorhombic crystal structure (sp. gr. *Pbcn*) for all the crystals with the unit cell parameters similar to those of the pure crystal reported in [12]. This paper reports on the magnetic properties and magnetic phase diagrams of three single crystals of $Pb_2Fe_{2-x}Mn_xGe_2O_9$ with different concentrations of Mn^{3+}: $x = 0$, 0.16, and 0.43. The true manganese content in the crystals was determined by X-ray fluorescence analysis on Hitachi TM-3000 and JEOL JSM-7001F scanning electron microscopes.

The field and temperature dependences of the magnetization for the $Pb_2Fe_{2-x}Mn_xGe_2O_9$ crystals were measured on a vibrating sample magnetometer (VSM) with a superconducting solenoid in magnetic fields of up to 70 kOe [13] and on a PPMS-9 Quantum Design Physical Property Measurement System.

2. Results and discussion. Magnetic phase diagrams of $Pb_2Fe_{2-x}Mn_xGe_2O_9$

2.1. Temperature dependencies of magnetization, x = 0, 0.16 and 0.43

We first note that Mn^{3+} substitution causes a modest reduction in the Néel temperature. For the pure crystal, $T_N = 45.2$ K [9]; this decreases to $T_N = 42.0$ K [10] at $x = 0.16$ and further to $T_N = 39.9$ K [11] at $x = 0.43$. The values of T_N were extracted from specific heat data for $x = 0$ and 0.16, and from the peak in the derivative dM/dT for $x = 0.43$. The most pronounced

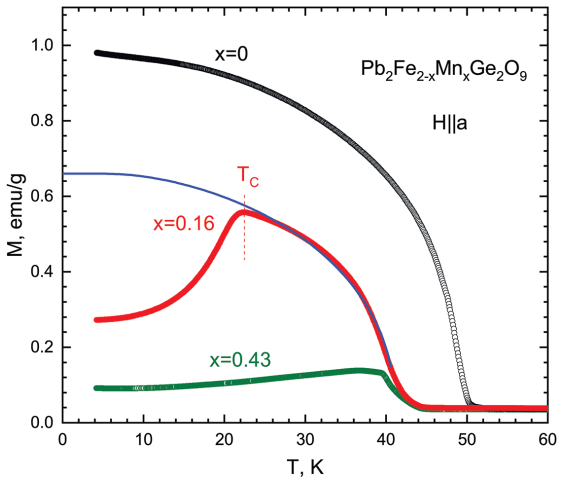

Fig. 1. Temperature dependences of magnetization for $Pb_2Fe_{2-x}Mn_xGe_2O_9$ single crystals with $x = 0$, 0.16, and 0.43 measured in a magnetic field $\mathbf{H} \parallel \mathbf{a}$, $H = 1$ kOe. From [10]

differences in the behavior of the temperature-dependent magnetization of the single crystals were observed for the magnetic field orientation $\mathbf{H} \parallel \mathbf{a}$. Fig. 1 shows the low-temperature portion of these dependences, measured in a magnetic field of 1 kOe. In the pristine crystal ($x = 0$), a magnetization induced by a weak ferromagnetic moment was observed for this orientation below the Néel temperature T_N. The signal increased monotonically upon cooling, following the temperature dependence expected for a spontaneous magnetic moment.

In the crystal with the maximum Mn^{3+} substitution level ($x = 0.43$), the magnetization measured for the same orientation is an order of magnitude smaller and remains virtually temperature-independent. In contrast, at an intermediate Mn^{3+} content ($x = 0.16$), the magnetization upon cooling below the Néel temperature initially exhibits behavior similar to that of the pure crystal. Then, upon reaching $T \approx 23$ K, a kink appears in the dependence, and the magnetization drops sharply with further cooling of the crystal.

In this crystal, the magnetization along the orthorhombic **b**- and **c**-axes also exhibits singularities at T_c, see Fig. 2. Specifically, along the **b**-axis, the magnetization remains almost constant from T_N down to T_c and then decreases upon further cooling. The opposite temperature behavior is observed along the orthorhombic **c**-axis: immediately below T_N, the magnetization shows a slight increase, then decreases until T_c, and below T_c it remains constant down to liquid helium temperature. Such behavior suggests that at T_c, the magnetic structure of the crystal with $x = 0.16$ undergoes a spontaneous phase transition. In contrast, for the crystals with $x = 0$ and $x = 0.43$, the temperature dependences of magnetization in the magnetically ordered region ($T < T_N$) are smooth for all three field orientations, indicating the absence of spontaneous phase transitions.

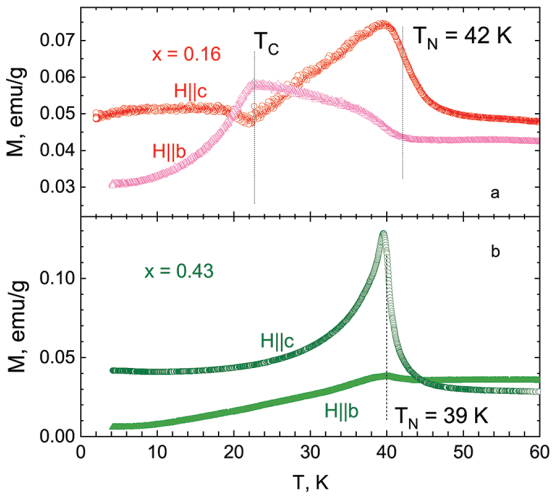

Fig. 2. Temperature dependences of magnetization for $Pb_2Fe_{2-x}Mn_xGe_2O_9$ single crystals with $x = 0.16$ and 0.43 measured in magnetic fields $\mathbf{H} \parallel \mathbf{b}$ and $\mathbf{H} \parallel \mathbf{c}$, $H = 1$ kOe. From [10, 11]

2.2. Field dependencies of the magnetization, x = 0, 0.16 and 0.43

It is convenient to begin the description of the field dependences of magnetization and the corresponding magnetic phase diagrams with the pure $Pb_2Fe_2Ge_2O_9$ single crystal. The magnetic properties of this crystal have been studied in Refs. [3,9]. The field dependences of magnetization for $Pb_2Fe_2Ge_2O_9$, measured at $T = 4.2$ K along the three orthorhombic axes, are shown in Fig. 3.

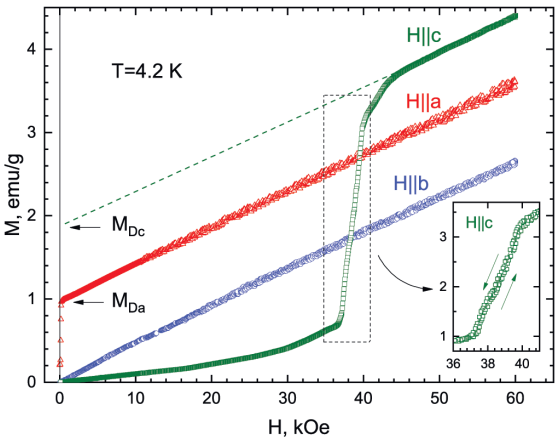

Fig. 3. Field dependences of the magnetization $Pb_2Fe_2Ge_2O_9$ single crystal measured at $T = 4.2$ K along the a-, b- and c-axes. From [9]

The dependences exhibit a form typical of an antiferromagnet with weak ferromagnetism. The spontaneous magnetic moment along the a-axis arises from the weak ferromagnetic canting of the antiferromagnetic sublattice moments in this direction. The field dependence of magnetization

for this orientation can be expressed as [14, 15]:

$$M_a = M_{Da} + \chi_\perp H = \chi_\perp (H_{Da} + H),$$
$$M_{Da} = \frac{H_{Da}}{H_E} M_0, \quad \chi_\perp = \frac{M_0}{H_E}, \tag{1}$$

Here, $M_{Da} = 0.99$ emu/g is the spontaneous weak ferromagnetic moment along the a-axis, $\chi_\perp = (4.33 \pm 0.005) \times 10^{-5}$ cm^3/g, H_{Da} is the Dzyaloshinskii effective field, and H_E is the exchange field. From the experimental data at $T = 4.2$ K, we obtained a value of $H_{Da} = 22.5$ kOe, which is close to the value of 21 kOe reported in Ref. [3]. In the calculation, we used $H_E = 780$ kOe, derived from the perpendicular susceptibility $\chi_\perp$, and a theoretical value of $M_0 = 230$ G.

In a magnetic field applied along the b-axis, the magnetization increases linearly up to 60 kOe. However, a sharp spin-flop transition is observed when the field is applied along the c-axis. This behavior indicates that the antiferromagnetic vector is directed along this axis. The critical field of the spin-flop transition is $H_C = 39$ kOe at $T = 4.2$ K. The weak hysteresis observed in the vicinity of the transition suggests that it is first-order. The temperature dependence of H_C has the typical form shown in Fig. 4.

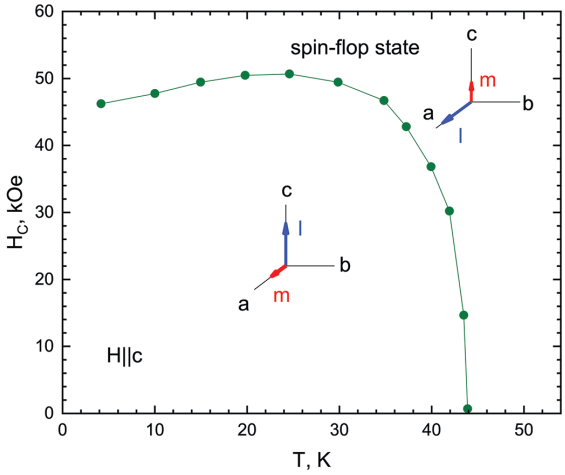

Fig. 4. Temperature dependence of the spin-flop critical field H_C for $Pb_2Fe_2Ge_2O_9$. Taken from [3]

Above the spin-flop transition field, the magnetization is described by an expression similar to Eq. (1), but with a different value of the spontaneous weak ferromagnetic moment, M_{Dc}, which exceeds M_{Da} by a factor of approximately 1.8. This value corresponds to a Dzyaloshinskii field of $H_{Dc} = 39.8$ kOe at $T = 4.2$ K. As shown in Ref. [14], the difference in the spontaneous moments measured along different orthorhombic axes arises from the different relative contributions of two mechanisms — Dzyaloshinskii–Moriya interaction and single-ion anisotropy — to the corresponding Dzyaloshinskii field:

$$H_{Dc} = D_{DM} + D_{si}, \qquad H_{Da} = D_{DM} - D_{si}. \tag{2}$$

Using Eq. (2), we determine the corresponding contributions at $T = 4.2$ K: $D_{DM} = 31.2$ kOe and $D_{SI} = 9.6$ kOe. Note that the Dzyaloshinskii–Moriya contribution dominates.

Given that all crystals of the $Pb_2Fe_{2-x}Mn_xGe_2O_9$ family possess the same *Pbcn* crystal structure, a common thermodynamic potential can be used to describe the magnetic structures.

This potential corresponds to a two-sublattice orthorhombic antiferromagnet with a second-order symmetry axis along the b-axis, relative to which the antiferromagnetic structure is even [14–16]:

$$F = \frac{A}{2}\mathbf{m}^2 + \frac{a_1}{2}m_x^2 + \frac{a_2}{2}m_y^2 + \frac{b_1}{2}l_x^2 + \frac{b_2}{2}l_z^2 + d_1 m_x l_z + d_2 m_z l_x - \mathbf{mh}, \qquad (3)$$

The expansion was made over the components of the ferromagnetic vector $\mathbf{m} = (\mathbf{M}_1 + \mathbf{M}_2)/(2M_0)$ and the antiferromagnetic vector $\mathbf{l} = (\mathbf{M}_1 - \mathbf{M}_2)/(2M_0)$; A is the exchange constant; a_1, a_2, b_1, and b_2 are the magnetic anisotropy constants; d_1 and d_2 are the constants at the invariants responsible for weak ferromagnetism; and $\mathbf{h} = \mathbf{H}\cdot 2M_0$. The indexes x, y, z correspond to orthorhombic axes a, b, c, respectively.

Eq. (3) shows that the weak ferromagnetic moment can only be formed in this crystal in the directions of the orthorhombic a- or c-axes. Moreover, according to the invariant $m_x l_z$, the moment in the a-axis direction can only exist at a nonzero component l_z of the antiferromagnetic vector, while the component l_x, due to the invariant $m_z l_x$, causes the moment m_z in the c-axis direction. This analysis confirms that in the $Pb_2Fe_2Ge_2O_9$ crystal, in weak magnetic fields, the antiferromagnetic vector $\mathbf{l}$ is directed along the orthorhombic c-axis, while the canting of the antiferromagnetic sublattices towards the a-axis creates a weak ferromagnetic moment in this direction.

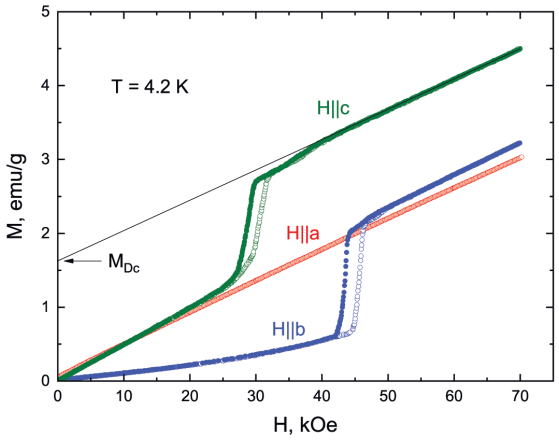

Fig. 5. Field dependences of magnetization for the $Pb_2Fe_{1.57}Mn_{0.43}Ge_2O_9$ crystal measured at $T = 4.2$ K in the three orthorhombic directions. From [11]

Let us now turn to the magnetic properties of the $Pb_2Fe_{2-x}Mn_xGe_2O_9$ crystal with the maximum Mn^{3+} ion content, $x = 0.43$ [11]. Fig. 5 presents field dependences of the magnetization measured on the crystal with $x = 0.43$ at $T = 4.2$ K along the three orthorhombic axes. In this case, the spontaneous weak ferromagnetism in the a-axis direction is absent. The magnetization jumps indicative of spin-reorientation transitions are observed in the directions of both the orthorhombic b- and c-axes. In both directions, the critical fields of the transition are temperature-dependent, tending to zero as the Néel temperature is approached. As an example, Fig. 6 shows a family of field dependences of the magnetization measured in the direction $\mathbf{H} \parallel \mathbf{c}$ at various temperatures. On the other hand, similar to the undoped $Pb_2Fe_2Ge_2O_9$ compound, under magnetization along the c-axis in fields above the orientational transition, a weak ferromagnetic state is also established and has the same weak ferromagnetic moment ($M_{Dc} \approx 1.8$ emu/g) as in the undoped crystal. Judging by the significant magnetic hysteresis in the region of spin-reorientation transitions, these transitions are first-order for both directions. The inset of Fig. 6 shows the temperature dependence of the weak ferromagnetic moment jump at the transition, which decreases monotonically as T_N is approached.

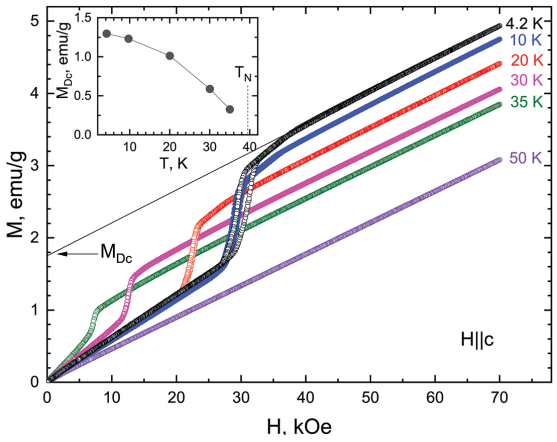

Fig. 6. Field dependences of magnetization for the $Pb_2Fe_{1.57}Mn_{0.43}Ge_2O_9$ crystal in the c-axis direction measured at different temperatures. Inset shows the temperature dependence of a jump of weak ferromagnetic moment at the transition. From [11]

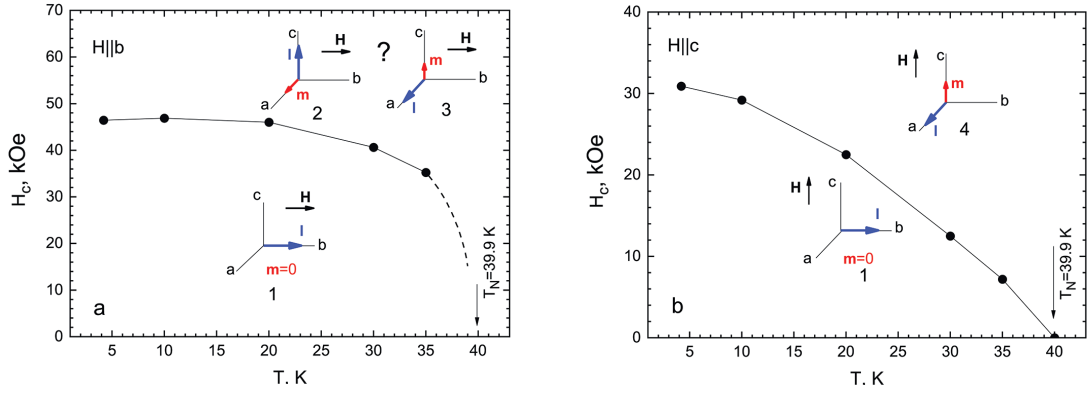

Fig. 7. Magnetic phase diagrams of the $Pb_2Fe_{1.57}Mn_{0.43}Ge_2O_9$ crystal at the magnetic field orientations (a) $\mathbf{H} \parallel \mathbf{b}$ and (b) $\mathbf{H} \parallel \mathbf{c}$. From [11]

The temperature dependences of the critical fields of the orientational transitions for the directions $\mathbf{H} \parallel \mathbf{b}$ and $\mathbf{H} \parallel \mathbf{c}$ are shown in Figs. 7a and 7b, which represent the magnetic phase diagrams for these two field directions. Let us now turn to the analysis of the possible magnetic states in different regions of these diagrams.

According to the form of the thermodynamic potential (3), which does not include the mixed invariants with l_y, the spontaneous weak ferromagnetism is absent in this case (see state 1 in Fig. 7a). The absence of spontaneous (i.e., for the magnetic field $\mathbf{H} \to 0$) weak ferromagnetism in this state is confirmed by the initial portions of the field dependences of magnetization for all orthorhombic axes (Fig. 5). Under magnetization along the b-axis, at low temperatures, the initial magnetic susceptibility ($\chi_\parallel$) below the critical field ($H < H_c$) is much weaker than the susceptibility ($\chi_\perp$) above the orientational transition; upon approaching the Néel temperature, this susceptibility difference decreases. Such a difference in susceptibilities, characteristic of a spin-flop transition, allows us to assert that in the ground state (as well as in weak magnetic fields) of the $Pb_2Fe_{1.57}Mn_{0.43}Ge_2O_9$ crystal, the antiferromagnetic vector $\mathbf{l}$ of the structure is directed along the orthorhombic b-axis, in contrast to the undoped crystal, where $\mathbf{l} \parallel \mathbf{c}$. Also noteworthy is the non-monotonic temperature dependence of the critical field H_C of the spin-flop

transition, with a maximum at $T \approx 10$ K; such behavior is inherent to this type of transition (compare with Fig. 4 for the undoped crystal).

The absence of the $m_y l_i$ invariants in the thermodynamic potential prevents the occurrence of weak ferromagnetism along the b-axis in the spin-flop state. However, in this state, weak ferromagnetism can arise in the transverse a or c direction, depending on orientation of the antiferromagnetic vector along the c- or a-axis in the spin-flop state (states 2 or 3 in Fig. 7a). Since, for this crystal, the anisotropy constants required for comparing the energies of these states are unknown, one of them can be chosen when measuring the field dependences of the transverse magnetization in the a- and c-axes directions for $\mathbf{H}\|\mathbf{b}$.

In this crystal, the most interesting case is magnetization along the c-axis, which is not of spin-flop nature and can be explained as follows. At this magnetization, when the magnetic field is perpendicular to the antiferromagnetic vector, the initial magnetization portion is determined by the magnetic susceptibility $\chi_\perp$. When a certain critical field is reached, the antiferromagnetic vector reorients stepwise to the orthorhombic a-axis direction, which is accompanied by a magnetization jump induced by the weak ferromagnetic moment occurring in the c-axis direction (state 4 in Fig. 7b, coinciding with state 3). As in the pure crystal, this moment is induced by the invariant $m_z l_x$ and the field dependence of the magnetization above the critical field is described by Eq. (3). Obviously, in this state, the field dependence is also determined by the perpendicular magnetic susceptibility $\chi_\perp$. The similar transitions were observed, for example, in orthorhombic antiferromagnets with weak ferromagnetism $YFeO_3$ and $YCrO_3$ [17, 18].

Thus, in the $Pb_2Fe_{1.57}Mn_{0.43}Ge_2O_9$ crystal, the magnetization jump of the spin reorientation in the c-axis direction is not related to the difference between the perpendicular and parallel susceptibilities, but originates from the occurrence of a weak ferromagnetic moment in the field-induced state. The different nature of the spin-reorientation transitions under magnetization along the b- and c-axes leads to different temperature dependences of the critical field what is observed in Figs. 7a and 7b.

Analysis of the magnetic structures of the $Pb_2Fe_{2-x}Mn_xGe_2O_9$ crystals with $x = 0$ and 0.43 showed that, after partial substitution of highly anisotropic Mn^{3+} ions for iron ions, the antiferromagnetic structure is preserved. However, due to the competition between the contributions of the iron and manganese subsystems, the magnetic phase diagrams of pure and Mn-substituted crystals are fundamentally different. In the undoped crystal, the magnetoanisotropic properties of which are only determined by the Fe^{3+} ion subsystem, the antiferromagnetic axis coincides with the orthorhombic c-axis. In this case, the slight sublattice canting induces a spontaneous weak ferromagnetic moment in the orthorhombic a-axis direction. Upon sufficiently strong substitution with $x = 0.43$, the contribution of the Mn^{3+} ion subsystem into the magnetic anisotropy of the crystal is dominant; therefore, the antiferromagnetic vector aligns in the orthorhombic b-axis direction and the weak ferromagnetism in the a-axis direction vanishes due to the symmetry prohibition. Thus, we can state that, in this crystal, the easy anisotropy axes for the iron and manganese ion subsystems are the c- and b-axes, respectively.

We examine also the magnetic properties and magnetic phase diagram of the single crystals $Pb_2Fe_{2-x}Mn_xGe_2O_9$ with the intermediate ($x = 0.16$) Mn^{3+} ion concentration [10]. Obviously, the competition of the contributions of the iron and manganese ion subsystems determines also the magnetic phase diagrams of this crystal. In this case, a Mn^{3+} content of $x = 0.16$ is fairly low; therefore, during the formation of magnetic structures, it may be important that the absolute values of the contributions of the iron and manganese subsystems may turn out to be similar in absolute value. It is known well that, if the absolute values of the competing contributions to the magnetic anisotropy are similar, inclined magnetic structures with an intermediate orientation of the antiferromagnetic vector $\mathbf{l}$ in one of the coordinate planes are often formed in a crystal. In particular, this is the cause for forming inclined magnetic structures in the $Pr_xY_{1-x}Fe_3(BO_3)_4$ crystals within a certain range of diamagnetic dilutions [6, 20]. Numerous cases of the formation of inclined magnetic structures were reported for rare-earth orthoferrites [19], the anisotropic

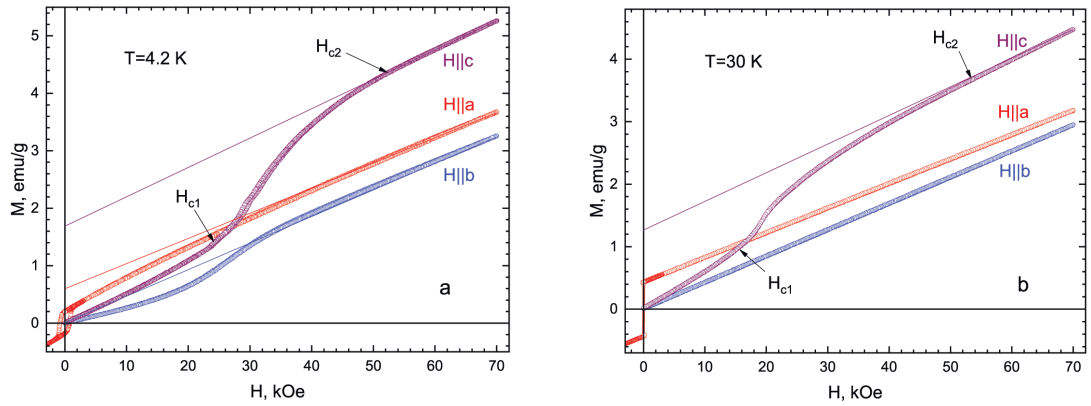

Fig. 8. Field dependences of the magnetization for the $Pb_2Fe_{1.84}Mn_{0.16}Ge_2O_9$ single crystal measured in the three orthorhombic directions at temperatures of T = (a) 4.2 and (b) 30 K. From [10]

properties of which are determined by the competition between the contributions of the iron and rare-earth ion subsystems.

The temperature dependences of the magnetization of $Pb_2Fe_{1.84}Mn_{0.16}Ge_2O_9$ presented above (Figs. 1 and 2) exhibit a spontaneous reorientation at T_c = 23 K. This finding corroborates the hypothesis of competing anisotropic contributions from the iron and manganese subsystems, which are comparable in magnitude. However, a comprehensive analysis of the magnetic structures and the construction of phase diagrams require the incorporation of field-dependent magnetization data acquired at various temperatures.

The field dependences of the magnetization also exhibit distinct behaviors in the temperature regions above and below T_c. Figs. 8a and 8b show the magnetization curves measured along the three orthorhombic axes at temperatures below and above T_c, respectively. At T = 4.2 K (Fig. 8a), the field dependences measured along the b- and c-axes are qualitatively similar to those of the crystal with x = 0.43. In both crystals, the magnetization increases nonlinearly after a certain threshold field. Above T_c (Fig. 8b), this behavior persists only for the $\mathbf{H}\|\mathbf{c}$ direction. In contrast, for $\mathbf{H}\|\mathbf{b}$, the magnetization depends linearly on the magnetic field over the entire range studied (up to 70 kOe).

The shape of the magnetization curves also changes for the $\mathbf{H}\|\mathbf{a}$ geometry. At T = 4.2 K, a wide hysteresis loop with a small remanent magnetization is observed, accompanied by a nonlinear field dependence. This contrasts with the x = 0.43 crystal, which exhibits no weak ferromagnetism in this direction. At temperatures above T_c, the remanent magnetization increases, and the field dependence becomes linear across the entire investigated field range.

A key issue in interpreting the magnetic study results and constructing the phase diagrams is the weak ferromagnetic moment — specifically, its existence, orientation, and magnitude.

We first consider the field dependences of the magnetization along the orthorhombic c-axis, shown in Figs. 8a and 8b. Notably, for all temperatures below T_N, the initial segments of these curves are linear and pass through the origin. This indicates the absence of a weak ferromagnetic moment ($m_z = 0$) in zero and low magnetic fields. According to the thermodynamic potential in Eq. (1), the weak ferromagnetic moment along the c-axis is governed by the invariant $m_z l_x$. Therefore, the observed behavior requires $l_x = 0$, implying that the antiferromagnetic vector $\mathbf{l}$ is confined to the bc plane. This conclusion is consistent with the proposed scenario in which the magnetic anisotropy arises from competing contributions from the Fe^{3+} and Mn^{3+} subsystems, whose easy axes are the orthorhombic c- and b-axes, respectively.

To determine the orientation of the antiferromagnetic vector within the bc plane, we now

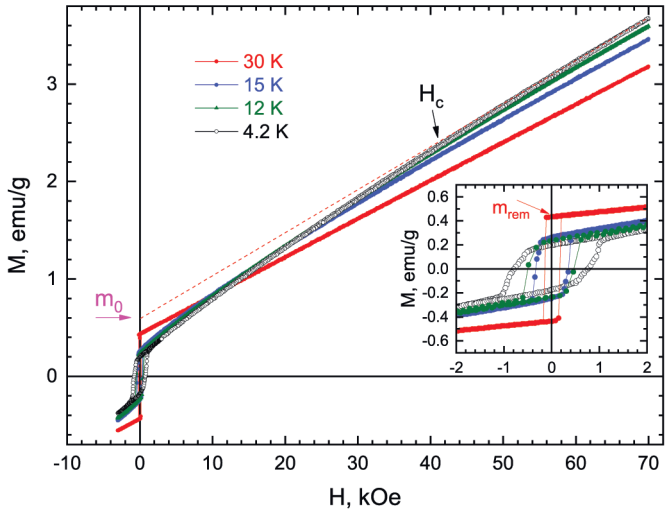

Fig. 9. Field dependences of the magnetization for the $Pb_2Fe_{1.84}Mn_{0.16}Ge_2O_9$ crystal in magnetic field **H** ∥ **a** at constant temperatures. Inset: enlarged hysteresis loops. From [10]

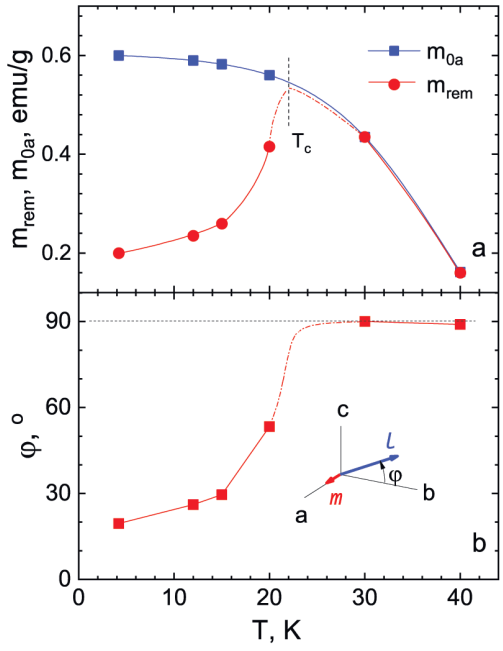

Fig. 10. Temperature dependences of (a) the remanent moment m_{rem} and weak ferromagnetic moment m_{0a} and (b) the angle between the orthorhombic b-axis and antiferromagnetic vector l in the *bc* plane. From [10]

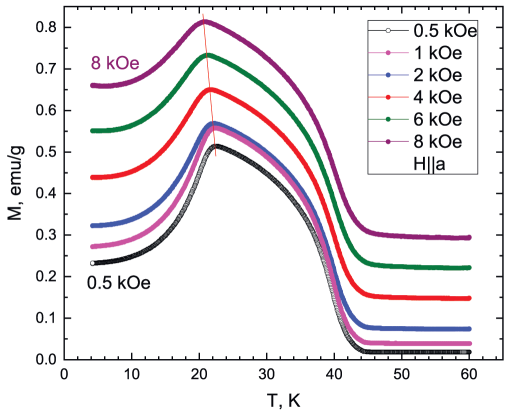

Fig. 11. Temperature dependences of the magnetization for the $Pb_2Fe_{1.84}Mn_{0.16}Ge_2O_9$ crystal in fixed magnetic fields **H** ∥ **a**. From [10]

examine the magnetic data for **H** ∥ **a** (Fig. 9). In this orientation, hysteresis loops characteristic of a weak ferromagnetic moment — arising from the invariant $m_x l_z$ — are observed at all

temperatures below T_N. The persistence of these loops implies that the component l_z is nonzero throughout the entire magnetically ordered region.

We propose that the remanent magnetization m_{rem} represents the portion of the weak ferromagnetic moment arising from the projection l_z of the antiferromagnetic vector $\mathbf{l}$ as it assumes an intermediate orientation within the bc plane. Conversely, the moment m_{0a} corresponds to the maximum weak ferromagnetic moment, achieved when $l_z = 1$.

For an arbitrary in-plane orientation of the vector $\mathbf{l}$ within the bc-plane, the remanent magnetization m_{rem} is governed by the equation [13]:

$$m_{rem} = M_0 \frac{H_D}{H_E} l_z, \tag{4}$$

where H_E and H_D denote the effective fields of the exchange and Dzyaloshinskii-Moriya interactions, respectively. The magnetic moment m_{0a} is also described by Eq. (4) for the case $l_z = 1$. By combining Eq. (4) with the experimentally observed ratio m_{rem}/m_{0a}, we can extract both the component l_z and the in-plane angle ϕ between the vector $\mathbf{l}$ and the crystallographic b-axis. At $T = 4.2$ K, we obtain $\phi = 20°$. The temperature evolution of this angle is presented in Fig. 10b.

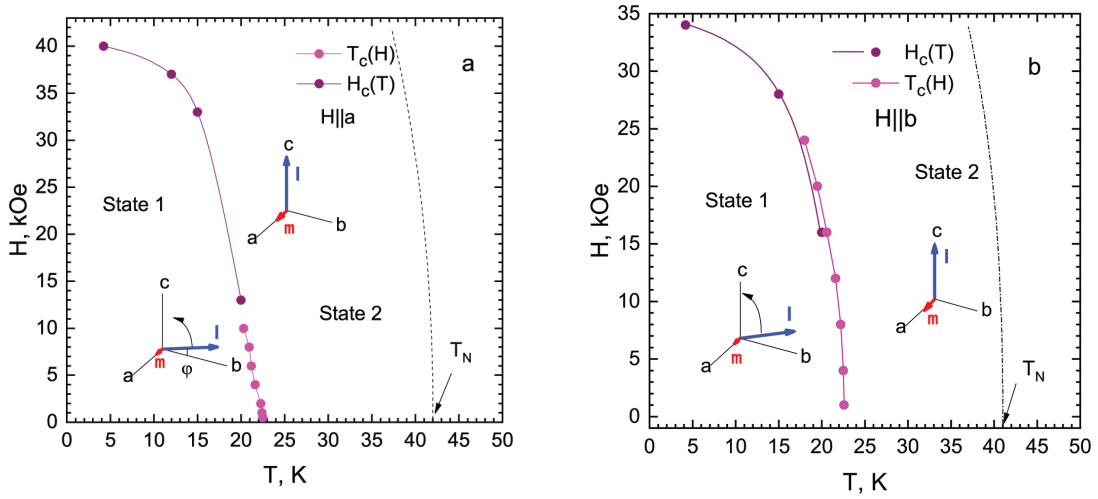

Fig. 12. Magnetic phase diagrams of the $Pb_2Fe_{1.84}Mn_{0.16}Ge_2O_9$ crystal at the magnetic field orientations: a – $\mathbf{H} \parallel \mathbf{a}$ and b – $\mathbf{H} \parallel \mathbf{b}$. From [10]

Thus, in the temperature range 4.2 K $< T < T_c$, the antiferromagnetic vector $\mathbf{l}$ undergoes a smooth rotation within the bc plane, from an initial intermediate orientation towards the orthorhombic c-axis. The absence of hysteresis in the vicinity of T_c indicates that this rotation ends with a second-order phase transition at $T = T_c$, at which point $\mathbf{l}$ becomes aligned with the c-axis.

The proposed magnetic structure offers a coherent explanation for the temperature dependences of the magnetization measured in fixed fields $\mathbf{H} \parallel \mathbf{a}$. The rotation of $\mathbf{l}$ towards the c-axis enhances the projection l_z, which in turn increases the remanent magnetization m_{rem} and accounts for the growth in magnetization as the temperature T_c is approached. Above this temperature, the measured magnetization is governed primarily by the temperature-dependent weak ferromagnetic moment m_{0a}.

In the resulting magnetic phase diagram for $\mathbf{H} \parallel \mathbf{a}$ (Fig. 12a) which is constructed from temperature and field dependences of magnetization [10], the field dependence of T_c defines the phase boundary, separating the inclined phase (State 1) from State 2.

As in the previous field geometry, the critical temperature T_c for $\mathbf{H} \parallel \mathbf{b}$ decreases with increasing field (Fig. 12b). Due to the inclined nature of the magnetic structure in State 1, the magnetization measured along the b-axis at $T < T_c$ comprises both parallel and perpendicular susceptibility contributions, with the latter typically dominating at low temperatures. Furthermore, in this orientation, the antiferromagnetic vector rotates not only with temperature but also with magnetic field for $T < T_c$. This rotation ends at the critical field H_c, where the nonlinear magnetization due to the perpendicular susceptibility becomes linear. The phase diagram (Fig. 12b), which is qualitatively similar to that for $\mathbf{H} \parallel \mathbf{a}$, features a common boundary between the rotating inclined phase (State 1) and State 2. The boundary is determined from the $T_c(H)$ and $H_c(T)$ curves, which show good agreement in the field range of 15–25 kOe.

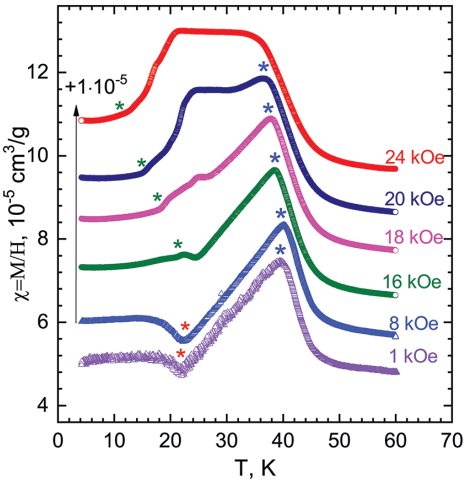

Fig. 13. Temperature dependences of the magnetization for the $Pb_2Fe_{1.84}Mn_{0.16}Ge_2O_9$ crystal normalized to the measurement field at fixed magnetic fields $\mathbf{H} \parallel \mathbf{c}$. From [10]

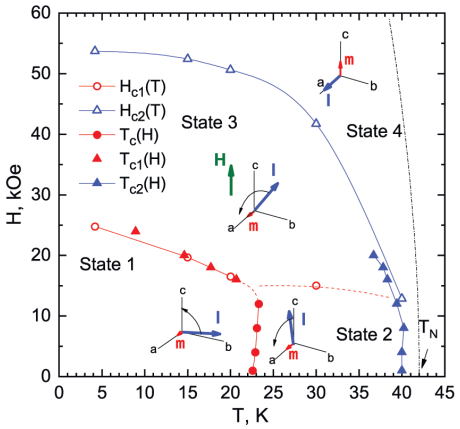

Fig. 14. Phase diagram of the $Pb_2Fe_{1.84}Mn_{0.16}Ge_2O_9$ crystal in magnetic field $\mathbf{H} \parallel \mathbf{c}$. From [10]

Of particular interest is the magnetic phase diagram for $\mathbf{H} \parallel \mathbf{c}$. Unlike the previous two field orientations, the rotation of the antiferromagnetic vector here occurs in a more complex way. This complexity stems from the magnetization behavior observed in the crystal with $x = 0.43$: in the Mn-substituted sample, this field configuration induces a rotation of the antiferromagnetic vector toward the orthorhombic a-axis.

Following the procedure used for the other two field orientations, the magnetic phase diagram for $\mathbf{H} \parallel \mathbf{c}$ was constructed from magnetization data. We analyzed both the field dependences measured at fixed temperatures and the temperature dependences obtained at fixed magnetic fields, as shown in Fig. 13. Based on their shape, the curves in this Figure fall into two distinct groups.

In weak magnetic fields ($H < 16$ kOe), the antiferromagnetic vector $\mathbf{l}$ rotates smoothly toward the c-axis with increasing temperature in the region below T_c (marked by red asterisks in Fig. 13). At $T = T_c$, the vector $\mathbf{l}$ becomes oriented along (or close to) this axis, resulting in a local minimum in the temperature dependence due to the contribution of the parallel magnetic susceptibility. The temperature T_c marks the boundary between State 1 and State 2 (see the phase diagram in Fig. 14). Above T_c (State 2), the vector $\mathbf{l}$ rotates toward the a-axis, and its projection l_x appears and increases with temperature. This rotation is accompanied by an almost linear increase in magnetization, caused by the growth of the weak ferromagnetic moment induced by the invariant $m_z l_x$. This process continues up to $T = T_{c2}$ (marked by blue asterisks

in Fig. 13), where the system transitions to State 4. In State 4, the magnetization decreases as the Néel temperature is approached.

In strong fields ($H > 18$ kOe), the field dependences for $\mathbf{H} \parallel \mathbf{c}$ (Figs. 8a and 8b) reveal that the rotation of $\mathbf{l}$ toward the a-axis also takes place at fixed temperatures with varying magnetic field. This rotation initiates at H_{c1} within State 3 and is manifested as a nonlinear increase in the magnetization field dependences, reflecting the onset of a weak ferromagnetic moment m_{0c} along the c-axis. An identical nonlinear magnetization growth is observed in the temperature dependences measured at fixed fields above 18 kOe for $T > T_{c1}$ (indicated by green asterisks in Fig. 13). For $T < T_c$, this rotation naturally commences from a temperature-dependent intermediate orientation of $\mathbf{l}$ within the bc-plane. Regardless of temperature (for $T < T_N$), the rotation of $\mathbf{l}$ culminates at the critical field H_{c2}, beyond which the field dependence of the magnetization becomes linear (Figs. 8a and 8b). The $H_{c2}(T)$ and $T_{c2}(H)$ curves form a common boundary with State 4, where $\mathbf{l}$ is oriented along the a-axis and the antiferromagnetic sublattices are canted along the c-axis.

It is worth mentioning that an important result of Refs. [9–11] was the discovery of sharp anomalies in the magnetodielectric properties, which were observed in crystals with $x = 0$ and $x = 0.43$ in the vicinity of certain spin-reorientation transitions. However, a discussion of the magnetodielectric properties of the investigated crystals lies beyond the scope of this paper, which is limited to studying the effect of substituting iron ions with highly anisotropic manganese ions on the magnetic structures and phase diagrams of $Pb_2Fe_{2-x}Mn_xGe_2O_9$ crystals.

Conclusion

We have performed a detailed investigation of the temperature and field dependences of the magnetization and constructed the magnetic phase diagrams for three single crystals of orthorhombic antiferromagnets from the $Pb_2Fe_{2-x}Mn_xGe_2O_9$ family: the pure compound ($x = 0$) as well as crystals with strong ($x = 0.43$) and intermediate ($x = 0.16$) substitution of Fe^{3+} ions by highly anisotropic Mn^{3+} ions.

A comparison of the magnetic phase diagrams of the pure $Pb_2Fe_2Ge_2O_9$ and the strongly substituted $Pb_2Fe_{1.57}Mn_{0.43}Ge_2O_9$ crystals reveals that the partial substitution of iron ions with highly anisotropic Mn^{3+} ions leads to a dramatic change in the magnetic phase diagram. In contrast to the ground state of the undoped crystal, where $\mathbf{l} \parallel \mathbf{c}$, the antiferromagnetic vector in the doped crystal reorients to the b-axis, and the weak ferromagnetism vanishes.

For the crystal with intermediate substitution ($x = 0.16$), the magnetoanisotropic contributions of the Fe^{3+} and Mn^{3+} ion subsystems are comparable in magnitude. Their competition gives rise to a spontaneous spin-reorientation transition at $T_c = 22$ K. The temperature of this transition depends on the strength and orientation of an applied magnetic field relative to the crystal's orthorhombic axes. Analysis of the magnetization data as a function of temperature and field for various orientations reveals that below T_c the crystal hosts an inclined magnetic structure. Within this structure, the antiferromagnetic vector undergoes a smooth rotation in the orthorhombic bc-plane as the temperature increases: it evolves from a direction close to the b-axis at $T = 4.2$ K toward the orthorhombic c-axis at $T = T_c$. This rotation also occurs at fixed temperatures below T_c upon increasing the magnetic field. In the temperature range $T_c < T < T_N$ for fields applied along the a- or b-axis, the antiferromagnetic vector is oriented along the orthorhombic c-axis.

Magnetic phase diagrams of the $Pb_2Fe_{1.84}Mn_{0.16}Ge_2O_9$ crystal were constructed in the field-temperature plane for various orientations of the magnetic field with respect to the crystal's orthorhombic axes. The most complex phase diagram is observed for $\mathbf{H} \parallel \mathbf{c}$. In addition to the states listed above, it features an additional inclined phase, where the antiferromagnetic vector rotates toward the orthorhombic a-axis as a function of temperature or magnetic field.

This study was carried out within the State Assignment of the Ministry of Science and Higher Education of the Russian Federation for the Kirensky Institute of Physics, Siberian Branch of the Russian Academy of Sciences.

References

[1] D.I.Khomskii, Multiferroics: Different ways to combine magnetism and ferroelectricity, *J. Magn. Magn. Mater.*, **306**(2006), 1. DOI: 10.1016/j.jmmm.2006.01.238

[2] S.Ivanov, R.Tellgren, H.Rundlof, N.Thomas, S.Ananta, Investigation of the structure of the relaxor ferroelectric $Pb(Fe_{1/2}Nb_{1/2})O_3$ by neutron powder diffraction, *J. Phys.: Condens. Matter*, **12**(2000), 2393. DOI: 10.1088/0953-8984/12/11/305

[3] G.A.Petrakovskii, M.A.Popov, A.D.Balaev et al., Magnetic properties of $Pb_2Fe_2Ge_2O_9$ single crystals, *Phys. Solid State*, **51**(2009), 1745. DOI: 10.1134/S1063783409090145

[4] A.A.Demidov, I.A.Gudim, E.V.Eremin, Magnetic properties of $Sm_0.7Ho_0.3Fe_3(BO_3)_4$, *JETP*, **115**(2012), 815.

[5] A.K.Zvezdin, A.M.Kadomtseva, Yu.F Popov et al., Magnetic anisotropy and magnetoelectric properties of $Tb_{1?x}Er_xFe_3(BO_3)_4$ ferroborates, *JETP*, **109**(2009), 68.

[6] C.Ritter, A.I.Pankrats, A.A.Demidov, D.A.Velikanov, V.L.Temerov, I.A. Gudim, Inclined magnetic structure of iron borate $PrY_{1-x}Fe_3(BO_3)_4$: a neutron diffraction study and crystal-field calculations, *Phys. Rev. B*, **91**(2015), 134416.

[7] A.Pankrats, M.Kolkov, A.Balaev, A.Shabanov, A.Vasiliev, Forming a ferrimagnetic-like structure in the $PbMn_{1-x}Fe_xBO_4$ (x=0.1) single crystal upon partial substitution, *J. Magn. Magn. Mater.*, **497**(2020), 165997.

[8] A.Pankrats, K.Sablina, M.Eremin et al., Ferromagnetism and strong magnetic anisotropy of the $PbMnBO_4$ orthoborate single crystals, *J. Magn. Magn. Mater.*, **414**(2016), 82.

[9] A.I.Pankrats, D.A.Balaev,S.E.Nikitin et al., Magnetic and thermodynamic properties and spin-flop-driven magnetodielectric response of the antiferromagnetic $Pb_2Fe_2Ge_2O_9$ single crystals, *J. Magn. Magn. Mater.*, **479**(2019), 114. DOI: 10.1016/j.jmmm.2019.02.026

[10] A.I.Pankrats, A.D.Balaev, S.A.Skorobogatov et al., Inclined Magnetic Structures and Magnetic Phase Diagrams for the $Pb_2Fe_{2-x}Mn_xGe_2O_9$ ($x = 0.16$) Single Crystal, *J. Magn. Magn. Mater.*, **563**(2022), 170021. DOI: 10.1016/j.jmmm.2022.170021

[11] A.Pankrats, M.Kolkov, A.Balaev, A.Freidman, A.Vasiliev, D.Balaev, Comparative study of the magnetic phase diagrams and spin-flop-driven magnetodielectric responses of the pure and Mn^{3+}-Doped $Pb_2Fe_2Ge_2O_9$ single crystals, *J. Magn. Magn. Mater.*, **534**(2021), 168023. DOI: 10.1016/j.jmmm.2021.168023

[12] J.Barbier, D.Levy, $Pb_2Fe_2Ge_2O_9$, the germanate analogue of the silicate mineral melanotekite, *Acta Cryst. C*, **54**(1998), 2.

[13] A.D.Balaev, Yu.V.Boyarshinov, M.M.Karpenko, B.P.Khrustalev, Prib. Tekh. Eksp. **3**(1985), 167tt.

[14] E.A.Turov, Physical properties of magnetically ordered crystals, Academic, New York, 1965.

[15] E.A.Turov, A.V.Kolchanov, V.V.Men'shenin, I.F.Mirsaev, V.V.Nikolaev, Symmetry and Physical Properties of Antiferromagnets, Fizmatlit, Moscow, 2001 (in Russian).

[16] S.N.Martynov, Single-ion mechanism of weak ferromagnetism and a spin-flop transition in one- and two-position antiferromagnets, *JETP Lett.*, **108**(2018), 196.

[17] V.M.Judin, A.B.Sherman, I.E.Mylnikova, Magnetic properties of $YFeO_3$, *Phys. Lett.*, **22**(1966) 554.

[18] J.S.Jacobs, H.F.Burne, L.M.Levinson, Field—induced spin reorientation in $YFeO_3$ and $YCrO_3$, *J. Appl. Phys.*, **42**(1971) 1631.

[19] K.P.Belov, A.K.Zvezdin, A.M.Kadomtseva, R.Z.Levitin, *Orientational Transitions in Rare-Earth Magnets*, Nauka, Moscow, 1979 (in Russian).

[20] A.I.Pankrats, S.M.Zharkov, G.M.Zeer, I.A.Gudim, Antiferromagnetic resonance and magnetic anisotropy in $Pr_xY_{1-x}Fe_3(BO_3)_4$ crystals in the region of the magnetic structure transformation «easy axis – easy plane», *Journal of Alloys and Compounds*, **909**(2022), 164821. DOI: 10.1016/j.jallcom.2022.164821.

Управление магнитной структурой и фазовой диаграммой орторомбических антиферромагнетиков $Pb_2Fe_{2-x}Mn_xGe_2O_9$ с помощью замещения Mn

Анатолий И. Панкрац
Институт физики им. Л. В. Киренского
Федеральный исследовательский центр КНЦ СО РАН
Красноярск, Российская Федерация

Аннотация. Работа представляет собой обзор исследований магнитных свойств и магнитных фазовых диаграмм трех изоструктурных орторомбических антиферромагнетиков семейства $Pb_2Fe_{2-x}Mn_xGe_2O_9$, с $x = 0$; 0.16 и 0.43. В чистом $Pb_2Fe_2Ge_2O_9$ магнитные свойства определяются только магнитными S-ионами Fe^{3+}. Магнитная структура этого кристалла характеризуется вектором антиферромагнетизма, ориентированным вдоль орторомбической оси c и слабоферромагнитным моментом вдоль оси a. Частичное замещение ионов Fe^{3+} сильноанизотропными ионами Mn^{3+} приводит к тому, что в кристалле с наиболее сильным замещением ($x = 0.43$) антиферромагнитный вектор переориентируется к направлению орторомбической оси b, при этом слабый ферромагнетизм пропадает. При промежуточном уровне замещения ($x = 0.16$) конкуренция анизотропных вкладов подсистем ионов Fe^{3+} и Mn^{3+} приводит к появлению спонтанного спин-переориентационного перехода при $T_c = 22$ K. Температурные и полевые зависимости намагниченности всех трех кристаллов анализировались на основе термодинамического потенциала, записанного с учетом элементов симметрии. На основе анализа построены фазовые диаграммы «магнитное поле — температура» для всех кристаллов при различных ориентациях поля относительно орторомбических осей.

Ключевые слова: антиферромагнетизм, слабый ферромагнетизм, спин-переориентационный переход, магнитные фазовые диаграммы, замещение Mn.

EDN: NUKMSY
УДК 621.793.18

The Stochastic Magnetic Microstructure Study of FeZrN Ferromagnetic Films Using Correlation Magnetometry

Eugene V. Harin*
Elena N. Sheftel
Valentin A. Tedzhetov†
Galina Sh. Usmanova
Igor O. Bannykh‡
Baikov Institute of Metallurgy and Materials Science RAS
Moscow, Russian Federation

Received 10.02.2026, received in revised form 27.03.2026, accepted 27.04.2026

Abstract. This article provides a brief literature review on the development of models describing the magnetization process in ferromagnets and the law of the approach to saturation magnetization (Akulov's law). An analytical approach for estimating the magnitude of effective local (inside the grain) magnetic anisotropy and the parameters of the magnetization autocorrelation function (on the stochastic domain scale) was developed by V. A. Ignatchenko and co-authors and it was called correlation magnetometry. Our experimental results are presented, confirming the applicability of the law of the approach to saturation magnetization and the correlation magnetometry method, in particular, to ferromagnetic FeZrN films.

Keywords: magnetron deposition, nanocrystalline films, X-ray diffraction, bcc Fe phase, magnetic microstructure, random anisotropy model, correlation magnetometry.

Citation: E.V. Harin, E.N. Sheftel, V.A. Tedzhetov, G.Sh. Usmanova, I.O. Bannykh, The Stochastic Magnetic Microstructure Study of FeZrN Ferromagnetic Films Using Correlation Magnetometry, J. Sib. Fed. Univ. Math. Phys., 2026, 19(4), 506–521. EDN: NUKMSY.

Introduction

Since 2000s, the authors have been engaged in interdisciplinary research, i.e., metal physics, physics of magnetic phenomena, materials science and technology for producing soft magnetic film materials. These studies are aimed at creating ferromagnetic Fe-based films with a nanocrystalline structure, the properties of which meet the requirements of constantly evolving magnetic electronics. Special attention is paid to the study of physical processes that determine the magnetic properties. The processes occurring at different levels of film structure are (1) the interaction of Fe ions with its environment (ions of other elements, Mössbauer spectroscopy), which determines the type of formed phases (crystalline and amorphous) and their magnetic state (ferromagnetic, paramagnetic, etc.), and (2) the exchange interaction between grains of ferromagnetic phase (correlation magnetometry), which determines the magnetic microstructure of films described by the random anisotropy model. It all started with a meeting with Rauf Sadykovich Iskhakov and Sergey Viktorovich Komogortsev at a conference in Yekaterinburg in 2007, who introduced us to the method of correlation magnetometry. Our collaborations with them [1–3] became our universities for the mastering of this method.

*ekharin@imet.ac.ru https://orcid.org/0000-0002-2068-5313
† https://orcid.org/0000-0003-3733-9713
‡ https://orcid.org/0000-0002-1866-9242

This article provides a brief literature review on the development of models describing the magnetization process of ferromagnets and the law of the approach to saturation magnetization (LASM). The analytical approach that makes it possible to estimate the magnitude of the effective local (inside the grain) magnetic anisotropy and the parameters of the autocorrelation function (on the scale of the stochastic domain) of magnetization was developed by Valter Alekseevich Ignatchenko and co-authors, and it was called correlation magnetometry. Our experimental results are presented, indicating the applicability of LASM and the method of correlation magnetometry to ferromagnetic FeZrN films of various chemical and phase compositions.

1. A brief history of the development of models describing the process of the approach to saturation magnetization

Ferromagnets below the Curie temperature have spontaneous magnetization, the measurement of which is not a trivial task. In the case of a single-phase polycrystal (or a randomly oriented single crystal), in order to equate the magnitude of its saturation magnetization M_s with spontaneous magnetization, it is necessary to extrapolate the measured magnetization M to an infinitely large magnetic field H. For this purpose, before the discovery of the physical laws describing the magnetization process of ferromagnets, the empirical LASM was used [4].

The event that advanced the development of physical models of the magnetization process of ferromagnets was the discovery by N. S. Akulov of the law of magnetocrystalline anisotropy [5]. This law made it possible to calculate the magnetic anisotropy constant K for an arbitrary orientation of a single crystal. Later, considering the energy of magnetic anisotropy of isotropic polycrystals, N.S. Akulov obtained a simple analytical expression for the LASM

$$M/M_s = 1 - cK^2/(HM_s)^2, \tag{1}$$

where c is a dimensionless coefficient that depends on the polycrystal structure [6]. Akulov's law does not take into account the exchange and dipole-dipole interactions between crystallites, therefore it is applicable to magnetization curves only in sufficiently high fields. At the same time, the introduction of the coefficient $(1/2)$ in the LASM

$$M/M_s = 1 - (1/2)cK^2/(HM_s)^2 \tag{2}$$

allows taking into account the dipole-dipole interaction in Akulov's law in external fields $H << 4\pi M_s$ [7].

It is known that the magnetization process, expressed as a magnetization curve, is influenced by different types of magnetic anisotropy. Magnetic anisotropy also determines the dependence of different properties on the external magnetic field. At the same time, the LASM, similar to Akulov's law, work for magnetostriction [8], magnetoelastic anisotropy caused by stresses of various nature [9, 10], for elastic modulus [11] and magnetoresistance [12]. It should be noted that the dipole-dipole interaction provides a modification [13] of the law of the approach to saturation magnetostriction similar to Akulov's law [7].

Further development of Akulov's law, obtained for an isotropic polycrystal, went in the directions of modeling various structural defects:

- textures of polycrystals [14];
- amorphous state [15];
- adding new terms of the form $M/M_s \sim 1 - 1/H^{1/2} - 1/H - 1/H^{3/2} - 1/^2 - \ldots$ to the dependency describing the LASM, where a certain type of defect was attributed to each power term [16–19].

A qualitatively different (model-free) approach was used by V. A. Ignatchenko and co-authors, based on the consideration of the spectral density of random functions describing the parameters

of the microstructure. This intermediate level of abstraction (the intermediate correlation function between structure and properties) allows this approach to be applied to any properties at the scale of a microstructure. This approach allows us to obtain the parameters of the magnetic microstructure from:

- the width of the ferromagnetic resonance line [20, 21];
- spin-wave resonance [22–24];
- the use of LASM in a magnetic field where the exchange interaction between grains is not suppressed by an external field (the magnitude of the magnetic field is below the field range of Akulov's law) [25, 26].

The latter case, called correlation magnetometry, is the most widespread [27, 28]. The method of correlation magnetometry makes it possible to determine not only the effective local (inside the grain) magnetic anisotropy from Akulov's law, but also the parameters of the autocorrelation function of magnetization (stochastic domain), determined by the competition of exchange interaction and local magnetic anisotropy. It should be noted that correlation magnetometry can estimate only a part of the parameters of the stochastic domain, whereas direct observations of the magnetization distribution are needed to determine the type of correlation function [3, 29].

2. Random anisotropy model and correlation magnetometry

The length of the exchange interaction R_L (magnetic autocorrelation radius) in nanocrystalline ferromagnets exceeds the grain size $2R_c$ (R_c is structural autocorrelation radius). As a result, the effective local magnetic anisotropy is averaged out on the scale of the exchange interaction; this leads to a correlation of magnetization on the $2R_L$ scale (random anisotropy model [30]). Such regions of magnetization are called stochastic domains $2R_L$, which are characterized by effective magnetic anisotropy $<K_{eff}>$, which determines the coercive field H_c of the material.

For H_c analysis, the widely used random anisotropy model establishes a dependence of the coercive field on the grain size of $2R_c$ to the sixth power, $H_c \sim {K_{eff}}^4 (2R_c)^6/(M_s A^3)$, where K_{eff} is the effective local magnetic anisotropy, and A is the exchange stiffness [31]. The reason for this dependence is the exchange interaction between grains, which suppresses local magnetic anisotropy [32].

When such a material is magnetized, three processes occur simultaneously, which, as the external magnetic field increases, dominate each other in sequence: (1) rotation of the magnetization of the entire stochastic domains, (2) a gradual decrease in the size of the stochastic domains down to the size of a ferromagnetic grain, and (3) rotation of the magnetization vectors inside individual grains. The description of these processes using autocorrelation functions is the basis of correlation magnetometry [32]. The latter consists of an analysis of the magnetization dispersion curves $d_m = f(H)$ (where $d_m = 1 - M(H)/M_s$) plotted on a log-log scale (Fig. 1a).

In the fields $H > H_R$ (the third process from the previous paragraph), there is no exchange correlation between the magnetization vectors in neighboring grains, and the magnetization process occurs by rotating the magnetization vectors inside the $2R_c$ regions. At $H > H_R$, the magnetization dispersion in the samples follows Akulov's law (green line in Fig. 1a):

$$d_m = \frac{1}{2}\left(\frac{D^{1/2} H_a}{H}\right)^2, \tag{3}$$

where H_a is the effective local anisotropy field corresponding to the radius R_c (we assume it to be equal to the radius of the grain) and D is the dispersion of anisotropy axes, which is equal to $1/15$ for randomly oriented uniaxial anisotropy axes. In the fields $H_L < H < H_R$ (the second process), the magnetization curve is described by the function (yellow line in Fig. 1a)

$$d_m = \frac{1}{2}\frac{(D^{1/2}H_a)^2}{H_R^{3/2}H^{1/2}}, \tag{4}$$

which indicates the existence of stochastic domains in the samples. H_R is the intersection field of Eq. (3) and (4). In the range $H < H_L$ (the first process), Akulov's law applies for the rotation of stochastic domains (red line in Fig. 1a)

$$d_m = \frac{1}{2}\left(\frac{D^{1/2}\langle H_a\rangle_2}{H}\right)^2. \tag{5}$$

H_L is the intersection field of Eq. (4) and (5).

At the same time, according to [33], the fitting of experimental magnetization curves (blue line in Fig. 1b) using the Eq.

$$M(H) = M_s[1 - (1/2)(D^{1/2}H_a)^2/(H^2 + H^{1/2}H_R^{3/2})], \tag{6}$$

in contrast to the consideration of $d_m = f(H)$, it allows us to determine simultaneously the saturation magnetization value M_s, the rms fluctuation of the local magnetic anisotropy field (inside the grain) $D^{1/2}H_a$ and the correlation field H_R. These values allow us to estimate the rms fluctuation of the anisotropy field of the stochastic domain $D^{1/2} < H_a >= (D^{1/2}H_a)^4/H_R^3 = 2D^{1/2} < K_{eff} > /M_s \approx H_c$ and the relative radius of the stochastic domain $R_L/R_c = (H_R/D^{1/2}H_a)^2$

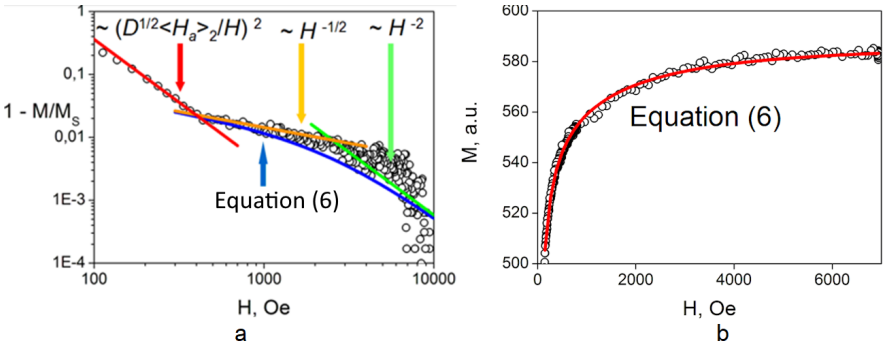

Fig. 1. Fitting of the magnetization dispersion (a) and the magnetization curve (b) by correlation magnetometry in a $Fe_{77}Zr_7N_{16}$ film [34]

3. Influence of chemical and phase composition of Fe-Zr-N system films on magnetic properties

For the study, films were selected whose compositions, when obtained by reactive magnetron deposition, should, in accordance with the scientific approach developed by us [35–36], belong to the Fe-ZrN quasi-binary diagram and contain 9–12 at. % Zr and 9–12 at. % N. However, the method of reactive magnetron deposition has the following features. (1) High sensitivity of the chemical composition of the as-deposited films to the slightest changes in the conditions of magnetron deposition. This leads to the fact that the resulting film can be contaminated with gas-forming elements (O, N, C) and turn into a 4-component material [37–39]. (2) The high cooling rate (10^{14} K/s) of the film on the substrate leads to the formation of a nonequilibrium phase state. It is represented by either a single-phase Fe-based amorphous state, or a two-phase Fe-based amorphous state with one of the phases of the Fe-Zr-N ternary system or the binary system (Fe-Zr, Fe-N and Zr-N). It is also possible to obtain metastable phases that do not form under equilibrium conditions [40–42]. To verify the described models and physical research

methods on our material, we selected films [42, 43] of the following compositions (Tab. 1). Some of the studied compositions are shown in Fig. 2. The variety of chemical composition of the films I-VI (Tab. 1) determines their variety of phase composition: αFe (I), a solid solution of αFe(Zr, N) (II, III), two-phase with iron nitride (IV, V) and X-ray amorphous (VI). The variety of phase composition determines the magnetic properties (Fig. 3): strong ferromagnets (I, II), in which saturation induction decreases with increasing alloying (III) and increasing nitrides (IV, V), and weak ferromagnets (VI).

Table 1. Chemical composition of FeZrN films

No.	Chemical composition, at. %
I	Fe
II	$Fe_{92.2}Zr_{3.0}N_{4.8}$
III	$Fe_{83.0}Zr_{9.5}N_{7.5}$
IV	$Fe_{89.6}Zr_{3.4}N_{7.0}$
V	$Fe_{88.7}Zr_{4.4}N_{6.9}$
VI	$Fe_{65.3}Zr_{34.7}$
VII	$Fe_{43.3}Zr_{34.8}N_{12.4}O_{9.6}$
VIII	$Fe_{72.4}N_{4.8}O_{22.8}$
IX	$Fe_{76.9}N_{4.8}O_{18.3}$
X	$Fe_{76.2}N_{4.9}O_{18.9}$
XI	$Fe_{72.0}N_{6.6}O_{21.4}$
XII	$Fe_{71.8}N_{8.3}O_{19.9}$
XIII	Fe
XIV	$Fe_{99.4}Zr_{0.6}$
XV	$Fe_{98.2}Zr_{1.8}$
XVI	$Fe_{97.1}Zr_{2.9}$
XVII	$Fe_{95.9}Zr_{4.1}$
XVIII	Fe
XIX	$Fe_{92.2}Zr_{3.0}N_{4.8}$
XX	$Fe_{88.7}Zr_{4.4}N_{6.9}$
XXI	$Fe_{78}Zr_{10}N_{12}$
XXII	$Fe_{77}Zr_{7}N_{16}$
XXIII	$Fe_{83.4}Zr_{7.7}N_{4.2}O_{4.7}$
XXIV	$Fe_{78}Zr_{9}N_{13}$

Under the conditions of magnetron deposition, the kinetic factor often prevails over the thermodynamic one, which leads to the appearance of phases that are present only in one of the binary diagrams. Therefore, in addition to ternary compounds (FeZrN), we studied binary compounds (FeN, FeZr). Various nitrides, including metastable nitrogenous martensite (Fig. 4), we obtained in binary films FeN (VIII-XII in Tab. 1) [43].

The solubility of Zr in αFe is practically absent under equilibrium conditions [44]. However, in the as-deposited FeZr films (XIII-XVII in Tab. 1), a supersaturated αFe(Zr) solid solution (Fig. 6a) and an amorphous phase were found [45], an indirect confirmation of the presence of the latter is the small grain size of the αFe(Zr), Fig. 6b.

FeNO films demonstrated a decrease in saturation magnetization with an increase in nitrogen content in the gas mixture (Fig. 5a), while an increase in coercive field is observed with a decrease in grain size (Fig. 5b), which, at first glance, contradicts the random anisotropy model, is explained by the phase composition and an increase in local magnetic anisotropy [43]. The shape of the hysteresis loops indicates the presence of two coercive fields (H_{c1} and H_{c2}, Fig. 5c),

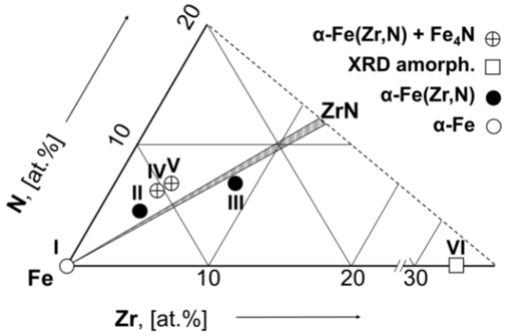

Fig. 2. Ternary Fe-Zr-N diagram and examples of the types of structure obtained in our work: αFe(I), a solid solution of αFe(Zr, N) (II, III), two-phase (IV, V) and X-ray amorphous (VI)

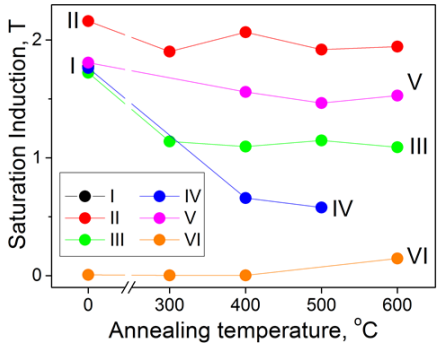

Fig. 3. Saturation induction of the films I-VI depending on the temperature of 1-h vacuum annealing (compositions are shown in Fig. 2)

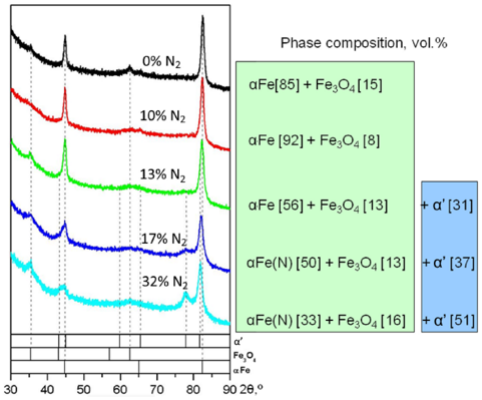

Fig. 4. X-ray diffraction of FeNO films (VIII-XII in Tab. 1) depending on the nitrogen content in the gas mixture during deposition (% N_2); and the phase composition of the films under study

which is explained by the two-mode distribution of stochastic domains with two anisotropy fields of stochastic domains in each film (Fig. 5d). The single-phase structure of the FeZr films (XIII-XVII in Tab. 1) is preferable to the multiphase structure in the FeNO films (they contain three ferromagnetic phases) to obtain predictable magnetic properties: saturation magnetization is

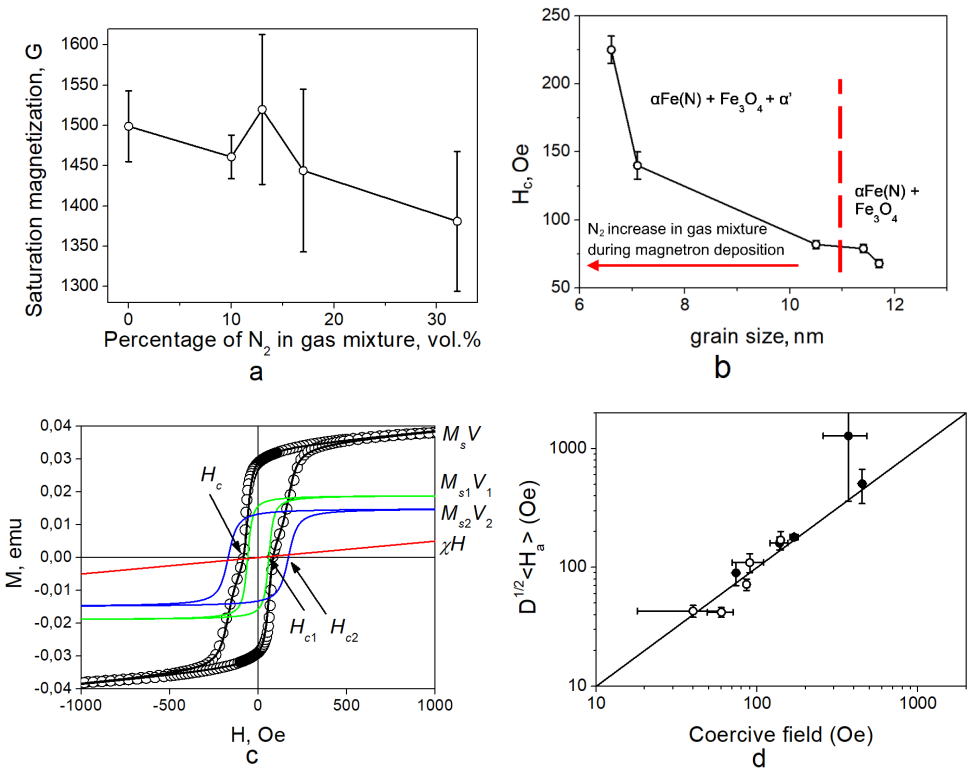

Fig. 5. Saturation magnetization (a), coercive field (b), decomposition of the hysteresis loop into two terms (c) and linear correlation of two coercive fields (H_{c1} and H_{c2}) and two anisotropy fields of the stochastic domain $D^{1/2} < H_a >$(d) in FeNO films (VIII-XII in the Tab. 1)

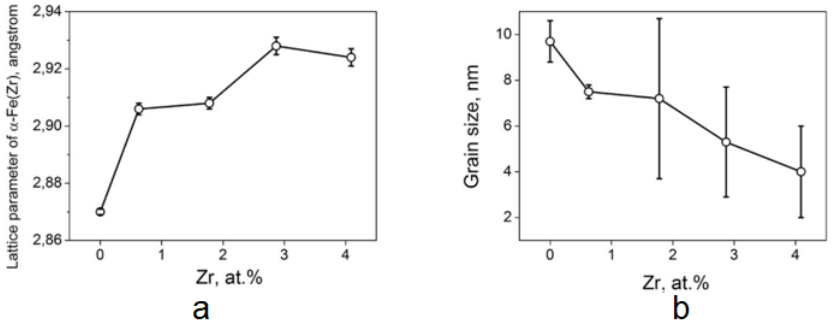

Fig. 6. Lattice parameter (a) and grain size (b) of the αFe(Zr) phase as a function of the Zr content in the FeZr films (XIII-XVII in Tab. 1)

slightly higher (Fig. 7a) and the coercive field obeys the dependence of grain size to the sixth power (Fig. 7b), unlike the FeNO films.

We found ZrN (Fig. 8a) in the films, including those with a high Zr content ($Fe_{43.3}Zr_{34.8}N_{12.4}O_{9.6}$, VII in Tab. 1). Excessive amounts of Zr cannot be coupled in nitride, so excess of Zr amorphizes the Fe-based phase. The Fe-based ferromagnetic phase in a paramagnetic amorphous matrix [46] behaves like a superparamagnet (Fig. 8b).

A feature of magnetron deposition is the possibility of obtaining a multilayer films (III and IV in Tab. 1). The multilayer structure [42] can significantly affect the shape of the magnetic hys-

teresis loops (Fig. 9). Transmission electron microscopy revealed an amorphous layer (Fig. 10a), which may be the cause of the complex shape of the hysteresis loop.

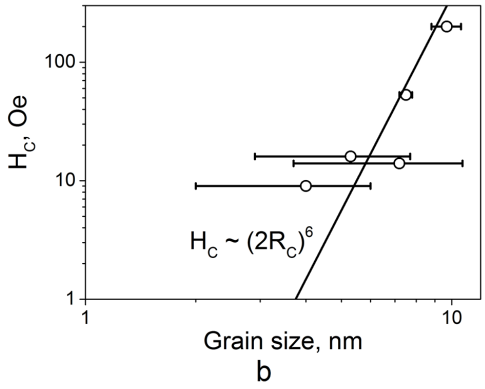

Fig. 7. Saturation magnetization (a) and coercive field (b) in the FeZr films (XIII-XVII in Tab. 1)

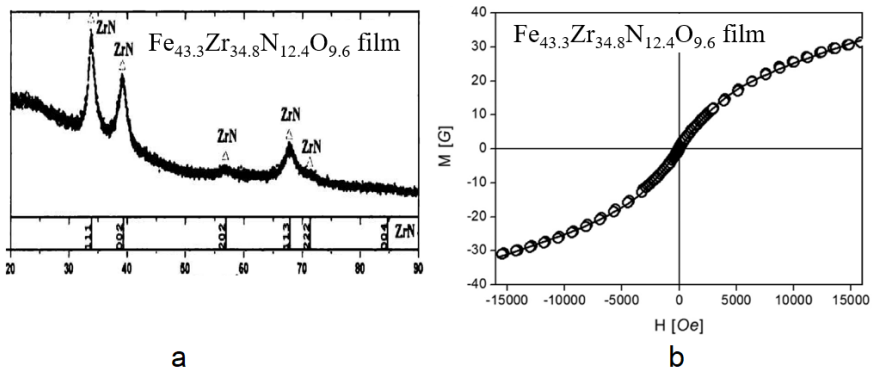

Fig. 8. X-ray diffraction (a) of film VII (Tab. 1), illustrating the formation of ZrN; the excessive zirconium in the films amorphizes iron, which forms a paramagnetic matrix with inclusions of isolated ferromagnetic grains in a superparamagnetic state (b), the magnetization curve of which can be approximated by the Langevin function (solid line)

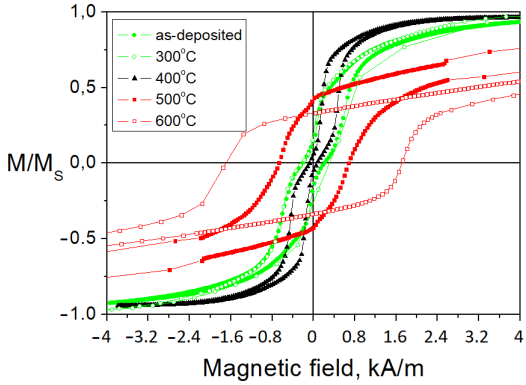

Fig. 9. Hysteresis loops of the films III (Tab. 1) at different annealing temperatures, showing the feature associated with the amorphous layer in the film, which disappears after annealing at temperatures of 500 and 600°C

Various iron nitrides were detected by electron diffraction (IV and V in Table 1, Fig. 10b). Vacuum annealing at temperatures up to 600°C confirmed the stability of the structure and made it possible to clarify the phase composition (Fig. 10b). The magnetic properties of films IV and V and the effect of annealing on them are discussed above (Fig. 3).

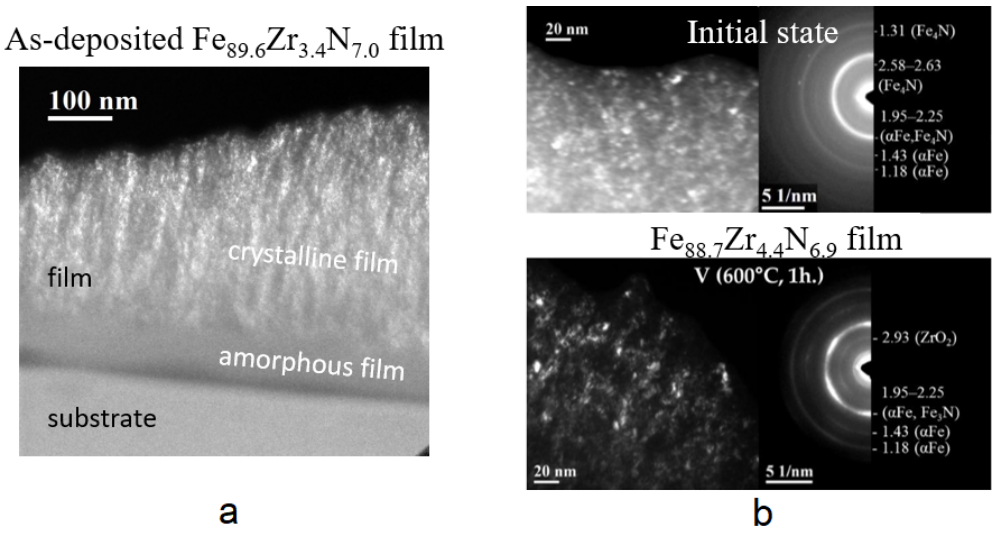

Fig. 10. a cross-section of the film IV showing the formation of an amorphous layer at the beginning of the magnetron deposition process (a); various Fe nitrides (film V) can be formed both during deposition (b) and during vacuum annealing at 600°C for 1 hour (b)

The final nanostructure is formed during subsequent annealing. Annealing of the obtained films leads to a shift of the phase state closer to equilibrium and partial nanocrystallization of the amorphous phase. The main purpose of annealing is fine regulation of the structure: reduction of residual macrostresses (XVIII-XX in Tab. 1, Fig. 11a) and depletion of supersaturated solid solution (Fig. 11b, I-VI in Tab. 1). At the same time, it was found that the size of the ferromagnetic grain increases slightly (Fig. 11b, I-VI in Tab. 1) [47]. The magnetic properties of films I-VI and the effect of annealing on them are discussed above (Fig. 3).

4. Application of the LASM and the method of correlation magnetometry to ferromagnetic FeZrN films

4.1. Local magnetic anisotropy and its effect on the size of the stochastic domain

Measurements of the local magnetic anisotropy H_a from the LASM give an effective value (see Section 3). We considered this value as the sum of four terms related to microstrain, grain boundaries, and phase composition [48]. The H_a value can be in a very wide range (Fig. 12a), which depend on the phase composition, solid solution, and environment of the ferromagnetic grain. As a result of the discussion of the random anisotropy model, we observe a correlation between the relative size of the stochastic domain and the coercive field (Fig. 12b).

The method of correlation magnetometry allows us to determine only the relative size of the stochastic domain, however, direct observations of the stochastic domain are possible by magnetic force microscopy. In Section 2, referring to the works [3, 29], it was noted that the exact form of the correlation function within the stochastic domain cannot be determined by correlation magnetometry. However, the analysis of the image obtained by magnetic force microscopy

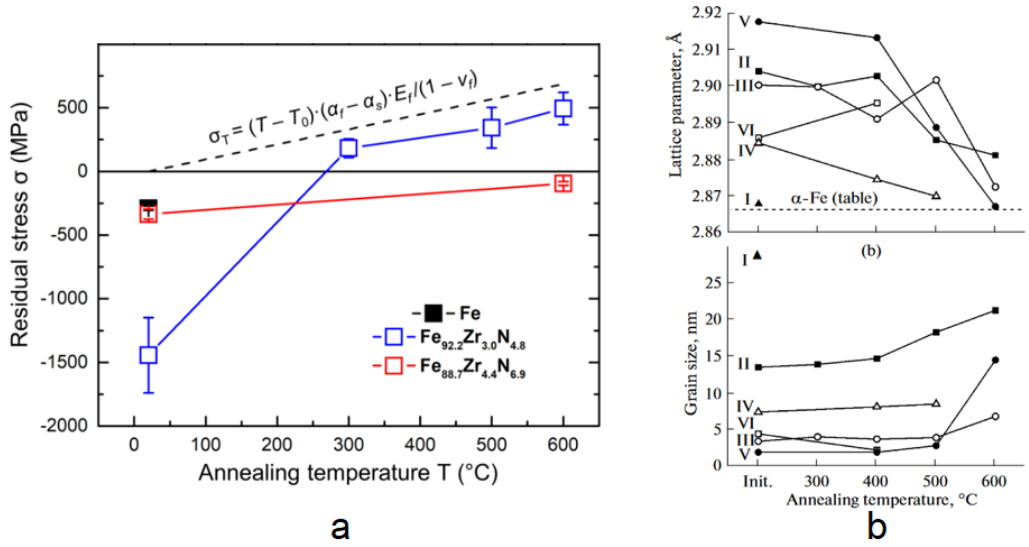

Fig. 11. Effect of vacuum 1-h annealing of films on: residual macrostresses (a, XVIII-XX in Tab. 1) and their comparison with thermal stresses due to the difference in thermal coefficients of the film and the substrate (dashed line), the lattice parameter of αFe (b, numbering corresponds to Fig. 2), the grain size of αFe (b)

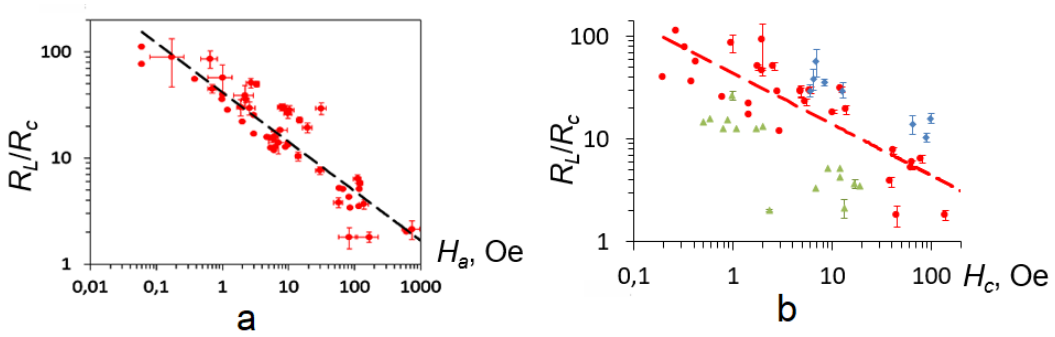

Fig. 12. Correlation of the relative size of the stochastic domain R_L/R_c and the field of local magnetic anisotropy H_a (a, dashed line is $R_L/R_c \sim H_a^{-2}$) or coercive field (b, dashed line is $R_L/R_c \sim H_c^{-1}$)

(Fig. 13), allowed us to quantify the type of correlation function from which the domain size in FeZrN films was determined (120 ± 9 nm, film XXI in Tab. 1), which was very close to the value estimated by correlation magnetometry (130 ± 40 nm) [3]. A comparison of the sizes of the stochastic domain obtained by magnetic force microscopy and correlation magnetometry on FeTiB films also provided a good match [49].

4.2. Rms fluctuation of the stochastic domain anisotropy field and the coercive field

From the large number of the studied films, we selected films of the composition $Fe_{77}Zr_7N_{16}$ (XXII in Tab. 1) with the phase composition of αFe (grain size of 2-23 nm), which most clearly show the effect of annealing on the magnetic microstructure. The rms fluctuation of the anisotropy field of the stochastic domain $D^{1/2} < H_a >$ is in good agreement with the two

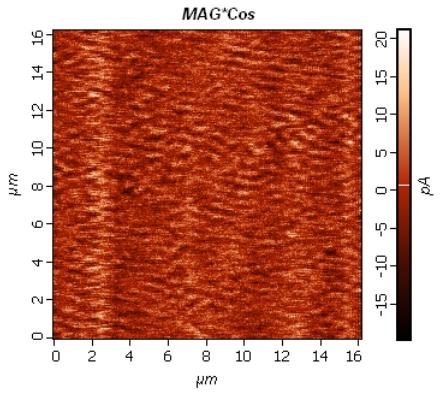

Fig. 13. Magnetic force microscopy of the $Fe_{78}Zr_{10}N_{12}$ film (XXI in Tab. 1)

values of the coercive field H_{c1} and H_{c2} (Fig. 14a). In addition, we confirmed the dependence of the two coercive fields H_{c1} and H_{c2} on the grain size $2R_c$ to the sixth power (Fig. 14b).

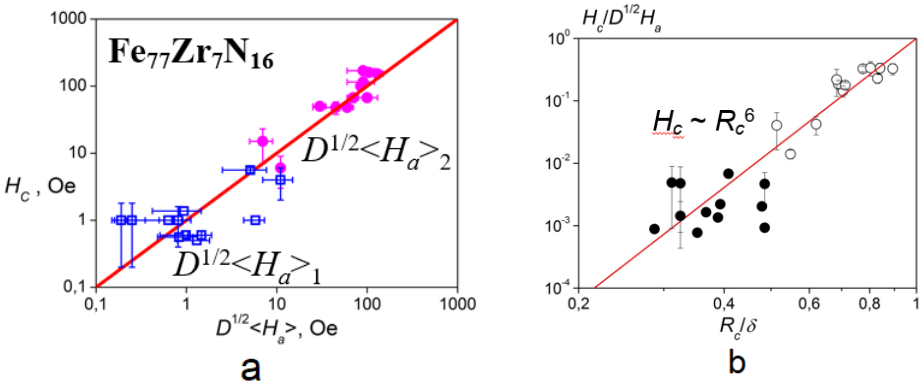

Fig. 14. Films XXII (Table 1): linear correlation of two coercive fields H_{c1} and H_{c2} and two anisotropy fields of the stochastic domain $D^{1/2} < H_a >_1$ and $D^{1/2} < H_a >_2$ (a); proportionality of the two coercive fields H_{c1} and H_{c2} to the sixth power of grain size (b), $H_c \sim (2R_c)^6$ [34]

4.3. The effect of the domain structure on microwave permeability

The permeability is a result of the above-mentioned parameters of the magnetic microstructure, $\mu \sim M_s / < H_a >$. The frequency dependence of μ and ferromagnetic resonance (FMR) also depend on magnetic anisotropy (Kittel equation) [50, 51]. The analysis of microwave permeability (Fig. 15) includes the following models: complex permeability, skin effect, FMR, Acher's law and Snoek limit, the influence of random anisotropy model parameters on FMR in FeZrN films (XXIII in Tab. 1).

5. Saturation induction of the FeZrN films

As mentioned at the beginning of Section 2, the discovery of the LASM was due to the need for accurate measurements of the saturation magnetization (induction) of ferromagnets. A large array of data obtained on FeZrN films made it possible for the first time to measure the effect of a nitrogen solid solution on the saturation induction of the αFe phase. The saturation induction of the films containing ZrN nitride (XXIV in Tab. 1) depends linearly on the volume fraction

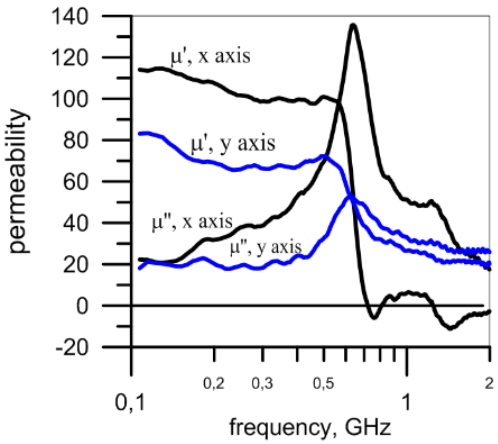

Fig. 15. Frequency dependence of the complex permeability measured in two orthogonal directions in the plane of the FeZrN film (XXIII in Tab. 1)

of the ferromagnetic phase, $B_s = {B_s}^{Fe} \bullet V_{\alpha Fe}$. At the same time, supersaturated solid solutions of αFe(Zr) and αFe(N) have different effects on saturation induction (in Fig. 16, induction is normalized to the volume fraction of αFe so that its value reflects dependence only on the solid solution). Annealing additionally affects the phase composition and supersaturated solid solution (lattice parameter in Fig. 16), which is reflected in the magnitude of saturation induction [52]. Thus, when the N content in the films is higher than Zr (N/Zr $>$ 1), N not coupled to ZrN nitride participates in the solid solution of αFe(N), which has a linear dependence of saturation induction on the N content in the solid solution, $B_s^{\alpha Fe(N)} = 2.15 - 0.17 \cdot N$, where N is expressed in at. % (Fig. 16).

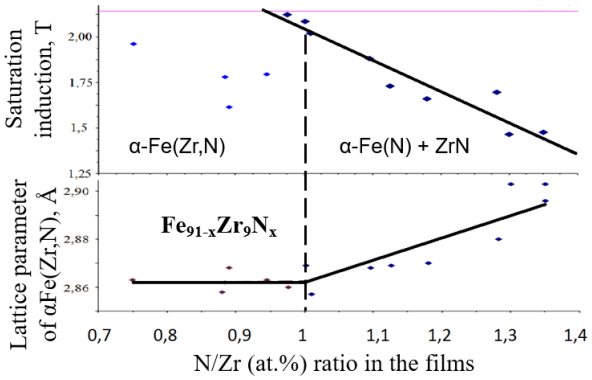

Fig. 16. Saturation induction (top) as a function of the N/Zr ratio (at. %) in films XXIV (Tab. 1) and the αFe lattice parameter, reflecting the N content in the solid solution (below)

Conclusions

Nanocrystalline ferromagnetic films of the Fe-Zr-N alloying system of various chemical and phase compositions with different values of magnetic microstructure parameters are considered. The applicability of the laws of the approach to saturation magnetization and the method of correlation magnetometry is confirmed for the films under study. For the first time, correlations between the coercive field, grain size and the anisotropy field of the stochastic domain have

been confirmed for the films of this system. The size of the stochastic domain depending on the parameters of the structure and the methods of its measurement are considered. For the first time, measurements of the size of a stochastic domain using correlation magnetometry and magnetic force microscopy have been compared. The effect of a nitrogen solid solution on the saturation induction of the αFe phase has been measured for the first time.

References

[1] E.N.Sheftel', S.V.Komogortsev, R.S.Iskhakov et al., Investigation of the Magnetic Properties and Magnetic Structure Parameters of Nanocrystalline $Fe_{79}Zr_{10}N_{11}$ Films, *Bulletin of the Russian Academy of Sciences: Physics*, **74**(2010), no. 10, 1449–1451. DOI: 10.3103/S1062873810100382

[2] E.N.Sheftel', E.V.Harin, S.V.Komogortsev, Study of the Physical Nature of the Soft Magnetic Properties of Fe–ZrN Nanocrystalline Films, *Russian Metallurgy (Metally)*, **2011**(2011), no. 9, 875–881. DOI: 10.1134/s0036029511090217

[3] S.V.Komogortsev, R.S.Iskhakov, E.N.Sheftel et al., Magnetization correlations and random magnetic anisotropy in nanocrystalline films Fe78Zr10N12, *Solid State Phenomena*, **190**(2012), 486–489. DOI: 10.4028/www.scientific.net/SSP.190.486

[4] P.Weiss, Les propriétés magnétiques de la pyrrhotine, *J. Phys. Theor. Appl.*, **4**(1905), no. 4, 469–508. DOI: 10.1051/jphystap:019050040046900

[5] N.Akulov, Zur Atomtheorie des Ferromagnetismus, *Z. Physik*, **54**(1929), 582–587. DOI: 10.1007/BF01338489

[6] N.S.Akulov, Über den Verlauf der Magnetisierungskurve in starken Feldern, *Z. Physik*, **69**(1931), 822–831. DOI: 10.1007/BF01339465

[7] T.Holstein, H.Primakoff, Magnetization Near Saturation in Polycrystalline Ferromagnets, *Phys. Rev.*, **59**(1941), no. 7, 388. DOI: 10.1103/PhysRev.59.388

[8] E.W.Lee, The Approach to Saturation Magnetostriction, *Proceedings of the Physical Society. Section A*, **67**(1954), no. 4, 381. DOI: 10.1088/0370-1298/67/4/409

[9] N.S.Akulov, L.V.Kirensky, Magnetic method for studying internal elastic stresses in ferromagnetic metals, *Journal of Technical Physics*, **9**(1939), no. 13, 1145–1150 (in Russian).

[10] L.Lanotte, C.Luponio, V.Tagliaferri, Magnetostriction in Ni rods under torsion: Critical stress and crystal anisotropy effect, *Il Nuovo Cimento D*, **10**(1982), no. 1, 215–224. DOI: 10.1007/BF02450080

[11] J.R.Cullen, S.Rinaldi, G.V.Blessing, Elastic versus magnetoelastic anisotropy in rare earth–iron alloys, *J. Appl. Phys.*, **49**(1978), no. 3, 1960–1965. DOI: 10.1063/1.324764

[12] V.S.Amral, J.B.Sousa, J.M.Moreira, et. al., Electrical resistivity and local magnetic order in random anisotropy amorphous ferromagnets, *Journal of Applied Physics*, **75**(1994), no. 10, 6513–6515. DOI: 10.1063/1.356932

[13] L.Neel, L'approche à la saturation de la magnétostriction, *J. Phys. Radium*, **15**(1954), no. 5, 376–378. DOI: 10.1051/jphysrad:01954001505037601

[14] M.Celasco, Saturation approach law of longitudinal magnetostriction in grain-oriented ferromagnetic cubic materials, *Nuovo Cim B*, **9**(1972), 425–439. DOI: 10.1007/BF02734457

[15] H.Kronmüller, J.Ulner, Micromagnetic theory of amorphous ferromagnets, *Journal of Magnetism and Magnetic Materials*, **6**(1977), 52–56. DOI: 10.1016/0304-8853(77)90073-7

[16] W.F.Brown, Theory of the Approach to Magnetic Saturation, *Physical Review*, **58**(1940), 736–743. DOI: 10.1103/PhysRev.58.736

[17] M.Fähnle, H. Kronmüller, The influence of spatially random magnetostatic, magnetocrystalline, magnetostrictive and exchange fluctuations on the law of approach to ferromagnetic saturation of amorphous ferromagnets, *Journal of Magnetism and Magnetic Materials*, **8**(1978), no. 2, 149–156. DOI: 10.1016/0304-8853(78)90114-2

[18] A Malozemoff, Laws of approach to magnetic saturation for interacting and isolated spherical and cylindrical defects in isotropic magnetostrictive media, *IEEE Transactions on Magnetics*, **19**(1983), no. 4, 1520–1523. DOI: 10.1109/TMAG.1983.1062583

[19] G.Diener, M.Posselt, A Self-Consistent Approach to the Ideal Magnetization in Heterogeneous Ferromagnetics, *phys. stat. sol. b*, **129**(1985), no. 2, 631-640.
DOI: 10.1002/pssb.2221290222

[20] V.A.Ignatchenko, Magnetic structure of thin magnetic films and ferromagnetic resonance, *Soviet Physics JETP*, **27**(1968), no. 1, 162–166.

[21] V.A.Ignatchenko, V.A.Felk, Exchange narrowing of magnetic resonance linewidths in inhomogeneous ferromagnets, *Phys. Rev. B*, **71**(2005), 094417.
DOI: 10.1103/PhysRevB.71.094417

[22] V.A.Ignatchenko, R.S.Iskhakov, Spin waves in a randomly inhomogeneous anisotropic medium, *Soviet Physics JETP*, **45**(1977), no. 3, 526–532.

[23] V.A.Ignatchenko, R.S.Iskhakov, Spin waves in amorphous and finely divided ferromagnets with allowance for dipole-dipole interaction, *Soviet Physics JETP*, **47**(1978), no. 4, 725–729.

[24] L.I.Deich, V.A.Ignatchenko, Magneto-elastic resonance in randomly inhomogeneous ferromagnets with zero-mean magnetostriction, *JETP*, **80**(1995), no. 3, 478–484.

[25] V.A.Ignatchenko, R.S.Iskhakov, G.V.Popov, Law of approach of the magnetization to saturation in amorphous ferromagnets, *Soviet Physics JETP*, **55**(1982), no. 5, 878–886.

[26] L.I.Deich, V.A.Ignatchenko, Influence of spatial fluctuations of the modulus of magnetization on the properties of amorphous ferromagnets, *Soviet physics JETP*, **72**(1991), no. 3, 453–460.

[27] E.M.Chudnovsky, W.M.Saslow, R.A.Serota, Ordering in ferromagnets with random anisotropy, *Phys. Rev. B*, **33**(1986), 251–261. DOI: 10.1103/PhysRevB.33.251

[28] R.S.Iskhakov, V.A.Ignatchenko, S.V.Komogortsev, A.D.Balaev, Study of magnetic correlations in nanostructured ferromagnets by correlation magnetometry, *JETP Letters*, **78**(2003), no. 10, 646–650. DOI: 10.1134/1.1644310

[29] A.Michels, R.N.Viswanath, J.G.Barker, R.Birringer, J.Weissmüller, Range of Magnetic Correlations in Nanocrystalline Soft Magnets , *Phys. Rev. Lett.*, **91**(2003), 267204.
DOI: 10.1103/PhysRevLett.91.267204

[30] G.Herzer, Modern soft magnets: Amorphous and nanocrystalline materials, *Acta Materialia*, **61**(2013), 718–734. DOI: 10.1016/j.actamat.2012.10.040

[31] G.Herzer, Nanocrystalline soft magnetic materials, *JMMM* , **112**(1992), no. 1-3, 258–262. DOI: 10.1016/0304-8853(92)91168-S

[32] R.S.Iskhakov, S.V.Komogortsev, Magnetic microstructure of amorphous, nanocrystalline, and nanophase ferromagnets, *Physics of Metals and Metallography*, **112**(2011), no. 7, 666–681. DOI: 10.1134/S0031918X11070064

[33] S.V.Komogortsev, E.A.Denisova, R.S.Iskhakov et al., Multilayer nanogranular films (Co40Fe40B20)50(SiO2)50/α-Si:H and (Co40Fe40B20)50(SiO2)50/SiO2: Magnetic properties, *J. Appl. Phys.*, **113**(2013), 17C105. DOI: 10.1063/1.4794361

[34] E.N.Sheftel, E.V.Harin, Two modes of magnetic structure of nanocrystalline FeZrN films prepared by oblique-angle magnetron sputtering, *Journal of Magnetism and Magnetic Materials*, **479** (2019), 84–87. DOI: 10.1016/j.jmmm.2019.02.027

[35] E.N.Sheftel, Soft Magnetic Nanocrystalline Films of Alloys of Fe—Refractory Interstitial Phase for Application in Devices for Magnetic Recording, *Inorganic Materials: Applied Research*, **1**(2010), no. 1, 17–24. DOI: 10.1134/S207511331001003X

[36] E.N.Sheftel, V.A.Tedzhetov, E.V. Harin, G.Sh. Usmanova, Films with nanocomposite structure αFe(N) +ZrN for soft magnetic applications , *Thin Solid Films*, **748**(2022), 139146. DOI: 10.1016/j.tsf.2022.139146

[37] A. Farhadizadeh, S. Ghasemi, P.Nurpour, M.Hamdi, H.Ghomi, The effect of magnetron sputtering parameters on the properties of TaZrN coatings: simulation and experiment , *Surfaces and Interfaces*, **30**(2022), 101926. DOI: 10.1016/j.surfin.2022.101926

[38] G.Greczynski, S.Mráz, L.Hultman, J.Schneider, Venting temperature determines surface chemistry of magnetron sputtered TiN films, *Applied Physics Letters* , **108**(2016), 041603. DOI: 10.1063/1.4940974

[39] E.N.Sheftel, V.A.Tedzhetov, E.V.Harin, G.Sh.Usmanova, A.L.Dyachkov, FeZrN films: Role of dc magnetron sputtering conditions in the formation of their elemental and phase compositions , *Thin Solid Films*, **698**(2020), 137876. DOI: 10.1016/j.tsf.2020.137876

[40] G.Liu, Y.Yang, X.Luo, B.Huang, P.Li, The phase, morphology and surface characterization of Ti–Mo alloy films prepared by magnetron sputtering, *RSC Advances*, **7**(2017), 52595–52603. DOI: 10.1039/c7ra10510j

[41] K.Chang, D.Music, T.Baben, D.Lange, H.Bolvardi, J.Schneider, Modeling of metastable phase formation diagrams for sputtered thin films, *Science and Technology of Advanced Materials* , **17**(2016), 210–219. DOI: 10.1080/14686996.2016.1167572

[42] E.N.Sheftel, V.A.Tedzhetov et al., FeZrN Films: Magnetic and Mechanical Properties Relative to the Phase-Structural State, *Materials*, **2022**(15), 137. DOI: 10.3390/ma15010137

[43] E.N.Sheftel, V.A.Tedzhetov, E.V.Harin, G.Sh.Usmanova, Phase composition and magnetic structure in nanocrystalline ferromagnetic Fe–N–O films, *Current Applied Physics*, **20**(2020), 1429-1434. DOI: 10.1016/j.cap.2020.09.009

[44] B.Samanta, P.Ramakrishna, S.Balakrishnan, K.Ananthasivan, Experimental determination of phase equilibria in the system Fe–Zr (0–100 at.% Zr) by using the technique, DSC, and XRD, *Calphad*, **78**(2022), 102458. DOI: 10.1016/j.calphad.2022.102458

[45] E.V.Harin, E.N.Sheftel, V.A.Tedzhetov, G.S.Usmanova, Two-Mode Stochastic Magnetic Structure in Nanocrystalline Soft Magnetic Fe–Zr Films, *Physica Status Solidi B*, **256**(2019), no. 10, 1900067. DOI: 10.1002/pssb.201900067

[46] E.N.Sheftel, E.V.Harin, V.A.Tedzhetov, et al. Magnetic structureandmagneticpropertiesofnanocrystalline and amorphousFe–Zr–N films, *Physica B*, **494**(2016), 13–19. DOI: 10.1016/j.physb.2016.04.033

[47] V.A.Tedzhetov, E.N.Sheftel, E.V.Harin, P.V.Kiryukhantsev-Korneev, Residual Stresses in Soft Magnetic FeTiB and FeZrN Films Obtained by Magnetron Deposition, *Coatings*, **11**(2021), 34. DOI: 10.3390/coatings11010034

[48] E.V.Harin, E.N.Sheftel, Micromagnetic Structure of Soft Magnetic Nanocrystalline Fe-Based Films, *Phys. Metals and Metallography*, **116**(2015), no. 8, 753–759. DOI: 10.1134/S0031918X15080074

[49] E.V.Harin, E.N.Sheftel, V.A.Tedzhetov et al., Comprehensive quantifying of the Fe-Ti-B film magnetic microstructure , *Thin Solid Films*, **807**(2024), 140544. DOI: 10.1016/j.tsf.2024.140544

[50] E.N.Sheftel, E.V.Harin et al., Static and high-frequency magnetic properties of nanocrystalline Fe-Zr-N films, *European Physical Journal: Web of Conferences*, **185**(2018), 04024. DOI: 10.1051/epjconf/201818504024

[51] E.N.Sheftel, E.V.Harin, V.A.Tedzhetov et al., FeZrN Films: Static and Microwave Magnetic Properties, *Inorganic Materials: Applied Research*, **15**(2024), no. 3, 760–765. DOI: 10.1134/S2075113324700187

[52] E.N.Sheftel, E.V.Harin, Fe-Zr-N films: Effect of nitrogen content and nitrogen-to-zirconium concentration ratio on saturation induction, *Materials Letters* , **229**(2018), 36–39. DOI: 10.1016/j.matlet.2018.06.110

Описание параметров магнитной микроструктуры ферромагнитных плёнок FeZrN методом корреляционной магнитометрии

Евгений В. Харин
Елена Н. Шефтель
Валентин А. Теджетов
Галина Ш. Усманова
Игорь О. Банных
Институт металлургии и материаловедения им. Байкова РАН
Москва, Российская Федерация

Аннотация. В настоящей статье приведен краткий литературный обзор, посвящённый развитию моделей, описывающих процесс намагничивания ферромагнетиков, и закону приближения намагниченности к насыщению (закон Акулова). Аналитический подход, позволяющий оценить величину эффективной локальной (внутри зерна) магнитной анизотропии и параметры автокорреляционной функции намагниченности (на масштабе стохастического домена), был развит В. А. Игнатченко с соавторами и получил название корреляционная магнитометрия. Приведены экспериментальные результаты авторов, подтвердившие применимость закона приближения намагниченности к насыщению и метода корреляционной магнитометрии, в частности, к ферромагнитным пленкам FeZrN.

Ключевые слова: магнетронное осаждение, нанокристаллические пленки, рентгеновская дифракция, ОЦК Fe фаза, магнитная микроструктура, модель случайной анизотропии, корреляционная магнитометрия.

EDN: SHTPLD
УДК 539.213.2

Galvanomagnetic and Magnetic Properties of Amorphous Alloys Based on Iron Group Elements

Ilkhomzhon Subkhankulov*
Engineering Physics Institute
Samarkand State University named after Sharof Rashidov
Samarkand, Uzbekistan
Gofur Dusmurodov†
Samarkand branch of the Tashkent University of Information Technologies named after Al-Khwarizmi
Samarkand, Uzbekistan
Sherzod A. Khomitov‡
Engineering Physics Institute
Samarkand State University named after Sharof Rashidov
Samarkand, Uzbekistan

Received 02.03.2026, received in revised form 03.04.2026, accepted 07.05.2026

Abstract. The paper presents the temperature dependences of the Hall coefficient and magnetization of alloys in amorphous and crystalline states based on Fe, Ni with additives of metalloids, at temperatures from room temperature to 1000 K. It is shown that with increasing temperature, crystallization occurs with the precipitation of various phases. The crystallization diagrams of the $Fe_{66,87}Ni_{24,7}Si_{4,93}B_{3,5}$ alloy are presented. It has been established that the relationship between the anomalous Hall coefficient and magnetization is such that in a certain temperature range there is a linear relationship between them.

Keywords: amorphous state, amorphous metal alloys, X-ray diffraction pattern, Hall coefficient, magnetization, Curie temperature, crystallization temperature.

Citation: I. Subkhankulov, G. Dusmurodov, Sh.A. Khomitov, Galvanomagnetic and Magnetic Properties of Amorphous Alloys Based on Iron Group Elements, J. Sib. Fed. Univ. Math. Phys., 2026, 19(4), 522–527. EDN: SHTPLD.

Introduction

Alloys based on transition metals with additions of metalloids belong to the class of promising objects of modern materials science. This is due to the unique properties in these alloys. For example, they have a high tensile strength, demonstrate high corrosion resistance and are used as magnetic materials in electronic equipment, etc. [1,2]. It should be noted that the specified characteristics of alloys based on iron group metals are manifested mainly in the nanocrystalline [3–5] and amorphous states. These alloys are used as protective coatings operating in aggressive environments and experiencing high mechanical stresses, and are also considered promising materials for the creation of magnetic field sensors, generators and converters of electrical energy [6]. The level of knowledge about the processes of glass transition and two-stage crystallization during subsequent annealing of initially amorphous alloys is insufficient, which limits the possibilities of their application over a wide range of temperatures. In this regard, in this work, a study was carried out on the thermophysical properties of amorphous alloys based on Fe and Ni with additives of Si and B at temperatures from room temperature to 1000 K.

*subhonqulov1955@gmail.com https://orcid.org/0009-0007-0561-4174
†dusmurodov@tiut.uz
‡sherxomitov@gmail.com https://orcid.org/0000-0003-4385-2943

1. Samples and research methodology

Amorphous alloys were obtained by rapid quenching of the melt on the surface of a rapidly rotating disk in the form of ribbons of $25\,\mu m$ in thickness [7].

The Hall coefficient of the samples was measured experimentally using a van der Pauw method with the High Temp Hall effect Measurement System [8]. Using this device, the Hall coefficient of amorphous plate-shaped alloys was studied in the temperature range from nitrogen to 1000 K.

To obtain information about structural changes, crystallization and Curie temperature in amorphous alloys, a vibrating magnetometer was used, which measured the temperature dependence of magnetization based on the vibrating magnetometer method [9].

In ferromagnetic alloys, the specific Hall resistance depends on the normal Hall coefficient, which depends on the magnetic field induction, and the anomalous Hall coefficient, which depends on the magnetization, that is, [10]:

$$\rho_n = R_0 B + R_S \cdot 4\pi I \tag{1}$$

In amorphous ferromagnetic alloys, the Hall coefficient is practically independent of temperature and in absolute value exceeds the corresponding coefficient in crystalline analogs.

Fig. 1 shows the dependences of the Hall coefficient $R_H(T)$ and magnetization $I_S(T)$ on temperature for the amorphous alloy $Fe_{66,87}Ni_{24,7}Si_{4,93}B_{3,5}$.

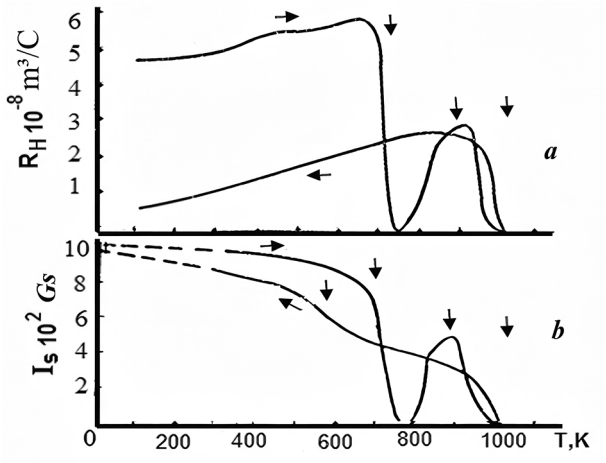

Fig. 1. Temperature dependences of the Hall coefficient $R_H(T)$ and magnetization $I_S(T)$ of the amorphous and crystalline states of the $Fe_{66,87}Ni_{24,7}Si_{4,93}B_{3,5}$ alloy

The Hall coefficient R_H varies from $4.6 \cdot 10^{-8}\ m^3/C$ to $5.9 \cdot 10^{-8}\ m^3/C$ in a nearly linear fashion over the temperature range of $100 - 660\,K$. At approximately $400\,K$, the $R_H = f(T)$ dependence shifts slightly upward, and starting at $780\,K$, the R_H coefficient decreases sharply and reaches zero. A decrease in R_H to zero indicates that the Curie temperature T_C of the amorphous state is near this value.

With a further increase in temperature, the Hall coefficient R_H increases again and at $T = 870\,K$ reaches a value of $R_H = 3 \cdot 10^{-8}\ m^3/C$, after which it decreases with increasing temperature and reaches zero at $T = 1000\,K$. The increase in the Hall coefficient 4 after the Curie temperature of the amorphous state is associated with the crystallization process of the sample, and the subsequent decrease in R_H to zero after crystallization is due to the Curie temperature of the crystalline state. Upon cooling after crystallization, the Hall coefficient R_H again increases from zero and at $T = 800\,K$ reaches a value of $2.8 \cdot 10^{-8}\ m^3/C$. With a further decrease in temperature, R_H decreases.

For this sample, the temperature dependence of magnetization $I_S = f(T)$ also exhibits an anomalous behavior, similar to that of $R_H(T)$. In the amorphous state, magnetization I_S decreases from 971G at 4 and reaches zero at 4, which, as noted above, corresponds to the Curie temperature of the amorphous state. With a further increase in temperature, I_S increases again and reaches $520G$ at $T = 860\,K$, after which it decreases again and reaches zero at $1000\,K$. This temperature corresponds to the Curie temperature of the crystalline state.

Upon cooling after crystallization, the magnetization I_S begins to increase from zero and reaches $868\,G$ at $T = 300\,K$. In this temperature range, characteristic bends in the $I_S(T)$ dependence are observed at values of $950\,K$, $610\,K$, and $500\,K$. In order to establish the causes of abrupt changes in physical properties under the influence of temperature, the sample was heated isothermally to temperatures at which anomalies were observed, and X-ray analysis was performed.

Based on the obtained results, it can be concluded that changes in the physical properties (mainly magnetic) of the amorphous alloy $Fe_{66,87}Ni_{24,7}Si_{4,93}B_{3,5}$ arise as a result of changes in the composition of the sample, that is, they are associated with the forming magnetic phases [11, 12].

Fig. 2 shows X-ray diffraction patterns of the $Fe_{66,87}Ni_{24,7}Si_{4,93}B_{3,5}$ alloy after isothermal heating at different temperatures.

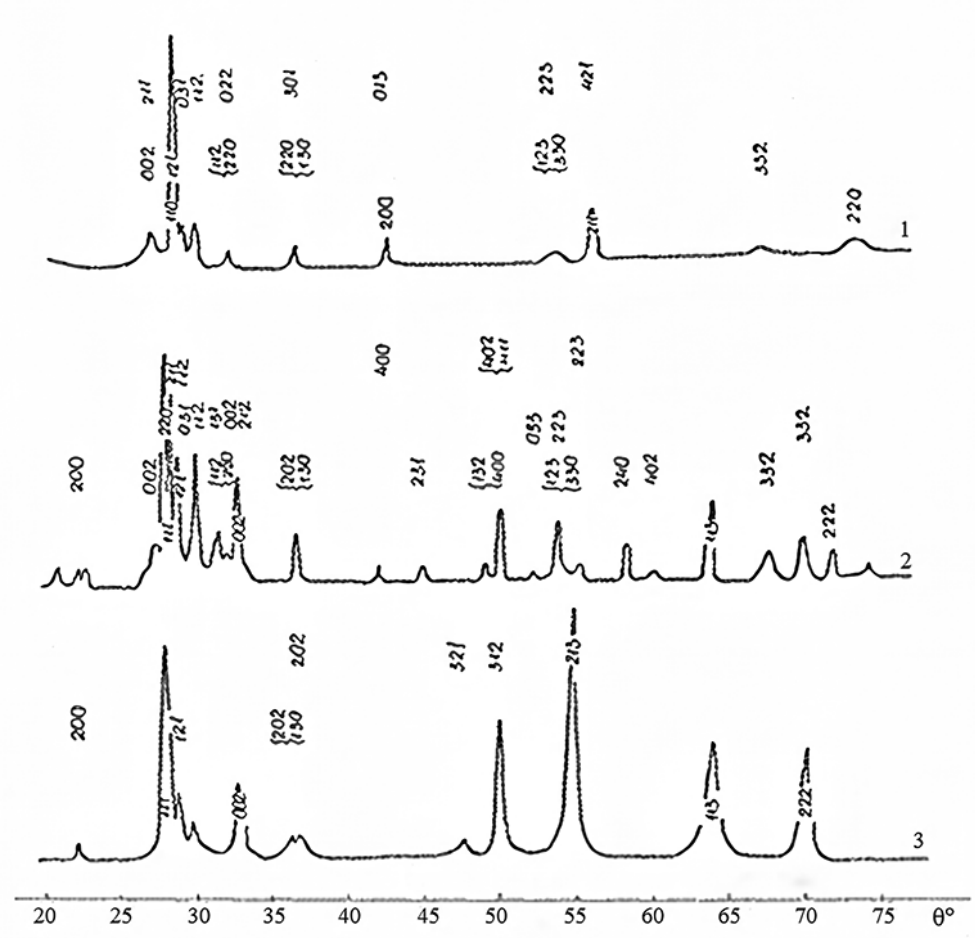

Fig. 2. X-ray diffraction patterns of amorphous alloy $Fe_{66,87}Ni_{24,7}Si_{4,93}B_{3,5}$ at different isothermal heating: I - 753 K, II - 853 K, III - initial crystalline form

In the $Fe_{66,87}Ni_{24,7}Si_{4,93}B_{3,5}$ sample, crystallization begins at $T = 770\,K$ with the formation of $\alpha - Fe$ crystals. Starting at $T = 865\,\mathrm{K}$, the amorphous matrix completely disappears, and the $\gamma - (Fe, Ni)$ phase with a lattice parameter $a = 0.357\,nm$ precipitates. At $T = 930\,K$, the following transitions are observed:

$$\alpha - Fe + A_1 \rightarrow \gamma - (Fe, Ni) + Fe_2B$$

Upon subsequent heating, a set of diffraction lines appears in the sample, corresponding to the following d/n values: 0.355; 0.307; 0.275; 0.251; 0.205; 0.1935; 0.1854; 0.1643 nm. Some of these lines are attributed to the $FeNi_3$ intermetallic compound, while the rest are associated with complex oxides or borosilicated compounds based on $Fe - Ni$ (phase B_2).

Crystallization of the amorphous alloy $Fe_{66,87}Ni_{24,7}Si_{4,93}B_{3,5}$ can be represented by the following scheme (APh — amorphous phase):

$$APh \xrightarrow{770K} APh + \alpha - Fe \xrightarrow{815\,K} APh + \alpha - Fe + A_1 \xrightarrow{865K} \alpha - Fe +$$

$$+\gamma - (Fe, Ni) + A_1 + B_2 \xrightarrow{930\,K} \gamma - (Fe, Ni) + Fe_2B + FeNi + B_2$$

As noted above, the anomalous Hall coefficient is directly related to magnetization. Therefore, we attempted to establish a relationship between the anomalous Hall coefficient and the square of magnetization [13–15]. In a certain temperature range, the following relationship was found between changes in ΔR_S and I_S^2, namely:

$$\Delta R_S = R_S(T) - R_S(T_B) = \alpha[I_S^2(T_B) - I_S^2(T)] \tag{2}$$

In this case, $R_S()$ is the Hall coefficient in the temperature range ($T < T_c$), and $R_S(T_B)$ is the Hall coefficient at room temperature; similarly, $I_S(T)$ is the magnetization at $T < T_C$ at any temperature in this range, and $I_S(T_B)$ is its value at room temperature.

Equation (2) expresses the relationship between the anomalous Hall coefficient and magnetization in a given temperature range.

Fig. 3 shows the relationship between the anomalous Hall coefficient and the square of magnetization for the amorphous and crystalline states of the $Fe_{66,87}Ni_{24,7}Si_{4,93}B_{3,5}$ alloy.

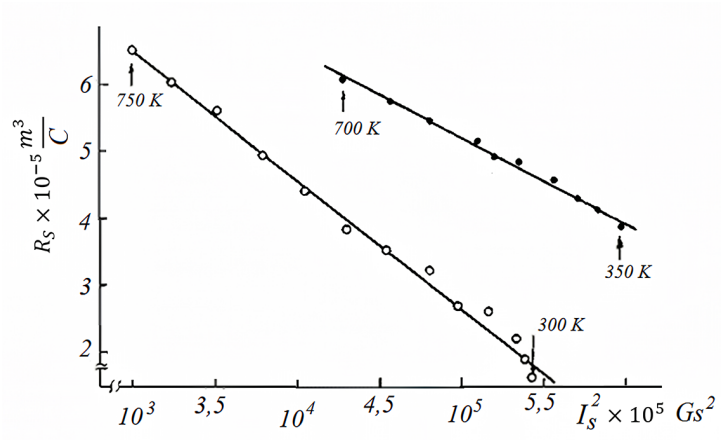

Fig. 3. Linear dependence between the anomalous Hall coefficient and magnetization for the $Fe_{66,87}Ni_{24,7}Si_{4,93}B_{3,5}$ alloy (····· — amorphous, °°°°° — crystalline state)

This dependence has also been established for several other amorphous alloys based on iron group elements. Tab. 1 lists the α values for the amorphous and crystalline states of several such

Table 1. Galvanomagnetic coefficient α for amorphous and crystalline alloys

Sample and its composition	Amorphous state		Crystalline state	
	Temperature range, K	$\alpha \cdot 10^{-13}$ $m^3/(C \cdot K)$	Temperature range, K	$\alpha \cdot 10^{-3}$ $m^3/(C \cdot K)$
$Fe_{66.87}Ni_{24.7}Si_{4.93}B_{3.5}$	350–600	0.86	300–600	1.023
$Fe_{40}Ni_{38}Mo_4B_{18}$	300–400	1.36	300–450	2.00
$Fe_{44.2}Ni_{44.2}Mo_{7.65}B_{3.95}$	350–700	2.06	300–750	2.29

alloys that satisfy equation (2), as well as the temperature range over which this dependence holds.

As can be seen from the values in the table and Fig. 3, there is a linear relationship between R_S and I_S^2 over a certain temperature range. This relationship is weaker in the amorphous state than in the crystalline state. This indicates that the contribution of phonons to the kinetic properties of amorphous alloys is smaller than in the crystalline state.

References

[1] K.Russew, L.Stojanova, Production, Properties and Applications of Glassy Metals, Springer, Berlin–Heidelberg, 2016. DOI: 10.1007/978-3-662-47882-0.

[2] O.K.Kuvandikov, I.Subkhankulov, D.H.Imamnazarov, Sh.A.Khomitov, Nature of exchange interaction in amorphous alloys based on metals of iron group with metalloids, *Metallofiz. i Noveishie Tekhnol.*, **44**(2022), no. 7, 823–829. DOI: 10.15407/mfint.44.07.0823.

[3] I.E.Permyakova, A.A.Ivanov, A.V.Shelyakov, Using the laser irradiation of amorphous alloys to create amorphous–nanocrystalline composites, *Bull. Russ. Acad. Sci. Phys.*, **85**(2021), 755–759.

[4] O.S. Trushin, A.A.Popov, A.N.Pestova et al., Nanostructuring at oblique angle deposition of cobalt, *Bull. Russ. Acad. Sci. Phys.*, **86**(2022), 542–545.

[5] R.A.Konchakov, A.S.Makarov, A.S.Aronin et al., Elastic dipoles in crystal and glassy aluminum and high-entropy $Fe_{20}Ni_{20}Cr_{20}Co_{20}Cu_{20}$ alloy, *JETP Lett.*, **115**(2022), 280–285. DOI: 10.1134/S0021364022100095.

[6] L.Y.Fetisov, Y.K.Fetisov, N.S.Perov et al., Magnetoelectric effect in amorphous FeNiSiC ferromagnet–piezoelectric planar structures, *Tech. Phys.*, **56**(2011), 485–490.

[7] I.V.Zolotukhin, Amorphous alloys, *Soros Educational Journal*, (1997), no. 4, 73 (in Russian).

[8] L.J. van der Pauw, Semiconductor Devices: Pioneering Papers, Springer, Berlin, 1991, 174–182. DOI: 10.1142/9789814503464_0017.

[9] I.Subkhankulov, B.Amonov, G.Bakaev, Sh.A.Khomitov, Magnetization of amorphous alloys at high temperatures and methods of measurement of magnetization, *Scientific Journal SamSU*, (2017), no. 1, 177–181.

[10] A.V.Kudrin, Galvanomagnetic properties of ferromagnetic nanostructures: A tutorial, Nizhny Novgorod State University, Nizhny Novgorod, 2011 (in Russian).

[11] I.B.Kekalo, Atomic structure of amorphous alloys and its evolution, Higher School, Moscow, 2006 (in Russian).

[12] O.Kuvandikov, N.S.Hamraev, R.M.Razhabov et al., Thermal characteristics of amorphous Fe–Ni–Si–C alloys, *Bull. Russ. Acad. Sci. Phys.*, **88**(2024), no. 12, 2055–2060.

[13] Yu.P. Irkhin, Sh.Sh. Abel'skii, Scattering on spin inhomogeneities and spontaneous Hall effect in ferromagnets, *Sov. Phys. Solid State*, **6**(1964), 1635 ([n Russian).

[14] O.Kuvandikov, I.Subkhankulov, R.Razhabov et al., Electrical resistance and Hall effect of amorphous ferromagnetic alloys of the FeNiSiC system, *AIP Conf. Proc.*, **3377**(2025), no. 1, 050006.

[15] O.Kuvandikov et al., The Hall effect in amorphous and crystalline $Fe_{60}Co_{20}Si_8B_{12}$ and $Fe_{58}Co_{20}Si_{12}B_{10}$ ferromagnetic alloys, *Bull. Russ. Acad. Sci. Phys.*, **88**(2024), no. 11, 1836–1842. DOI: 10.31857/S0367676524110259.

Гальваномагнитные и магнитные свойства аморфных сплавов на основе элементов железной группы

Илхомжон Субханкулов
Инженерно-физический институт Самаркандского государственного университета им. Шарофа Рашидова
Самарканд, Узбекистан

Гофур Дусмуродов
Самаркандский филиал Ташкентского университета информационных технологий им. аль-Хорезми
Самарканд, Узбекистан

Шерзод Хомитов
Инженерно-физический институт Самаркандского государственного университета им. Шарофа Рашидова
Самарканд, Узбекистан

Аннотация. В работе приводятся температурные зависимости коэффициента Холла и намагниченности сплавов в аморфном и кристаллическом состояниях на основе Fe, Ni с добавками металлоидов, при температурах от комнатной до 1000 K. Показано, что с ростом температуры кристаллизация происходит с выделением различных фаз. Представлены схемы кристаллизации сплава $Fe_{66,87}Ni_{24,7}Si_{4,93}B_{3,5}$. Установлена зависимость между аномальным коэффициентом Холла и намагниченностью, что в определенном интервале температур между ними существует линейная зависимость.

Ключевые слова: аморфное состояние, аморфные металлические сплавы, рентгенограмма, коэффициента Холла, намагниченность, температура Кюри, температура кристаллизации.

EDN: XMBUXC
УДК 537.635

Ferromagnetic Resonance of Superparamagnetic Fe_2O_3/SiO_2 Composites

Sergey V. Stolyar*
Oksana A. Li†
Krasnoyarsk Science Center, Federal Research Center KSC SB RAS
Krasnoyarsk, Russian Federation
Siberian Federal University
Krasnoyarsk, Russian Federation
Nikita M. Boev
Siberian Federal University
Krasnoyarsk, Russian Federation
Kirensky Institute of Physics, Federal Research Center KSC SB RAS
Krasnoyarsk, Russian Federation
Roman N. Yaroslavtsev‖
Anna V. Tyumentseva‡
Anna O. Shokhrina
Krasnoyarsk Science Center, Federal Research Center KSC SB RAS
Krasnoyarsk, Russian Federation
Alexandre M. Vorotynov
Kirensky Institute of Physics, Federal Research Center KSC SB RAS
Krasnoyarsk, Russian Federation
Rauf S. Iskhakov¶
Kirensky Institute of Physics, Federal Research Center KSC SB RAS
Krasnoyarsk, Russian Federation
Samarkand State University named after Sharof Rashidov
Samarkand, Uzbekistan
Irina G. Vazhenin§
Siberian Federal University
Krasnoyarsk, Russian Federation
Kirensky Institute of Physics, Federal Research Center KSC SB RAS
Krasnoyarsk, Russian Federation
Yurii L. Raikher**
Institute of Continuous Media Mechanics, Ural Branch of Russian Academy of Sciences
Perm, Russian Federation

Received 10.02.2026, received in revised form 31.03.2026, accepted 07.05.2026

Abstract. γ-Fe_2O_3/SiO_2 powders with an average particle size of 10 nm were studied using ferromagnetic resonance (FMR). The frequency and temperature dependences of the FMR parameters were analyzed within the framework of the anisotropic superparamagnet model. Saturation magnetization M = 300 G, magnetic anisotropy constant $K \approx 1.8{\cdot}10^5$ erg/cm^3, and exchange surface anisotropy constant $K_u \approx 1.2{\cdot}10^{-2}$ erg/cm^2 were determined for the prepared powders.

Keywords: nanoparticles, ferromagnetic resonance, hyperthermia.

*stol@iph.krasn.ru https://orcid.org/0000-0003-4310-091X
† https://orcid.org/0000-0003-2541-9003 ‖ https://orcid.org/0000-0002-6791-7492
‡ https://orcid.org/0000-0002-2269-0298 ¶ https://orcid.org/0000-0001-6077-2211
§ https://orcid.org/0000-0002-0271-5996 ** https://orcid.org/0000-0002-6167-6528

Citation: S.V. Stolyar, O.A. Li, N.M. Boev, R.N. Yaroslavtsev, A.V. Tyumentseva, A.M. Vorotynov, R.S. Iskhakov, I.G. Vazhenina, Yu.L. Raikher, Ferromagnetic Resonance of Superparamagnetic Fe_2O_3/SiO_2 Composites, J. Sib. Fed. Univ. Math. Phys., 2026, 19(4), 528–536. EDN: XMBUXC.

Introduction

The interest, growing over the past several decades, to the magnetic properties of ferropowders stems from two major factors: the development of new synthesis methods that allow for the targeted modification of chemical composition, size, shape, and surface condition of nanoparticles, and the wide range of their potential practical applications. Contrast agents for magnetic resonance imaging, drug delivery systems, heating mediators in magnetic hyperthermia of tumor cells—these are just a few most known practical applications of magnetic nanoparticles in biomedicine. Magnetic hyperthermia exploits the local heating entailed by the magnetization reversal of nanoparticles in alternating magnetic fields of frequency $f \lesssim 1$ MHz and amplitude up to 300 Oe. The heat generated in such a way disrupts the homeostasis of tumor cells ruining them [1,2], the attained heating power ranges $P_t \sim 100$ W/g.

As an alternative to the low-frequency strategy, in Refs. [3,4] a different concept of the magnetothermal effect was proposed, which allows for increasing P_t by an order of magnitude. This approach employs the phenomenon of ferromagnetic resonance (FMR) that is resonant excitation of the nanoparticle magnetic moment precession which is accompanied by intense energy dissipation. In addition to biomedical applications, the FMR-induced thermal effect may also be of interest in materials science [5], paleontology, and geology [6].

FMR, as such, is widely used as a facile and reliable method for measuring the magnetic parameters (magnetization, various types of anisotropy, exchange interaction constants, etc.) of magnetic nanoparticles [7]. In general, there are two ways to record the FMR data: either to use a broadband line under a fixed external magnetic field and vary the microwave frequency, or to use a fixed-frequency resonator and sweep the applied field strength.

In the macroscopic theory, the magnetic characteristic of a single-domain particle is its magnetic moment m with the magnitude $m = MV$, where M is the magnetization of the ferro(ferri)magnet and V the particle volume. The magnetodynamics of a single-domain particle accompanied by dissipation is described by the Landau–Lifshitz–Gilbert equation [8]:

$$\dot{m} = -\gamma(m \times H_{eff}) - \frac{\alpha\gamma}{m}(m \times (m \times H_{eff})), \tag{1}$$

where γ is the gyromagnetic ratio and α the damping parameter that determines the relaxation time of the precession of vector m:

$$\tau = (\alpha\gamma H_{eff})^{-1}. \tag{2}$$

The effective magnetic field H_{eff} in equation (1) is the sum of external field H, the magnetic anisotropy field H_K and the demagnetizing field of the sample. Provided that, besides the constant field H, the particle is subjected to a high-frequency microwave (AC) field of frequency ω_r and amplitude h, orthogonal to the external field H, the resonant absorption of microwave energy becomes possible. In the framework of the linear response theory, the AC field excitation of the particle may be described in terms of the magnetic susceptibility χ'' that, due to the presence of damping, comes out as a complex quantity. Close to the frequency ω_r, at which the resonant absorption occurs, the imaginary component χ'' — it defines the energy absorption — attains maximum.

FMR in powder materials exhibits a number of unique features compared to their bulk counterparts. This is primarily due to the small size of the grains and, consequently, their large specific

surface area. As the coordination number of magnetically active atoms on the particle surface is lower than in the interior, this leads to formation of various types of surface magnetic anisotropy [9]. Another peculiarity of nanoparticles is their superparamagnetic behavior occurring within a certain temperature range. Due to ever present thermal fluctuations, the particle magnetic moment experiences a stochastic magnetic field $H_f \sim k_B T/MV$; here T is temperature and k_B the Boltzmann constant. For sufficiently small values of the V/T ratio, H_f becomes comparable to the strength of the regular external and/or internal (anisotropy) magnetic fields. Because of that, the particle magnetic moment becomes involved in an intense rotary diffusion process essentially similar to Brownian motion. Remarkably, in the superparamagnetic regime a nanoparticle still remains single-domain, i.e., keeps its internal spin ordering. In other words, the magnetic moment undergoes orientational fluctuations as a single entity. A vast number of studies have been devoted to the theoretical investigation of FMR in superparamagnetic nanoparticles [10–15].

Meanwhile, the number of experimental studies that reveal influence of the superparamagnetic effect of nanoparticles on their FMR properties is extremely limited [16]. Developing this line of research, in [17] the ferromagnetic resonance spectra of nickel ferrite ($NiFe_2O_4$) nanopowder were investigated. To interpret the experimental results, we used a theoretical model describing an isotropic superparamagnet, i.e., the particles with a negligible intrinsic magnetic anisotropy.

In this paper we present the results of a FMR study of composite superparamagnetic powders Fe_2O_3/SiO_2. We remark that silicon dioxide coating significantly improves the dispersibility of magnetic nanoparticles in biological fluids and, moreover, provides a platform for improving their functionalization [18]. The here-presented data was obtained in two independent series of experiments. In the tests of the first type, frequency scanning was performed at room temperature under a fixed bias field. In the tests of the second type, the microwave field frequency was fixed (X-band, $f = 9.48$ GHz) and the FMR measurements were carried out in the temperature range from 20 K to 300 K. As the Fe_2O_3/SiO_2 nanoparticles possess a non-negligible intrinsic magnetic anisotropy, to interpret the experimental results, the anisotropic superparamagnet model [11] was used.

1. Materials and methods

To prepare a γ-Fe_2O_3 powder, iron salts ($FeCl_3$ and $FeCl_2$) were used in a 2 :1 molar ratio in an aqueous solution. 500 mg of the salt mixture was dissolved in 92 mL of distilled water and subjected to mechanical stirring for 10 minutes. Then, 8 mL of a 25% aqueous ammonia solution was added to the mixture and incubated under constant stirring for 30 minutes. The final pH after adding the aqueous ammonia was 10–11. The resulting magnetic precipitate was collected using a neodymium magnet and washed with distilled water until the pH reached neutrality. The particles were coated with silicon oxide using tetraethoxysilane (TEOS). 20 mg of nanoparticles were suspended in an ethanol-water mixture (9 :1) and sonicated for 3 minutes using an UZTA-0.4/22-OM ultrasonic dispergator. Then, under continuous mechanical stirring, 500 μL of TEOS was added dropwise to the suspension. The mixture was incubated at room temperature for 3 hours under constant stirring. The γ-Fe_2O_3/SiO_2 nanoparticle precipitate was washed with distilled water and collected using a magnet.

Particle morphology was studied using a Hitachi HT7700 transmission electron microscope. Temperature-dependent FMR studies were performed using a Bruker ELEXSYS 560 spectrometer operating in the X-band (9.48 GHz). Differential absorption curves (dP/dH) were recorded, where P is the absorbed power and H is the magnetizing field strength. The field-frequency dependences of the powders were studied using a broadband ferromagnetic resonance spectrometer at 300 K in the frequency range from 100 MHz to 10 GHz and fields up to 1500 Oe [19]. In the experiment, the real and imaginary parts of the magnetic permeability μ were measured.

2. Results and discussion

Fig. 1(a) shows a transmission electron microscope image of Fe_2O_3/SiO_2 composite powders. The Fe_2O_3 particles had a nearly spherical shape. Fig. 1(b) shows the particle size distribution of Fe_2O_3 in the Fe_2O_3/SiO_2 composite.

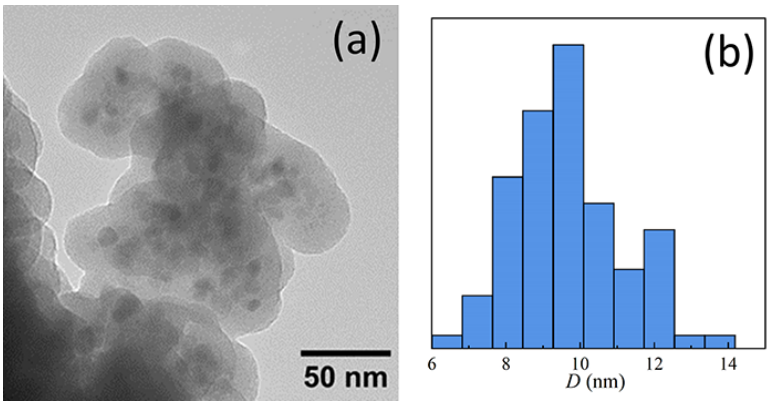

Fig. 1. TEM image of particles (a) and size distribution (b)

Fig. 2 shows the differential microwave absorption characteristics (FMR curves) of the prepared Fe_2O_3/SiO_2 powders, recorded at different temperatures. The resonance field H_r and the line width ΔH, determined from the experimental FMR spectra, are shown in Fig. 3a. The temperature dependence of the normalized intensity I of the FMR resonance curve, which was determined as the product of the line width ΔH and the height of the differential absorption curve $I = \Delta H \cdot dP/dH$, is shown in Fig 3b. The maximum in the temperature dependence $I(T)$ at $T = 200$ K may within reason be associated with the superparamagnetic blocking temperature T_B^{FMR} of the nanoparticles. The maximum intensity of the FMR resonance curve at the blocking temperature T_B^{FMR} has previously been repeatedly observed in γ-Fe_2O_3/SiO_2 composite systems [20] and in γ-Fe_2O_3 nanoparticles [21].

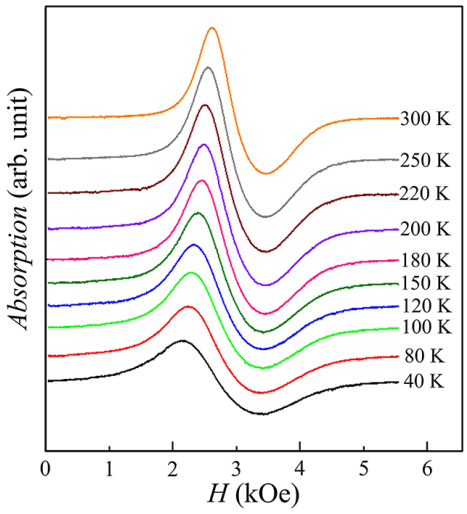

Fig. 2. Experimental FMR spectra at different temperatures

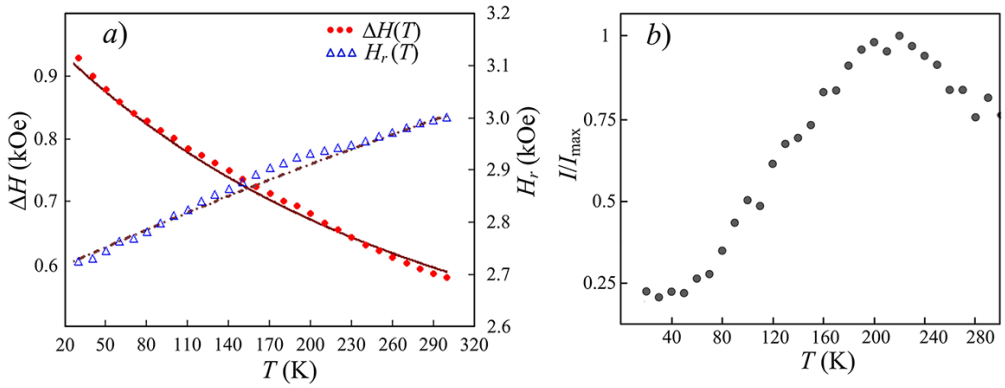

Fig. 3. (a) Temperature dependences of the resonance field H_r and line width ΔH, (b) temperature dependence of FMR intensity

Fig. 4 shows the frequency dependence of the imaginary component of magnetic permeability $\mu'' = 4\pi\chi''$ for different values of external field. The dependence of resonant frequency $f_r = \omega_r/2\pi$ on the magnitude H of magnetizing field is shown in Fig. 5. For the prepared γ-Fe_2O_3/SiO_2 particles, the field-frequency dependence can be approximated by expression $2\pi f_r \approx \gamma^* H + 2\pi f_0$ at $\gamma^* \approx 2{\cdot}10^7$ Hz/Oe for magnetization fields $H > 600$ Oe. The $2\pi f_0$ term indicates the presence of magnetic anisotropy in the nanoparticles. For comparison, the inset in Fig. 5 shows the field-frequency dependence of isotropic superparamagnetic (intrinsic magnetic anisotropy is negligible) $NiFe_2O_4$ powder taken from [17]. For an isotropic superparamagnet, the frequency-field dependence is in general well approximated by a straight line passing through the origin: $2\pi f_r \approx \gamma H$ for $\gamma = 1.8{\cdot}10^7$ Hz/Oe. Deviations from the linear dependence $2\pi f_r \approx \gamma H$ occur only in weak fields ($H \lesssim 300$ Oe).

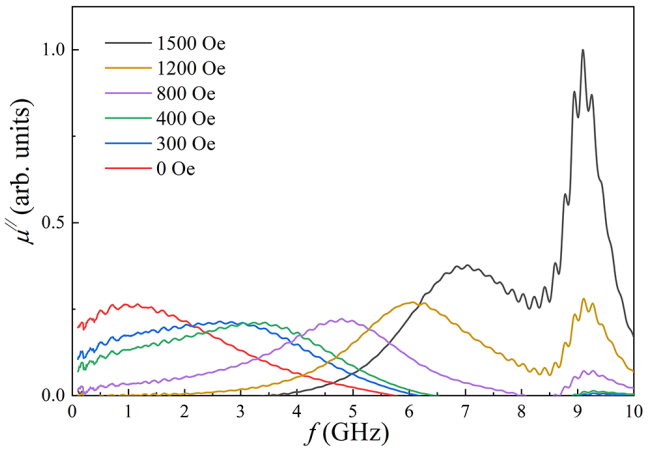

Fig. 4. Frequency dependences of the imaginary μ'' part of the complex magnetic permeability for different values of H

The average size of γ-Fe_2O_3 magnetic inclusions in γ-Fe_2O_3/SiO_2 composite powders is 10 nm (see Fig. 1). The blocking temperature T_B^{FMR}, estimated from the temperature dependence of the intensity of the FMR absorption curve (see Figs. 2 and 3b) is ≈ 200 K. This value is in fair agreement with the estimation of T_B for γ-Fe_2O_3/SiO_2 composites on the base of magnetometric

measurements of $M(H,T)$ [22]. In Ref. [22] using the ZFC-FC protocol, the average blocking temperature was determined to be $T_B^{M(H)} \approx 77$ K.

In [11], the temperature dependences of the resonant frequency ω_r and dynamic magnetic susceptibility of a superparamagnetic particle with uniaxial magnetic anisotropy were calculated. After averaging over random distribution of the anisotropy axes, the expression for the resonant field (resonant frequency) has been presented in the form

$$H_r = \omega/\gamma - H_a \frac{L_2^2}{L_1} - H_u, \tag{3}$$

where $L_1 = \coth\xi - 1/\xi$ and $L_2 = 1 - 3L_1/\xi$ are the Langevin functions, $\xi = (\omega\mu_P)/(\gamma k_B T)$; here μ_P is the magnetic moment of the particle, and H_a is the magnetic anisotropy field. We have added one more term to the right-hand side of equation (3): the unidirectional exchange anisotropy field H_u [9]. This type of surface anisotropy is caused by a spin-glass state acquired by the atomic magnetic moments of the surface. The peculiarity of this type of surface anisotropy is that orientationally the H_u field follows the direction of the externally applied field. Fig. 3 shows the experimental data on the resonance field, as well as the fitting curve plotted using expression (3); for that, H_a, H_u и μ_P were used as fitting parameters. Assuming the saturation magnetization to be equal to magnetization of maghemite (300 G), the particle diameter d and the anisotropy constant K were calculated and are also listed in the table. The table also shows the exchange anisotropy constant K_u, which was determined using formula $K_u = (H_u M d)/6$.

Table 1. Fitting parameters of the experimental curves: $H_r(T)$, $\Delta H(T)$ and $\omega(H)$. M is the magnetization, H_a is the internal anisotropy field, μ_P is the magnetic moment of the particle, d is the particle diameter, K is the uniaxial magnetic anisotropy constant

	H_a, Oe	μ_p, emu	H_u, Oe	K_u, erg/cm^2	d, nm	K, erg/cm^3
$H_r(T)$	1000	$16.12{\cdot}10^{-17}$	310	$1.4{\cdot}10^{-2}$	11.0	$1.22{\cdot}10^5$
$\Delta H(T)$	1519	$15.7{\cdot}10^{-17}$	–	–	10.0	$1.80{\cdot}10^5$
$\omega(H)$	1170	$20.8{\cdot}10^{-17}$	245	$1.2{\cdot}10^{-2}$	10.8	$1.85{\cdot}10^5$

The FMR line width ΔH, defined in [11] as the distance along the field axis between the maximum and minimum of the curve $d\chi''/dH$ has the form:

$$\Delta H(T) = \frac{3}{2} H_a \frac{L_2}{L_1} + \frac{2\alpha\omega(\xi - L_1)}{\sqrt{3}\xi\gamma L_1}. \tag{4}$$

In the anisotropic superparamagnet model that we used, the FMR linewidth, see equation (4), is described by the sum of two contributions: the inhomogeneous broadening (the first term), caused by the spread in the anisotropy field directions, which dominates at low temperatures, and the superparamagnetic contribution, which dominates in the fluctuation region at high temperatures. Fig. 3 shows the fitting curve for the experimental points of the $\Delta H(T)$ dependence, obtained using equation (4). The fitting parameters are given in the Tab. 1. It renders also the uniaxial anisotropy constant, which was determined from relationship $K = H_a M/2$.

The field-frequency dependence shown in Fig. 5 was also fitted using expression (4). The fitting parameters are listed in the Tab. 1.

The parameters given in Tab. 1, were obtained as a result of fitting the experimental curves $H_r(T)$, $\Delta H(T)$ and $\omega(H)$, first, on the requirement that they agree with each other, and secondly, that they agree with the literature data obtained on γ-Fe_2O_3 powders of the corresponding sizes [9].

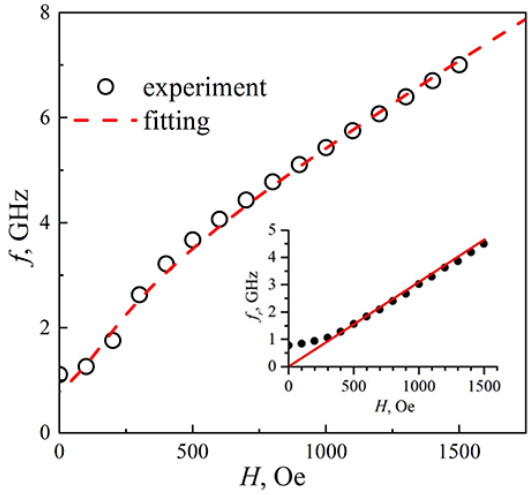

Fig. 5. Dependence of the resonant frequency ω_r on the external field H, determined by the permeability imaginary component μ''. Inset: field-frequency dependence of isotropic superparamagnetic $NiFe_2O_4$ powder [17]

Conclusion

Composite powders of γ-Fe_2O_3/SiO_2 with average maghemite inclusions of size $\sim$ 10 nm were prepared using coprecipitation. FMR curves were measured at frequency f = 9.48 GHz in the temperature range from 20 K to 300 K. The imaginary part of the magnetic permeability was measured using a broadband FMR spectrometer in the frequency range from 100 MHz to 10 GHz and in the fields up to 1500 Oe. The obtained temperature dependences of the resonance field $H_r(T)$, linewidth $\Delta H(T)$, and field-frequency dependence $\omega_r(H)$ were analyzed in the framework of the anisotropic superparamagnet theory. Fitting the experimental curves $H_r(T)$, $\Delta H(T)$, and $\omega_r(H)$ we have arrived at the following evaluations: the saturation magnetization M $\approx$ 300 G, the magnetic anisotropy constant $K \approx 1.8{\cdot}10^5$ erg/cm^3, the exchange surface anisotropy constant $K_u = 1.2{\cdot}10^{-2}$ erg/cm^2. This set of magnetic parameters — extracted with the aid of FMR measurements — turns out to be in fairly good consistence with the literature data obtained by a variety of methods.

This study was carried out within the State Assignment for the "Krasnoyarsk Science Center", Siberian Branch of the Russian Academy of Sciences.

References

[1] R.Hergt, S.Dutz, R Müller, M.Zeisberger, Magnetic particle hyperthermia: nanoparticle magnetism and materials development for cancer therapy, *J. Phys. Condens. Matter.*, **18**(2006), no. 38. DOI: 10.1088/0953-8984/18/38/S26.

[2] C.Martinez-Boubeta, K.Simeonidis, A.Makridis et al., Learning from Nature to improve the heat generation of iron-oxide nanoparticles for magnetic hyperthermia applications, *Sci. Rep.*, **3**(2013), no. 1, 1652. DOI: 10.1038/srep01652

[3] M.-K.Kim, J.Sim, J.-H.Lee, M.Kim, S.-K.Kim, Dynamical origin of highly efficient energy dissipation in soft magnetic nanoparticles for magnetic hyperthermia applications, *Phys. Rev. Appl.*, **9**(2018), no. 5, 054037. DOI: 10.1103/PhysRevApplied.9.054037

[4] J.-H.Lee, B.Kim, Y.Kim, S.-K.Kim, Ultra-high rate of temperature increment from superparamagnetic nanoparticles for highly efficient hyperthermia, *Sci. Rep.*, **11**(2021), no. 1, 4969. DOI: 10.1038/s41598-021-84424-1

[5] N.Yoshikawa, T.Kato, Ferromagnetic resonance heating of Fe and Fe_3O_4 by 5.8 GHz microwave irradiation, *J. Phys. D. Appl. Phys.* , **43**(2010), no. 42, 425403. DOI: 10.1088/0022-3727/43/42/425403

[6] D.Walton, S.Snape, T.C.Rolph, J.Shaw, J.Share, Application of ferrimagnetic resonance heating to palaeointensity determinations, *Phys. Earth Planet. Inter.*, **94**(1996), no. 3-4, 183–186. DOI: 10.1016/0031-9201(95)03094-8

[7] I.Benguettat-El Mokhtari, D.S.Schmool, Ferromagnetic resonance in magnetic oxide nanoparticules: A short review of theory and experiment, *Magnetochemistry*, **9**(2023), no. 8, 191. DOI: 10.3390/magnetochemistry9080191

[8] A.G.Gurevich, Magnetic Resonance in Ferrites and Antiferromagnets, Moscow, Nauka, 1973, 591.

[9] V.P.Shilov, Yu.L.Raikher, J.-C. Bacri, F.Gazeau, R.Perzynski, Effect of unidirectional anisotropy on the ferromagnetic resonance in ferrite nanoparticles, *Phys. Rev. B.*, **60**(1999), no. 17, 11902–11905. DOI: 10.1103/PhysRevB.60.11902

[10] I.S.Poperechny, Yu.L.Raikher, Ferromagnetic resonance in uniaxial superparamagnetic particles, *Phys. Rev. B.*, **93**(2016), no. 1, 014441. DOI: 10.1103/PhysRevB.93.014441

[11] Yu.L.Raikher, V.I.Stepanov, Thermal fluctuation effect on the ferromagnetic-resonance lineshape in disperse ferromagnets, *JETP*, **102**(1992), no. 4, 1409–1423.

[12] F.Gazeau, V.Shilov, J.C.Bacri et al., Magnetic resonance of nanoparticles in a ferrofluid: evidence of thermofluctuational effects, *J. Magn. Magn. Mater.*, **202**(1992), no. 2-3, 535–546. DOI: 10.1016/S0304-8853(99)00156-0

[13] R.S.Gekht, V.A.Ignatchenko, Yu.L.Raikher, M.I.Shliomis, Magnetic resonance of an isotropic superparamagnet, *JETP*, **43**(1976), no. 4, 677–683.

[14] R.S. de Biasi, T.C.Devezas, Anisotropy field of small magnetic particles as measured by resonance, *J. Appl. Phys.*, **49**(1978), no. 4, 2466–2469. DOI: 10.1063/1.325093

[15] E.de Biasi, C.A.Ramos, R.D.Zysler, Size and anisotropy determination by ferromagnetic resonance in dispersed magnetic nanoparticle systems, *J. Magn. Magn. Mater.*, **262**(2003), no. 2, 235–241. DOI: 10.1016/S0304-8853(02)01496-8

[16] F.Gazeau, J.Bacri, F.Gendron et al., Magnetic resonance of ferrite nanoparticles, *J. Magn. Magn. Mater.*, **186**(1998), no. 1-2, 175–187. DOI: 10.1016/S0304-8853(98)00080-8

[17] S.V.Stolyar, O.A.Li et al., Heating of superparamagnetic powders via the ferromagnetic resonance mode, *J. Appl. Phys.*, **139**(2026), no. 1, 013901. DOI: 10.1063/5.0302922

[18] A.V.Tyumentseva, S.V.Komogortsev, R.N.Yaroslavtsev et al., Silica–iron oxide magnetic composite particles for in vitro cell separation: Synthesis, possibilities, and effects on cell metabolism, *ACS Appl. Bio Mater.*, **8**(2025), no. 10, 8643–8654. DOI: 10.1021/acsabm.5c00587

[19] A.V.Izotov, B.A.Belyaev, N.M.Boev et al., Ferromagnetic resonance line broadening and shift effect in nanocrystalline thin magnetic films: Relation with crystalline and magnetic structure, *J. Alloys Compd.*, **900**(2022), 163416. DOI: 10.1016/j.jallcom.2021.163416

[20] R.Berger, J.-C.Bissey, J.Kliava, H.Daubric, C.Estournés, Temperature dependence of superparamagnetic resonance of iron oxide nanoparticles, *J. Magn. Magn. Mater.*, **234**(2001), no. 3, 535–544. DOI: 10.1016/S0304-8853(01)00347-X

[21] N.E.Domracheva, A.V.Pyataev, R.A.Manapov, M.S.Gruzdev, Magnetic resonance and Mössbauer studies of superparamagnetic γ-Fe_2O_3 nanoparticles encapsulated into liquid-crystalline poly(propylene imine) dendrimers, *ChemPhysChem.* , **12**(2011), no. 16, 3009–3019. DOI: 10.1002/cphc.201100363

[22] S.V.Stolyar, R.N.Yaroslavtsev, A.V.Tyumentseva et al., Manifestation of stoichiometry deviation in silica-coated magnetite nanoparticles, *J. Phys. Chem. C.*, **126**(2022), no. 17, 7510–7516. DOI: 10.1021/acs.jpcc.2c00349

Ферромагнитный резонанс суперпарамагнитных композитов Fe_2O_3/SiO_2

Сергей В. Столяр
Оксана А. Ли
Федеральный исследовательский центр КНЦ СО РАН
Красноярск, Российская Федерация
Сибирский федеральный университет
Красноярск, Российская Федерация
Никита М. Боев
Институт физики им. Л. В. Киренского, ФИЦ КНЦ СО РАН
Красноярск, Российская Федерация
Сибирский федеральный университет
Красноярск, Российская Федерация
Роман Н. Ярославцев
Анна В.Тюменцева
Анна О. Шохрина
Федеральный исследовательский центр КНЦ СО РАН
Красноярск, Российская Федерация
Александр М. Воротынов
Институт физики им. Л. В. Киренского, ФИЦ КНЦ СО РАН
Красноярск, Российская Федерация
Рауф С. Исхаков
Институт физики им. Л. В. Киренского, ФИЦ КНЦ СО РАН
Красноярск, Российская Федерация
Самаркандский государственный университет имени Шарофа Рашидова
Самарканд, Узбекистан
Ирина Г. Важенина
Институт физики им. Л. В. Киренского, ФИЦ КНЦ СО РАН
Красноярск, Российская Федерация
Юрий Л. Райхер
Институт механики сплошных сред, УрО РАН
Пермь, Российская Федерация

Аннотация. Методом ферромагнитного резонанса (ФМР) изучены порошки γ-Fe_2O_3/SiO_2 со средним размером 10 нм. Частотные и температурные зависимости параметров ФМР анализировались в рамках модели анизотропного суперпарамагнетика. Определены намагниченность насыщения M = 300 Гс, константа магнитной анизотропии $K \approx 1.8{\cdot}10^5$ erg/cm^3, константа обменной поверхностной анизотропии $K_u = 1.2{\cdot}10^{-2}$ erg/cm^2 изготовленых порошков.

Ключевые слова: наночастицы, ферромагнитный резонанс, гипертемия

Journal of Siberian Federal University. Mathematics & Physics 2026, 19(4), 537–559

EDN: SWYHOH
УДК 51(9)

Superparamagnetic Particles: Introduction to Theoretical Description of the Magnetodynamics

Yuriy L. Raikher*
Institute of Continuous Media Mechanics
Ural Branch of the Russian Academy of Sciences
Perm, Russian Federation

Received 03.02.2026, received in revised form 05.03.2026, accepted 07.04.2026

Abstract. The goal of this paper is to present a brief comprehensive review text on the theoretical framework that provides basic description of the magnetodynamics of single-domain superparamagnetic particles. It is shown how the classical framework (Landau–Lifshitz and Gilbert equations) are modified for the case of superparamagnetic behavior where temperature explicitly enters the equations since the deterministic dynamics is replaced by the stochastic one that is rendered by either the kinetic (Fokker-Planck-like) equation for the distribution function or by the set of equations which link the statistical moments of growing order. As an initial step, the conventional macroscopic (phenomenological) description of magnetodynamics of a ferromagnet particle is outlined and discussed.

Keywords: superparamagnetism, single-domain particles, orientational distribution function, magnetodynamics.

Citation: Y.L. Raikher, Superparamagnetic Particles: Introduction to Theoretical Description of the Magnetodynamics, J. Sib. Fed. Univ. Math. Phys., 2026, 19(4), 537–559. EDN: SWYHOH.

Introduction

Well below the Curie temperature, the fine particles of ferromagnets and ferrites in a certain size range acquire non-trivial behavior known as *superparamagnetism* that in some way may be looked at as the rotary Brownian motion of the particle magnetic moments. As a result, the observable properties of the particles as such and of their assemblies become strongly temperature-affected. In here we do not touch the nanosuspensions of such particles in fluids although these systems, which are widely known as *magnetic fluids* or *ferrocolloids*, make an important and interesting class of composite media of multi-purpose destination including biotechnology and medicine. The point is that all the new and newest applications notwithstanding, the standard situation, where the nanoparticles are considered as fully trapped in a solid matrix still attracts a lot of attention. The 'customers' for the knowledge of the behavior of fine magnetic particles in wide temperature ranges and under magnetic fields of arbitrary frequency and amplitudes come from the numerous community of researches and engineers who work on developing and improvement of materials and methods of magnetic data recording or intentional heating (hyperthermia) of the composites whereto the nanoparticles are embedded.

The mathematical basis for the theory of superparamagnetism is formed by the technique of solving the orientational rotary diffusion (Fokker–Planck-like) equation by reducing this partial derivative equation to an infinite set of ordinary differential equations that describes the time evolution of the statistical moments of the distribution function. The latter renders either the probability density $W(\boldsymbol{\mu}, t)$ for the angle coordinates of the magnetic moment $\boldsymbol{\mu}$ or $W(\boldsymbol{n}, t)$ that is the distribution for the components of the orientational tensor of the particle geometry

*raikher@icmm.ru https://orcid.org/0000-0002-6167-6528

axis $\boldsymbol{n}$. In a number of cases the joint distribution function $W(\boldsymbol{\mu}, \boldsymbol{n}, t)$ is considered. The obtained equations are finally solved numerically by sweep methods. It has turned out that the said algorithm is very efficient for this type of problems since the emerging matrices are rather sparse. A completely different (at the first sight) method is described in the book [1]. It uses the formalism of the continued fractions and provides the expressions for the solutions of the Fokker–Planck equation which, when written symbolically, look as exact ones, see [2]. However, any conversion of a continued fraction into some particular result needs a numerical procedure. In fact, both methods (sweep and continued fraction) are identical by its content, meaning and ability. In Sections 5 and 6 we present in detail the scheme of application of the sweep method taking the case of a single-domain particle with easy-axis magnetic anisotropy as an instructive example. However, first, to be consistent, in Sections 2–4 the necessary basic notions of the theory of superparamagnetism are given.

1. Single-domain ferromagnetic particles

Fine magnetic particles are unique physical objects with remarkable properties which differ greatly from those of their parent massive materials. The source of this difference, which has numerous and diverse manifestations, is the fact that in fine particles surface effects become comparable with or dominating over the bulk ones. Notably, just this condition suffices to outline the range of spatial scales where the notion of *a fine magnetic particle* turns up.

Here we discuss the fundamental issues, estimations and analysis of the equilibrium and dynamic properties of fine particles made of a ferromagnet or ferrite. That is why from the very beginning we introduce the most important notations for 'global' usage. In particular, we adopt the macroscopic (continuum) approach to magnetodynamics assuming simultaneously that the temperature is well below the Curie point. This viewpont was shaped up by W. F. Brown [3] and since then is known as *micromagnetism*. In the micromagnetic framework one treats the magnetization of the ferromagnetic material as a vector of constant length that we denote as

$$\boldsymbol{M} = M\boldsymbol{e}, \tag{1}$$

thus introducing $\boldsymbol{e}$, the unit vector of magnetization. The value of magnetization M is of the order of saturation magnetization M_s of the corresponding bulk material and typically ranges from 0.3 to 1.5 kG. Another unit vector, $\boldsymbol{n}$, we associate with the uniaxial magnetic anisotropy whose direction is imposed either by the crystallographic structure of the particle or by the anisometricity of its body. For estimates we suppose that the particle non-sphericity is not too strong, so that all the three dimensions are close to d, the mean diameter; thence for the particle volume one gets $V \simeq \pi d^3/6$. This formally excludes the cases of needle-like (acicular) or disc-like fine magnetic grains. However, if necessary, the estimates could be easily modified for these cases.

In the absence of external fields, the volume density of free energy of a magnetic material with a uniaxial internal anisotropy writes

$$F = \frac{1}{2}\,\alpha M^2\,(\nabla \boldsymbol{e})^2 - K_v(\boldsymbol{e}\cdot\boldsymbol{n})^2 - \frac{1}{2}\,M(\boldsymbol{e}\cdot\boldsymbol{H}_d). \tag{2}$$

Here $\nabla\boldsymbol{e} = \partial e_i/\partial x_j$ is the second rank tensor, $\alpha \sim 10^{-12}\,\mathrm{cm}^2$ is a parameter called *the exchange rigidity constant*, K_v is the volume density of the magnetic anisotropy energy which normally ranges $K_v \sim 10^4 - 10^6\,\mathrm{erg/cm}^3$. The first term in Eq. (2) yields the macroscopic form of the non-uniform exchange interaction induced by spin non-collinearity. The second one renders the contribution of the spin-orbit interaction (crystal field) that determines the energetically favorable directions of the magnetization inside the ferromagnetic (ferrite) sample. The last (magnetostatic) term is caused by the so-called demagnetizing field H_d, i.e., the energy of the

'magnetic poles' emerging at the surface of a sample either magnetized by an external field or possessing a spontaneous magnetization.

The volume energy density in the form (2) implies that a sample of finite size is considered. Indeed, the presence of the demagnetizing, also called *the magnetostatic*, term is solely due to the assumed existence of a surface or interface where the magnetic poles appear. Following the authors of review papers [4, 5], one may divide the fine-particle effects in two categories. The effects of the first category stem from just the finiteness of the size. The other category comprises the effects which are due to the specific properties of the surface that differ from those of the bulk: broken atomic bonds, deficiency of neighboring atoms, etc. In this context, the appearance of the magnetostatic term in Eq. (2) is a finite-size effect, see Ref. [3] for example.

By definition, the demagnetizing term in Eq. (2) is non-zero for the cases where the particle is magnetized in such a way that it creates in the outer space a magnetic (*stray*) field. We remark that the magnetostatic term does not require that magnetization is uniform over the sample. It is right its interplay with the the first two terms of Eq. (2) that entails the most well-known magnetic surface effect: the existence of uniformly magnetized, i.e., single-domain particles. We remind that ordinary magnetic materials, either metals or ferrites, on a usual spatial scale (μm and greater) in the absence of an external field are always multi-domain.

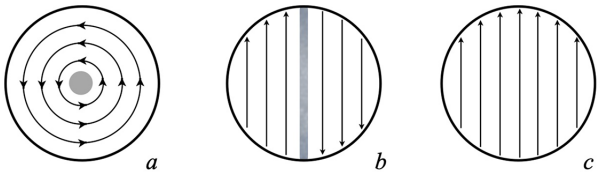

Fig. 1. Schematic view of nanoparticle domain structures: (a) a magnetically soft particle, no distinctive domain wall, in the central part the structure is 3D to avoid singularities; (b) a magnetically hard particle with a narrow domain wall; (c) a single-domain particle

To estimate the spatial scale below which single-domain state becomes possible, let us compare alternative situations illustrated by Fig. 1. In a uniformly magnetized particle $\mathcal{F}_{\rm ms}$ is minimum, and the energy increment is caused by the stray field. Near the surface the magnitude of H_d equals $4\pi M/3$ that yields the particle energy $\delta\mathcal{F}_{\rm ms} \sim -H_d M v \sim \mu M \sim M^2 d^3$, where $\mu = MV$ is the total magnetic moment. On the other hand, a sample with a closed magnetic flux (multi-domain) has zero net magnetic moment and thus is in the minimum with respect to $\mathcal{F}_{\rm ms} = 0$ 'paying' for that by a non-uniform spatial distribution of magnetization and thus causing the energy increment from the non-uniform exchange term:

$$\delta\mathcal{F}_{\rm ex} \sim \alpha(M^2/d^2)\, v \sim \alpha M^2 d; \tag{3}$$

note that here we assume that $M^2 \gg K_v$ so that the sample is effectively isotropic. Evidently, the particle will be magnetized non-uniformly (the reference length is the particle dimension) as long as $\delta\mathcal{F}_{\rm ex} < \delta\mathcal{F}_{\rm ms}$. Under the reversed condition, the state of minimal energy corresponds to a uniform magnetization, i.e., the particle becomes a single magnetic domain. Estimation of the maximum size of single-domainnes for a magnetically isotropic particle yields

$$d_* = \sqrt{\alpha} \sim 10^{-6}\,\text{cm} = 10\ \text{nm}. \tag{4}$$

In the case of magnetically hard particles ($M^2 \ll K_v$) the main term opposing the magnetostatic one is the uniaxial anisotropy. Here, as the first step, one needs to estimate the surface tension of the domain wall. On doing that, see textbooks [6, 7] or the original paper [8], instead of Eq. (4) one gets

$$d_* = \sqrt{\alpha K}/M. \tag{5}$$

At $K \sim 10^6\,\mathrm{erg/cm^3}$ and $M \sim 10^3\,\mathrm{G}$ this estimation is of the same order of magnitude as that of Eq. (4). Therefore, one arrives at the conclusion that the conventional term *single-domain particles* has in fact quite a precise meaning expressed by the condition $d \lesssim 10$ nm.[†]

Denoting the interatomic distance in a crystalline substance by a_0, one gets a well-known estimate for the fraction of the atoms residing at the particle surface. For $d \simeq 10$ nm and a_0 about 0.2 nm, one has

$$c \sim 6a_0/(d - 6a_0) \simeq 14\% \tag{6}$$

which number grows drastically when d goes below 10 nm. Evidently, c renders also the fraction of spins deprived of a full set of neighbors.

Incomplete and distorted atomic surrounding creates for a spin a situation where those crystal field contributions, which self-average for a bulk spin, remain non-zero. Under such conditions, a surface spin experiences an enhanced crystal field, and its local (single-ion) magnetic anisotropy is different (usually, higher) than that for a bulk one. This mechanism does not reduce to just geometrical restrictions and, right as implied by the classification of Ref. [4], represents the situation where the surface possesses some special properties different from those of the bulk. The existence of surface magnetic anisotropy has numerous experimental verifications in both films and fine particles but its origin is still not completely clear. In fact, the modern phenomenology did not proceed much beyond the fundamental concept worked out by Néel in 1954 [12]. In this approach the surface anisotropy is described at the macroscopic level by a specific energy parameter K_s and the direction of the local easy (or hard) magnetization axis. Then the surface energy density is written as

$$F_s = -K_s\,(\boldsymbol{e}\cdot\boldsymbol{\nu})^2\,, \tag{7}$$

where $\boldsymbol{\nu}$ is the unit vector of the surface easy axis. From the symmetry considerations Néel [12] and, after him, Brown [3] associated $\boldsymbol{\nu}$ with the direction of the normal to the particle surface. According to the same work by Néel, the surface energy density is estimated as $K_s \sim \pi\ell M^2$, where $\ell \sim 10\,\mathrm{nm}$ is some characteristic length of the order of 10 nm. For example, for a well-known ferrite γ-Fe_2O_3 (maghemite) which has $M \simeq 400\,\mathrm{G}$ this gives $K_s \sim 5 \times 10^{-2}\,\mathrm{erg/cm^2}$.

2. Superparamagnetic effect

The main idea of superparamagnetism first put forward in 1949 by Néel [13] and cast to a comprehensive form by Bean and Livingston [14], is that thermal fluctuations inside a solid particle can strongly affect the state of magnetization of this particle. The superparamagnetic effect in its basic form is expressed by a simple relationship

$$\tau = \tau_0\,\exp(U_a/kT), \tag{8}$$

where U_a is the particle magnetic anisotropy energy[‡]. The pre-factor τ_0 in Eq. (1) is some microscopic time characteristic of a particular magnetic material; typical values of τ_0 lie in the range 10^{-9}–$10^{-11}\,\mathrm{s}$. The estimations for U_a follow from the above-given expressions for the anisotropy energy: $U_a \sim K_v V$ or $U_a \sim K_s S$, where V and S are the particle volume and lateral area, respectively.

By its physical meaning, Eq. (8) is the reference time, which the magnetic moment $\boldsymbol{\mu}$ of a single-domain particle spends in a given energy minimum of the depth U_a at a given temperature T. In other words, during time intervals $t < \tau$ the particle behaves as a permanent magnet.

[†]We remark that the given estimation examples are rather heuristic. A more rigorous approach to the problem was outlined by Brown [9]. Concerning the modern developments of the problem see Refs. [10, 11] and references therein.

[‡]Here we do not distinguish between free energy $\mathcal{F}$ and internal energy U of the particle since no change of its aggregate state is expected. The possible thermal effect is included in the thermal dependence of the material parameters like M or K.

At longer times, $t > \tau$, the probability is high that under thermal fluctuations $\boldsymbol{\mu}$ will reverse at least once. This means the loss of 'memory' of the initial state. At $t \gg \tau$ the particle magnetic moment behaves exactly as that of an atom in a paramagnetic gas. The only difference is in the value of the magnetic moment. Indeed, we discuss room (and lower) temperatures, i.e., the range well below the Curie point of usual ferromagnets/ferrites. This means that microscopically the particle remains a spin-ordered object comprising about 10^5 coherently oriented spins. Thence its magnetic moment $\boldsymbol{\mu} = MV\boldsymbol{e}$ (albeit randomly rotating) is super-high in comparison with that of a paramagnetic atom. That is why the effect had acquired its name.

Imagine that we use a PC with a hard disk, where the size of the magnetic grains in the working layer is progressively diminished. At first, one will see a positive effect: with smaller particles the resolution of recording will enhance, and the PC will be able to write and read a growing amount of data. Then, on further diminution of the particle size, the time τ will become comparable with the mean time interval between writing and reading, and some symptoms like a dementia disease will show up — fits of forgetfulness and occasional memory blackouts. Further 'grinding' of the particles will finally lead to a complete mess: the disk, consuming huge lumps of data will be forgetting them immediately. At the attempt of reading, only random (white) noise will emerge, complete amnesia. According to the existing estimates [15], we enter the epoch when the areal density of records in commercially available devices will reach $1\,\mathrm{Tbit} = 10^{12}\,\mathrm{bit}$ per square inch. How far one may go beyond that? The main limitation on miniaturization of the magnetic recording devices is imposed by superparamagnetism.

This fundamental law of magnetic recording is expressed by Eq. (8). Such non-hysteretic (*superparamagnetic*) behavior is universal and occurs in any ferrite or ferromagnet had it been sufficiently dispersed to the nanosize range.

Let us estimate the size at which the superparamagnetic behavior of the particles becomes important. A reasonably high value of the volume magnetic anisotropy is $K \sim 1.5{\cdot}10^6\,\mathrm{erg/cm^3}$. Using it, we find that at room temperature ($kT \sim 4{\cdot}10^{-14}\,\mathrm{erg}$), the ratio ($U_a/kT \sim 40$ (stability of the record during 10 years) is ensured with the particles of volume $V \gtrsim 10^{-18}\,\mathrm{cm^3}$. Assuming the particle to be spherical, for its linear size (diameter) one finds $d \sim 12\,\mathrm{nm}$. Comparing that with the estimations given in Section 1, one finds that superparamagnetic behavior should be inherent to single-domain particles.

Now let us estimate the density of particle distribution over the surface. The area that one particle occupies equals $S_1 \sim d^2 \sim 1.5\cdot10^{-12}\,\mathrm{cm^2}$. Consider the grains organized in a square lattice with the minimal center-to-center distance $2d$ in order to reduce the stray fields of the neighbors. With such a pattern the number density of the particles is $\sim 10^{12}$ per square inch, that is right about $1\,\mathrm{Tbit/inch^2}$. About the same value one finds if for the particles not bulk but surface magnetic anisotropy with the density $K_s \sim 1\,\mathrm{erg/cm^2}$ is assumed. This simple estimate coincides by the order of magnitude with that derived in a more sophisticated way [15]. To be reasonable, one has to consider 1 Tbit level as a prospective rather than real assertion, since it is based on the assumption that the dimensions of the writing and reading heads are of the order of d. As yet, with allowance for a finite size of a head and the fact that one bit is written at the cluster of several grains.

We remark, however, that the above-discussed transition to the regime of spontaneous remagnetizing of particles is an undesirable effect only if to look at it from the magnetic data storage viewpoint. It to treat the problem more broadly, from the position of general physics, it becomes clear that to investigate both the spontaneous motion of the magnetic moment (free orientational diffusion) and its forced diffusion motion makes not at all less interest than the magnetodynamic studies restricted effectively to the $T = 0$ domain. The main merit of the physics of nanoparticles is that the theory that is being developed, allows to go through all the important size range and to get an adequate account of the rôle of thermofluctuational effects. By this, one gets the description of the phenomena from its dynamic-like end (large particles and/or low temperatures) to its essentially diffusional limit (small particles and/or high temperatures).

In particular, with respect to the magnetic recording this shows where one should part with the hopes for further condensing of the stored data.

As it has been found, the fluctuational domain, where noise effects are very pronounced, is very interesting as such and is very rich in novel effects [16]. Right in the systems, where the ability to oscillations is suppressed by strong noisy motion (overdamped oscillator), there were discovered the so-called *stochastic resonance* [17, 18] and, maybe yet less known but not to the least interesting *noise-* and *force-induced resonances* [19–22]. The fact that single-domain magnetic particles in the superparamagnetic regime ($U_a/kT \sim 1$) are extremely convenient (one may say, perfect) objects for observation and investigation of the phenomena of such a kind had been commented on many times [23–29]. Inspired by the idea, theoretical models equivalent to that of a single-domain particle were introduced to describe the functional properties of magnetoresistive heads [30–32].

3. Superparamagnetiic effect on closer inspection

3.1. Reference time scales. Magnetodynamic equation

The phenomenological equation which determines the motion of the magnetic moment of a ferromagnetic sample is known under the generic name of *Landau–Lifshitz–Gilbert equation* and has two basic modifications. The first form

$$\frac{d\boldsymbol{e}}{dt} = -\gamma\,(\boldsymbol{e}\times\boldsymbol{H}_e) - \alpha\gamma\,(\boldsymbol{e}\times(\boldsymbol{e}\times\boldsymbol{H}_e)) \tag{9}$$

had been proposed in [8]. When applied to a single-domain particle, the notations in Eq. (9) mean: $\boldsymbol{e}$ the unit vector of the magnetic moment, γ is the gyromagnetic ratio for electrons, α is the non-dimensional constant (the constant of spin-lattice relaxation) which determines the rate of damping of the Larmor precession of the vector $\boldsymbol{\mu}$. The magnitude of the latter is $\mu = MV_m$, where V_m is the volume of that part of the particle which possesses bulk ferromagnetic properties. Thus we allow for the fact that a particle of a total volume V may bear a 'dead' shell on its surface [33, 34] or that the particle surface layer may be effectively demagnetized due to its specific magnetic structure, see [4, 35, 36] for particular examples. The effective magnetic field $\boldsymbol{H}_e$ in Eq. (9) sums up all the internal and external fields acting on the vector $\mu\boldsymbol{e}$. The schematic presentation of the torques acting on vector $\boldsymbol{e}$ — according to (9) they contribute to the angular velocity $d\boldsymbol{e}/dt$ — is given in Fig. 2.

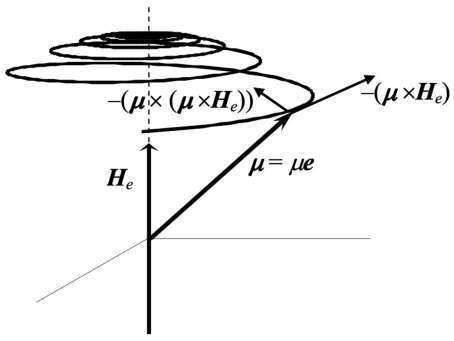

Fig. 2. Schematic view of the torques experienced by the magnetic moment perturbed from its equilibrium position

The alternative form of the magnetodynamic equation was introduced by Gilbert in [37, 38]:

$$\frac{d\boldsymbol{e}}{dt} = -\gamma^* \left(\boldsymbol{e} \times \boldsymbol{H}_e\right) + \alpha_0 \left(\boldsymbol{e} \times \frac{d\boldsymbol{e}}{dt}\right). \tag{10}$$

As one sees from comparison, Landau-Lifshitz and Gilbert equations do differ in the form of the damping term. Specifically, the Gilbert equation embodies explicitly the hypothesis of linear irreversible thermodynamics which states that dissipation is proportional to the rate of change of the corresponding dynamic variable. Note the presence of the time derivative of $\boldsymbol{e}$ in both parts of the equation. Soon afterwards it had been proven — see [39] — that Eqs. (9) and (10) are in fact identical and transform into each other upon the replacement:

$$\gamma^* = \gamma(1+\alpha_0^2), \qquad \alpha = \alpha_0\,. \tag{11}$$

Owing to the coincidence of α and α_0, further on we omit the subscript at the damping parameter. However, for the magnetic materials with enhanced level of dissipation the Gilbert form is more appropriate. Indeed, consider it for a simple isotropic ferromagnet under the combination of a constant (magnetizing) field and a weak probing field $\propto \exp(-i\omega t)$. Setting $H_e = H_0$ and associating (as in a standard experiment) the resonance field with the value of H_0 which delivers maximum to the out-of-phase (imaginary) component of the linear dynamic susceptibility $\chi(\omega)$ at $\omega_0 = \gamma H_0$, in the $\alpha \ll 1$ limit we find

$$H_0^{(\mathrm{res})} = \frac{\omega_0}{\gamma^*}\,\sqrt{2\sqrt{1+\alpha^2} - (1+\alpha^2)} \simeq \frac{\omega_0}{\gamma^*}\,\left(1 - \frac{1}{8}\,\alpha^4\right). \tag{12}$$

With regard to that, one may consider the dependence of H_{res} on α as a weak one. Meanwhile, in the Landau-Lifshitz terms one has in the same limit:

$$H_0^{(\mathrm{res})} = \frac{\omega_0}{\gamma}\,\sqrt{\frac{2}{(1+\alpha^2)^{3/2}} - \frac{1}{1+\alpha^2}} \simeq \frac{\omega_0}{\gamma(1+\alpha^2)}. \tag{13}$$

Comparing Eqs. (12) and (13), one sees that the Landau-Lifshitz resonance field contains additional factor $\propto 1/(1+\alpha^2)$, and thus is more sensitive to α than the Gilbert one. Of course, at $\alpha \to 0$ both approaches coincide. The dependences of the Gilbert and Landau–Lifshitz resonance fields on α are shown in Fig. 3. Turning of H_0^{res} into zero at $\alpha = \sqrt{3}$ and its nonexistence at greater α's means that in this range function $\chi''(H_0)$ has no maximum and diminishes monotonically as its argument grows.

In the framework of the standard linear response theory the relaxation times of precession are determined in the $\alpha \ll 1$ limit according to the generic formula $\tau = (\alpha\gamma H)^{-1}$. Setting the field equal to its resonance value, one gets

$$\tau = \begin{cases} 1/\alpha\omega_0 & \text{Gilbert case,} \\ (1+\alpha^2)/\alpha\omega_0 & \text{Landau-Lifshitz case.} \end{cases}$$

For the case when the external magnetizing field is absent, the reference relaxation time of precession is defined upon assuming that the particle possesses uniaxial magnetic anisotropy with the energy density K. Then the Larmor precession in the intrinsic anisotropy field is considered, and the generic formula for the relaxation time emerges as $\tau = M/2\alpha\gamma K$. Specifying it for the two representations, one gets

$$\tau_0 = \begin{cases} M(1+\alpha^2)/2\alpha\gamma^* K & \text{Gilbert case,} \\ M/2\alpha\gamma^* K & \text{Landau-Lifshitz case,} \end{cases}$$

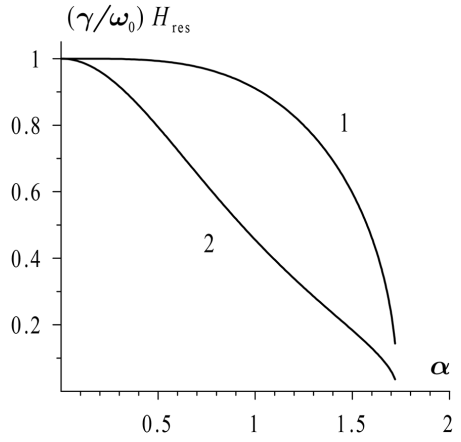

Fig. 3. Comparison of the resonance fields as functions of the damping parameter in the Gilbert (1) and Landau–Lifshitz (2) representations.

which expressions coincide at $\alpha \to 0$. Therefore, τ_0 provides a basic reference time scale for high-frequency magnetic processes in a single-domain particle in the absence of external fields and thermal fluctuations. To estimate τ_0 by the order of magnitude we take $M \sim 400\,\mathrm{G}$ and $K \sim 10^6\,\mathrm{erg/cm^3}$ that is typical for a nanodispersed ferrite, set $\alpha = 0.1$ (moderate quality factor of the precession) and recall that $\gamma \simeq 1.7{\cdot}10^7\,\mathrm{rad/Oe}$. This yields $\tau_0 \sim 10^{-10}\,\mathrm{s}$.

3.2. Rotary mobility coefficient of the magnetic moment

We choose a spherical coordinate frame with the polar axis directed along vector $\boldsymbol{H}_e$. Then the basic vectors of the problem write as

$$\boldsymbol{H}_e = (0,\, 0,\, H_e), \qquad \boldsymbol{e} = (\sin\vartheta\cos\varphi,\, \sin\vartheta\sin\varphi,\, \cos\vartheta).$$

According to Eqs. (9) and (10), when having been deviated from its equilibrium position $\boldsymbol{e} \parallel \boldsymbol{H}_e$ or $\vartheta = 0$, the magnetic moment $\boldsymbol{e}$ begins to precess around the direction of $\boldsymbol{H}_e$. Scalar multiplication of Eq. (9) by H_e, shows that under zero dissipation ($\alpha = 0$) this precession is unceasing. At non-zero damping the same multiplication yields

$$\left(\boldsymbol{H}_e \cdot \frac{d\boldsymbol{e}}{dt}\right) = -\alpha\gamma\,(\boldsymbol{e}\cdot\boldsymbol{H}_{\mathrm{eff}})^2 + \alpha\gamma H_e^2,$$

where from after dividing by H_e one gets

$$\frac{de_z}{dt} = -\alpha\gamma H_e\left(\cos^2\vartheta - 1\right) \quad \text{or} \quad \frac{d\vartheta}{dt} = -\alpha\gamma H_e\sin\vartheta. \tag{14}$$

The quantity $d\vartheta/dt$ is the component of the angular velocity $\boldsymbol{\Omega}$ of the magnetic moment in the direction perpendicular to Oz axis, i.e., to the field $\boldsymbol{H}_{\mathrm{eff}}$. In Eq. (14) it is the dissipative torque which strives to bring the magnetic moment back to its equilibrium position $\vartheta = 0$. With allowance for the constancy of the length μ of the magnetic moment, Eq. (14) in vector form writes as

$$\boldsymbol{\Omega}_\perp = \frac{\alpha\gamma}{\mu}\,(\,\mu\boldsymbol{e}\times\boldsymbol{H}_e)_\perp\,. \tag{15}$$

As it shows, the coefficient

$$b^{(\mathrm{LL})} = \alpha\gamma/\mu \tag{16}$$

has the meaning of the rotary mobility of the magnetic moment with respect to its relaxational (i.e., towards its equilibrium position) motion. Indeed, in the Landau–Lifshitz equation this coefficient establishes proportionality between the torque exerted on the vector $\boldsymbol{\mu}$ and the angular velocity of the latter normal to the precession axis. Using the correspondence relationships (11), one finds that the mobility coefficient rendered by Gilbert equation (10) has the form

$$b^{(\mathrm{G})} = \frac{\alpha\gamma^*}{\mu(1+\alpha^2)}. \tag{17}$$

In the afore-presented forms of the magnetodynamic equation, the mobility coefficients in different ways depend on the precession damping parameter. The one found from Landau–Lifshitz equation is directly proportional to the parameter α, see formula (16). The respective coefficient from Gilbert equation, see Eq. (17), turns out to be a non-monotonic function: $b^{(\mathrm{G})}(\alpha)$ passes through a maximum at $\alpha \sim 1$. As Eqs. (9) and (10) show, in this range the angular velocities $d\varphi/dt$ of the precessional (azimuthal) and $d\vartheta/dt$ of the relaxational (meridional) motions become comparable. This is a crossover between two limiting regimes. At low dissipation ($\alpha \ll 1$) the magnetic moment prior to settle in the equilibrium position makes a lot of turns around the direction of $\boldsymbol{H}_e$. In the opposite case $\alpha \gtrsim 1$ the motion of vector $\boldsymbol{e}$ hardly has time to accomplish a single turn. In qualitative terms, at small α the non-equilibrium $\vartheta \neq 0$ 'lives' due to the gyromagnetic properties of the magnetic moment: one may treat gyromagnetism as a kind of rotary inertia. Consequently, in this limit the growth of α accelerates relaxation. In the opposite case, at large α gyromagnetism is irrelevant, see formula (17), and the motion of vector $\boldsymbol{e}$ is the meridional 'crawl' to the direction of the field. In this situation the parameter α plays the same role as the viscosity in an ordinary fluid: its growth stretches the non-equilibirity lifetime, so it is quite natural that the mobility is inversely proportional to α.

3.3. Rotary diffusion coefficient for the magnetic moment

In the presence of thermal fluctuations, i.e., at a finite temperature T, the magnetic moment, quiescent or moving, experiences perturbations with the reference energy $\frac{1}{2}kT$ per each degree of freedom. To take the thermofluctuational factor into account, one has to insert a random torque to the magnetodynamic equation. This can be done by adding formally random magnetic field $\boldsymbol{H}_f$ to the regular one. Then the random torque will take the form $\mu(\boldsymbol{e} \times \boldsymbol{H}_f)$. At the next step, assuming that the noise is white, the correlation function $\langle\, \boldsymbol{H}_f^2(t)\,\rangle$ is evaluated. This approach was first used by Brown [40] and afterwards was advanced, see review articles [41, 42], and book [2]. Being interested in brevity and simplicity, we shall use another method based on the equation of motion for the distribution function of the magnetic moment. Under the action of fluctuations the magnetic moment, no matter is it or not entrained in some regular motion, is with necessity subjected to a Brownian process and undergoes random thermal walks. Given that, the angular coordinates of $\boldsymbol{e}$ are no longer dynamical variables; for instance, the notion of angular trajectory of $\boldsymbol{e}$ becomes meaningless. Instead, the description is formulated in terms of distribution function $W(\boldsymbol{e}, t)$ of the coordinates of the vector $\boldsymbol{e}$. Namely, $W(\boldsymbol{e}, t)\, d\boldsymbol{e}$ equals the probability to find the magnetic moment vector in the element $d\boldsymbol{e}$ of the solid angle; it is convenient to define this function on the surface of a unit sphere. The relationship rendering the evolution of $W(\boldsymbol{e}, t)$ (the Fokker–Planck equation) emerges as a continuity equation for the probability flux at this surface:

$$\frac{\partial W}{\partial t} = -\mathrm{Div}\, \boldsymbol{Q}, \tag{18}$$

where the operator Div involves only the angular variables.

To construct the probability flux vector $\boldsymbol{Q}$, one starts with the relationship

$$\boldsymbol{H}_{\mathrm{eff}} = -\frac{1}{\mu}\,\frac{\partial U}{\partial \boldsymbol{e}},$$

where $U(\boldsymbol{e})$ is the part of the magnetic energy of the particle which depends solely on the magnetic moment orientation. Then formula (15) writes

$$\boldsymbol{\Omega} = -\frac{\alpha\gamma}{\mu}\,(\mu\boldsymbol{e}\times\nabla)\,U,$$

where the gradient is taken only with respect to the angular variables. Evidently, the angular velocity $\boldsymbol{\Omega}$ pertains to the regular (drift) motion of $\boldsymbol{e}$ so that the full probability flux is the sum

$$\boldsymbol{Q} = \boldsymbol{\Omega}W + \boldsymbol{Q}_{\rm diff}\,; \tag{19}$$

here the second term accounts for the diffusion flux. We take the latter in the weak non-equilibrium approximation, i.e., as the Fick law:

$$\boldsymbol{Q}_{\rm diff} = -D(\boldsymbol{e}\times\nabla)\,W \tag{20}$$

where the diffusion coefficient D has to be evaluated. In Eq. (20) when writing the spatial derivative we have taken into account that the function W is defined at the surface of a unit sphere with no radial (parallel to $\boldsymbol{e}$) gradients. Thence the gradient operator reduces to

$$\widehat{\boldsymbol{J}} = (\boldsymbol{e}\times\nabla),$$

which coincides, see book [43], for example, with the infinitesimal rotation operator or (adding a numeric factor) with the angular momentum operator in quantum mechanics.

Substituting the explicit expressions for $\boldsymbol{\Omega}$ and $\boldsymbol{Q}_{\rm diff}$ in Eq. (19), we transform it to

$$\boldsymbol{Q} = -\frac{\alpha\gamma}{\mu}\,W\,\widehat{\boldsymbol{J}}U - D\widehat{\boldsymbol{J}}W = -W\widehat{\boldsymbol{J}}\left[\frac{\alpha\gamma}{\mu}\,U + D\ln W\right]. \tag{21}$$

In equilibrium, the Boltzmann distribution

$$W_0 \propto \exp(-U/T), \tag{22}$$

holds, and the probability flux vanishes. (From now on we set the Boltzmann constant k equal unity.) Substituting Eq. (22) in (21), one gets

$$-W_0\widehat{\boldsymbol{J}}U\left[\frac{\alpha\gamma}{\mu} - \frac{D}{T}\right] = 0,$$

which is evidently satisfied at

$$\left[\frac{\alpha\gamma}{\mu} - \frac{D}{T}\right] = 0.$$

From here follows the rotary diffusion coefficient

$$D^{(\rm LL)} = \alpha\gamma T/\mu = \alpha\gamma T/MV_m\,. \tag{23}$$

Note that as soon as the rotary mobility coefficient had been found, Eq. (23) might have been written down right away using the Einstein formula. This is equally valid for both Landau–Lifshitz and Gilbert representations of the magnetodynamic equation. Using formula (17) one finds

$$D^{(\rm G)} = \alpha\gamma^* T/MV(1+\alpha^2). \tag{24}$$

Defining operation Div as scalar multiplication of operator $\widehat{\boldsymbol{J}}$ by the flux vector, one rewrites the continuity equation (18) as

$$\frac{\partial W}{\partial t} = -\widehat{\boldsymbol{J}}\,\boldsymbol{Q},$$

and then with the aid of Eq. (21) obtains the Fokker–Planck kinetic equation (FPE) in the form

$$2\tau_D \frac{\partial W}{\partial t} = \widehat{\boldsymbol{J}}\, W\, \widehat{\boldsymbol{J}} \left[\frac{U}{T} + \ln W\right]; \tag{25}$$

here the rotary diffusion (Debye) time is

$$\tau_D^{(\mathrm{LL})} = (2D)^{-1} = MV_m/2\alpha\gamma T. \tag{26}$$

This relaxation time — to be specific, we have written it in the Landau-Lifshitz representation — has the anticipated behavior: the smaller the precession damping constant the slower the particle magnetic moment approaches its equilibrium position. For nanoparticles, typical values of the material parameters are $M \lesssim 10^3\,\mathrm{G}$, $V_m \sim 10^{-18}\,\mathrm{cm}^3$, $\alpha \sim 0.1$. Substituting them in formula (26) at $\gamma \approx 2 \times 10^8\,\mathrm{rad/Oe{\cdot}s}$ and room temperature one obtains $\tau_D \sim 10^{-9}\,\mathrm{s}$.

Note a close resemblance between the reference time of the internal rotary diffusion of the magnetic moment and Debye time

$$\tau_B = 3\eta V/T \tag{27}$$

of 'external' rotary diffusion of a spherical particle of volume V in an isotropic liquid with viscosity η. Comparing formulas (26) and (27), one introduces the coefficient of effective magnetic viscosity of a ferromagnet [41] as

$$\eta_m^{(\mathrm{LL})} = M/6\alpha\gamma. \tag{28}$$

In the Landau–Lifshitz representation the orientational diffusion time (26) is the greater the weaker is the precession damping coefficient. However, as it was already noted, such a behavior looks reasonable at small damping but is difficult to understand under strong one when the motion is aperiodic. In this respect, the interpretation of magnetic viscosity that follows from the Gilbert representation seems rather intelligible. Indeed, using the diffusion coefficient from Eq. (28), one finds for the orientation relaxation time

$$\tau_D^{(\mathrm{G})} = (2D)^{-1} = Mv_m(1+\alpha^2)/2\alpha\gamma^* T. \tag{29}$$

Accordingly, from comparison of Eqs. (29) and (27) for the effective magnetic viscosity one gets

$$\eta_m^{(\mathrm{G})} = \frac{M(1+\alpha^2)}{6\alpha\gamma} \propto \begin{cases} 1/\alpha & \text{for } \alpha \ll 1 \\ \alpha & \text{for } \alpha \gg 1 \end{cases}. \tag{30}$$

which means different characteristic behaviors in weak and strong precession damping limits.

From FPE (23) it follows that in the absence of internal and external fields ($U = 0$) the parameter τ_D exhaustively determines the response time of the system to a weak external excitation. For example, it is τ_D and only it which determines the dispersion of the magnetic susceptibility in a magnetically isotropic particle.

3.4. Relaxation of the magnetic moment in an anisotropic particle

Thermofluctuational behavior of the magnetic moment in a magnetically anisotropic particle acquires new features in comparison with the isotropic case and, accordingly, extends the set of relaxation times. Consider a single-domain particle with the easy-axis anisotropy given by

$$U_a = -KV_m\,(\boldsymbol{e}\cdot\boldsymbol{n})^2 = -KV_m\,\cos^2\vartheta, \tag{31}$$

where $\boldsymbol{n}$ is the unit vector of the easy axis and ϑ is the angle between the direction of the particle magnetic moment $\boldsymbol{e}$ and $\boldsymbol{n}$. Expression (31) establishes that in the internal configurational space

of a particle at $\vartheta = \pi/2$ there exists the energy barrier of the height Kv_m, which separates the two minima, $\vartheta = 0$ and $\vartheta = \pi$ corresponding to the orientations $\boldsymbol{e} \parallel \boldsymbol{n}$ and $\boldsymbol{e} \parallel -\boldsymbol{n}$. At finite temperatures, i.e., in the presence of fluctuations, the characteristic parameter for the system is the non-dimensional ratio

$$\sigma = KV_m/T \tag{32}$$

of the magnetic energy to the thermal one. Evidently, at $\sigma \ll 1$ the motion of the particle magnetic moment very much resembles the case of free diffusion ($U = 0$); thence in this limit the relaxation time $\tau(\sigma)$ is close to τ_D.

Essentially different is the situation of a high potential barrier or, equivalently, of low temperature; both these conditions are expressed by the relation $\sigma \gg 1$. Applying the Boltzmann law (22) to the two-well potential (31), one arrives at the conclusion that the orientational probability is almost totally localized in exponentially small vicinities of the easy directions $\vartheta = 0$ and $\vartheta = \pi$; at full equilibrium the populations of both wells are equal.

Kinetics of establishing orientational equilibrium in a single-domain particle in the presence of thermal fluctuations is described by FPE (25). We write it down in spherical coordinates at the surface of a unit sphere. Assuming that all the functions in depend only on the meridional angle ϑ, we get

$$\frac{\partial W}{\partial t} = -\mathrm{Div}\,\boldsymbol{Q} = -\frac{1}{\sin\vartheta}\,\frac{\partial}{\partial\vartheta}\,[\,\sin\vartheta\cdot Q_\vartheta\,] = \frac{1}{2\tau_D}\,\frac{1}{\sin\vartheta}\,\frac{\partial}{\partial\vartheta}\,\left[\sin\vartheta\left(\frac{W}{T}\,\frac{dU_a}{d\vartheta} + \frac{dW}{d\vartheta}\right)\right]. \tag{33}$$

The expression for the probability flux vector

$$\boldsymbol{Q} = Q_\vartheta\,\boldsymbol{i}_\vartheta\,, \qquad Q_\vartheta = -\frac{1}{2\tau_D}\,\left(\frac{W}{T}\,\frac{dU_a}{d\vartheta} + \frac{dW}{d\vartheta}\right), \tag{34}$$

(in the considered situation it has only the ϑ-component) coincides with the above introduced definition (21).

Full solution of FPE (33) is a rather complicated task. There exists numerous literature on the analysis of the problem for various forms of the potential function, see review article [44] or book [2], for example. To get a simple estimation of the orientation relaxation time of the observable (i.e., statistically averaged) magnetic moment at $\sigma \gg 1$ we follow Ref. [40], where Kramers approximation [44,45] is used. The main point is that the full non-stationary problem is replaced by an effective steady one. It is assumed that inside the energy minima (potential wells) the equilibrium is achieved in a short time and is not affected by the interwell diffusion. Between the wells there exists a stationary flux as it is required by the balance between the diffusion and force terms in FPE. Therefore, the probability flux $\boldsymbol{Q}$ couples two compact spots in the orientational space which are localized at the poles ($\vartheta = 0,\ \pi$) of the unit sphere. Accordingly, on the total flux the requirement of non-divergency is imposed stating that in the whole coordinate interval except for the vicinities $[0, \vartheta_1]$ and $[\vartheta_2, \pi]$, the quantity $B \equiv \sin\vartheta\cdot Q_\vartheta$ is constant. Substituting here Q_ϑ from Eq. (34), one arrives at the condition

$$B = -\frac{\sin\vartheta}{2\tau_D}\left(\frac{dW}{d\vartheta} + \frac{W}{T}\,\frac{dU_a}{d\vartheta}\right). \tag{35}$$

That states that the interwell probability flux is non-zero and vanishes only in the case of true equilibrium, i.e., when the global Boltzmann distribution is attained.

Denoting the populations of the wells as n_1 (around $\vartheta = 0$) and n_2 (around $\vartheta = \pi$), we write the normalizing condition for the distribution function $W(\vartheta)$ as

$$\int W(\vartheta)\,d\Gamma = 2\pi\int_0^\pi W(\vartheta)\,\sin\vartheta\,d\vartheta = 1,$$

so that $n_1 + n_2 = 1$. Now we multiply Eq. (33) by $\sin\vartheta$ and integrate the result over ϑ in the interval $[0, \pi]$. Then the left-hand part of the equation turns into zero as a derivative of a constant. On the same grounds — B is constant — will turn into zero the right-hand part as well. In the high-barrier approximation the obtained probability conservation law means the balance between the populations of the polar regions:

$$\frac{dn_1}{dt} + \frac{dn_2}{dt} = 0. \tag{36}$$

On the other hand, according to Eq. (36) the probability flux is

$$\frac{dn_1}{dt} = -\frac{dn_2}{dt} = -2\pi B.$$

Indeed, integration of the right-hand side of Eq. (33) on transforming the volume integral into a surface one reduces to a sum of products of the quantity B and the unit outer normal vectors: on entering the region (close to $\vartheta = 0$) and on quitting it (close to $\vartheta = \pi$). Moreover, the exact position of the boundary over which the flux is calculated does not matter.

We multiply Eq. (35) by $\exp(U_a/T)$ and integrate from ϑ_1 to ϑ_2, taking the latter as the respective borders of the populated polar regions. This yields

$$W(\vartheta_2)\, e^{U_a(\vartheta_2)/T} - W(\vartheta_1)\, e^{U_a(\vartheta_1)/T} = -2\tau_D B \int_{\vartheta_1}^{\vartheta_2} \frac{e^{U_a/T}\, d\vartheta}{\sin\vartheta}. \tag{37}$$

In the right-hand side of this formula we make the following:
1) replace the potential by its expansion in series in the vicinity of the summit of the potential curve:

$$\frac{U_a(\vartheta)}{T} = \frac{U_a(\pi/2)}{T} + \frac{1}{2T}\,\frac{d^2U_a}{d\vartheta^2}\,(\pi/2 - \vartheta)^2 = -\sigma\,(\pi/2 - \vartheta)^2\,; \tag{38}$$

2) replace $\sin\vartheta$ by its value at the summit, i.e., by unity;
3) assuming drastic diminution of the integrand under deviation of the integration variable from $\pi/2$, we proceed to infinite integration limits $(-\infty, \infty)$. After that the integral evaluates easily, and Eq. (37) assumes the form

$$W(\vartheta_2)\, e^{U_a(\vartheta_2)/T} - W(\vartheta_1)\, e^{U_a(\vartheta_1)/T} = 2\tau_D B\sqrt{\frac{\pi}{\sigma}}\,.$$

Upon substituting energy (38) the rate of population change is presented as

$$\frac{\tau_D}{\sqrt{\pi\sigma}}\,\frac{dn_1}{dt} = W(\vartheta_2)\, e^{U_a(\vartheta_2)/T} - W(\vartheta_1)\, e^{U_a(\vartheta_1)/T}. \tag{39}$$

To close the last equation, we use the above-introduced hypothesis that in each well there exists an independent local Boltzmann distribution. To be specific, let us take the region around the pole $\vartheta = 0$ and present the distribution function at the interval$[0, \vartheta_1]$ in the form

$$W(\vartheta)\big|_{\vartheta\leq\vartheta_1} = W(0)\, e^{-U_a/T} = W(0)\, e^{\sigma}\, e^{-\sigma\vartheta^2}, \tag{40}$$

where $W(0)$ is a constant. In the last of equalities (40), making use of being close to the minimum, the exact potential is replaced by its expansion in a series up to quadratic order. The distribution function integrated over the interval $[0, \vartheta_1]$ must equal population n_1, that is

$$n_1 = 2\pi \int_0^{\vartheta_1} W(\vartheta)\big|_{\vartheta\leqslant\vartheta_1} \sin\vartheta\, d\vartheta = 2\pi W(0)\, e^{\sigma} \int_0^{\infty} e^{-\sigma\vartheta^2}\, \vartheta\, d\vartheta = \frac{\pi}{\sigma}\, W(0)\, e^{\sigma}.$$

This establishes the coefficient $W(0)$ in formula (40). Repeating the same considerations for the potential minimum located near $\vartheta = \pi$, one finds finally for the 'localized' distribution functions:

$$W(\vartheta)\big|_{\vartheta\leqslant\vartheta_1} = \frac{\sigma}{\pi}\, n_1 e^{-\sigma\vartheta^2} \qquad (\vartheta_1 \ll 1),$$
$$W(\vartheta)\big|_{\vartheta\geqslant\vartheta_2} = \frac{\sigma}{\pi}\, n_2 e^{-\sigma(\pi-\vartheta)^2} \qquad (\pi - \vartheta_2 \ll 1). \tag{41}$$

We use formulas (41) to transform the right-hand part of Eq. (39) and get

$$W(\vartheta_2)\, e^{U_a(\vartheta_2)/T} - W(\vartheta_1)\, e^{U_a(\vartheta_1)/T} = \\ = \frac{\sigma}{\pi}\, n_2 e^{-\sigma\vartheta_2^2}\, e^{-\sigma}\, e^{\sigma\vartheta_2^2} - \frac{\sigma}{\pi}\, n_1 e^{-\sigma\vartheta_1^2}\, e^{-\sigma}\, e^{\sigma\vartheta_1^2} = \frac{\sigma}{\pi}\, e^{-\sigma}\, (n_2 - n_1)\,. \tag{42}$$

In result, one arrives at a simple kinetic equation, which describes the evolution of populations in a two-level system:

$$\frac{e^\sigma}{\sigma}\sqrt{\frac{\pi}{\sigma}}\,\tau_D\,\frac{d}{dt}\,n_1 = -\frac{e^\sigma}{\sigma}\sqrt{\frac{\pi}{\sigma}}\,\tau_D\,\frac{d}{dt}\,n_2 = (n_2 - n_1)\,.$$

Closing it, i.e., writing in terms of the non-equilibrium population $(n_1 - n_2)$, one finally obtains

$$\frac{d}{dt}\,(n_1 - n_2) = -\frac{2\sigma}{\tau_D e^\sigma}\sqrt{\frac{\sigma}{\pi}}\,(n_1 - n_2)\,,$$

wherefrom immediately follows the expression for characteristic time of magnetic relaxation

$$\tau(\sigma) = \frac{e^\sigma}{2\sigma}\sqrt{\frac{\pi}{\sigma}}\,\tau_D. \tag{43}$$

Evidently, due to its exponential dependence on the parameter $\sigma = KV_m/T$, the quantity $\tau(\sigma)$ may grow virtually unboundedly. This is a specific property of the solution of any Kramers problem.

Wrapping up the calculation of formula (43), first performed by W. F. Brown [40], let us remind the conditions under which the Kramers approximation may be applied. First of all, this is a sufficient height of the barrier ($\sigma \gg 1$) and, in gyromagnetic problems, a sufficiently high value of the precession damping parameter. Recalling in this connection the above-presented discussion of the expressions for the orientation diffusion time in the Landau–Lifshitz and Gilbert representations, we settle on the decision that the Gilbert representation is more adequate. This, in turn, means that τ_D should be expressed with the aid of Eq. (29). In fact, the problem of the intrinsic relaxation time in a magnetic nanoparticle is much wider. For example, one may justly ask what will happen if the magnetic damping would be sufficiently low, and the Larmor precession would be a pronounced and a long-living process. An account on the theory of thermally activated phenomena including the low- and high-damping limits as well as the crossover behavior bridging them one can find in the review article by Coffey, Garanin and McCarthy [44].

4. Moment equations

Equations for macroscopic characteristic of magnetic particles can be obtained by performing ensemble averaging, i.e., averaging corresponding microscopic quantities with a distribution function that satisfies Eq. (25). In below, we use the standard notation for these averages:

$$\langle \ldots \rangle = \int \ldots W\, d\Omega,$$

where Ω is the set of pertinent phase variables; for a quiescent single-domain particle it is the set of angles describing orientation of vector $\boldsymbol{e}$.

For example, for the dimensionless magnetization $\langle \boldsymbol{e} \rangle$ of an assembly of magnetically isotropic particles, where

$$U = -\mu(\boldsymbol{e}\cdot\boldsymbol{H}),$$

one gets from Eq. (25)

$$2\tau_D \frac{\partial}{\partial t}\langle e_i \rangle = \xi\,(\delta_{ik} - \langle\, e_i e_k \,\rangle)\;\; h_k - 2\langle\, e_i \,\rangle, \tag{44}$$

where $\xi = \mu H/T$ and $\boldsymbol{h} = \boldsymbol{H}/H$ is the unit vector of external field. Equation (44) describes the evolution of the first moment of the distribution function. However, it contains the second moment, and thus is coupled with higher terms. This chain-linking turns out to be infinite: the equation for the second moment includes the third one and so on. Thus one may find out that, as it usually happens in kinetic problems, the Fokker–Planck equation (partial derivative equation) for the distribution function is equivalent to an infinite set of ordinary differential equations for the moments of this function.

Another important and instructive example is a single-domain magnetic particle with a uniaxial anisotropy described by the expression

$$U = -KV_m\,(\boldsymbol{e}\cdot\boldsymbol{n})^2 - \mu\,(\boldsymbol{e}\cdot\boldsymbol{H}), \tag{45}$$

which is in use in this paper. With the energy function (45), the equation for the dimensionless magnetization following from Eq. (25) writes

$$2\tau_D \frac{\partial}{\partial t}\langle\, e_i \,\rangle = 2\sigma\,(n_i n_k \langle\, e_k \,\rangle - n_k n_l \langle\, e_i e_k e_l \,\rangle) + \xi\,(\delta_{ik} - \langle\, e_i e_k \,\rangle)\; h_k - 2\langle e_i \rangle\,, \tag{46}$$

where the right-hand side incorporates both second and third statistical moments.

To write down Eq. (46) as well as (44), we used after Ref. [46] the distribution function moments presented as Cartesian tensors. However, when solving the orientational problem, it is more natural to use the set of spherical functions. Choosing spherical coordinates for the unit vectors $\boldsymbol{e}$, $\boldsymbol{n}$, and $\boldsymbol{h}$ as (θ,φ), $(0,0)$, $(\psi,0)$, respectively, i.e., taking $\boldsymbol{n}$ as the polar axis of the frame, one gets

$$(\boldsymbol{e}\cdot\boldsymbol{h}) = \cos\psi\,\cos\theta + \sin\psi\,\sin\theta\,\cos\varphi, \tag{47}$$

so that Eq. (45) may be rewritten as

$$U = -KV_m\,\cos^2\theta - \mu H\,(\cos\psi\,\cos\theta + \sin\psi\,\sin\theta\,\cos\varphi), \tag{48}$$

Then the non-stationary solution of the kinetic equation (25) with the energy function (48) is sought in the form of the spherical harmonics expansion

$$W_{\boldsymbol{e}}(\theta,\varphi,t) = \sum_{l=0}^{\infty}\sum_{m=-l}^{l} b_{l,m}(t)\,\frac{2l+1}{4\pi}\,\frac{(l-|m|)!}{(l+|m|)!}\,X_l^{m*}(\boldsymbol{e},\boldsymbol{n}). \tag{49}$$

In Eq. (49) symbols $X_l^m(\boldsymbol{a},\boldsymbol{b})$ denote the so-called non-normalized spherical harmonics defined as

$$X_l^m(\boldsymbol{a},\boldsymbol{b}) = P_l^m(\cos\alpha)\,e^{im\beta}, \tag{50}$$

where P_l^m are associated Legendre polynomials. The angles α and β are the coordinates of the unit vector $\boldsymbol{a}$ in the spherical coordinate frame with the polar axis set along the unit vector $\boldsymbol{b}$. Functions (50) are connected to the conventional (normalized) spherical harmonics by the relationship

$$Y_l^m = \sqrt{\frac{2l+1}{4\pi}\,\frac{(l-|m|)!}{(l+|m|)!}}\;X_l^m. \tag{51}$$

The time dependence in Eq. (49) is determined by the quantities $b_{l,m}(t)$, which appear to be the moments of the distribution function:

$$b_{l,m}(t) = \left\langle P_l^m(\cos\theta) e^{im\varphi} \right\rangle, \tag{52}$$

These complex coefficients one finds by solving numerically the infinite set of differential recurrence relations obtained by substitution of expansion (49) into Eq. (25):

$$\begin{aligned} 2\tau_D \frac{d}{dt}\, b_{l,m} + l(l+1)b_{l,m} - 2\sigma \Bigg[& \frac{(l+1)(l+m-1)(l+m)}{(2l-1)(2l+1)}\, b_{l-2,m} + \\ & + \frac{l(l+1)-3m^2}{(2l-1)(2l+3)}\, b_{l,m} - \frac{l(l-m+2)(l-m+1)}{(2l+1)(2l+3)}\, b_{l+2,m} \Bigg] - \\ & - \frac{\xi\cos\psi}{2l+1}\, [(l+1)(l+m)b_{l-1,m} - l(l-m+1)b_{l+1,m}] - \\ & - \frac{\xi\sin\psi}{2(2l+1)}\, [(l+1)(l+m-1)(l+m)b_{l-1,m-1} + \\ & + l(l-m+2)(l-m+1)b_{l+1,m-1} - (l+1)b_{l-1,m+1} - lb_{l+1,m+1}] = 0. \end{aligned} \tag{53}$$

Equations (53) are valid for $m \geqslant 1$, and one does not need to consider the negative values of m because of the symmetry of Eq. (49) with respect to the replacement $m \to -m$ that yields $b_{l,-m} = b_{l,m}$. However, the case $m = 0$ is somewhat special, and the corresponding equation that closes the set (53) is to be derived separately. On doing that, it writes in the form

$$\begin{aligned} 2\tau_D \frac{d}{dt}\, b_{l,0} + l(l+1)b_{l,0} - 2\sigma \Bigg[& \frac{(l-1)l(l+1)}{(2l-1)(2l+1)}\, b_{l-2,0} + \\ & + \frac{l(l+1)}{(2l-1)(2l+3)}\, b_{l,0} - \frac{l(l+1)(l+2)}{(2l+1)(2l+3)}\, b_{l+2,0} \Bigg] - \\ & - \frac{\xi\cos\psi}{2l+1}\, l(l+1)(b_{l-1,0} - b_{l+1,0}) + \frac{\xi\sin\psi}{2l+1}\, [(l+1)b_{l-1,1} + lb_{l+1,1}] = 0. \end{aligned} \tag{54}$$

The kinetic equation (25) with the energy function (45) first studied by Brown [40] since then has been investigated extensively [41, 46–51]. However, due to mathematical difficulties the case of arbitrary orientation of the external and anisotropy fields, i.e., vectors $\boldsymbol{h}$ and $\boldsymbol{n}$, has been addressed not so long ago. The numerical solution of the relaxation problem for $\boldsymbol{h}$ and $\boldsymbol{n}$ crossed under an arbitrary angle for the first time was given in Ref. [52].

5. Methods of solution

In general case, Eqs. (53) and (54) present infinite sets of the five-term (pentadiagonal) recurrence relations with respect to the index l. In certain special cases ($\xi = 0$ or $\sigma = 0$), they reduce to three-term (tridiagonal) recurrence relations. In this section the sweep procedure for solving of such sets is described. This method, also known as *the Thomas algorithm*, is widely used for handling the recurrence relations entailed by the finite-difference approximation applied for solving differential equations, see Ref. [53], for example. In our case, the recurrence relation that follows from expansion (53) of the distribution function in the basis of orthogonal spherical functions, treated with the sweep method, as explained below, renders the numerical representation of the exact solution of the recurrence relations.

5.1. Solution of the three-term scalar recurrence relationships

Consider the three-term inhomogeneous recurrence relationship

$$A_l b_{l-1} + B_l b_l + C_l b_{l+1} = f_l\,, \qquad l = 1, 2, 3 \ldots, \tag{55}$$

with b_0 being a given quantity (initial condition). The sweep method is realized by Eq. (55) to a two-term recurrence equation by means of the sweep coefficients, which relate to each other the neighboring terms as

$$b_l = \alpha_l b_{l-1} + \gamma_l\,, \quad b_{l+1} = \alpha_{l+1} b_l + \gamma_{l+1}\,. \tag{56}$$

Substituting Eq. (56) into (55), one gets

$$A_l b_{l-1} + (B_l + C_l\alpha_{l+1}) b_l + C_l\gamma_{l+1} = f_l\,. \tag{57}$$

Comparison of Eqs. (56) and (57) yields the two-term backward recurrence for the sweep coefficients

$$\alpha_l = -\frac{A_l}{B_l + C_l\alpha_{l+1}}\,, \qquad \gamma_l = \frac{f_l - C_l\gamma_{l+1}}{B_l + C_l\alpha_{l+1}}\,. \tag{58}$$

For practical calculations one has to choose a large enough $l = L$ and set α_{L+1} and γ_{L+1} to zero. Then, upon implementing the backward recurrence relationships (58) until $l = 1$, one evaluates the full set of the sweep coefficients. By an upward iteration of (56) one can find all the terms b_l with the indices $l = 1, \ldots L$. Due to the stability of both iteration processes the initial error, caused by truncation of the infinite recurrences (58), dissolves in the course of iterations and finally becomes less then computer zero. The desired accuracy is attained by varying the cutoff index number L; normally, the higher σ or ξ in Eqs. (53 and 54), the higher L is to be used. In this sense, one may call the solutions obtained *numerically exact*.

5.2. Solution of the five-term scalar recurrence relationships

Now we consider a five-term inhomogeneous recurrence relationship

$$A_l b_{l-2} + B_l b_{l-1} + C_l b_l + D_l b_{l+1} + E_l b_{l+2} = f_l, \qquad l = 1, 2, 3 \ldots\,, \tag{59}$$

with b_0 being a given quantity (initial condition). In the literature on the solution of the Fokker-Planck Equation (see, for example, Refs. [1, 2]) the five-term *scalar* recurrence relationship is usually reduced to a three-term *vector* one, by pairing the neighboring even and odd terms into a two-component columnar matrices (vectors). Here we show how to solve Eq. (59) by the sweep method, which is more feasible to realise. For this purpose, we introduce three sets of sweep coefficients which couple the neighboring terms. They are as follows

$$\begin{aligned} &b_l = \alpha_l b_{l-1} + \beta_l b_{l-2} + \gamma_l\,, \quad b_{l+1} = \alpha_{l+1} b_l + \beta_{l+1} b_{l-1} + \gamma_{l+1}\,, \\ &b_{l+2} = (\alpha_{l+2}\alpha_{l+1} + \beta_{l+2}) b_l + \alpha_{l+2}\beta_{l+1} b_{l-1} + \gamma_{l+2} + \alpha_{l+2}\gamma_{l+1}\,. \end{aligned}$$

Substituting relations (60) into Eq. (59) one gets

$$\begin{aligned} A_l b_{l-2} + (B_l + D_l\beta_{l+1} + E_l\alpha_{l+2}\beta_{l+1}) b_{l-1} + [C_l + D_l\alpha_{l+1} + \\ + E_l(\alpha_{l+2}\alpha_{l+1} + \beta_{l+2})]\, b_l = f_l - (D_l + E_l\alpha_{l+2})\gamma_{l+1} - E_l\gamma_{l+2}\,. \end{aligned} \tag{60}$$

On comparing Eqs. (60) and (60) one finds the three-term backward recurrences for the sweep coefficients which read

$$\begin{aligned}
\alpha_l &= -\frac{B_l + D_l\beta_{l+1} + E_l\alpha_{l+2}\beta_{l+1}}{C_l + D_l\alpha_{l+1} + E_l(\alpha_{l+2}\alpha_{l+1} + \beta_{l+2})},\\
\beta_l &= -\frac{A_l}{C_l + D_l\alpha_{l+1} + E_l(\alpha_{l+2}\alpha_{l+1} + \beta_{l+2})},\\
\gamma_l &= \frac{f_l - (D_l + E_l\alpha_{l+2})\gamma_{l+1} - E_l\gamma_{l+2}}{C_l + D_l\alpha_{l+1} + E_l(\alpha_{l+2}\alpha_{l+1} + \beta_{l+2})}.
\end{aligned} \tag{61}$$

As in the above-described case, when performing practical calculations of sweep coefficients one has to choose a large enough $l = L$ and set all the sweep coefficients of the higher orders to zero. Then implementation of the backward recurrence relationships (61) until $l = 1$ will render the full set of the sweep coefficients. With the aid of the upward iteration of (60) one can find then all the terms b_l within interval $l = 1, \dots L$.

5.3. Solution of vector recurrence relationships

In the previous subsection we have mentioned a method to solve a pentadiagonal scalar recurrence relation by reducing it to tridiagonal vector recurrence relationships. After that, the problem may be solved as it is described in Subsection 6.2 with the only exception that all the coefficients of Eq. (55) must be treated as matrices. The matrix sweep coefficients, calculated according to the rules of the matrix algebra, now take the form

$$\boldsymbol{\alpha}_l = -(\boldsymbol{B}_l + \boldsymbol{C}_l\boldsymbol{\alpha}_{l+1})^{-1}\boldsymbol{A}_l\,, \quad \boldsymbol{\gamma}_l = -(\boldsymbol{B}_l + \boldsymbol{C}_l\boldsymbol{\alpha}_{l+1})^{-1}(\boldsymbol{f}_l - \boldsymbol{C}_l\boldsymbol{\gamma}_{l+1})\,, \tag{62}$$

where the superscript -1 means the inversion of the matrix. By the upward iteration of

$$\boldsymbol{b}_{l+1} = \boldsymbol{\alpha}_{l+1}\boldsymbol{b}_l + \boldsymbol{\gamma}_{l+1} \tag{63}$$

one can find all the vectors $\boldsymbol{b}_l$.

Eqs. (53) and (61) are also able to yield the vector recurrence relationships for the case of a skew bias field, that is when vectors $\boldsymbol{h}$ and $\boldsymbol{n}$ are not parallel. In this case one should ascribe to each b_l as many as $2l + 1$ components, corresponding to different values of the azimuthal index m. Another problem, involving vector recurrence relationships, is a steady-state nonlinear oscillations of b_l in a high AC field. To study the harmonic content of the nonlinear response, one has to expand all the moments $b(t)_l$ in the Fourier series. Then the Fourier coefficients may be treated as the components of a columnar vector. This situation will be considered more than once throughout the present paper.

We end up this section with formulas delivering the solution of the pentadiagonal recurrence relationships (59) and (60), where coefficients must be treated as matrices and the variables b_l as columnar vectors. Then for the matrix sweep coefficients one gets

$$\begin{aligned}
&\boldsymbol{\alpha}_l = -\boldsymbol{\Delta}^{-1}(\boldsymbol{B}_l + \boldsymbol{D}_l\boldsymbol{\beta}_{l+1} + \boldsymbol{E}_l\boldsymbol{\alpha}_{l+2}\boldsymbol{\beta}_{l+1})\,, \quad \boldsymbol{\beta}_l = -\boldsymbol{\Delta}^{-1}\boldsymbol{A}_l\,,\\
&\boldsymbol{\gamma}_l = \boldsymbol{\Delta}^{-1}\left(\boldsymbol{f}_l - (\boldsymbol{D}_l + \boldsymbol{E}_l\boldsymbol{\alpha}_{l+2})\boldsymbol{\gamma}_{l+1} - \boldsymbol{E}_l\boldsymbol{\gamma}_{l+2}\right),
\end{aligned} \tag{64}$$

where

$$\boldsymbol{\Delta} = \boldsymbol{C}_l + \boldsymbol{D}_l\boldsymbol{\alpha}_{l+1} + \boldsymbol{E}_l(\boldsymbol{\alpha}_{l+2}\boldsymbol{\alpha}_{l+1} + \boldsymbol{\beta}_{l+2})\,.$$

Conclusion

The above-presented explanations are, clearly, just the initial step introducing the theory of magnetodynamics of superparamagnetic particles. As thermal fluctuations are the essential factor affecting all throughout the particle properties, the theoretical description used the theory of random (stochastic) processes to account for the situation. This framework is based on the kinetic Fokker–Planck-like (also known as rotary diffusion) equation solved either directly or by transforming it to a chain-linked set of moment equations. The specifics of fine particles is that in the majority of cases they are single-domain, and this entails a relative simplicity (low order) of the resulting equations.

For the pertinent sets of the moment equations, efficient numerical schemes of solution have been developed nowadays. These schemes are rather flexible as to allow one include many additional factors, e.g., surface magnetic anisotropy along with the bulk one [54, 55]. Although not described here, the theory is also feasible to be extended to the cases of high and ultra-high frequencies of the applied field where the ferromagnetic resonance comes to effect. Even quite special cases where the 'inertia' of the magnetic moment should be taken into account are considered [56]. As well, the above-developed conceptual framework is very useful for the theory of magnetic fluids, the systems where fine particles are suspended in a fluid that adds to their conventional (internal) superparamagnetism the external one caused by their ability to mechanically rotate. Finally, the issue that is beyond the frame of the present subject — single particles without interaction — but logically following from it, is the problem of how does the interparticle interaction (magnetostatic or other) affect the properties of the fine particle assemblies like magnetic fluids or solid nanocomposites, see [57] and the discussion therein, for example.

The work was carried out in the framework of the state-budget financed theme No. 126020916888-9.

References

[1] H.Risken, The Fokker-Planck Equation, Methods of Solutions and Applications. Springer, Berlin, 1989.

[2] W.T.Coffey, Yu.P.Kalmykov, The Langevin Equation. With applications to Stochastic Problems in Physics, Chemistry and Electrical Engineering. World Scientific, Singapore, 2012.

[3] W.F.Brown, Micromagnetics, Wiley-Interscience, New York–London, 1963.

[4] X.Batlle, A.Labarta, Finite-size effects in fine particles: magnetic and transport properties, *Journal of Physics D: Applied Physics*, **35**(2002), R15–R42.
DOI: 10.1088/0022-3727/35/6/201

[5] X.Batlle, A.Labarta, O.Iglesias, From finite size and surface effects to glassy behaviour in ferrimagnetic nanoparticles, In: D. Fiorani, editor, Surface Effects in Magnetic Nanoparticles, Springer, 2005, 105–140.

[6] S.Chikatzumi, Physics of Magnetism. Wiley, New York, 1964.

[7] L.D.Landau, E.M.Lifshitz, Electrodynamics of Continuous Media. Pergamon, Oxford, 1984.

[8] L.D.Landau, E.M.Lifshitz On the dispersion of magnetic permeability of ferromagnetic bodies, *Physikalische Zeitschriften der Sowjetunion*, **8**(1935), 153–162; reprinted in Collected Works of L. D. Landau, Pergamon, London, 1965, no. 18, 101–114.

[9] W.F.Brown, The fundamental theorem of the theory of fine ferromagnetic particles, *Annals of the New York Academy of Sciences*, **147**(1969), 463–488. DOI: 10.1111/j.1749-6632.1969.tb41269.x

[10] A.Aharoni, Introduction to the Theory of Ferromagnetism. Clarendon, Oxford, 1996.

[11] A.Aharoni, Brown's "fundamental theorem" revisited, *Journal of Applied Physics*, **90**(2001), 4645–4650. DOI: 10.1063/1.1407313

[12] L.Néel, Anisotropie magnetique superficielle et surstructures d'orientation, *Journal de Physique et le Radium*, **15**(1954), 225–239.

[13] L.Néel, Influence des fluctuations thermiques sur l'aimantation de grains ferromagnetiques tr'es fins, *Comptes Rendus de l'Academie des Sciences (Paris)*, **228**(1949), 664–666.

[14] C.P.Bean, J.D.Livingston, Superparamagnetism, *Journal of Applied Physics*, **30**(1959), 120S–129S. DOI: 10.1063/1.2185850

[15] A.Moser, K.Takano et al., Magnetic recording: advancing into the future, *Journal of Physics D: Applied Physics*, **35**(2002), R157–R167. DOI: 10.1088/0022-3727/35/19/201

[16] L.Gammaitoni, P.Hänggi, P.Jung, F.Marchesoni, Stochastic resonance, *Reviews of Modern Physics*, **70**(1998), 223–287. DOI: 10.1103/RevModPhys.70.223

[17] R.Benzi, A.Sutera, A.Vulpiani, The mechanism of stochastic resonance, *Journal of Physics A: Mathematical and General Physics*, **14**(1981), L453–L458. DOI: 10.1088/0305-4470/14/11/006

[18] R.Weisenfeld, F.Moss, Stochastic resonance and the benefits of noise: from ice ages to crayfish and squids, *Nature*, **373**(1995), 33–36. DOI: 10.1038/373033a0

[19] R.Bartussek, P.Hänggi, P.Jung, Stochastic resonance in optical bistable systems, *Physical Review E*, (), 49:3930–3939, 1994. DOI: 10.1103/PhysRevE.49.3930

[20] P.Jung, P.Talkner, Suppression of highre harmonics at noise induced resonances, *Physical Review E*, **51**(1995), 2640–2643. DOI: 10.1103/PhysRevE.51.2640

[21] Yu.L.Raikher, V.I.Stepanov, Selective suppression of the higher harmonics of magnetization in a superparamagnetic system, *Physics of the Solid State*, **43**(2001), 279–283. DOI: 10.1103/PhysRevLett.86.1923

[22] Yu.L.Raikher, V.I.Stepanov, Noise- and force-induced resonances in noisy rotary oscillations of classical spins, *Phys. Rev. Lett .*, **86**(2001), 1923–1926. DOI: 10.1103/PhysRevLett.86.1923

[23] A.N.Grigorenko, V.I.Konov, P.I.Nikitin, Magnetostochastic resonance, *Soviet Journal of Experimental and Theoretical Physics Letters*, **52**(1990), 593–596.

[24] E.K.Sadykov, Stochastic resonance in small-particle magnetics. I. radiospectroscopic study, *Journal of Physics C: Condensed Matter*, **4**(1992), 3295–3298.

[25] L.B.Kiss, Z.Gingl, Z.Márton et al., 1/f noise in systems showing stochastic resonance, *Journal of Statistical Physics*, **70**(1993), 451–462. DOI: 10.1007/BF01053981

[26] A.N.Grigorenko, P.I.Nikitin, A.N.Slavin, P.Y.Zhou, Experimental observation of magnetostochastic resonance, *Journal of Applied Physics*, **76**(1994), 6335–6337. DOI: 10.1063/1.358258

[27] Yu.L.Raikher, V.I.Stepanov, Stochastic resonance in single-domain particles, *Journal of Physics C: Condensed Matter*, **6**(1994), 4137–4145. DOI: 10.1088/0953-8984/6/22/013

[28] Yu.L.Raikher, V.I.Stepanov, Stochastic resonance and phase shifts in single-domain particles, *Physical Review B*, **52**(1994), 3493–3498. DOI: 10.1103/PhysRevB.52.3493

[29] A.N.Grigorenko, P.I.Nikitin, G.V.Roschepkin, Frequency mixing phenomena in a bistable system, *Journal of Applied Physics*, **79**(1996), 6113–6115. DOI: 10.1063/1.362104

[30] N.Smith, P.Arnett, White-noise magnetization fluctuations in magnetoresistive heads, *Applied Physics Letters*, **78**(2001), 1448–1450. DOI: 10.1063/1.1352694

[31] V.L.Safonov, H.N.Bertram, "dynamic-thermal" reversal in a fine micromagnetic grain: Time dependence of coercivity, *Journal of Applied Physics*, **87**(2000), 5681–5683. DOI: 10.1063/1.372488

[32] N.Smith, Modeling of thermal magnetization fluctuations in thin-film magnetic devices, *Journal of Applied Physics*, **90**(2001), 5768–5773. DOI: 10.1063/1.1402146

[33] R.Kaiser, G.Miskolczy, Magnetic properties of stable dispersions of subdomain magnetite particles, *Journal of Applied Physics*, **41**(1970), 1064–1072. DOI: 10.1063/1.1658812

[34] X.Zianni, K.N.Trohidou, J.A.Blackman, Effect of surface anisotropy on the coercive field of small magnetic particles, *Journal of Applied Physics*, **81**(1970), 4739–4740. DOI: 10.1063/1.365447

[35] V.P.Shilov, J.-C.Bacri, F.Gazeau, F.Gendron, R.Perzynski, Yu.L.Raikher, Ferromagnetic resonance in ferrite nanoparticles with uniaxial surface anisotropy, *Journal of Applied Physics*, **85**(1970), 6642–6647. DOI: 10.1063/1.370173

[36] V.P.Shilov, Yu.L.Raikher, J.-C.Bacri, F.Gazeau, R.Perzynski, Effect of unidirectional anisotropy on the ferromagnetic resonance in ferrite nanoparticles, *Physical Review B*, **60**(1999), 11902–11905. DOI: 10.1103/PhysRevB.60.11902

[37] T.L.Gilbert, A phenomenological theory of damping in ferromagnetic materials, *Physical Review*, **100**(1955), 1243. This reference reproduces the biblio data customarily referred to until 2004. However, in the PR archive (PROLA) this paper cannot be found. In 2004 the original work had been reprinted in full in [38].

[38] T.L.Gilbert, A phenomenological theory of damping in ferromagnetic materials, *IEEE Transactions on Magnetics*, **40**(2004), 3443–3449. DOI: 10.1109/TMAG.2004.836740

[39] G.V.Skrotskii, L.V.Kurbatov, Phenomenological theory of ferromagnetic resonance rom finite size and surface effects to glassy behaviour in ferrimagnetic nanoparticles. In: S.V.Vonsovsii, editor, Ferromagnetic Resonance, pages, Pergamon, Oxford, 1966, 12–77.

[40] W.F.Brown, Thermal fluctuations in single-domain particles, *Physical Review*, **130**(1963), 1677–1686. DOI: 10.1103/PhysRev.130.1677

[41] Yu.L.Raikher, M.I.Shliomis, Effective field method for orientational kinetics of magnetic fluids and liquid crystals, *Advances in Chemical Physics Series*, **87**(1994), 595–751. DOI: 10.1002/9780470141465.ch8

[42] Yu.L.Raikher, V.I.Stepanov, Nonlinear dynamic susceptibilities and field-induced birefringence in magnetic fluids, *Advances in Chemical Physics Series*, **129**(2004), 419–588. DOI: 10.1002/047168077X.ch4

[43] L.D.Landau, E.M.Lifshitz, Quantum Mechanics, Pergamon, Oxford, 1959.

[44] W.T.Coffey, D.A.Garanin, D.J.McCarthy, Crossover formulas in the kramers theory of thermally activated escape rates – application to spin systems, *Advances in Chemical Physics Series*, **117**(2001), 483–766.

[45] C.W.Gardiner, Handbook of Stochastic Methods, Springer Series in Synergetics, Springer, Berlin, 1985.

[46] Yu.L.Raikher, M.I.Shliomis, Theory of dispersion of the magnetic susceptibility of fine ferromagnetic particles, *Soviet Journal of Experimental and Theoretical Physics*, **40**(1974), 526–532.

[47] A.Aharoni, Effect of a magnetic field on the superparamagnetic relaxation time, *Physical Review*, **177**(1969), 793–796. DOI: 10.1103/PhysRev.177.793

[48] A.Aharoni, Relaxation time of superparamagnetic particles with cubic anisotropy, *Physical Review B*, **7**(1976), 1103–1107. DOI: 10.1103/PhysRevB.7.1103

[49] A.Aharoni, Susceptibility resonance and magnetic viscosity, *Physical Review B*, **46**(1994), 5434–5441. DOI: 10.1103/PhysRevB.46.5434

[50] W.T.Coffey, D.S.F.Crothers, Yu.P.Kalmykov et al., Exact analytic formula for the correlation time of a single-domain ferromagnetic particle, *Physical Review E*, **49**(1994), 1869–1882. DOI: 10.1103/PhysRevE.49.1869

[51] W.T.Coffey, D.S.F Crothers, Yu.P.Kalmykov, J.T.Waldron, Constant-magnetic field effect in Néel relaxation of single-domain ferromagnetic particles, *Physical Review B*, **51**(1995), 15947–15956. DOI: 10.1103/PhysRevB.51.15947

[52] W.T.Coffey, D.S.F.Crothers, J.-L.Dormann et al., Effect of an oblique magnetic field on the superparamagnetic relaxation time, *Physical Review B*, **52**(1995), 15951–15965. DOI: 10.1103/PhysRevB.52.15951

[53] C.A.J.Fletcher, Computational Technique for Fluid Dynamics, Vol. 1, Springer, Berlin, 1988.

[54] D.A.Balaev, I.S.Poperechny, A.A.Krasikov et al., Dynamic magnetization of "ε-Fe2O3 in pulse field: Evidence of surface effect, *Journal of Applied Physics*, **117**(2015), 063908. DOI: 10.1063/1.4907586

[55] D.A.Balaev, I.S.Poperechny, A.A.Krasikov et al., Dynamic remagnetisation of CoFe2O4 nanoparticles: thermal fluctuational thawing of anisotropy, *Journal of Physics D: Applied Physics*, **54**(2021), 275003. DOI: 10.1088/1361-6463/abf371

[56] S.V.Titov, W.T.Coffey, Yu.P.Kalmykov, M.Zarifakis, A.S.Titov, Inertial magnetization dynamics of ferromagnetic nanoparticles including thermal agitation, *Physical Review B*, **103**(2021), 144433. DOI: 10.1103/PhysRevB.103.144433

[57] A.O.Ivanov, O.B.Kuznetsova, Applying the modified mean-field model to superparamagnetic nanoparticles, *Journal of Chemical Physics*, **164**(2026), 021001. DOI: 10.1063/5.031011

Суперпарамагнитные частицы: введение в теоретическое описание магнитодинамики

Юрий Л. Райхер
Институт механики сплошных сред УрО РАН
Пермь, Российская Федерация

Аннотация. Цель работы — кратко и доступно изложить теоретическую схему, с помощью которой описывается магнитодинамика однодоменных суперпарамагнитных частиц. Показано, как классическая картина (уравнения Ландау–Лифшица и Гильберта) модифицируется для случая суперпарамагнитного поведения, так что температура явным образом входит в уравнения, поскольку детерминистическая динамика уступает место стохастической. Для этого используются или кинетическое (типа Фоккера-Планка) уравнение, или система уравнений, связывающая статистические моменты возрастающего порядка. В качестве первого шага, вводится с пояснениями стандартное макроскопическое (феноменологическое) описание магнитодинамики частицы ферромагнетика.

Ключевые слова: суперпарамагнетизм, однодоменные частицы, ориентационная функция распределения, магнитодинамика.

EDN: XQFDQI
УДК 537.611.3

Coupled Dynamics of Magnetic Vortices with Different Polarities in a Small-diameter Spin-transfer Nano-oscillator

Evgenii G. Ekomasov*
Radmir A. Faskhutdinov
Daniil K. Kabanov†
Victor S. Kudashev
Institute of Physics and Technology
Ufa University of Science and Technology
Ufa, Russian Federation

Received 16.02.2026, received in revised form 10.04.2026, accepted 13.05.2026

Abstract. We investigate the dynamics of two dipolar-coupled magnetic vortices with different polarities in a small-diameter spin-transfer nano-oscillator under the influence of a spin-polarized electric current. Using micromagnetic modeling, we demonstrate the existence of three distinct vortex motion regimes separated by two critical current values. A near-linear dependence of the oscillation frequency and the vortex core orbit radius on the spin-polarized current magnitude is obtained. The results are compared with the case of coupled vortex dynamics of identical polarity.

Keywords: generalized Landau–Lifshitz–Gilbert equation, magnetic vortices, spin-transfer nano-oscillator, coupled oscillator dynamics.

Citation: E.G. Ekomasov, R.A. Faskhutdinov, D.K. Kabanov, V.S. Kudashev, Coupled Dynamics of Magnetic Vortices with Different Polarities in a Small-diameter Spin-transfer Nano-oscillator, J. Sib. Fed. Univ. Math. Phys., 2026, 19(4), 560–569. EDN: XQFDQI.

Introduction

A promising direction in spintronics is the development of nanoelectronic devices in which the magnetization dynamics of a system can be excited by a spin-polarized current [1–3]. Such magnetic nanostructures are used for creating advanced radiofrequency applications, as their magnetization oscillation frequencies can be tuned by applying external magnetic fields and currents [4, 5].

Spin-transfer nano-oscillators (STNOs) attract significant research interest [6–9]. Often, such multilayer structures consist of two magnetic layers separated by a non-magnetic spacer [10]. Given certain geometric dimensions, a magnetic vortex can be realized as the ground state in these structures [11, 12]. At the center (or core) of the vortex, in a region approximately 10 nm in size, the magnetic moment points out-of-plane perpendicularly. In other areas, the magnetic moment lies within the plane of the magnetic film. The magnetization at the vortex center can have two opposite directions, or vortex polarities (up or down), which can be used to encode digital signals "0" or "1". Vortex-based STNOs can also find application as vortex nanoscale spin-torque generators [10] and as programmable building blocks for neuromorphic computing systems [13].

For practical applications, the study of the structure, statics, and dynamics of magnetic vortices is of great importance [14, 15]. The structure and static properties of magnetic vortices

*ekomasoveg@gmail.com
†danya.kabanov.95@mail.ru

in isolated nanodisks and in STNOs with a vortex state in a single free magnetic layer have been studied quite thoroughly [15, 16]. Cases where the second, fixed magnetic layer in an STNO can have either uniform or non-uniform magnetization have been considered [10, 17–19]. It has been shown that when a spin-polarized current is passed through a single-vortex STNO, the vortex can start moving along different types of orbits (e.g., a stationary circular orbit, chaotic motion, etc.) [20–22]. Effective differential equations for the vortex core coordinates, which accurately describe the gyrotropic motion of the vortex, have been proposed [23, 24]. The mechanisms for switching the chirality and polarity of a magnetic vortex, both by polarized current and by pulsed or constant magnetic fields, have also been investigated [25, 26]. In [27], laser excitation of magnetization dynamics without applying external fields was used to induce transient changes in the structure and dynamics of a magnetic vortex. The linear and nonlinear dynamics of mutually coupled magnetic vortices in two STNOs, excited either by an external harmonic magnetic field or by a spin-polarized current, have been studied [28].

Numerous experimental and theoretical works have been devoted to studying the dynamics of magnetostatically coupled magnetic vortices in STNOs where both magnetic disks are in a vortex state (see, e.g., [29–35]). The properties of such a system significantly depend on the mutual orientation of the magnetization in the vortex cores. The influence of the STNO diameter on the coupled vortex dynamics under a spin-polarized current has been investigated [34–39]. The existence of several critical current values separating different regimes of coupled vortex dynamics was discovered. One of them is the gyrotropic oscillations of magnetostatically coupled vortices with a constant frequency, which has current limitations. When the current magnitude exceeds a critical value for large and medium-diameter STNOs, after the vortex in the thicker layer reaches a critical velocity, a dynamic switching of this vortex's polarity occurs [34, 39, 40]. This indicates the possibility of controlling vortex polarity using direct current under zero magnetic field conditions. For small STNO diameters, in the case of vortices with identical polarity and chirality, vortex expulsion from the disk edge is observed [37–39]. However, it has been shown that in modern experiments, a signal can only be observed for the case of vortices with different polarities [41]. Therefore, this work investigates the influence of current on the dynamics of coupled vortices with different polarities and identical chirality in a small-diameter STNO equal to 120 nm.

1. Fundamental equations and results

The generalized Landau-Lifshitz equation (GLE) describing the nonlinear magnetization dynamics in each magnetic layer includes an additional spin-transfer torque term $\mathbf{T}_{s.t.}$ [3] responsible for the interaction between the current and the magnetization, and can be written as:

$$\dot{\mathbf{M}} = -\gamma \left[\mathbf{M} \times \mathbf{H}_{eff}\right] + \frac{\alpha}{\mathrm{M}_s}\left[\mathbf{M} \times \dot{\mathbf{M}}\right] + \mathbf{T}_{s.t.} \tag{1}$$

where $\mathbf{M}$ is the magnetization vector, γ is the gyromagnetic ratio, M_s is the saturation magnetization, α is the Gilbert damping parameter. The effective field $\mathbf{H}_{eff}$ represents the sum of the external magnetic field, and the magnetostatic and exchange interaction fields.

$$\begin{gathered} \mathbf{T}_{s.t.} = -\frac{\gamma_0 a_j}{\mathrm{M}_s}\mathbf{M} \times \left[\mathbf{M} \times \mathbf{m}_{ref}\right] + \gamma b_j \left[\mathbf{M} \times \mathbf{m}_{ref}\right], \\ a_j = \frac{\hbar}{2\left|e\right|}\frac{1}{d}P\frac{1}{M_s}J_e,\ b_j = \beta a_j,\ \ \beta \sim 0.05 - 0.2, \end{gathered} \tag{2}$$

where $\hbar$ is Planck's constant, e is the electron charge, d is the thickness of the magnetic layer, J_e is the current density, P is the current polarization, and $\mathbf{m}_{ref}$ is the unit vector along the

magnetization of the reference layer. The GLE is a complex integro-differential equation that, in the general case, can only be solved using numerical methods.

We investigate a spin-transfer nano-oscillator in the form of a multilayer nanocylinder with a circular cross-section and a diameter of 120 nm, which has been previously studied experimentally [30]. It consists of three layers: a "thick" magnetic permalloy layer (15 nm thick), an intermediate non-magnetic spacer layer (10 nm thick), and a "thin" magnetic permalloy layer (4 nm thick). The permalloy composition is Ni80Fe20, abbreviated as Py. For numerical calculations, we use the following magnetic parameters [30]: $M_s = 700$ erg Gs /cm^3 for the "thick" and $M_s = 600$ erg Gs /cm^3 for the "thin" magnetic layers; exchange stiffness $A = 1.2 \times 10^{-6}$ erg / cm for the "thick" layer and $A = 1.12 \times 10^{-6}$ erg / cm for the "thin" magnetic layer; Gilbert damping constant $\alpha = 0.01$; gyromagnetic ratio $\gamma = 2.0023 \times 10^7$ (Oe s)$^{-1}$.

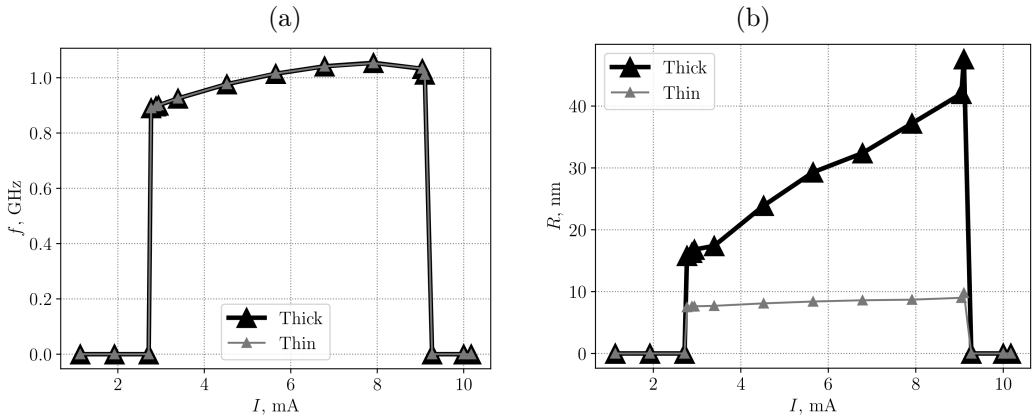

Fig. 1. Dependence of (a) the frequency and (b) the radius of stationary coupled vortex core oscillations on the current magnitude

For the numerical calculation of the structure and coupled dynamics of the magnetic vortices, we used the SpinPM software package for micromagnetic modeling [10]. With its help, the dependencies of the magnetization projections on the coordinate axes versus time (e.g., $M_x = M_x(t)$)) were obtained. Using these dependencies, the oscillation period and the corresponding frequency value were determined from the peaks in the magnetization. To verify the accuracy of the determined frequencies, Fourier analysis was also used, which provided identical values.

The motion of the coupled magnetic vortices in the STNO was excited by a spin-polarized current with a polarization of $P = 0.1$, flowing perpendicular to the plane of the layers. For definiteness, the case where the current flows from top to bottom, from the thin layer to the thick one, is considered. We further investigate the structure in which, at the initial moment, the vortex chiralities in both Py layers are identical and correspond to the twist direction of the Oersted field induced by the current. The vortex polarities are opposite: in the upper thin layer, the core magnetization is directed downward, while in the lower thick layer, it is directed upward.

For the case of coupled vortex dynamics with identical polarity in a similar STNO, it is known that there exist three critical values of current on the dependence of oscillation frequencies on the magnitude of the spin-polarized current [37]. The first of these limits the region of decaying vortex motion, the second limits the region of stationary vortex motion, and the third limits the region where the vortex in the thick layer is expelled beyond the disk edge. For the case of coupled vortex dynamics with opposite polarities, the numerical calculation results revealed the presence of two critical current values (Fig. 1a). The first one, $I_1 = 2.77$ mA (4.64 mA for the case of vortices with identical polarity), limits the region where decaying oscillations of the vortices in the thin and thick layers exist. The interval of current values between $I_1 = 2.77$ mA

and $I_2 = 9.15$ mA (between 4.64 mA and 7.35 mA for the case of vortices with identical polarity) defines the region where stationary oscillations of the vortices in both layers exist. It should be noted that for the case of vortices with opposite polarities, the range of currents supporting a stationary regime of coupled vortex oscillations increases substantially, and the value of the minimum required current decreases significantly. Due to their coupled motion, the oscillation frequencies of both vortices have identical values. Their values increase almost linearly with the current. The oscillation radii of the vortex cores also increase almost linearly with the current magnitude (Fig. 1b), with the increase in the oscillation radius of the vortex core in the thick magnetic layer being much greater than that in the thin layer. At a current equal to or greater than $I_2 = 9.15$ mA, the regime of vortex expulsion beyond the disk edge is observed in both magnetic layers.

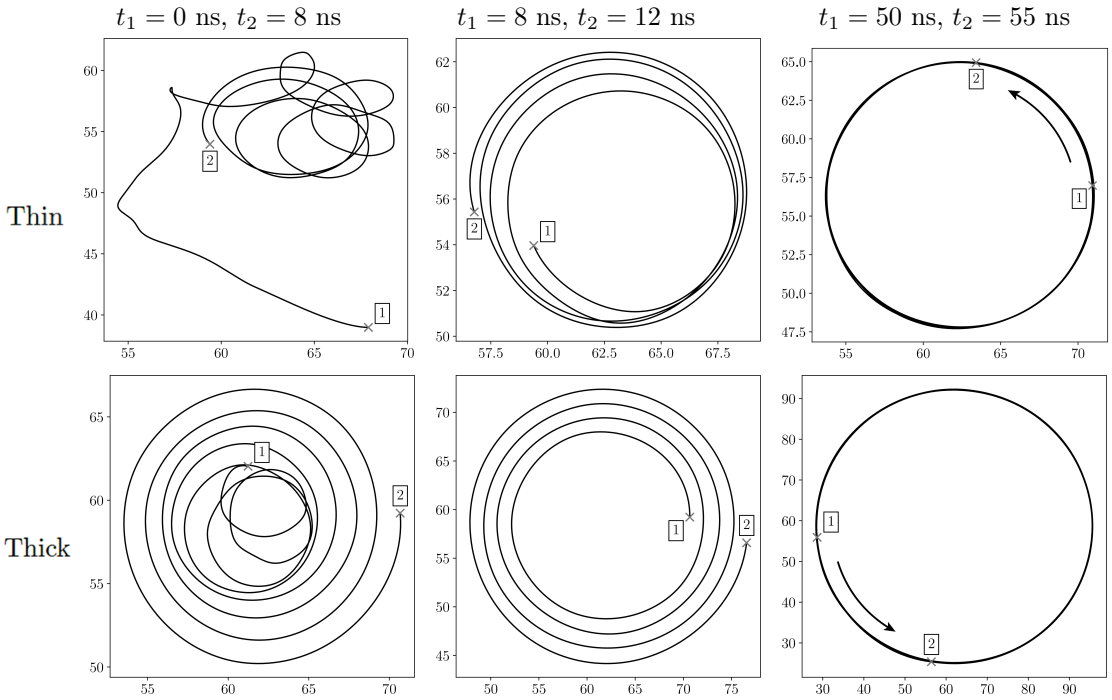

Fig. 2. Trajectory of the vortex core motion in the thin layer (top row) and in the thick layer (bottom row). The first column corresponds to the time interval from 0 ns to 8 ns, the second column from 8 ns to 12 ns, and the third column from 50 ns to 55 ns. $I = 6.78$ mA

Let us examine how the system under study transitions to a stationary oscillation regime. For this purpose, we take a current magnitude greater than the first critical current, for example, I = 6.78 mA. At the initial moment, the vortex cores are located on opposite sides relative to the disk center. This is caused by magnetostatic interaction. Note that in the case of identical vortex polarities, the core of the vortex in the thin magnetic layer and the core of the vortex in the thick magnetic layer are located on the same side of the nanocylinder center. After the current is switched on, a nonlinear stage of vortex dynamics is initially observed in both the thin and thick layers (first row in Fig. 2). The vortices begin to move in different directions—clockwise in the thin layer and counterclockwise in the thick one. Subsequently, due to interaction with the vortex in the thick magnetic layer, the vortex in the thin layer stops and begins moving counterclockwise, just like the vortex in the thick layer. It should be noted that a similar motion scenario was previously observed for vortices with opposite polarities in medium and

large-diameter nanocylinders [34, 38, 40]. This stage of vortex motion lasts several nanoseconds after the current is switched on. After this, the vortices begin to spiral out (second row in Fig. 2), and the trajectory of their core motion is a screw line. The figures show that at identical moments in time, the vortex cores lie on a straight line passing through the center of their orbit but on opposite sides of it and move in the same direction. Approximately 27 ns after the start of motion, the vortices settle into a constant circular orbit (third row in Fig. 2).

Let us further investigate the dynamics of vortex expulsion from the layer. For this purpose, we consider the case of a current equal to the critical value I = 9.15 mA. As in the previously considered case, when the current is switched on, the vortices begin moving in opposite directions. After several nanoseconds, the vortex in the thin layer stops and begins moving in the opposite direction. Subsequently, the vortex cores move along a screw line in the same direction for several tens of nanoseconds, after which they reach a certain maximum orbit radius (the vortex in the thick layer is already practically at the very edge of the disk), and their orbits cease to increase rapidly (Figs. 3a and 3b). The vortices move in this manner for approximately 150 nanoseconds (Figs. 4a and 4b). Although the vortex in the thick layer has approached close to the disk

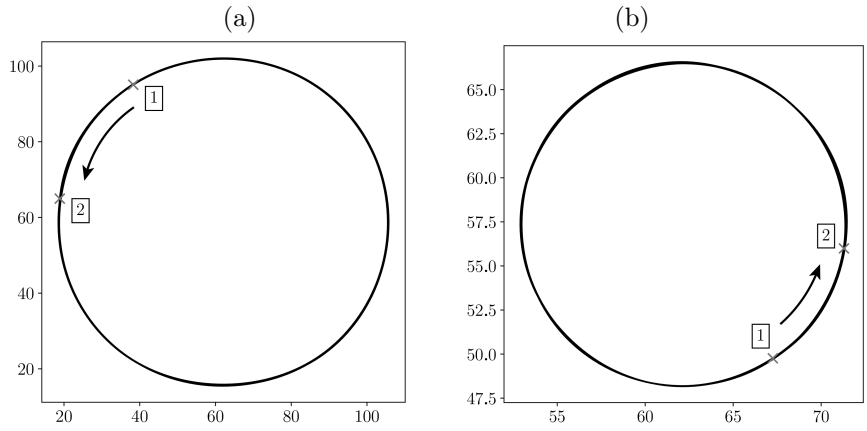

Fig. 3. Trajectory of the vortex core motion before expulsion in (a) the thin layer and (b) the thick layer. Points 1 and 2 correspond to time instances of 60 ns and 64 ns, respectively. $I = 9.15$ mA

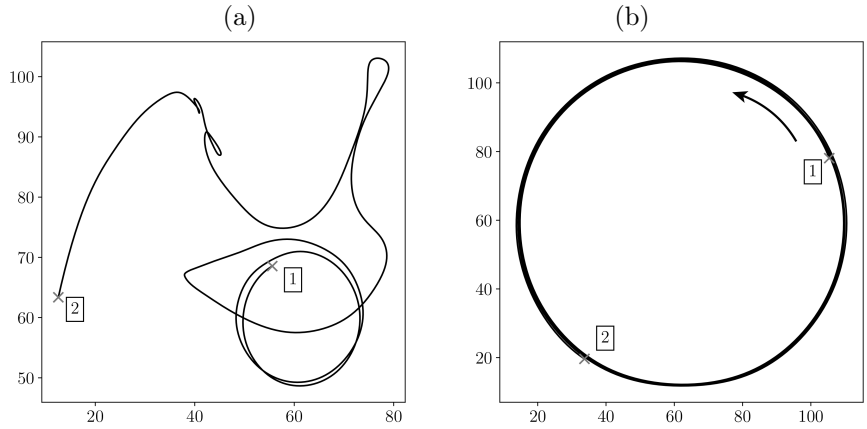

Fig. 4. Trajectory of the vortex core motion before expulsion in (a) the thin layer, where point 1 corresponds to 210 ns and point 2 to 217.8 ns; and (b) the thick layer, where point 1 corresponds to 208 ns and point 2 to 212.2 ns. $I = 9.15$ mA

edge, its circular structure outside the core region remains practically undisturbed. At 212 ns, a noticeable portion of the vortex in the thick layer already extends beyond the disk edge. At 214.4 ns, the vortex is no longer present on the disk (see Fig. 5). After this, the nature of the vortex motion in the thin layer changes abruptly (see Fig. 4a), the trajectory becomes highly nonlinear, the vortex core position rapidly approaches the edge, and at 217.4 ns it is expelled from the disk.

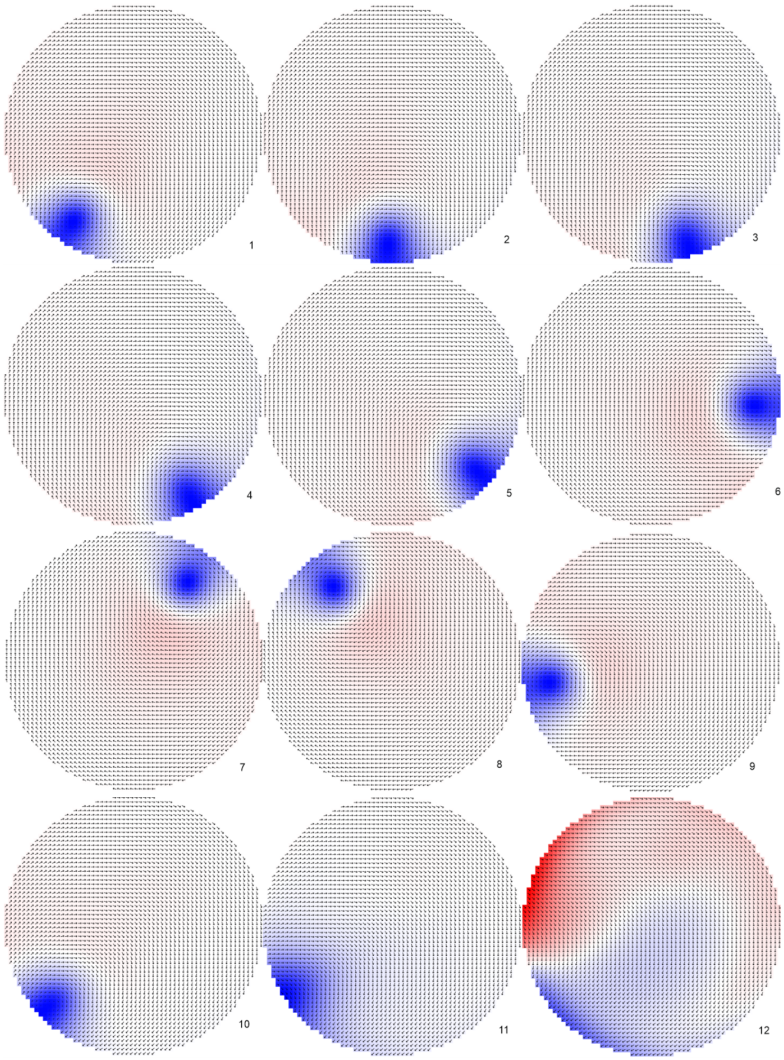

Fig. 5. Magnetization structure in the thick magnetic layer at different time instances: 1 – 212.2 ns; 2 – 212.4 ns; 3 – 212.6 ns; 4 – 212.8 ns; 5 – 213.0 ns; 6 – 213.2 ns; 7 – 213.4 ns; 8 – 213.6 ns; 9 – 213.8 ns; 10 – 214.0 ns; 11 – 214.2 ns; 12 – 214.4 ns

Conclusion

Using micromagnetic modeling, the dynamics of two coupled magnetic vortices with different polarities in a small-diameter spin-transfer nano-oscillator under the influence of a spin-polarized electric current has been investigated. The possible vortex trajectories over a time period of approximately 250 ns are described. A comparison with the case of two coupled magnetic vortices

of identical polarity is performed. It is found that, unlike the case of vortices with identical polarity, only two critical current values exist, separating the different vortex motion regimes: decaying oscillations, stationary oscillations, and vortex expulsion from the nanocylinder. The possibility of controlling the frequency and radius of the stationary vortex motion over a wider range of current values than in the case of vortices with identical polarity is demonstrated.

It is also worth noting that the long-standing friendship and collaboration between magnetologists from Ufa and their colleagues in Krasnoyarsk is largely linked to Walter Alexeevich Ignatchenko. His seminal works on thin magnetic films—investigating domain and stochastic magnetic structure, features of the remagnetization process, spin-wave and magnetoelastic resonance, and domain wall resonance—have been thoroughly studied and actively cited by scientists from Ufa. Our scientific community has also shown great interest in the comprehensive theoretical and experimental approach he developed with his students for studying randomly inhomogeneous media. His ideas, research methods, and results have been utilized in teaching special courses to students specializing in theoretical physics at our university.

The work was carried out within the framework of the state assignment, Agreement No. 075-03-2024-123/1 dated February 15, 2024, Topic No. 324-21.

References

[1] J.C.Slonczewski, Current-driven excitation of magnetic multilayers, *J. Magn. Magn. Mater.*, **159**(1996), L1–L7.

[2] N.Locatelli, V.Cros, J.Grollier, Spin-torque building blocks, *Nat. Mater.*, **13**(2014), 11–20. DOI: 10.1038/nmat3823

[3] A.K.Zvezdin, A.V.Khvalkovskiy, K.A.Zvezdin, The generalized Landau-Lifshitz equation and spin transfer processes in magnetic nanostructures, *Phys. Usp.*, **51**(2008), 412–417. DOI: 10.3367/UFNr.0178.200804i.0436

[4] S.Manipatruni, D.E.Nikonov, I.A.Young, Beyond CMOS computing with spin and polarization, *Nat. Phys.*, **14**(2018), 338–343. DOI: 10.1038/s41567-018-0101-4

[5] S.Fusil, V.Garcia, A.Barthélémy, M.Bibes, Magnetoelectric devices for spintronics, *Annu. Rev. Mater. Res.*, **44**(2014), 91–116.

[6] I.V.Barashenkov, A.Chernyavsky, Stable solitons in a nearly PT-symmetric ferromagnet with spin-transfer torque, *Physica D*, **409**(2020), 132481.

[7] S.Jiang, L.Yao, S.Wang et al., Spin-torque nano-oscillators and their applications, *Appl. Phys. Rev.*, **11**(2024), 041309.

[8] A.Slavin, V.Tyberkevych, R.Verba, Auto-oscillations and phase-locking in a multimode spin-torque oscillator, *Low Temp. Phys.*, **51**(2025), 804–812. DOI:10.1063/10.0036804

[9] A.Litvinenko, P.Sethi, C.Murapaka et al., Analog and digital phase modulation and signal transmission with spin-torque nano-oscillators, *Phys. Rev. Appl.*, **16**(2021), 024048. DOI: 10.1103/PhysRevApplied.16.024048

[10] K.A.Zvezdin, E.G.Ekomazov, Spin currents and nonlinear dynamics of vortex spin-transfer nano-oscillators, *Phys. Met. Metallogr.*, **123**(2022), 219–228. DOI: 10.1134/S0031918X22030140

[11] N.A.Usov, S.E.Peschany, Vortex magnetization distribution in a thin ferromagnetic cylinder, *Phys. Met. Metallogr.*, **78**(1994), 13–20.

[12] K.L.Metlov, Equilibrium large vortex state in ferromagnetic disks, *J. Appl. Phys.*, **113**(2013), 223905.

[13] T.Bóhnert, Y.Rezaeiyan, M.S.Claro, Weighted spin-torque nano-oscillator system for neuromorphic computing, *Commun. Eng.*, **2**(2023), 65.

[14] A.B.Borisov, Two-dimensional magnetic vortices, *Phys. Met. Metallogr.*, **125**(2024), 1548–1576.

[15] A.B.Borisov, E.G.Ekomazov, Three-dimensional vortex structures, *Phys. Met. Metallogr.*, **126**(2025), 379–422.

[16] H.Vigo-Cotrina, S.Urcia-Romero, A.P.Guimaräes, Influence of perpendicular uniaxial anisotropy on the switching of a magnetic vortex, *J. Appl. Phys.*, **137**(2025), 013909.

[17] M.Stebliy, A.Jenkins, L.Benetti, R.Ferreira, Experimental study of a vortex spin-torque oscillator in an MTJ with a vortex polarizer, *arXiv preprint*, arXiv:2511.04761.

[18] A.Khvalkovskiy, J.Grollier, V.Cros, Nonuniformity of a planar polarizer for spin-transfer-induced vortex oscillations at zero field, *Appl. Phys. Lett.*, **96**(2010), 212507. DOI:10.1063/1.3441405

[19] A.Hanif, A.A.Rahim, H.Maab, Vortex dynamics in a spin valve nanopillar having hybrid polarizer and magnetostatic coupling, *Physica B*, **668**(2023), 415203. DOI:10.1016/j.physb.2023.415203

[20] B.A.Ivanov, C.E.Zaspel, Excitation of spin dynamics by spin-polarized current in vortex state magnetic disks, *Phys. Rev. Lett.*, **99**(2007), 247208.

[21] K.Y.Guslienko, O.V.Sukhostavets, D.V.Berkov, Nonlinear magnetic vortex dynamics in a circular nanodot excited by spin-polarized current, *Nanoscale Research Letters*, **9**(2014), 386. DOI: 10.1186/1556-276X-9-386

[22] S.Petit-Watelot, J.Kim, A.Ruotolo et al., Commensurability and chaos in magnetic vortex oscillations, *Nat. Phys.*, **8**(2012), 682–687.

[23] K.Y.Guslienko et al., Eigenfrequencies of vortex state excitations in magnetic submicron-size disks, *J. Appl. Phys.*, **91**(2002), 8037–8039.

[24] S.de Wergifosse, C.Chopin, F.Abreu Araujo, Quantitative and realistic description of the magnetic potential energy of spin-torque vortex oscillators, *Phys. Rev. B*, **108**(2023), 174403. DOI: 10.1103/PhysRevB.108.174403

[25] T.Okuno, K.Shigeto, T.Ono, K.Mibu, T.Shinjo, MFM study of magnetic vortex cores in circular permalloy dots: behavior in external field, *J. Magn. Magn. Mater.*, **240**(2002), 1–6.

[26] A.V.Khvalkovskiy, A.N.Slavin, J.Grollier, K.A.Zvezdin, K.Y.Guslienko, Critical velocity for the vortex core reversal in perpendicular bias magnetic field, *Appl. Phys. Lett.*, **96**(2010), 022504.

[27] M.Fanciulli, M.Pancaldi, A.Stanciu, Magnetic Vortex Dynamics Probed by Time-Resolved Magnetic Helicoidal Dichroism, *Phys. Rev. Lett.*, **134**(2025), 156701. DOI: 10.1103/PhysRevLett.134.156701

[28] A.A.Matveev, A.R.Safin, S.A.Nikitov, Exceptional points in coupled vortex-based spin-torque oscillators, *Phys. Rev. B*, **108**(2023), 174443.

[29] K.Y.Guslienko, K.S.Buchanan, S.D.Bader, V.Novosad, Dynamics of coupled vortices in layered magnetic nanodots, *Appl. Phys. Lett.*, **86**(2005), 223112. DOI:10.1063/1.1929078

[30] N.Locatelli, A.E.Ekomasov, A.V.Khvalkovskiy et al., Reversal process of a magnetic vortex core under the combined action of a perpendicular field and spin transfer torque, *Appl. Phys. Lett.*, **102**(2013), 062401.

[31] S.S.Cherepov, B.C.Koop, A.Y.Galkin et al., Core-Core dynamics in spin vortex pairs, *Phys. Rev. Lett.*, **109**(2012), 097204.

[32] E.Holmgren, A.Bondarenko, B.A.Ivanov, V.Korenivski, Resonant pinning spectroscopy with spin-vortex pairs, *Phys. Rev. B*, **97**(2018), 094406.

[33] V.Sluka, A.Kakay, A.M.Deac, D.E.Burgler, C.M.Schneider, R.Hertel, Spin-torque-induced dynamics at fine-split frequencies in nano-oscillators with two stacked vortices, *Nat. Commun.*, **6**(2015), 6409.

[34] A.E.Ekomasov, S.V.Stepanov, K.A.Zvezdin, E.G.Ekomasov, Spin current induced dynamics and polarity switching of coupled magnetic vortices in three-layer nanopillars, *J. Magn. Magn. Mater.*, **471**(2019), 513–517.

[35] A.A.Hamadeh, A.Koujok, D.R.Rodrigues et al., Diverse dynamics in interacting vortices systems through tunable conservative and non-conservative coupling strengths, *Commun. Phys.*, **8**(2025), 85.

[36] A.A.Hamadeh, A.Koujok et al., Core Reversal in Vertically Coupled Vortices: Simulation and Experimental Study, *IEEE Trans. Nanotechnol.*, **23**(2024), 549–553.
DOI: 10.1109/TNANO.2024.3420249

[37] A.E.Ekomasov, S.V.Stepanov, K.A.Zvezdin, E.G.Ekomasov, Influence of perpendicular magnetic field and polarized current on the dynamics of coupled magnetic vortices in a thin nanocolumnar trilayer conducting structure, *Phys. Met. Metallogr.*, **118**(2017), 328–333.
DOI: 10.1134/S0031918X17020028

[38] E.G.Ekomasov, S.V.Stepanov, K.A.Zvezdin, N.G.Pugach, G.I.Antonov, The effect of the spin-polarized current on the dynamics and structural changes of magnetic vortices in a large-diameter three-layer conducting nanocylinder, *Phys. Met. Metallogr.*, **122**(2021), 197–204.

[39] S.V.Stepanov, V.N.Nazarov, K.A.Zvezdin, E.G.Ekomasov, Edge vortices and C-state in vortex spin torque nanooscillators, *J. Magn. Magn. Mater.*, **562**(2022), 169758.
DOI: 10.1016/j.jmmm.2022.169758

[40] G.I.Antonov, E.G.Ekomasov, K.A.Zvezdin, N.G.Pugach, A New Stationary Mode of Coupled Oscillations in a Three-Layer Spin-Transfer Nano-Oscillator at High Currents, *Phys. Met. Metallogr.*, **125**(2024), 33–40.

[41] N.Locatelli et al., Improved Spectral Stability in Spin-Transfer Nano-Oscillators: Single Vortex Versus Coupled Vortices Dynamics, *IEEE Trans. Magn.*, **51**(2015), 1400304.
DOI:10.1109/TMAG.2015.2414903

Связанная динамика магнитных вихрей разной полярности в спин-трансферном наноосцилляторе малого диаметра

Евгений Г. Екомасов
Радмир А. Фасхутдинов
Даниил К. Кабанов
Виктор С. Кудашев
Институт физики и технологий
Уфимский университет науки и технологий
Уфа, Российская Федерация

Аннотация. Проведено исследование динамики двух дипольно-связанных магнитных вихрей разной полярности в спин-трансферном наноосцилляторе малого диаметра под действием спин-поляризованного электрического тока. С помощью микромагнитного моделирования показано наличие трех возможных режимов движения вихрей, разделяемых двумя критическими значениями тока. Получена близкая к линейной зависимость частоты и радиуса осцилляций вихрей от величины спин-поляризованного тока. Проведено сравнение результатов со случаем связанной динамики вихрей одинаковой полярности.

Ключевые слова: обобщенное уравнение Ландау–Лифшица–Гильберта, магнитные вихри, спин трансферный наноосциллятор, связанная динамика осцилляторов.